Laser Materials Processing for NASA's Aerospace Structural Materials

Project Report
(ODURF Contract # 104041)

Dr. Karthik Nagarathnam
Principal Investigator
&
Thomas A. Hunyady
Graduate Research Assistant

Applied Research Center
College of Engineering and Technology
Old Dominion University
12050 Jefferson Avenue, Suite 623
Newport News, VA 23606
Tel: 757-269-5641; Fax: 757-269-5644

karthik@odu.edu
tomh@jlab.org

Submitted
To

Karen M. B. Taminger
Technical Monitor
NASA Langley Research Center
MS 188A
Hampton, VA 23681

Tel: 757-864-3131; Fax: 757-864-3131
k.m.taminger@larc.nasa.gov

January 22, 2001

TABLE OF CONTENTS

ABSTRACT.....4

INTRODUCTION AND LITERATURE BACKGROUND.....5

Energy Requirements for Laser Materials Processing

Laser Surface Engineering

Built-up Freeform Fabrication

Laser Welding, Machining, and Other Manufacturing Applications

Comparison of Laser Types

EXPERIMENTAL SETUP AND PROCEDURES.....8

Laser System and Other Experimental Equipment

Laser Equipment

Optical System

Positioning Equipment

Shield Gas and Ventilation Systems

Powder Delivery System

Experimental Materials Preparation and Analysis

Test Specimens

Substrate Test Coupons

Alloy Cladding Powder

Sectioning, Polishing and Etching

Digital Imaging

Optical Microscopy (OM)

Scanning Electron Microscopy (SEM)

Secondary Ion Mass Spectroscopy (SIMS)

Energy Dispersive Spectroscopy (EDS)

Microhardness and Toughness Testing

X-Ray Diffraction (XRD)

RESULTS AND DISCUSSION.....12

Experimental Parameters

Laser Processing of Ti-6Al-4V

Laser Processing of Al 2219

Laser Processing of Al 2090

Summary of Phase I Research

Phase II

CONCLUSIONS FROM THE RESEARCH FINDINGS.....15

PROJECT ACCOMPLISHMENTS.....15

New Research Lab Establishment

Fabrication of Key Experimental Components

Acquisition and Testing of Essential Motion Controller

SUMMARY AND FUTURE OF MANUFACTURING IN SPACE.....16

ACKNOWLEDGMENTS.....16

REFERENCES.....17

TABLES.....18

FIGURES.....44

APPENDIX A: CONTINUOUS WAVE CO_2 LASER BEAM WELDING DATA FOR AL ALLOYS.....145

APPENDIX B: PULSED LASER BEAM DATA FOR AL ALLOYS.....147

APPENDIX C: CONTINUOUS WAVE CO_2 LASER BEAM WELDING DATA FOR TITANIUM ALLOYS.....148

APPENDIX D: LASER SHOCK PROCESSING DATA OF ALUMINUM ALLOYS.....149

APPENDIX E: TORNADO ND:YAG LASER SPECIFICATIONS.....152

APPENDIX F: GLOSSARY OF TERMS FOR LASER CHARACTERISTICS.....155

APPENDIX G: THERMOPHYSICAL PROPERTIES AND TYPICAL MELT ENERGY CALCULATIONS FOR TITANIUM AND ALUMINUM ALLOYS.....159

APPENDIX H: COMPARISON CHART OF VARIOUS LASERS.....160

ABSTRACT

Lasers are useful for performing operations such as joining, machining, built-up freeform fabrication, and surface treatment. Due to the multifunctional nature of a single tool and the variety of materials that can be processed, these attributes are attractive in order to support long-term missions in space. However, current laser technology also has drawbacks for space-based applications. Specifically, size, power efficiency, lack of robustness, and problems processing highly reflective materials are all concerns. With the advent of recent breakthroughs in solid-state laser (e.g., diode-pumped lasers) and fiber optic technologies, the potential to perform multiple processing techniques in space has increased significantly. A review of the historical development of lasers from their infancy to the present will be used to show how these issues may be addressed. The review will also indicate where further development is necessary to realize a laser-based materials processing capability in space. The broad utility of laser beams in synthesizing various classes of engineering materials will be illustrated using state-of-the art processing maps for select lightweight alloys typically found on spacecraft. Both short- and long-term space missions will benefit from the development of a universal laser-based tool with low power consumption, improved process flexibility, compactness (e.g., miniaturization), robustness, and automation for maximum utility with a minimum of human interaction. The potential advantages of using lasers with suitable wavelength and beam properties for future space missions to the moon, Mars and beyond will be discussed.

The laser processing experiments in the present report were performed using a diode pumped, pulsed/ continuous wave Nd:YAG laser (50W max average laser power), with a 1064 nm wavelength. The processed materials included Ti-6Al-4V, Al-2219 and Al-2090. For Phase I of this project, the laser process conditions were varied and optimized to see the effects on melt-quenching, cladding/alloying (using the pre-placed powder technique), and cutting. Key parameters such laser power, pulse repetition frequency, process speed and shield gas flow and the observed process characteristics such as plasma formation during laser/material interaction, have been reported for all experimental runs. Preliminary materials characterization of select samples was carried out using various microscopy, diffraction, spectroscopy and microhardness test methods, and reported. Select nitridation results of Ti-6Al-4V using nitrogen assist gas indicated the successful formation of hard titanium nitrides with much higher hardness (2180 kg_f/mm^2). A cost-effective and simple powder delivery system has been successfully fabricated for the further experimentation in Phase II.

INTRODUCTION AND LITERATURE BACKGROUND

The development of a universal, multifunctional tool is essential to support long-term missions in space. In addition to maximized utility, launch costs and the availability of power in space are the primary constraints that will determine whether a tool is sufficiently useful to be included in any mission (with or without a human presence). Lasers are useful for performing operations such as surface engineering, built-up freeform fabrication, joining, and machining (Nagarathnam and Taminger, 2001). Additionally, lasers are capable of performing these processes on a wide variety of different materials, including metals, ceramics, polymers, and composites. These attributes are attractive in supporting long-term space missions due to the multifunctional nature of a single tool and the variety of materials that can be processed.

However, when considering space-based applications, current laser technology also has significant drawbacks, which need to be addressed. Current lasers tend to be large, have low power efficiency, have significant maintenance requirements, and have difficulty with processing highly reflective materials such as aluminum. Currently, since launch costs per pound are extremely high and the available power supplies are quite limited, these drawbacks are not insignificant.

With the advent of recent breakthroughs in solid-state laser (e.g., diode-pumped Nd:YAG lasers) and fiber optic technologies, the potential to perform multiple processing techniques in space is increasing significantly. Aluminum is a very common material for satellite and spacecraft structures, so techniques need to be developed to be able to effectively process highly reflective materials like aluminum to increase the utility of the laser as a space-based tool. Recent developments in laser technology are potentially enabling for both short- and long-term space missions to explore the limits of innovative processing strategies which combine low power consumption, improved process flexibility, compactness (e.g., miniaturization) and robustness.

Energy Requirements for Laser-Assisted Materials Processing

Figure 1 shows general regimes for various material processing parameters for both pulsed and continuous wave lasers. Short pulses (ns, ps or fs) with high peak power densities are desirable for laser shock processing, drilling, machining, and ablation applications. In general, longer pulses (ns or ms) or continuous wave lasers are preferred for melting, freeform fabrication, and welding operations, as well as hybrid combinations of processing such as melt-quenching/heat treatment. Laser chemical vapor deposition and laser surface transformation hardening require lower power densities and interaction times as compared to processes involving melting and vaporization.

Representative laser processing research efforts and the resulting properties (e.g., grain refinement, less segregation, enhancement of corrosion resistance, an increase in microhardness, fatigue strength improvement) of aluminum and titanium based alloys are summarized in Table 1. These results demonstrate that both CO_2 and Nd:YAG lasers are capable of performing numerous operations on highly reflective, non-ferrous alloys.

Laser Surface Engineering

Materials have been traditionally processed in such a way that their properties were optimized with respect to bulk as well as surface constraint requirements. This is an inherently difficult task as the properties required at the surface (fatigue, wear and corrosion) are often very different from those in bulk form (strength and toughness). The

use of lasers represents a significant development with the potential for optimizing engineered surfaces without compromising the bulk properties.

Laser surface modification has been proven to improve the wear resistance and/or high temperature corrosion resistance in several ferrous and non-ferrous alloy systems. Alternatively, coatings treated by other processing techniques such as plasma spraying or electroplating may be modified with laser beams. Lasers in the infrared regions (~1064 nm in wavelength) have also been used to process materials such as aluminum, titanium and copper alloys. Unlike conventional castings or heat treatment, it is possible to have much higher cooling rates with laser processing. These rapid solidification rates yield superior fine-grained microstructures with metastable crystalline and/or amorphous phases, uniform alloy composition, and extended solubility of alloying elements.

Built-up Freeform Fabrication

Shallow depth of penetration of laser energy into the bulk material can be a benefit, as seen in the surface engineering field. However, to affect bulk material properties with laser processing, techniques originally developed for laser surface cladding or alloying needs to be applied in a built-up process. One built-up freeform fabrication process employs a laser beam to create a small melt pool on the surface of a metallic substrate. Metallic powder is fed into the molten pool in a layer-by-layer process. This results in a fully dense, structural part, built directly from computer-aided design models, without molds, tooling, or machining. The resulting microstructure throughout the bulk is typically much finer than that in conventionally produced materials due to the rapid solidification kinetics associated with the small melt pool. Due to the ability to blend alloy powders, it is possible to produce unique materials that are compositionally tailored and functionally graded in a unitized structure. The process is flexible enough to be able to build near-net shaped parts in complex geometries (which can be net-shape if surface roughness is not an issue). Although not documented in other materials to date, two distinctly different microstructures were obtained in Ti-6Al-4V with different laser settings (Schlienger, 1998). This provides evidence that not only compositions but also microstructures may be controlled and tailored during the fabrication process.

Laser freeform fabrication, using fiber optic delivery, has tremendous potential for revolutionizing the use of lasers in space manufacturing applications because it provides a means by which to build up structures. This process can be modified to use wire feed to eliminate the handling of powder feedstock in a zero or low-gravity atmosphere. Typically, the process is performed in a glove box under inert gas shielding, but the enclosure and gas shielding requirements can be eliminated in the vacuum of space. The built-up freeform fabrication process is computer controlled, and could be fully automated to operate with minimal human intervention. All of these attributes are advantageous for crewed or uncrewed space manufacturing applications.

Laser Welding, Machining, and Other Manufacturing Applications

Lasers are useful in other areas of manufacturing such as welding, micro-machining, solid-state transformation hardening, melt quenching, melt-particle injection, and surface processing. Lasers can also be used on most materials, including ferrous, non-ferrous, ceramic, cermet and composite engineering materials. For example, autogenous laser welding has been successfully performed on numerous ferrous and non-ferrous alloys. Laser welding produces very small heat affected zones and typically requires no post-weld heat treatment. Precision laser micro-machining can be accomplished on a variety of different materials, including metal matrix composites (MMC's). This is significant as MMC's can cause rapid tool wear in traditional machining because of the hard reinforcement phase within the more ductile metal matrix. Nd:YAG lasers have been used to micro-machine SiC reinforced aluminum composites without a large heat affected zone or recast layer (Nagarathnam, et al., 1997). Since lasers are non-contacting, they do not suffer tool wear. Lasers are also capable of machining extremely

delicate details using a small beam diameter and, with fiber optic technology, can perform keyhole drilling. Laser melt-particle injection is used to create in-situ composite coatings by melting only the substrate and injecting hard particles like oxides or carbides during the co-deposition.
The required laser power density, specific energy and interaction time requirements typical for CO_2 laser materials processes are given in Table 2. From Table 2, it becomes obvious that surface melting processes require much higher power densities when compared to solid-state transformation hardening. When using solid-state lasers with shorter wavelengths (1064 nm or lower), the reflectivity problems with aluminum alloys are reduced significantly. The required energy densities and times are correspondingly reduced due to higher absorbtivities, thereby also reducing the input energy requirements.

Based on several experimental findings, typical laser processing maps were developed for surface engineering applications, and are shown for laser surface melt quenching (Figure. 2), laser surface alloying (Figure. 3), laser surface cladding (Figure. 4), laser beam welding (Figure. 5a,b and Appendices A, B, and C) (Nagarathnam and Mazumder, 1996), and laser shock processing (Berthe et al., 1998, Appendix D). These laser-processing maps show the required laser parameters for a variety of ferrous and non-ferrous based alloys for each of the different techniques. Processing maps are useful for defining key laser variables for processing new alloys, and for comparing the range of laser settings used for performing different laser techniques. Most of these techniques can be carried out with the same laser setup by proper choice of fixturing. Addition of feedstock supply and computer-controlled positioning capability can expand a standard laser arrangement to be capable of built-up freeform fabrication. Thus, if a single type of laser can attain the range of settings in these different processing maps, that laser would be extremely versatile in performing many different processing operations on a variety of materials.

Comparison of Laser Types

The theory of light emission dates back to Albert Einstein in 1916. Einstein's theory was brought to reality with Theodore Maiman's engineering use of a ruby laser in 1960. For the past four decades, the CO_2 laser has been the workhorse in various industrial materials processing applications. Over the past decade however, the yttrium aluminum garnet (YAG) solid-state laser has become increasingly more popular for manufacturing applications, due to better absorptivity and the ability to use fiber optics for beam transport.

In pulsed solid-state lasers such as Nd:YAG, Q-switching is commonly used to obtain pulses of various lengths and frequencies (up to 50 MHz). Using a frequency doubling technique, the 1064 nm wavelength can be sent through aligned crystals such as lithium niobate (LBO) to obtain a visible green wavelength (532 nm). The rod geometry of the YAG has been modified into a slab- or face-pumped geometry to generate very high peak powers with reduced thermal lensing and beam distortion. The diode-pumped solid-state laser has a much longer life (several thousands of hours) than that of the krypton arc lamp-pumped lasers, which lasts only few hundred hours. The laser diodes used for pumping have higher brightness, monochromaticity, and more efficient coupling with the lasing medium such as neodymium ions. The compact size of these diodes is also very attractive in reducing the thermal losses in these types of lasers. Some solid-state lasers such as the Ti-sapphire laser are capable of ultra-short pulses (picosecond or femtosecond). Although attractive for diagnostics, micro/nano-machining and ablation in a small scale, this type of laser is less suitable for melting/cladding processes.

A number of alternative lasers with varying wavelengths (Appendix F) and power levels are also available. Both fast axial flow and transverse flow continuous wave gas lasers are available with high power levels up to 100 kW. Among the pulsed lasers, the transverse excitation atmospheric (TEA) laser is popular in attaining high peak power levels of ~1MW, higher pulse energy (10 J) and greater pulse length (2-3 ms). Excimer UV lasers (KrF, XeCl) are pulsed chemical lasers with UV wavelengths, very short pulse lengths, and high peak, but fairly low average power

levels of only a few watts. Copper vapor lasers (532 nm wavelength) exhibit intermediate average and high peak power levels. Chemical oxygen-iodine lasers (COIL, 1315 nm wavelength) have scalable high power levels up to 40 kW. However, chemical and gas lasers are typically bulky in size and require handling chemicals, frequent maintenance, and elaborate cooling systems. These features tend to make them less attractive for processing in space.

Semiconductor lasers are the most compact of all laser types. Semiconductor lasers are typically GaAs, GaAlAs (750-870 nm wavelength), and InGaAs (900-1000 nm wavelength). The power requirements for semiconductor lasers are substantially lower than for other types of lasers, and cooling requirements are minimal. Although these semiconductor (diode) lasers are available at low power levels, they can be used for efficient pumping of solid-state lasers (Appendix E). The desirable wavelengths for optimum energy absorption of reflective alloys include visible (511 nm) to near-infra-red (1064 nm), which are found in diode-pumped solid-state lasers. The wall plug efficiency of lamp-pumped Nd:YAG lasers is only 2%, while diode-pumped solid-state lasers possess about 8% efficiency. CO_2 lasers have a typical efficiency rating of approximately 12%. However, the advent of semiconductor lasers as pumping sources has increased efficiencies up to 30-40%. Although the demonstrated increases in efficiency are encouraging, because of the strict power limitations that exist in space, further improvements are required to make space-based laser manufacturing feasible.

EXPERIMENTAL SETUP AND PROCEDURES

Laser System and Other Experimental Equipment

Laser Equipment

The experimental setup for all laser-processing experiments is shown in Figures 6a and b. This includes the laser equipment, motion controller, focusing optics, shield gas delivery and powder delivery systems. The laser used in the present study was a 50 W Spectra-Physics Nd:YAG laser, which emits a 1064nm wavelength beam (specifications in Appendix E). From the specifications it can be seen that the laser can be operated both in pulsed and continuous wave mode. When used in the pulsed mode, the pulse repetition frequency (PRF) can be varied from 0.2 to 80 kHz. Additionally, the average laser power decreases slightly from 50 kHz to about 10 kHz and then shows a drastic decrease at much lower PRFs (e.g., <10 KHz). The pulse energy per shot increases with shorter pulse durations and decreasing PRFs. In continuous wave (CW) mode or operating at a high PRF, the laser is amenable for processes involving melting and cladding. Although the average power of the laser decreases at lower PRF's, the total energy per pulse increases. This makes the laser more suitable for other operations such as cutting and drilling. The empirically obtained laser power characteristics, measured as a function of diode current (from 20 to 46.3 A) for both CW and pulsed mode (50kHz of pulse repetition frequency), are shown in Figures 7a and b. It is also apparent from these findings that there is a threshold value of diode current (20 A) above which the measured laser power increases in a non-linear way for both CW and pulsed beam modes.

Optical System

The beam emitted from the laser is an unfocused beam of diameter ~2mm. The beam is then diverted downwards by a CVI Optics 2" diameter mirror, positioned at an angle of 45 degrees relative to the level of the laser (Fig 8). The mirror is specially constructed to reflect in excess of 99% of incident radiation at 1064 nm. The beam then passes through a 1" diameter plano-convex lens of focal length, f=100mm. The now-focused beam then impinges

on the test coupon, which has been placed at some optimum focal position of about 100 mm where the laser beam energy density was found to be the maximum. The laser beam was always viewed after wearing safety goggles (with optical density of 4.5 and above) and using an infrared viewer. The infrared viewer was a hand-held type of model # 7215 made by Electrophysics Corporation. Additionally, "Zap-It" papers were used for beam alignment. For beam alignment, the laser was operated in continuous wave mode with approximately 20 A of diode current with a minimum of power for safety reasons. It is also recommended that laser beam alignment should not be conducted in the pulsed mode with very high laser power densities, especially when attempting to focus the beam.

Positioning Equipment

The test coupon itself is mounted and clamped onto a Velmex two-axis, computer-controlled linear stage. This arrangement allows movement of the target without risking disruption of the optical focusing equipment. The positioning stage has a number of different features (Table 3), including the capability of movement in both the x and y directions in steps as small as 5-8 mils. In the z direction, the precision is 20-30 microns (Table 3). Preliminary calibration of the linear speed along the x-axis is shown in Figures 9a-c.

The motion of the stage is controlled by software provided by Ability Systems, Inc, operating from a Windows 98 equipped, Pentium-class PC. This software, called Indexer LPT software, employs Hewlett-Packard Graphics Language (HPGL) commands to control the stage in much the same way as an old-style plotter is controlled. The HPGL commands are transmitted via 2 extra parallel port cards installed in the PC. The corresponding cables are attached to a translator/controller unit, which in turn, controls the actual operation of the stage step motors. Through a command-line programming interface, the Indexer LPT software also allows the stage to move in complex 2 and 3 dimensional patterns as desired.

Shield Gas and Ventilation Systems

The test coupons were bathed in a laboratory grade helium (He) gas envelope, delivered at a rate of 10 SCFH. Exhaust gases and metal vapors were collected by a custom-designed ventilation system (Figure 10). The intake was placed approximately 2 feet above the target area and was designed to allow for the collection of He without diverting the flow of shield gas before it could bathe the target area. The waste vapors and gases were then collected by the building ventilation system.

Powder Delivery System

The powder delivery system used in this experiment was a gravity-fed, manually controlled copper tube, with a powder reservoir located at the top of the tube (Figure 11). The powder reservoir was a 15cm long, 3cm diameter, transparent acrylic tube. This feature allowed the operator to quickly determine the amount of powder remaining in the feeder. At the top of the acrylic tube, a custom-machined fitting made of nylatron plastic and equipped with a rubber o-ring, acted as a stopper. The stopper was drilled through its longitudinal axis and equipped with a pneumatic fitting on its top surface. A tube from the shield gas bottle supplied He to the powder mixture to reduce the possibility of any premature reaction of the powder. This arrangement also allowed the shield gas to be delivered directly to the site of the powder-laser beam interaction while minimizing the risk of powder displacement from the larger, adjacent shield gas flow tube.

The acrylic tube was mounted on a machined brass sleeve that was tapered internally to retard the flow of the powder. Soldered to the bottom of the brass sleeve was a ¼" O.D. copper tube, equipped with a manually controlled butterfly valve. The valve was placed in the flow path, midway between the brass sleeve and the tube exit. The placement of the valve allowed the flow of the powder to be adjusted without forcing the operator to come in close proximity of the laser beam. The copper tube was of sufficient length and flexibility to place the tube exit within 3mm of the target/ laser beam interaction point. Copper was chosen as the feed tube material because of its high thermal conductivity/ reflectivity. These properties would allow the tube to have a higher resistance to any effects caused by the unintended impingement of the laser beam on the tube.

Experimental Materials Preparation and Analysis

Test Specimens

Three different alloys, Ti-6Al-4V, Al-2219, and Al-2090 were received as sheet/plate from NASA Langley. Their thermophysical properties are shown in Appendix G. These as-received samples were first partially sectioned using a power hacksaw into small specimens of approx. ½" square. These specimens were then polished, etched and subjected to different analysis techniques in order to ascertain the properties of each in the condition in which it was received (Figures 12a-e and Figures 13a-c). The rolled texture was observed in Ti-6Al-4V and the age-hardened microstructures were apparent for Al alloys.

Substrate Test Coupons

The as-received bulk material was also sectioned into a number of 2" x 4 ½ " test coupons. The sectioning was accomplished with an industrial, water/oil cooled band saw, operating at an extremely low cutting speed of less than 50 blade-feet/min to prevent warping of the test coupon. Each specimen was then rinsed with tap water, and cleaned in an ultrasonic bath using acetone followed by isopropyl alcohol, each for a period of five minutes. The specimens were then allowed to air dry before being placed in plastic bags in order to minimize contamination.

Alloy Cladding Powder

There were two alloy powders used in this experiment. The first powder used was Ti-6Al-4V obtained from Starmet Corporation. This powder ranged in size from 45 to 300 μm. The other alloy powder (Al-2219) was mechanically blended from elemental powders obtained from the Alfa-AESAR Corporation (Table 4). Due to the pellet nature of zirconium, it was not added to the other alloying elements in the elemental powder form. Due to its low concentration, this is not especially critical, considering that especially in laser processing produces greater solidification rates with grain refinement.

Sectioning, Polishing & Etching

The laser-processed test coupons were sectioned perpendicular to the process track for microscopy and other analyses. Each sample was in turn polished successively by 180, 240, and 400-grit SiC sandpaper, using water as lubricant. The samples were then chemically etched by a solution of 10ml HF acid, 5ml HNO_3 acid and 85ml H_2O for 30 s to 1 minute. Each specimen was then rinsed with tap water, and cleaned in an ultrasonic bath using acetone and then isopropyl alcohol respectively, each for a period of five minutes. The specimens were then allowed to air dry before being placed in holding containers in order to minimize contamination.

Digital Imaging

The visual records of the as-processed samples were obtained using both Nikon and Kodak digital cameras (Figures14a-l).

Optical Microscopy (OM)

The processed test coupons were examined and imaged with a Nikon optical microscope, using a variety of magnification settings (Figures 15a-m).

Scanning Electron Microscopy (SEM)

The microstructures of the test specimens and of the substrate test coupons were investigated using a Scanning Electron Microscope (SEM) set at an operating voltage of 15kV and various magnification settings ranging from 88x to 9000x (Figures 16a-p).

Secondary Ion Mass Spectroscopy (SIMS)

Two of the selected samples (laser nitrided Ti-6Al-4V and Al-2219 alloyed on to Ti-6Al-4V substrate) were subjected to analysis by use of the Secondary Ion Mass Spectrometry (SIMS) technique. In this instance, Physical Electronics manufactured the SIMS machine used and the operating voltages for both positive (for heavy elements) and negative SIMS (for detecting light elements such as nitrogen and oxygen) were set to 15kV. The results are demonstrated in Figures 17a-u.

Energy Dispersive Spectroscopy (EDS)

The same samples used for SIMS were also subjected to analysis by the use of Energy Dispersive Spectroscopy technique. The results of this analysis are demonstrated in Figures 18a-y.

Microhardness and Toughness Testing

The microhardness characteristics of the same samples used for EDS and SIMS (Table 5) were obtained using a Shimadzu Type M Vickers Microhardness Tester. The test loads used were 300, 500 and 1000g for a static loading time of 15 seconds. The visual search for cracking under the static indentation loads was used as a qualitative measure of toughness for the tested samples.

X-Ray Diffraction (XRD)

The X-Ray Diffraction (XRD) analysis (Figures 19a-b) was performed on the same samples using both Phillips and Rigaku model x-ray diffractometers. In both cases, the anode was a standard Cu anode with a wavelength of 1.54056 Å. The operating voltage and tube current were set to 40 kV and 30mA, respectively. The scan angle range was from 10 to 130 degrees with a step size of 0.05 degrees, and a step time of 1s.

RESULTS AND DISCUSSION

Experimental Parameters

Preliminary energy calculations of the three experimental alloys are given in Appendix G. A number of different experimental parameters were varied in order to obtain the research findings contained herein. Some examples of these parameters include diode current, laser power, pulse repetition frequency, and process speed. These parameters and the observed effects of laser/material interaction mechanisms such as melt quenching, cladding/alloying and cutting, and the plasma characteristics of each experimental run, are listed in Tables 6a-w.

Laser Processing of Ti-6Al-4V

The results of the laser melt-quenched Ti-6Al-4V samples with or without He assist gas showed the following trends: In the case of continuous wave laser processing experiments, it is evident from Figure 20a that as the laser power was increased by increasing the diode current, the widths of melt and the heat affected zones (as evidenced by the different color zones) were found to increase.

The results of laser processing experimental runs performed at various pulse repetition frequencies on Ti-alloy samples at fairly constant diode current are shown in Figure 20b. It was evident that at lower pulse repetition frequencies, the laser pulse energy is high enough to cause sufficient cutting of the samples (due to vaporization) as opposed to melting. The threshold PRF was between 1 (Figure 15a) and 5 KHz for the Ti-alloy samples in this study. The cutting mechanism also produced blue plasma accompanied by significant noise as opposed to white plasma. The color variations of the plasma also provided supporting evidence of the physical mechanism change from melting to cutting in the test samples. The approximate heights of the plasma in select cases including the color changes above the sample surface were listed in Tables 6a-w. The plasma color observations were made after viewing the laser/sample interaction regions with the help of safety goggles (as always!!). Some of the blue colored heat affected regions in laser melted Ti-6Al-4V indicated to a certain degree the insufficient shielding in the process and also undesirable plasma heating of the substrate. Therefore it is essential to consider the right shield gas flow conditions to minimize such a heating effect. It was also noted that when the laser pulse frequency was increased, the extent of heat-affected region was also increased.

The results of cladding experiments with pre-placed Ti-6Al-4V alloy powder were also very encouraging. The clad beads looked fairly continuous, well bonded, and crack-free. At constant laser power, the increase in process speed was found to decrease the processed depth.

The only surface cleaning treatment for the experimental Ti-plates was done using acetone and isopropyl alcohol in conjunction with an ultrasonic cleaner before the actual tests. The experimental results provided encouraging evidence that the laser beam absorption properties (hence energy coupling) of the Ti-alloy samples were adequate in the as-received condition. This eliminates the need for any other absorbent coatings to be placed on the substrate. This was verified both in laser melt-quenched and laser cladding experiments by pre-placing a thin layer of alloy powder on the substrate. Without He gas, the observed plasma size above the surface was found to increase slightly with some smoking streaks from the interaction zones. Figure 14d shows the heat-affected zone without He as compared to that with He. This smoking effect was minimized by using He shield gas, flowing at a rate of 10 SCFH at the source.

The XRD results (Figure. 13a) of the as-received Ti-6Al-4V microstructures (Figure. 12a) revealed the presence of α-Ti (HCP) and β-Ti (BCC) phases. Additionally, the relative intensity variations and absence of some peaks (e.g., β-Ti) indicated the texture effect. The preliminary observations on Ti-samples indicated columnar dendritic morphology in the laser melt-quenched microstructures (Figure. 16b) with spacings of ~2-6 microns. The microstructures of the pre-placed 2219 alloy on Ti-6Al-4V substrate also revealed grains of (Figures. 16c, d, e, and f) of 5 to 10 microns. This is indicative of the presence of higher cooling rates even at low process speeds, unlike traditional casting or heat treatment. The interface between the Al-2219 alloyed layer and the Ti-substrate was free from any noticeable cracking or porosity. This demonstrates that the He shielding was adequate for the pre-placed powder coating experiments. The hardness tests (Table 5) revealed a substantial increase in the hardness of Al-2219 alloyed coating on Ti-substrate by a factor of ~5 as compared to that of as-received Ti-6Al-4V. These results are potentially applicable for the production of in-situ wear and corrosion resistant high temperature coatings made of intermetallic phases such as aluminides, without any vacuum requirement. The SIMS results revealed the presence of Cu, Ti, and Al in the coating regions, which was confirmed by the EDS results (Figures. 18o-y). The XRD results indicated the possible presence of compounds such as Cu_3Al and/or Al_2Ti, for example. For further confirmation, a more detailed microchemistry analysis of various phase constituents and XRD scans at much lower scan rates, will be carried out in Phase II of this study.

The hardness results of Al-2219 alloyed coatings (Table 5) provided no evidence of cracking under the test loads used in this study. This indicates the possession of significant toughness in addition to being much harder.

The laser nitrided samples shown in Figures. 14l and 16g-i demonstrate the formation of outer and inner layers (2 to 3 distinct regions) in the microstructure. Please refer to Table 6v for laser nitridation process conditions. Figure. 18a – n show the EDS results of the different nitrided regions. Indicated are the presence of the major element Ti and a small amount of Al. The XRD results shown in Figure. indicate the presence of variable stoichiometry compounds of Ti and N (e.g., Ti_3N_{2-X}). Additionally, the laser nitridation process parameters need to be optimized to eliminate cracking. For example when the laser was used in the pulsed mode (10 kHz), cracking was observed where it was absent in cw mode. This can be explained due to minimization of the stresses incurred during the less severe quenching of the cw mode (Figure. 16j). Of course, one can also produce crack-free coatings by using appropriately higher PRF for example.

The SIMS results revealed a similar trend of Ti-enrichment in the outer regions, with little Al present (Figures. 17m –u). The designation "Area A" in these figures, refer to the outer layers of the nitrided zone. To detect elements such as nitrogen and oxygen (e.g. <Z=20), negative SIMS was performed and is shown. SIMS results were also obtained for Areas B, C and D respectfully, which refers to progressively deeper layers, and ending with the untreated substrate.

Laser Processing of Al-2219

One of the technical strategies used to increase the initial coupling of the laser energy with the substrate material, is outlined below. The surface of the as-received Al-2219 test coupons was sprayed with a layer of energy absorbing black paint before several experimental runs. This practice of using energy absorbent coatings is fairly common when, for example, a CO_2 laser is used for heat treatment of steel surfaces. This is due to the higher reflectivity exhibited by the untreated steel surface.

In the present study, the laser process conditions used were higher laser power (at a diode current of 46.3 amps) and a constant process speed of 0.5 ipm in both cw and pulsed (PRF of 1 kHz) wave modes. The results yielded interesting melting and cutting on the highly reflective Al-2219 alloy. The results were not nearly as interesting for Ti-6Al-4V. The laser was successful in melting the Al-2219 (Figures. 15e, g and Figure. 16k) using highly energetic

pulses without pre-placed powder. The microhardness (Table 5) of the laser melt-quenched layer was found to be slightly higher than that of the untreated material. The processed layer depth was very small as compared to those obtained with Ti-6Al-4V and Al-2090 due to the much higher conduction losses of Al-2219. Figures. 15c, 15f, 15h and Figures 16 l and m reveal the effect of low PRF runs in which cutting was found to occur. Figure. 15 d shows both the central groove and laser melt-quenched edge microstructures of black painted Al-2219. Preliminary cladding results of Al-2219 using cw mode and by pre-placing the alloy powder showed some bonding after processing (as shown in the visual record). With high power density cw lasers, it is possible to increase the processed layer depth using powder melting onto an Al-2219 substrate. The XRD results (Figure. 13c) of the as-received Al 2219 microstructures (Figure. 12b and 12c) revealed the presence of α-Al (FCC) as the major phase present.

Laser Processing of Al-2090

Laser melt-quenched results of Al-2090 microstructures as observed from the top surface, are shown in Figures 15i – m as well as in Figures 16o-p. The rapidly solidified cellular grain boundaries are apparent, as is the lack of porosity and cracking, as evidenced from these micrographs. It was also found that the black painting of the surface prior to laser processing was not needed for Al-2090 due to its relatively lower thermal conductivity (as compared to Al-2219). The XRD results (Figure. 13b) of the as-received Al-2090 microstructures (Figure. 12d and 12e) revealed the α-Al (FCC) as the major phase.

Summary of Phase I Research

In Phase I of the research project, what have been presented are the feasibility findings, which will be used for further exploration in Phase II. The laser given by the vendor to the PI's project is a brand new state-of-the-art laser, which has not yet been used in conjunction with manufacturing. This laser has far superior characteristics, which are suitable for a melting/cladding study as compared to any of the other available lasers at ARC-ODU at the time of experimentation. That is one of the major reasons to choose this type of laser for this challenging and exploratory study. It is also noted that all of the above-mentioned experiments were performed using a 100 mm focal length lens, a much smaller multi-mode (e.g., with M^2 of 14 or so) laser beam size (e.g., 30 to 100 micron size, and a larger depth of field (constant power density within this depth of field). The process speeds used in this study are relatively slow due to the lower power densities possible with this laser. The reason why we chose a larger focal length is to accommodate the shield gas and powder delivery nozzles. This arrangement is also advantageous in that it is possible to explore other focal length lenses as well. For example, the focused laser power densities and energies can be increased using a shorter focal length lens (e.g., 50 mm).

Phase II

Phase II is planned to be a continuation of the work begun in Phase I. Specifically, further laser cladding experiments and free-form fabrication of samples for Ti-6Al-4V and Al-2219 have been proposed. A more efficient powder delivery method, and a continuous wave Nd:YAG laser with higher average power (e.g., 500W) and relatively larger beam diameter, are planned to be utilized. It is expected that this will help to increase the processed layer depth and width by substantially increasing the melting of the cladding alloy powder. These changes also have the added benefit of increasing the process speed by a substantial margin. Typical cost comparison of selected available laser equipment is provided in Appendix H for easy reference. The initial experiments in Phase II are planned to be performed using a vendor-supplied laser, loaned to the PI. This is viewed as the most cost-effective method of experimentation before a recommendation is issued (if needed) relating to the purchase of the primary laser to be used in future R&D. The PI is also currently seeking cost-sharing assistance from the ODU College of

Engineering in this regard. Additional details are to be provided in a separate Phase II proposal submitted by the PI to NASA Langley Research Center.

CONCLUSIONS FROM THE RESEARCH FINDINGS

The following conclusions were drawn from the experimental results of the present research investigation:

- Ti-6Al-4V samples can be successfully laser melted/cladded using the pulsed/cw Nd:YAG laser
- Dense, crack-free and well-bonded melt-quenched layers/coatings were produced in single layers
- Key laser variables such as laser power, pulse repetition frequency and process speed had direct influence on the laser-processed geometry such as melt width, kerf width and heat affected zone.
- The low repetition frequencies of the pulsed laser (e.g., 1 kHz) produced cutting in both Ti-6Al-4V, Al-2219, and Al-2090, whereas melt-quenching was obtained using high PRF (20 kHz or higher) and continuous wave beam modes
- Ti-6Al-4V and Al-2090 samples were laser processed without any energy absorbent black coatings
- Absorbent coatings were found to be beneficial to increase the initial laser energy coupling of Al-2219 samples
- The laser processed microstructures were much finer than those of the untreated substrate materials, indicating higher cooling rates
- In-situ production of hard aluminide and nitride coatings, with excellent hardness properties, on Ti-6Al-4V was demonstrated

PROJECT ACCOMPLISHMENTS

The following list provides some of the project accomplishments under this research grant:

New Research Lab Establishment
Fabrication of Key Experimental Components
Acquisition and Testing of Essential Motion Controller
Groundwork for the Preliminary Research Findings and Phase II Study
Collaborative ARC/ODU Paper for STAIF-2001 Conference
Educational and Research Support from NASA Langley

SUMMARY AND FUTURE OF LASER MANUFACTURING IN SPACE

With launch costs and power constraints in space in mind, the development of a multifunctional tool would have potential for actual application in short- or long-term space missions. Laser power efficiencies have been improved from 2% to as much as 40%. Fiber optic delivery has greatly increased the flexibility of laser manufacturing by expanding the ability to treat complex geometries and inaccessible areas with less difficulty. Shorter wavelengths, higher reliability, lower input power requirements with greater efficiency, low maintenance requirements, the ability to use fiber optic beam delivery, and the compact size of diode pumped solid-state lasers, are all factors which will potentially serve the needs of in-space manufacturing. They are also suitable from a multifunctional perspective, but significant improvements in power efficiency are necessary for applicability in space missions. These lasers are inherently well suited to be used as a multifunctional tool because they have characteristic wavelengths and power outputs suitable for most laser materials processing techniques. The continuing development of these types of lasers is currently addressing manufacturing issues, which will also impact the ability to modify these systems for space-based manufacturing. Establishing an in-space laser manufacturing capability will require significant improvements over state-of-the-art laser technology in power efficiency, maximized life with minimal maintenance, and the ability to operate using DC input power.

ACKNOWLEDGMENTS

This research project was supported by NASA Langley Research Center under grant #104041.

REFERENCES

Abboud, J. H., and West, D. R. F., "Processing Aspects of Laser Surface Alloying of Titanium with Aluminum," *Mat. Sci. & Tech.*, 7 No. 4, 353-356 (1991).

Almeida., et al., "Laser Alloying of Aluminum Alloys with Chromium," *Surf. & Coatings Tech.*, **70**, 221-229 (1995).

Berthe et al., "Laser-Shock Surface Processing of Materials," Chapter 12, ASM Surface Engineering Series, **1**, 465-504 (1998)

Bharti, A., Sivakumar R., and Goel, D. B., *J. of Laser Appl.*, March, p. 43 (1989).

Coyle, et al., "Laser Welding in the Assembly of a High Reliability Al Alloy Amplifier Housing," in *Proc. of the Intl. Conf. on the Appl. of Lasers & Electro-Optics (ICALEO)*, San Diego, CA, Nov. 1997, pp. 75-82.

Fu, Y., and Batchelor, A. W., "Laser Alloying of Aluminum Alloy AA6061 with Ni and Cr. Part II. The Effect of Laser Alloying on the Fretting Wear Resistance," *Surf. & Coatings Tech.*, **102**, 119-126 (1998).

Das, D. K., et al., "Evolution of Microstructure in Laser Surface Alloying of Aluminum with Nickel," *Mat. Sci. & Eng.*, **A174**, 75-84 (1994).

JCPDS: International Centre for Diffraction Data, File Numbers: 44-1294, 44-1288, 04-0787, 25-0012.

Katsuna, M., et al., *Welding in the World*, **31** No. 2, 126-135 (1993).

Kelly, J., Nagarathnam, K., and Mazumder, J., "Processing and Characterization of Laser Cladded Cu-Sn-Zn Coatings on Cast Aluminum Alloys," in *Proc. of the Intl. Conf. on the Appl. of Lasers & Electro-Optics (ICALEO)*, San Diego, CA, Nov. 1995, **80**, pp. 477-486.

Kelly, J., Nagarathnam, K., and Mazumder, J., "Laser Cladding of Cast Aluminum-Silicon Alloys for Improved Dry Sliding Wear Resistance," *J. of Laser Appl.*, **10** No. 2, 45-54 (1998).

Nagarathnam, K., "Processing and Characterization of Laser-Synthesized Overcoats for Surface Engineering," Ph.D. Thesis, Dept. of Mechanical and Industrial Eng., Univ. of Illinois at Urbana-Champaign, Oct. 1994.

Nagarathnam, K., "Laser Processing Data for Reflective Alloys", Unpublished Research Work, 1995-1997.

Nagarathnam, K., and Komvopoulos, K., "Microstructural Analysis and Oxidation Behavior of Laser Processed Fe-Cr-Al-Y Alloy Coatings," *Met. Trans. A*, **27A**, 381-390 (1996).

Nagarathnam, K., and Mazumder, J., "Laser Heat Treatment," LIA Handbook Chapter of Laser Materials Processing, Magnolia Publishing Company, Oklahoma City, OK, (2000).

Nagarathnam, K., and Mazumder, J., "Development of Processing Maps and Comprehensive Database for the Laser Beam Welding of Various Engineering Materials," *DARPA Project Reports*, Oct. 1994-1996.

Nagarathnam, K., Chen, X., and Mazumder, J., "Scientific Implications in High Peak Power Nd:YAG Laser Material Removal of Al-30% SiC Composite," International Mechanical Eng. Conf. & Exposition (IMEC & E), *Recent Adv. in Solids/Structures & Appl. of Met. Mat.*, **369**, 389-398 (1997).

Nagarathnam, K., and Taminger, K. M. B., "Technology Assesment of Laser-Assisted Materials Processing in Space," the Space Technology and Applications International Forum-2001, *CP 552,* M.S. El-Genk, editor, *Paper Published by the American Institute of Physics (2001).*

Ramaswamy, et al., "CO_2 and Nd:YAG Laser Beam Welding of 6114-T4 Aluminum Alloy for Automotive Applications," *J. of Laser Appl.*, **12** No. 3, 101-115 (2000).

Schlienger, M. E., et al., "Titanium Processing with LENS," TMS Annual Mtg., San Antonio, TX, Feb. 1998.

Spectra-Physics Manual, "Tornado- Diode Pumped, Cw/Q-Switched Infrared Laser-User's Manual, Sections 1-1 to 8-4, Rev.2, February 2000.

Whitaker, I., et al., "Microstructural Characterization of CO_2 Laser Welds in the Al-Li Based Alloy 8090," *J. of Mat. Sci.*, **28** No. 20, 5469-5477 (1993).

Table 1. Typical Processing Parameters and Results of Laser-Processed Al, Ti and Cu-Based Materials.

Material	Type of Laser Process	Laser Type Used	Typical Process Parameters	Comments	Reference
7175 Al substrate/ Cr alloying	Laser surface alloying	Continuous wave CO_2	Power Density: 120-260 kW/cm^2 Interaction Time: .04-.3 s Scanning Rate: 5, 10 mm/s Remelting Rate: 10, 20 mm/s	VHN=155 (Cr-alloyed Al) VHN = 300 (Cr-alloyed 7175); reduced porosity after remelting; improved pitting corrosion resistance with Cr; Al_7Cr, $Al_{11}Cr_2$ & α-Al phases	Almeida, et al., 1995
Ti substrate/ Al alloying	Laser surface alloying	Continuous wave CO_2	Power: 1.8 kW Beam Diameter: 3 mm Process Speed: 3-20 mm/s Powder Feed: 0.03-0.11 g/s	Alloy is homogeneous & reproducible; alloy build-up thickness: 0.2 -0.9 mm; 17-80% Al concentration with increase in powder feed rates	Abboud, et al., 1991
Ti-6Al-4V substrate/ C alloying	Laser surface alloying	Continuous wave CO_2	Laser Power: 3 kW Process Speed: 40-100 ipm	Dendritic & cellular structures; roughness decreases from 50 to 10 microns & chemical homogeneity improves as # of scans incr. from 0 to 4	Bharti, et al., 1989
6061 Al substrate/ Ni, Cr alloying	Laser surface alloying	Continuous wave Nd:YAG	Power Density: 30 J/mm^2 Beam Diameter: 2 mm Scanning Rate: 6 mm/s	Fretting wear & coefficient of friction reduced significantly	Fu, et al., 1998
Pure Al substrate/ Ni alloying	Laser surface alloying	Pulsed Nd:YAG	Power: 120 W Pulse Width: 4 ms Repetition Rate: 10 Hz Speed: 2.1 mm/s % Overlap of Tracks: 65%	α-Al, lamellar eutectic of α-Al & Al_3Ni and primary Al_3Ni dendrites depending on the Ni contents (6-15% in alloyed zone)	Das, et al., 1994
Cu substrate/ Al alloying	Laser surface alloying	Pulsed Nd:YAG	Power: 160W Beam Size: 0.45 mm Pulse Duration: 2 ms Frequency: 10 Hz Process Speed: 1 mm/s	Non-ferrous martensitic microstructures; improved mechanical strength & wear resistance	Nagarathnam, 1995-1997

Table 1 (Contd.). Typical Processing Parameters and Results of Laser-Processed Al, Ti and Cu-Based Materials.

Material	Type of Laser Process	Laser Type Used	Typical Process Parameters	Comments	Reference
316L stainless steel substrate/ MCrAlY alloy coatings	Laser surface cladding	Continuous wave Nd:YAG	Laser Power: 0.6-2.4 kW Process Speed: 0.53-4.23 mm/s Powder Feed Rate: 0.083 g/s Beam Delivery: fiber optic	Homogeneous single phase α-Fe-Cr-Al microstructure with sufficient yttrium; 15- 150 microns grain sizes; improved high temperature oxidation resistance at 1200°C	Nagarathnam, et al., 1996
Cast 390 & 333 Al-Si alloy substrate/ Sn & Mn-Bronze alloy coatings	Laser surface cladding	Continuous wave CO_2	Power: 2.3-2.5 W Process Speed: 14-16 mm/s Powder Feed Rate: 0.7 g/s Specific Energy: 34-48 J/mm^2	Fine grained microstructure of primary α-phase and eutectic interdendritic phases; increased hardness, toughness & improved sliding wear resistance	Kelly, et al., 1995, 1998
2219, 5083, 6063 Al	Laser beam welding	Continuous wave CO_2	Power: 3, 4, 6 and 8 kW	Penetration depths: 3.25, 4.30, 6.5, & 7.10 mm	Katsuna, et al., 1993
6061, 4047 Al	Laser beam welding	Pulsed Nd:YAG	Power: 20 W Pulse Duration: 7 ms Frequency: 1 Hz Shield Gas: Ar	Successful welding	Coyle, et al., 1987
6111-T4 Al	Laser beam welding	Continuous wave Nd:YAG	Power: 2 kW Weld Speed: 42 – 63 mm/s Beam Diameter: 0.5 mm Sheet metal thickness: 1 mm Beam Delivery: 1 mm fiber optic	Reduced weld hardness due to solutionizing effect; cellular dendrites in fusion zone with equiaxed grains at weld center; successful autogenous butt welding; no post weld heat treatment	Ramaswamy, et al., 2000

Table 1 (Contd.). Typical Processing Parameters and Results of Laser-Processed Al, Ti and Cu-Based Materials.

Material	Type of Laser Process	Laser Type Used	Typical Process Parameters	Comments	Reference
8090 Al	Laser beam welding	Continuous wave CO_2	Power: 1.5-3.8 kW Scanning Rate: 20-120 mm/s Beam Diameter: 0.25 mm Coaxial He Flow: 40 l/min Sheet Thickness: 2-3.2 mm (60 mm/s-full weld penetration) 4 mm (60 mm/s-partial weld penetration)	2-5 micron secondary dendrite arm spacing; columnar & equiaxed grains; fine scale δ' (Al_3Li) ppts. within α-phase; increased hardness; porosity along weld centerline	Whitaker, et al., 1993
Al-30% SiC particulate composite	Laser micro-machining	Diode-pumped Nd:YAG	Wavelengths: 532 nm (green) at 35 W 1064 nm (IR) at 85-90 W Power: 35-90 W Modes: Q-switch+ Mode Lock: 150 ps pulses (13 ns apart) at 76 MHz Q-Switch (5 kHz & 300 ns) Process time: Up to 180 s Assist Gas: 45 psig O_2	Straight & angular holes; no recast layer & heat affected zone under optimum conditions; hole depths: 85-420 microns; hole width: 30-425 microns; higher material removal rate at 532 nm wavelength	Nagarathnam, et al., 1997

Table 2. CO_2 Laser Materials Processing Parameters for Various Surface Engineering Applications.

Surface Engineering Process	Laser Power Density (Power/Beam Area), kW/cm^2	Specific Energy (Power/Beam Size Speed), J/cm^2	Laser Beam Interaction Time (Beam Size/Speed), s
Laser Surface Transformation Hardening	0.8-40	0.3-60	0.04-9
Laser Surface Melt-Quenching	2.5-7000	0.3-200	0.001-9
Laser Surface Alloying	3-40000	1-200	0.001-10
Laser Surface Cladding	3-150	1-100	0.1-10
Laser Melt-Particle Injection	30-310	5-30	0.04-0.55

Table 3: Specifications of Velmex Bi-Slide™ 2-Axis Linear Stage

	Lead Screw Pitch (in/rev)	Slide Travel (in)	Speed Limit (ipm)	Resolution (1 Step = 6.3μm)
X-Axis	0.4	30	180	5-8 mils
Y-Axis	0.4	15	180	5-8 mils
Z-Axis	0.1	10	45	20-30 microns

Table 4: Composition of Mechanically Blended Al-2219

Component	Wt. %	Wt of Component Elements (g)
Al	93	93.08
Cu	5.8 - 6.8	6.304
Fe	Max 0.3	not used
Mg	Max 0.02	not used
Mn	0.2 - 0.4	not used
Si	Max 0.2	not used
Ti	0.02 - 0.1	0.0605
V	0.05 - 0.15	0.1157
Zn	Max 0.1	not used
Zr	0.1 - 0.25	0.1835
Total:		**100g**

Table 5: Microhardness Test Results

Material	Load (g)	Time (s)	Trial Number	Horizontal Distance (μm)	Vertical Distance (μm)	Hardness Values (kg_f/mm^2)		
						Obtained	Calculated (Average)	Expected
As-Received Ti-6Al-4V	500	15	1	49	48.6	389	378	396
	500	15	2	48.5	52.5	363		
	500	15	3	51	47.7	381		
	1000	15	1	68.3	70.5	385	378	396
	1000	15	2	71.4	69.8	372		
As-Received Al-2090	300	15	1	60.8	59.7	153	151	
	300	15	2	66.1	58	145		
	300	15	3	62	58	155		
As received Al-2219	300	15	1	62	57.5	156	154	149
	300	15	2	61	60.4	151		
	500	15	1	79.3	80.3	146	147	149
	500	15	2	78.3	76.6	149		
	500	15	3	80.1	79.3	146		
Laser Nitrided Ti-6Al-4V - Substrate (11-01-2000 TC4 R1)	500	15	1	45.4	47.2	433	452	
	500	15	2	45.9	44.5	454		
	500	15	3	43.5	45.4	469		
Laser Nitrided Ti-6Al-4V Inner Layer of Nitrided Zone (11-01-2000 TC4 R1)	1000	15	1	34.1	33.2	1639	1582	
	1000	15	2	36.0	33.7	1527		
	1000	15	3	34.4	34.2	1580		
Laser Nitrided Ti-6Al-4V Outer Layer of Nitrided Zone (11-01-2000 TC4 R1)	1000	15	1	28.1	30.2	2180	2180	
Al-2219 PPP on Ti-6Al-4V Substrate – Alloyed Zone (10-30-2000 TC4 R3)	300	15	1	18.3	19.6	1547	1768	
	300	15	2	19.0	19.1	1529		
	300	15	3	15.9	15.7	2228		
Al-2219 PPP on Ti-6Al-4V Substrate Substrate Region (10-30-2000 TC4 R3)	300	15	1	39.7	38.5	364	370	
	300	15	2	37.8	40.0	368		
	300	15	3	37.0	39.5	379		
Laser Melted Al-2219 - Kerf	500	15	1			493	494	
	500	15	2			487		
	500	15	3			501		

Tables 6a-w: Experimental Parameters and Observed Effects

Table 6a

Date: 10-03-2000 Test Coupon 1				
Material: Untreated Ti-6Al-4V Process Type: Surface Melting				
Beam Mode: CW Shield Gas: None Process Speed (v): 100 mm/min				
Run Number	Diode Current (A)	Ave. Laser Power (W)	HAZ Width (μm)	Comments
1^	25	9.6		Zigzag pattern observed
2^	30	22.4	1193.8	Melting observed
3^	35	32.68	1701.8	Melting observed
4^	40	38.2	1727.2	Melting observed
5^	46.3	41.4	1930.4	1mm yellow plasma observed

^ Measurements obtained from photographic analysis

Table 6b

Date: 10-03-2000 Test Coupon 2				
Material: Untreated Ti-6Al-4V Process Type: Surface Melting				
Beam Mode: PRF=20 kHz Shield Gas: He @ 10 SCFH Process Speed (v): 100 mm/min				
Run Number	Diode Current (A)	Ave. Laser Power (W)	HAZ Width (μm)	Comments
1^	20			Melting observed
2^	25		482.6	Melting observed
3^	30		787.4	Melting observed
4^	35		1371.6	Melting observed
5^	40		1447.8	Melting observed
6^	46.3	~35	1549.4	Melting observed

^ Measurements obtained from photographic analysis

Table 6c

Date: 10-03-2000 Test Coupon 3				
Material: Untreated Ti-6Al-4V Process Type: Surface Melting				
Beam Mode: PRF=50 kHz Shield Gas: None Process Speed (v): 100 mm/min				
Run Number	Diode Current (A)	Ave. Laser Power (W)	HAZ Width (μm)	Comments
1^	20	0.2		No effect
2^	25	8.9	533.4	Some plasma observed
3^	30	20.5	787.4	Some plasma observed
4^	35	30.9	1219.2	
5^	40	34.1	2032.0	

^ Measurements obtained from photographic analysis

Table 6d

Date: 10-03-2000 Test Coupon 4								
Material: Untreated Ti-6Al-4V Process Type: Surface Melting								
Shield Gas: He @ 10 SCFH Process Speed (v): 100 mm/min								
Run Number	Diode Current (A)	Ave. Laser Power (W)	PRF (kHz)	Melt Width (μm)	HAZ Depth (μm)	Kerf Width (μm)	Kerf Depth (μm)	Comments
1+	46.3	~35	1			70	112.4	Sparks observed 10mm plasma observed
2+	46.3	~35	5			331.2	250.4	10mm plasma observed
3+	46.3	~35	10	342	35.6			
4+	46.3	~35	20	380	42.8			No sparks observed <1mm plasma observed
5+	46.3	~35	40	432	87.2			<1mm plasma observed
6+	46.3	~35	60	356	92			<1mm plasma observed
7+	46.3	~35	80	233.6	42			Erratic track pattern

+ Measurements obtained from optical microscopy

Table 6e

Date: 10-09-2000 Test Coupon(s): 1 & 2						
Material: Untreated Ti-6Al-4V Process Type: Surface Melting						
Beam Mode: CW Shield Gas: None Focal Position: 114.3 mm						
Run Number	Diode Current (A)	Ave. Laser Power (W)	Process Speed (mm/min)	Travel Distance (mm)	HAZ Width (μm)	Comments
1^	46.3	41.4	50.8	50.8		
2^	46.3	41.4	25.4	38.1		
3^	46.3	41.4	50.8	25.4	3362	
4^	46.3	41.4	25.4	25.4	3838	
5^	46.3	41.4	12.7	25.4	5427	
General Comments						Wider melt zones at lower speeds Warping of substrate Oxidation observed No sparking

^ Measurements made by photographic analysis

Table 6f

Date: 10-09-2000 Test Coupon(s): 3					
Material: Untreated Al-2219 Process Type: Surface Melting					
Beam Mode: CW Shield Gas: None Focal Position: 114.3 mm					
Run Number	Diode Current (A)	Ave. Laser Power (W)	Process Speed (mm/min)	Travel Distance (mm)	Comments
6	46.3	41.4	50.8	50.8	No observable HAZ
7	46.3	41.4	25.4	50.8	Run aborted
8	46.3	41.4	25.4	50.8	<1mm yellow plasma observed
9	46.3	41.4	12.7	50.8	

Table 6g

Date: 10-10-2000 Test Coupon(s): 1						
Material(s): Untreated Ti-6Al-4V Substrate and Ti-6Al-4V PPP Process Type: PPP Melting						
Beam Mode: CW Shield Gas: He @ 10 SCFH Focal Position: 114.3 mm						
Run Number	Diode Current (A)	Ave. Laser Power (W)	Voltage (V)	Process Speed (mm/min)	Travel Distance (mm)	Comments
1	46.3	41.4	10.73	50.8	50.8	Melting observed
2	46.3	41.4	10.73	25.4	38.1	Overlapped into first track
3	46.3	41.4	10.73	25.4	25.4	1mm plasma observed
4	46.3	41.4	10.73	25.4	25.4	2mm plasma observed
5	46.3	41.4	10.73	25.4	25.4	Yellowish layer present on surface

Run Number	Clad Width (μm)	Clad Height (μm)	Clad Depth (μm)	Comments
3*	264.7	70.0	12.7	Partial Width Measurement
4*	40.5	8.4		Result due to discontinuous clad layer
5*	449.6	68.8		

* Measurements obtained from scanning electron microscopy

Table 6h

Date: 10-10-2000 Test Coupon(s): 2							
Material(s): Untreated Ti-6Al-4V Substrate and Ti-6Al-4V PPP Process Type: PPP Melting							
Beam Mode: CW Shield Gas: None Focal Position: 114.3 mm							
Run Number	Diode Current (A)	Ave. Laser Power (W)	Voltage (V)	Process Speed (mm/min)	Travel Distance (mm)	HAZ Width (μm)	Comments
6	46.3	41.4	10.73	12.7	50.8		Some melting observed Track is extremely narrow
7^	46.3	41.4	10.73	12.7	50.8	5425	<1mm plasma observed
8^	46.3	41.4	10.73	25.4	50.8	4953	<1.5mm white plasma observed
9^	46.3	41.4	10.73	50.8	50.8	3325	<1.5mm white plasma observed

^ Measurements made by photographic analysis

Table 6i

Date: 10-10-2000 Test Coupon(s): 3								
Material(s): Untreated Al-2219 Substrate and Al-2219 PPP Process Type: PPP Melting								
Shield Gas: None Focal Position: 114.3 mm								
Run Number	Diode Current (A)	Ave. Laser Power (W)	Voltage (V)	Beam Mode (kHz)	Process Speed (mm/min)	Travel Distance (mm)	Processed Width (μm)	Comments
10	46.3	41.4	10.73	CW	12.7	50.8		<.5mm white plasma observed No sparking present Powder layer was relatively thick
11^	46.3	41.4	10.73	CW	12.7	50.8	647	Powder layer thickness reduced on this run <.5mm white plasma observed
12^	46.3	41.4	10.73	CW	12.7	50.8	747	Performed along same track as 11 to see if remelting occurs
13^	46.3	~35	10.73	1	12.7	50.8	993	Thick powder layer <.5mm of blue plasma observed No sparking observed
14^	46.3	~35	10.73	10	12.7	50.8	827	<.25mm plasma No pushing of powder layer to side of track

^ Measurements made by photographic analysis

Table 6j

Date: 10-13-2000 Test Coupon(s): 1							
Material(s): Untreated Ti-6Al-4V Process Type: Surface Melting							
Shield Gas: None Focal Position: 114.3 mm							
Run Number	Diode Current (A)	Ave. Laser Power (W)	Beam Mode (kHz)	Process Speed (mm/min)	Travel Distance (mm)	HAZ Width (μm)	Comments
1^	20	41.4	CW	12.7	38	2311	Melting observed White plasma observed
2^					44.5	2616	Switched from shield gas to no shield gas in middle of run
General Comments							Demo sample for NASA Sponsor

^ Measurements made by photographic analysis

Table 6k

Date: 10-13-2000 Test Coupon(s): 2						
Material(s): Untreated Al-2219 Process Type: Surface Melting						
Shield Gas: None Focal Position: 114.3 mm						
Run Number	Diode Current (A)	Ave. Laser Power (W)	Beam Mode (kHz)	Process Speed (mm/min)	Travel Distance (mm)	
1	20	41.4	CW	12.7	38	
2						
General Comments						Demo sample for NASA Sponsor

Table 6l

Date: 10-27-2000 Test Coupon(s): 1							
Material(s): Black Painted Al-2090 Process Type: Black Paint Melting							
Shield Gas: He @ 10 SCFH Focal Position: 114.3 mm							
Run Number	Diode Current (A)	Ave. Laser Power (W)	Voltage (V)	Beam Mode (kHz)	Process Speed (mm/min)	Travel Distance (mm)	Comments
1	46.3	41.4	10.73	CW	12.7	25.4	
2	46.3	41.4	10.73	CW	12.7	25.4	
3	46.3	41.4	10.73	CW	12.7	25.4	High speed Test
4	46.3	~35	10.73	20	12.7	25.4	Plasma Observed
5	46.3	~35	10.73	1	12.7	25.4	<1mm blue plasma observed Cutting observed High pitched, audible noise present
6	46.3	~35	10.73	.2	12.7	25.4	<1mm blue plasma observed Cutting observed High pitched, audible noise present Noise is higher pitched than previous run
A	46.3	~35	10.73	10	12.7	25.4	Little noise
B	46.3	~35	10.73	10	12.7	25.4	Two passes on same track-melting observed

Run Number	Melt Width (μm)	Melt Depth (μm)	Kerf Depth (μm)	Kerf Width (μm)	Track Width (μm)	Comments
4*					405.7	63.8 μm grain size (top central zone) 33.0 μm(near interface) 2-4 μm at interface
5+			149.2	104.4		
6+			149.2	89.2		Measurement to be redone
A+	461.6	128.6				

+ Measurements obtained from optical microscopy

* Measurements obtained from scanning electron microscopy

Table 6m

Date: 10-27-2000 Test Coupon(s): 2							
Material(s): Untreated Al-2090 Process Type: Melting/Cutting							
Shield Gas: He @ 10 SCFH Focal Position: 114.3 mm							
Run Number	Diode Current (A)	Ave. Laser Power (W)	Voltage (V)	Beam Mode (kHz)	Process Speed (mm/min)	Travel Distance (mm)	Comments
7	46.3	~35	10.73	.2	12.7	25.4	Audible sound present
8	46.3	~35	10.73	1	12.7	25.4	Audible sound present Blue plasma observed NO SHIELD GAS USED
9	46.3	~35	10.73	1	12.7	25.4	Audible sound present Blue plasma observed
10	46.3	~35	10.73	20	12.7	25.4	Small amount of plasma observed
11	46.3	41.4	10.73	CW	12.7	25.4	Small amount of plasma observed
12	46.3	~35	10.73	10	12.7	25.4	Small amount of plasma observed
13	46.3	~35	10.73	5	12.7	25.4	Small amount of plasma observed
14	46.3	~35	10.73	7.5	12.7	25.4	Audible sound present Blue plasma observed
C	46.3	~35	10.73	10	12.7	25.4	2 passes performed on this track Small amount of plasma observed

Run Number	Kerf Width (μm)	Kerf Depth (μm)	Comments
7+	78.8	161.6	Burr width 211.2 μm; Burr height 69.2 μm
8+	84.4	61.2	Burr width 317.2 μm
9+	62.0	29.6	Burr width 225.2 μ; Burr height 76.4 μm
13+	126.8	91.2	Burr width 68.8 μ; Burr height 20.0 μm
14+			
C+			
General Comments		This series of tests was conducted on the reverse side of Test Coupon 1	

+ Measurements obtained from optical microscopy

Table 6n

Date: 10-30-2000 Test Coupon(s): 1							
Material(s): Black Painted Ti-6Al-4V strip with Al foil Process Type: Welding							
Shield Gas: He @ 10 SCFH Focal Position: 114.3 mm							
Run Number	Diode Current (A)	Ave. Laser Power (W)	Voltage (V)	Beam Mode (kHz)	Process Speed (mm/min)	Travel Distance (mm)	Comments
1	46.3	~35	10.73	10	12.7	25.4	<1mm plasma observed Audible sound present
2	46.3	~35	10.73	20	12.7	25.4	<1mm plasma observed Audible sound present Lower pitched than previous run
General Comments					Al foil was placed dull side up to enhance coupling		

Table 6o

Date: 10-30-2000 Test Coupon(s): 2							
Material(s): Black Painted Al-2219 Process Type: Cutting							
Shield Gas: He @ 10 SCFH Focal Position: 114.3 mm							
Run Number	Diode Current (A)	Ave. Laser Power (W)	Voltage (V)	Beam Mode (kHz)	Process Speed (mm/min)	Travel Distance (mm)	Comments
1	46.3	~35	10.73	10	12.7	25.4	<1mm of blue plasma present Audible noise present
2	46.3	~35	10.73	.2	12.7	25.4	<1mm of blue plasma present Audible noise present
3	46.3	~35	10.73	15	12.7	25.4	<1 mm of white plasma present Quieter than previous runs
4	46.3	~35	10.73	20	12.7	25.4	<1 mm of white plasma present Quieter than previous runs
5	46.3	41.4	10.73	CW	12.7	25.4	<1 mm of white plasma present Quieter than previous runs Less melting than previous runs

Table 6p

Date: 10-30-2000 Test Coupon(s): 3							
Material(s): Untreated Al-2219 Process Type: Melting/Cutting							
Shield Gas: He @ 10 SCFH Focal Position: 114.3 mm							
Run Number	Diode Current (A)	Ave. Laser Power (W)	Voltage (V)	Beam Mode (kHz)	Process Speed (mm/min)	Travel Distance (mm)	Comments
1	46.3	~35	10.73	10	12.7	25.4	<1mm blue plasma observed Some audible noise present
2	46.3	~35	10.73	.2	12.7	25.4	<1mm blue plasma observed Some audible noise present
3	46.3	~35	10.73	20	12.7	25.4	<1mm blue plasma observed No audible noise present
4	46.3	~35	10.73	1	12.7	25.4	Intense blue plasma observed <1mm in height
5	46.3	~35	10.73	15	12.7	25.4	1mm blue plasma observed No audible noise present
6	46.3	41.4	10.73	CW	25.4	25.4	No effect
7	46.3	41.4	10.73	10	25.4	25.4	<1mm plasma observed No audible noise present f changed to 100 mm
8	46.3	41.4	10.73	10	25.4	25.4	More audible noise than #7 Better coupling f changed to 108mm
9	46.3	41.4	10.73	10	25.4	25.4	Cutting observed f changed to 109.5mm
10	46.3	41.4	10.73	10	25.4	25.4	<1mm plasma observed f changed to 114.3mm

+ Measurements obtained from optical microscopy

* Measurements obtained from scanning electron microscopy

Table 6p (Contd.)

Date: 10-30-2000	Test Coupon(s): 3				
Material(s): Untreated Al-2219	Process Type: Melting/Cutting				
Shield Gas: He @ 10 SCFH	Focal Position: 114.3 mm				
Run Number	Kerf Width (μm)	Kerf Depth (μm)	Melt Depth (μm)	Melt Width (μm)	Comments
1+	126.8	141.2	125.5		
2+	50.8	114.4	44.6		Recast layer and burr formation observed
3+					Cellular grains observed from top
4+	136.8	138.8			No observable HAZ
6*					
8*				229.5	
10*	53.3	150.3	167.0	100.3	Grooving observed
General Comments			This series of tests was conducted on the reverse side of Test Coupon 2 Focal position in runs 7-10 was varied for effect		

Table 6q

Date: 10-30-2000 Test Coupon(s): 4							
Material(s): Black Painted Ti-6Al-4V Substrate & Al-2219 PPP Process Type: PPP Cladding							
Shield Gas: He @ 10 SCFH Focal Position: 114.3 mm							
Run Number	Diode Current (A)	Ave. Laser Power (W)	Voltage (V)	Beam Mode (kHz)	Process Speed (mm/min)	Travel Distance (mm)	Comments
1	46.3	~35	10.73	10	12.7	25.4	Powder was pushed aside 6mm on both sides of track when shield gas was not present
2	46.3	41.4	10.73	CW	12.7	25.4	NO SHIELD GAS Large amount of smoke present without shield gas Gas turned on halfway thru track run HAZ and smoke reduced significantly with presence of He shield gas
3	46.3	41.4	10.73	CW	12.7	25.4	<1mm plasma No audible noise present
4	46.3	~35	10.73	50	12.7	25.4	<1mm plasma No audible noise present
5	46.3	~35	10.73	30	12.7	25.4	<1mm plasma No audible noise present
6	46.3	~35	10.73	20	12.7	25.4	<1mm plasma No audible noise present

Date: 10-30-2000 Test Coupon(s): 4									
Material(s): Black Painted Ti-6Al-4V Substrate & Al-2219 PPP Process Type: PPP Cladding									
Shield Gas: He @ 10 SCFH Focal Position: 114.3 mm									
Run Number	Melt Width (μm)	Melt Depth (μm)	HAZ Depth (μm)	HAZ Width (μm)	Boundary Layer Thickness (μm)	Clad Width (μm)	Clad Height (μm)	Clad Depth (μm)	Comments
1*	307.44	288.3	448.4	467.5	39.9	546.8			
3*						712.1	323.2	244.7	
5*						737.9	504.2		

* Measurements obtained from scanning electron microscopy

Table 6r

Date: 11-01-2000 Test Coupon(s): 1							
Material(s): Untreated Al-2090 Substrate & Ti-6Al-4V PPP Process Type: PPP Cladding							
Shield Gas: He @ 10 SCFH Focal Position: 114.3 mm							
Run Number	Diode Current (A)	Ave. Laser Power (W)	Voltage (V)	Beam Mode (kHz)	Process Speed (mm/min)	Travel Distance (mm)	Comments
1	46.3	~35	10.73	10	12.7	25.4	>1mm of plasma observed Audible noise present Large amount of sparking present
2	46.3	~35	10.73	15	12.7	25.4	>1mm of plasma observed Audible noise present Large amount of sparking present
3	46.3	~35	10.73	20	12.7	25.4	>1mm of plasma observed Audible noise present Large amount of sparking present
4	46.3	~35	10.73	50	12.7	25.4	>1mm of plasma observed Audible noise present Large amount of sparking present
5	46.3	41.4	10.73	CW	12.7	25.4	>1mm of plasma observed Audible noise present Large amount of sparking present
6	46.3	41.4	10.73	CW	12.7	25.4	>1mm of plasma observed Audible noise present Large amount of sparking present

+ Measurements obtained from optical microscopy

* Measurements obtained from scanning electron microscopy

Table 6r (Contd.)

Date: 11-01-2000 Test Coupon(s): 1						
Material(s): Untreated Al-2090 Substrate & Ti-6Al-4V PPP Process Type: PPP Cladding						
Shield Gas: He @ 10 SCFH Focal Position: 114.3 mm						
Run Number	Clad Width (μm)	Clad Depth (μm)	Clad Height (μm)	HAZ Width (μm)	HAZ Depth (μm)	Comments
1+				302.4	167.6	
2+				170.8	60.8	
3+				241.2	128.4	
5*	304.9	88.0	54.3			
6*	358.5	52.7	42.0			
General Comments				Shield gas turned off and turned on halfway thru runs 3 and 4 Smoke and sparks present during absence of shield gas Level of audible noise decreased as PRF increased		

Table 6s

Date: 11-01-2000 Test Coupon(s): 2							
Material(s): Black Painted Ti-6Al-4V Substrate & Al-2219 PPP Process Type: PPP Cladding							
Shield Gas: He @ 10 SCFH Focal Position: 114.3 mm							
Run Number	Diode Current (A)	Ave. Laser Power (W)	Voltage (V)	Beam Mode (kHz)	Process Speed (mm/min)	Travel Distance (mm)	Comments
1	46.3	~35	10.73	10	12.7	25.4	10mm of plasma observed Audible noise present Large quantity of small sparks present Powder was pushed to one side Track width 10mm NO SHIELD GAS
2	46.3	~35	10.73	10	12.7	25.4	10mm of plasma observed Audible noise present Large quantity of small sparks present Powder was pushed to one side Track width 10mm
3	46.3	~35	10.73	20	12.7	25.4	2mm of plasma observed Lower level audible noise present Large quantity of small sparks present in all directions up to 100mm from target Powder was pushed to one side Track width 7mm NO SHIELD GAS
4	46.3	~35	10.73	20	12.7	25.4	Same level of audible noise as previous run Intermittent sparking, 50mm from target in all directions 1mm of white plasma observed Track width 5mm

Date: 11-01-2000 Test Coupon(s): 2							
Material(s): Black Painted Ti-6Al-4V Substrate & Al-2219 PPP Process Type: PPP Cladding							
Shield Gas: He @ 10 SCFH Focal Position: 114.3 mm							
Run Number	Diode Current (A)	Ave. Laser Power (W)	Voltage (V)	Beam Mode (kHz)	Process Speed (mm/min)	Travel Distance (mm)	Comments
5	46.3	~35	10.73	50	12.7	25.4	No noise, sparks, or smoke observed Plasma <1mm high observed Track width < 5mm
6	46.3	41.4	10.73	CW	12.7	25.4	No noise, sparks, or smoke observed Plasma <1mm high observed Track width < 5mm HAZ much narrower than previous runs

Table 6t

Date: 11-01-2000 Test Coupon(s): 2						
Material(s): Black Painted Ti-6Al-4V Substrate & Al-2219 PPP Process Type: PPP Cladding						
Shield Gas: He @ 10 SCFH Focal Position: 114.3 mm						
Run Number	Clad Width (μm)	Clad Depth (μm)	Clad Height (μm)	HAZ Width (μm)	HAZ Depth (μm)	Comments
1+	525.6	245.2		790.4	607.2	
2+	336.4	366.4				
3+	772.0	232.8	390.8			
4+	485.2	296.4				
5+	346.4	48.8		346.4	98.0	
6+	377.6	44.8	50.8			

+ Measurements obtained from optical microscopy

Table 6u

Date: 11-01-2000 Test Coupon(s): 3								
Material(s): Black Painted Al-2219 Substrate & Ti-6Al-4V PPP Process Type: PPP Cladding								
Shield Gas: He @ 10 SCFH Focal Position: 114.3 mm								
Run Number	Diode Current (A)	Ave. Laser Power (W)	Voltage (V)	Beam Mode (kHz)	Process Speed (mm/min)	Travel Distance (mm)	Clad Width (μm)	Comments
1^	46.3	~35	10.73	10	12.7	25.4	688	High pitched noise present 1mm white plasma observed Large sparks observed 30mm from target in all directions NO SHIELD GAS
2^	46.3	~35	10.73	10	12.7	25.4	678	High pitched noise present 1mm white plasma observed Small sparks observed 10mm from target in all directions 7mm track width
3^	46.3	~35	10.73	20	12.7	25.4	781	Lower level of audible noise present Intermittent sparking observed in direction of gas flow
4^	46.3	~35	10.73	50	12.7	25.4	1398	No noise or sparks observed <1mm yellow plasma observed
5^	46.3	41.4	10.73	CW	12.7	25.4	1234	No noise or sparks observed <1mm yellow plasma observed

^ Measurements made by photographic analysis

Table 6v

Date: 11-01-2000 Test Coupon(s): 4							
Material(s): Untreated Ti-6Al-4V Process Type: Nitridation							
Shield Gas: N2 @ 10 SCFH Focal Position: 114.3 mm							
Run Number	Diode Current (A)	Ave. Laser Power (W)	Voltage (V)	Beam Mode (kHz)	Process Speed (mm/min)	Travel Distance (mm)	Comments
1	46.3	41.4	10.73	CW	12.7	25.4	No plasma, sparking or smoke observed
2	46.3	41.4	10.73	CW	12.7	25.4	No plasma, sparking or smoke observed
3	46.3	41.4	10.73	CW	12.7	25.4	No plasma, sparking or smoke observed
4	46.3	41.4	10.73	CW	12.7	25.4	No sparking or smoke observed <1mm yellow plasma observed For 10 seconds, wave mode changed to 25 kHz Changed back to CW after 10 seconds
5	46.3	~35	10.73	20	12.7	25.4	1mm white plasma observed Brown stripe down middle of track observed
6	46.3	~35	10.73	10	12.7	25.4	Blue plasma observed, brighter than previous runs Audible, high pitched noise present Cutting at center of track observed
7	46.3	~35	10.73	15	12.7	25.4	Less noise than previous run Sparking observed, 20mm in all directions
8	46.3	~35	10.73	5	12.7	25.4	Very high pitched noise present Sparks and streaks present for 10mm in all directions 2mm blue plasma observed

Run Number	Melt Width (μm)	Melt Depth (μm)	HAZ Depth (μm)	HAZ Width (μm)	Interface Layer Thickness (μm)	Comments

Date: 11-01-2000 Test Coupon(s): 4						
Material(s): Untreated Ti-6Al-4V Process Type: Nitridation						
Shield Gas: N2 @ 10 SCFH Focal Position: 114.3 mm						
1*	385.2	173.8	318.6	505.5	61.2	
7*	254.3	438.7	607.5	594.6		

* Measurements obtained from scanning electron microscopy

Table 6w

Date: 11-01-2000 Test Coupon(s): 5							
Material(s): Black Painted Al-2219 Substrate & Al-2219 PPP Process Type: PPP Cladding							
Shield Gas: He @ 10 SCFH Focal Position: 114.3 mm							
Run Number	Diode Current (A)	Ave. Laser Power (W)	Voltage (V)	Beam Mode (kHz)	Process Speed (mm/min)	Travel Distance (mm)	Comments
1	46.3	41.4	10.73	CW	12.7	25.4	No plasma, sparking or smoke observed
2	46.3	~35	10.73	20	12.7	25.4	No plasma, sparking or smoke observed
3	46.3	~35	10.73	10	12.7	25.4	NO SHIELD GAS Audible noise present Blue plasma observed Shield gas turned on halfway thru run
4	46.3	~35	10.73	15	12.7	25.4	Less noise than previous run <1mm white plasma observed
5	46.3	~35	10.73	50	12.7	25.4	No plasma, sparking or smoke observed

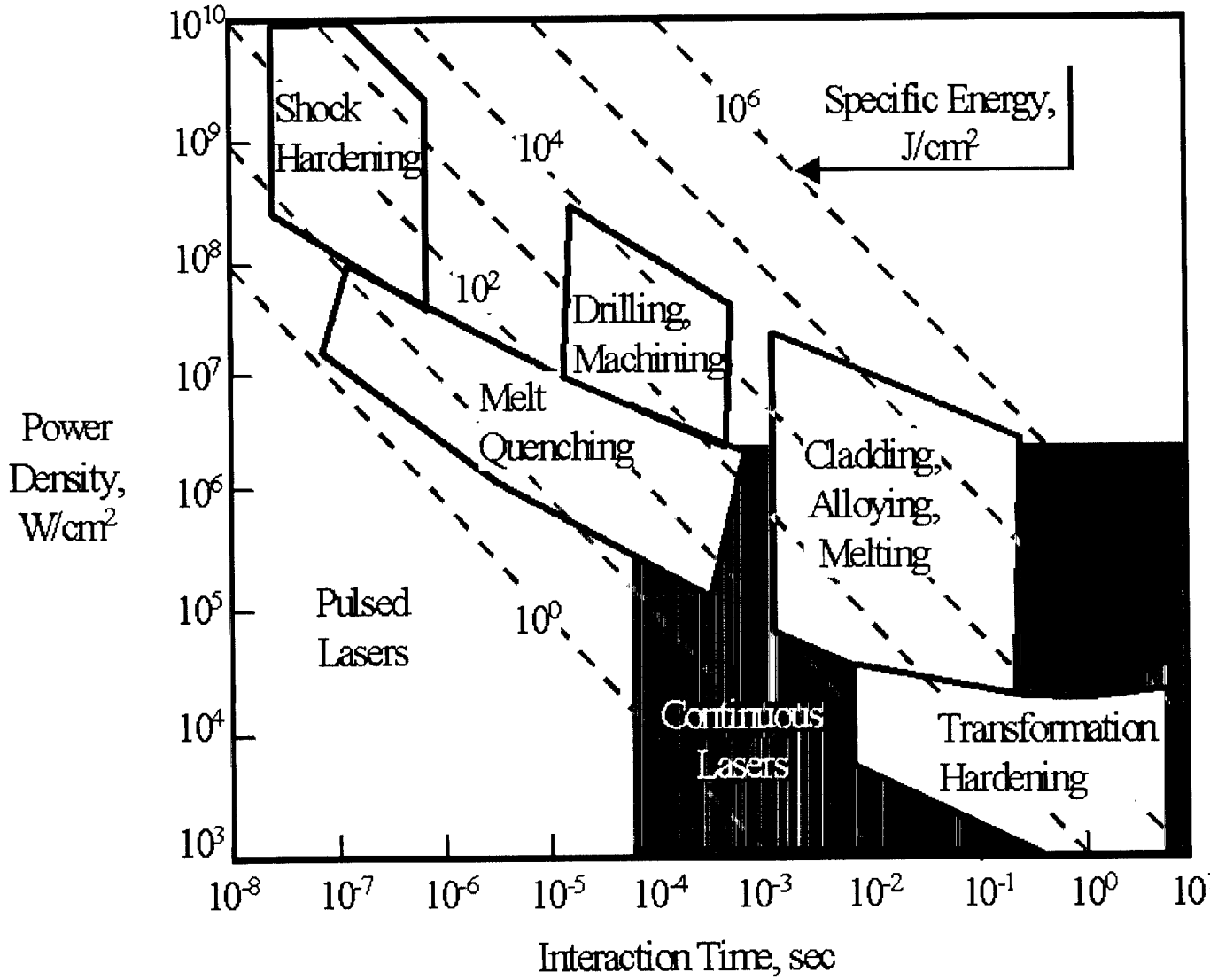

Figure 1: Laser beam power density, specific energy and interaction times for various regimes

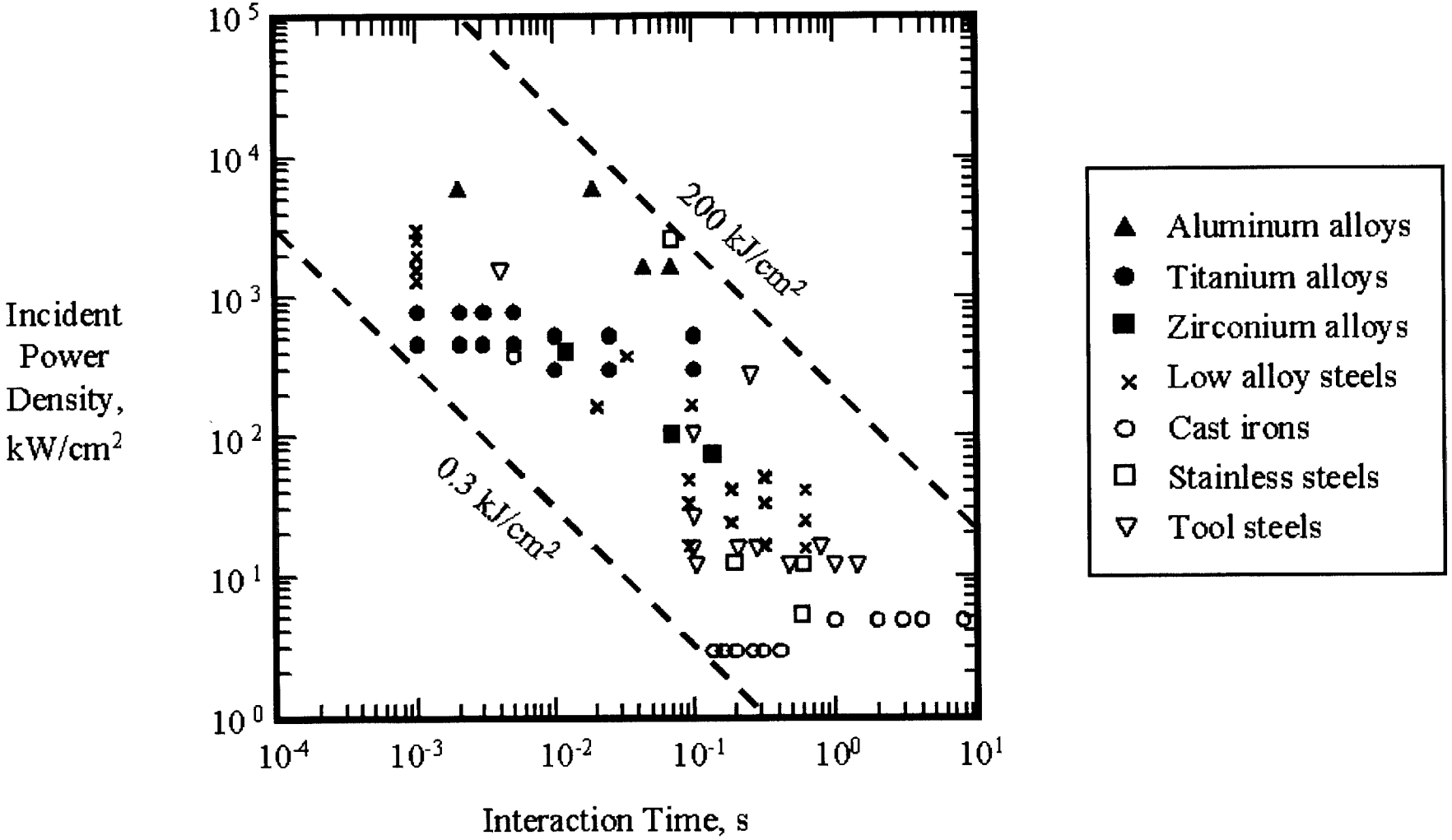

Figure 2: Processing map for laser surface melt quenching

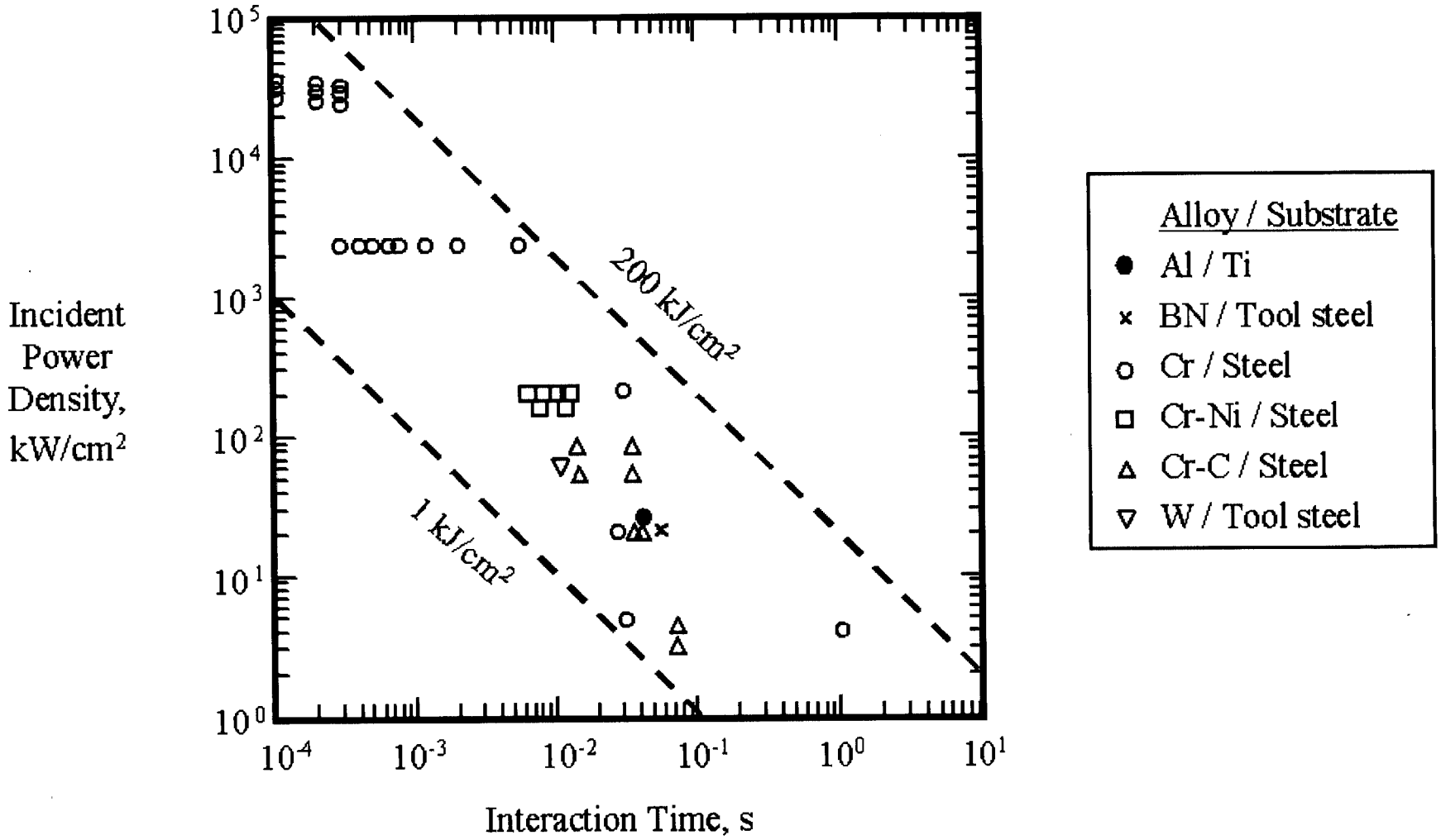

Figure 3: Processing map for laser surface alloying

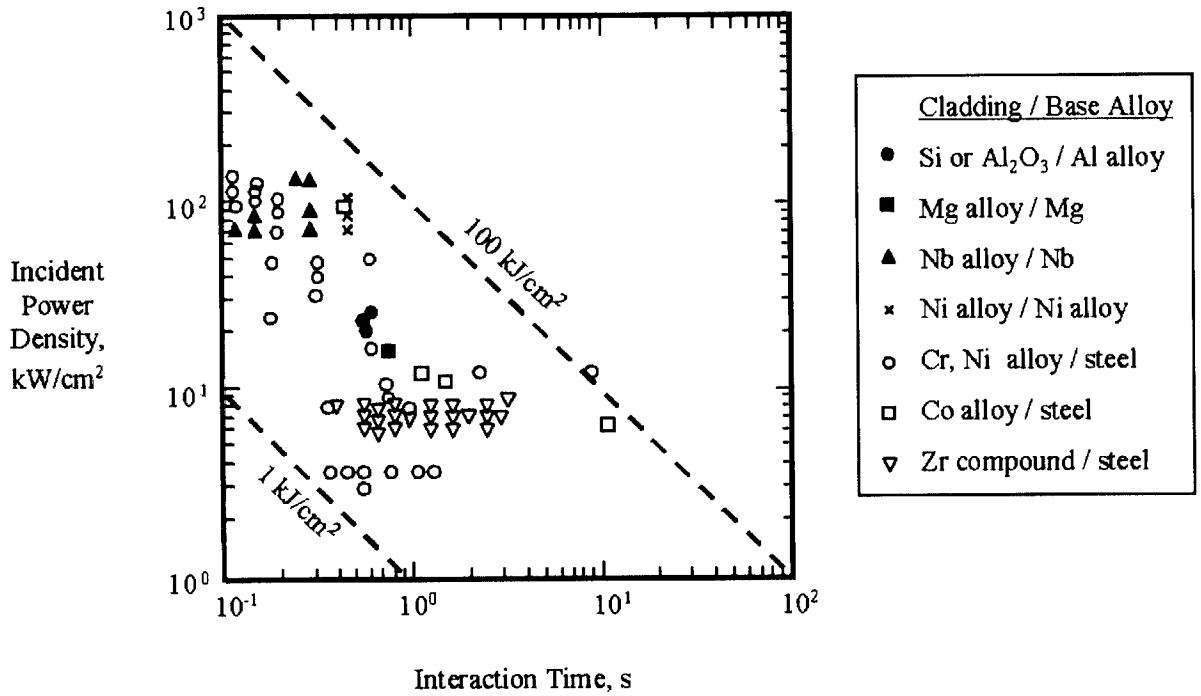

Figure 4: Processing map for laser surface cladding

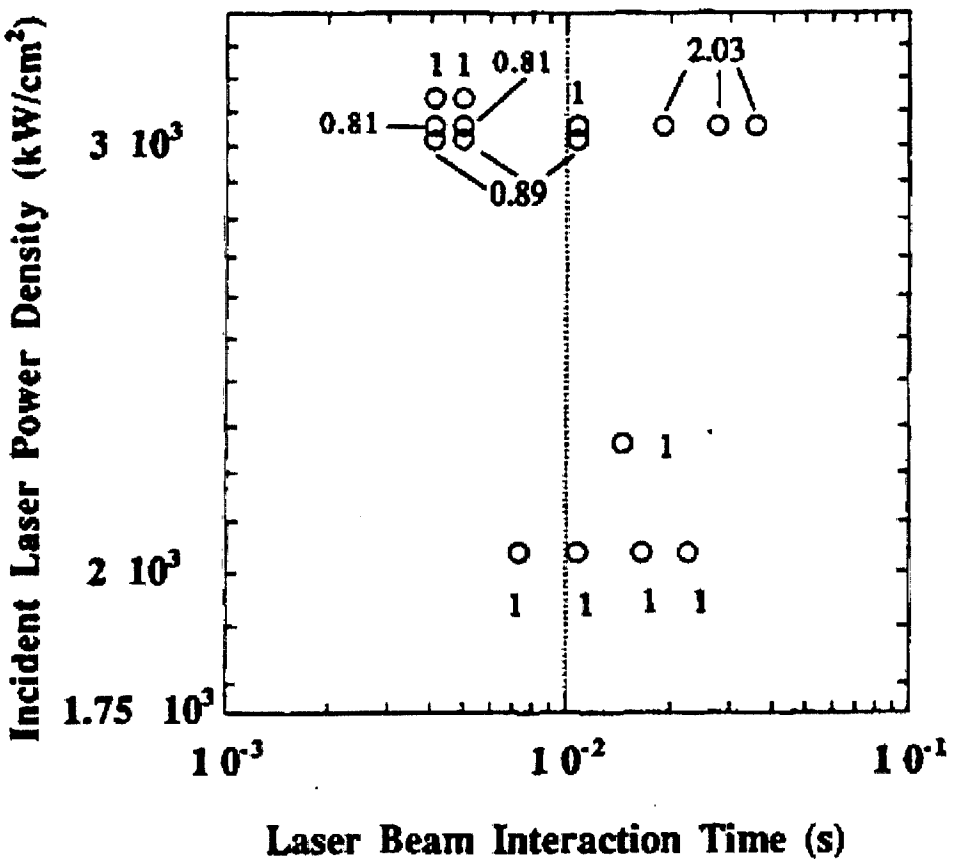

All dimensions in the plot refer to weld depth in mm.

Figure 5a: CO_2 Laser Welding Data for Ti-6Al-4V

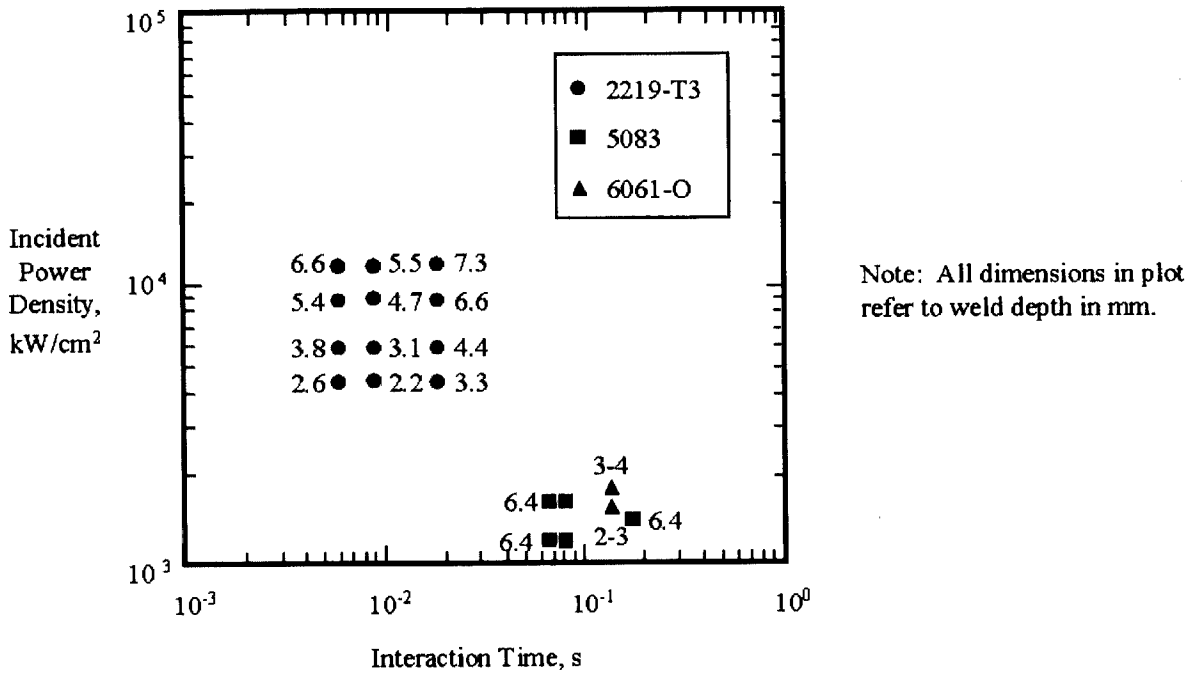

Figure 5b: Processing map for laser welding of aluminum alloys

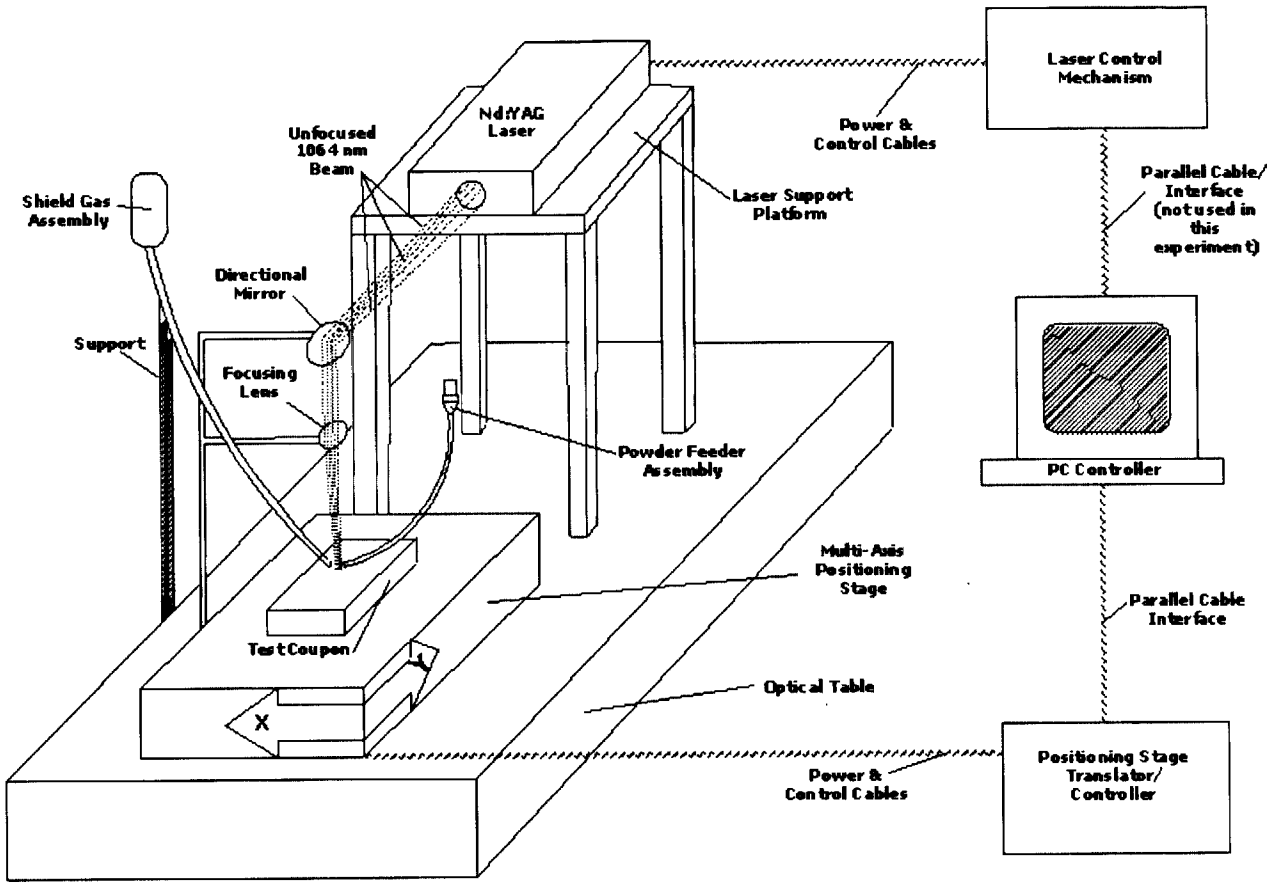

Figure 6a: Experimental Setup Overview

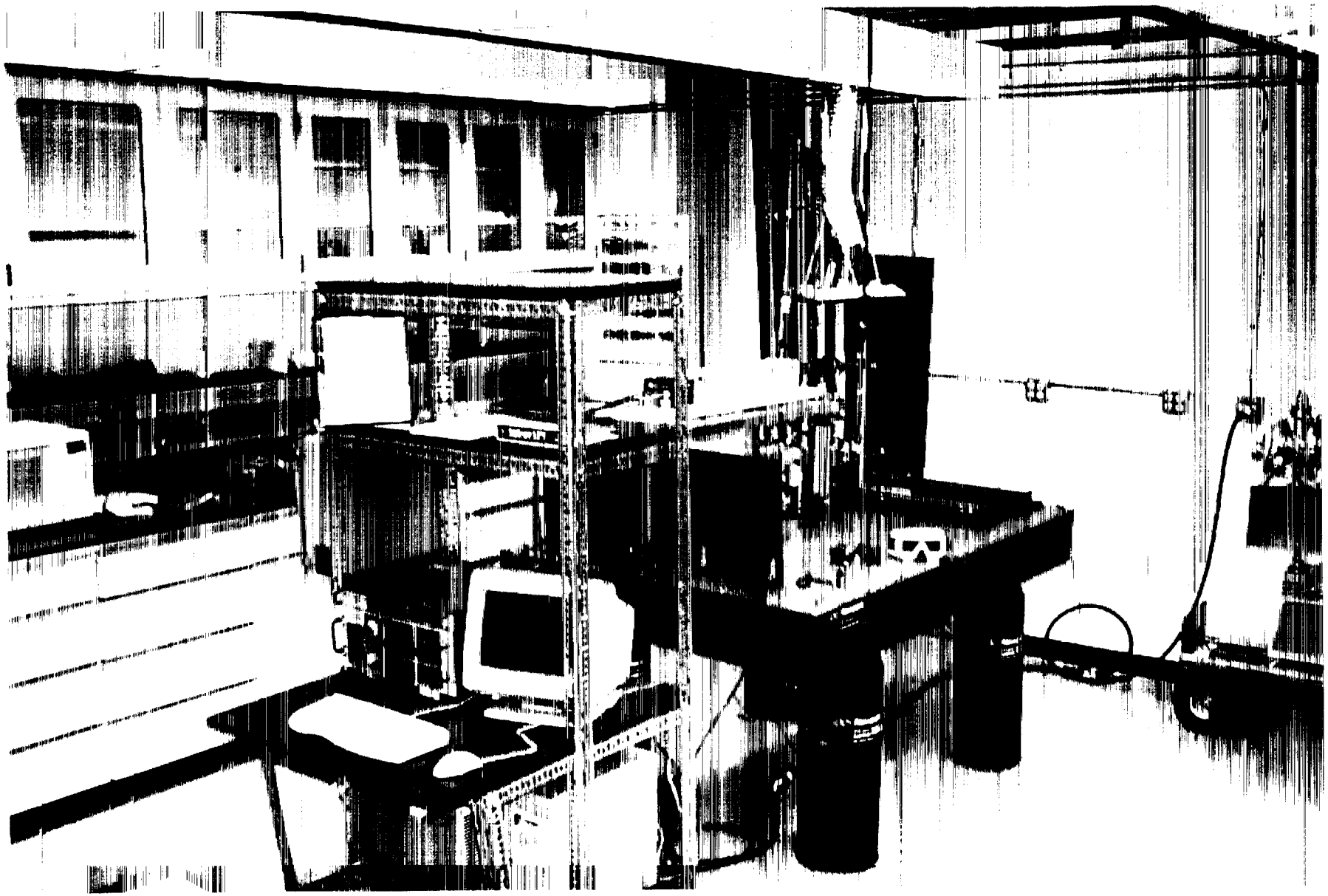

Figure 6b: Experimental Arrangement

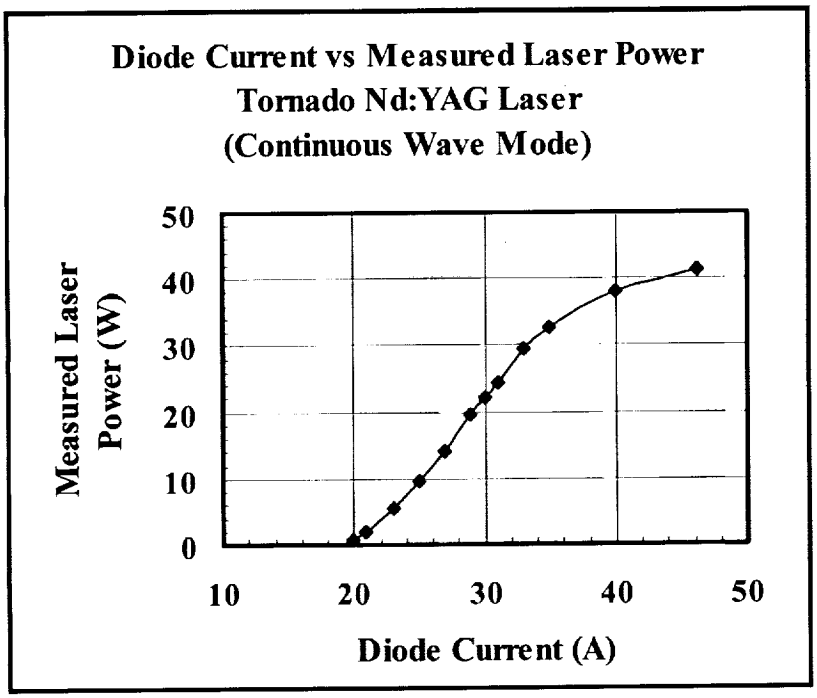

Figure 7a: Laser Power vs. Diode Current Characteristics (Continuous Wave Mode)

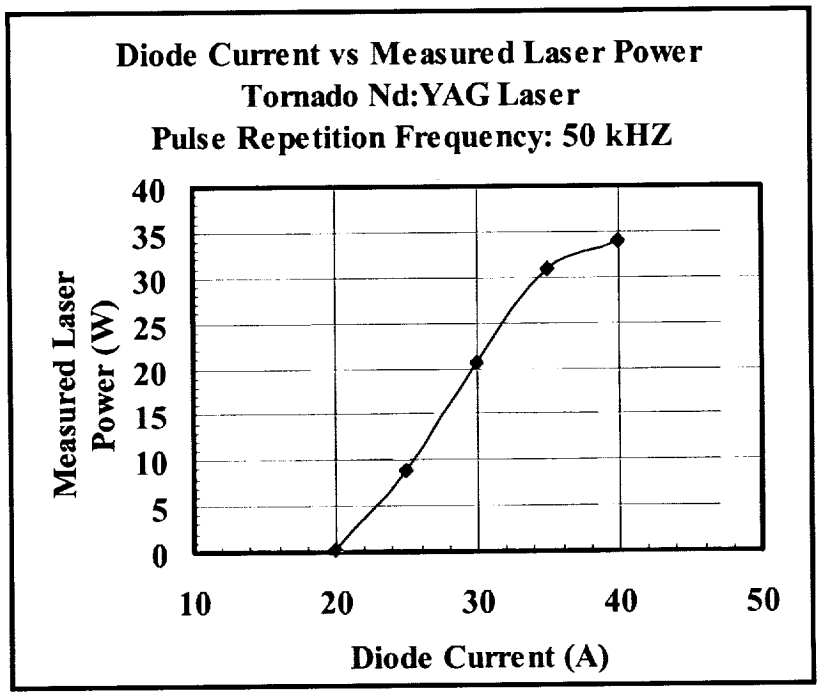

Figure 7b: Laser Power vs. Diode Current Characteristics (Pulsed Mode with PRF = 50 kHz

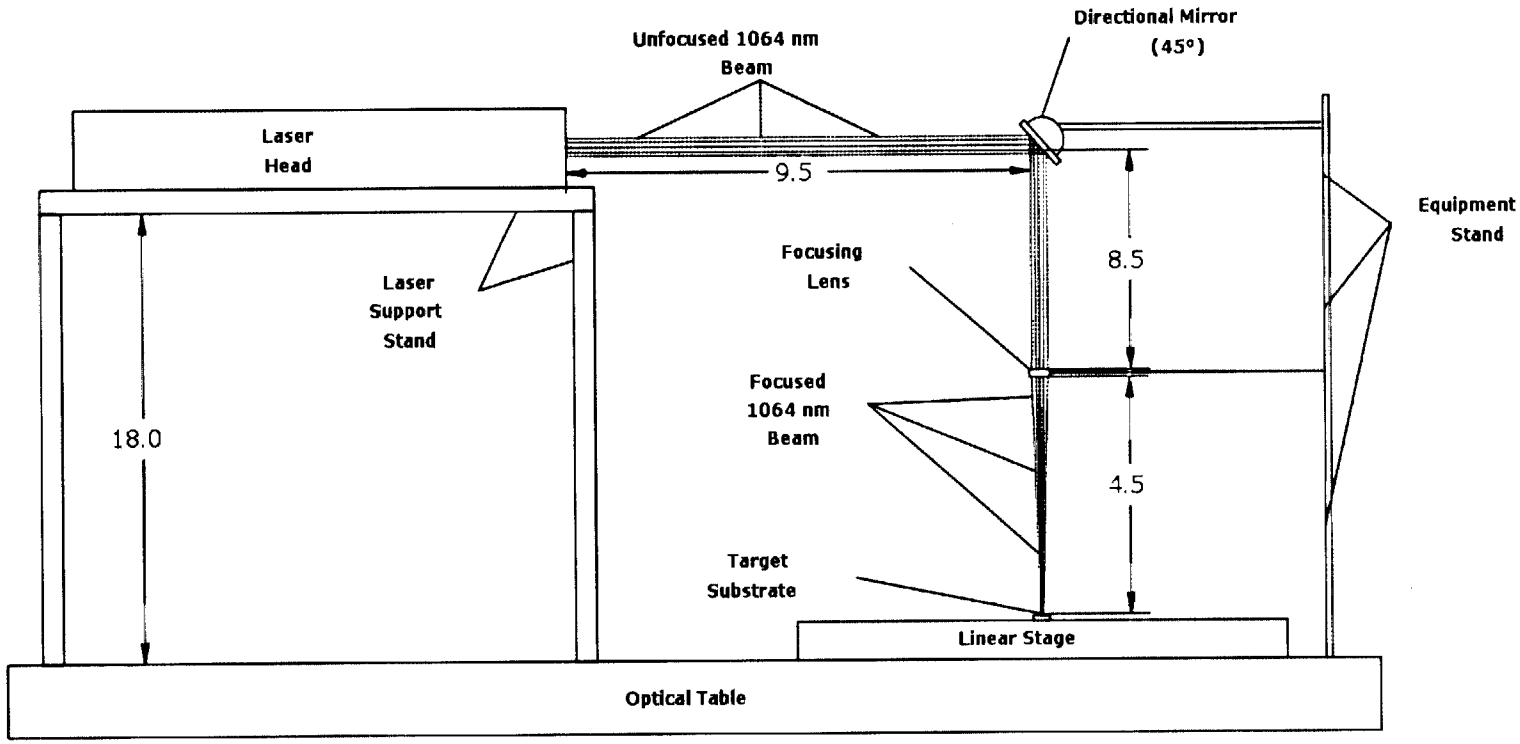

Figure 8: Laser Beam Directional Diagram
(All Dimensions in Inches--Not Drawn to Scale)

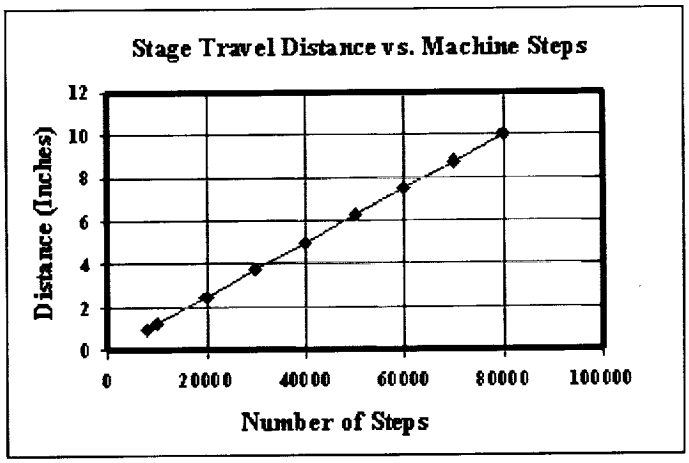

Figure 9a: Stage Travel Distance vs Number of Machine Steps Traveled

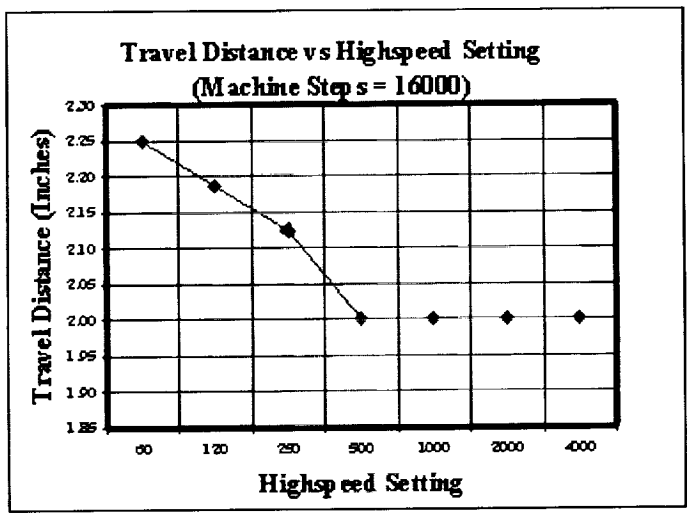

Figure 9b: Travel Distance at Various Machine Highspeed Settings

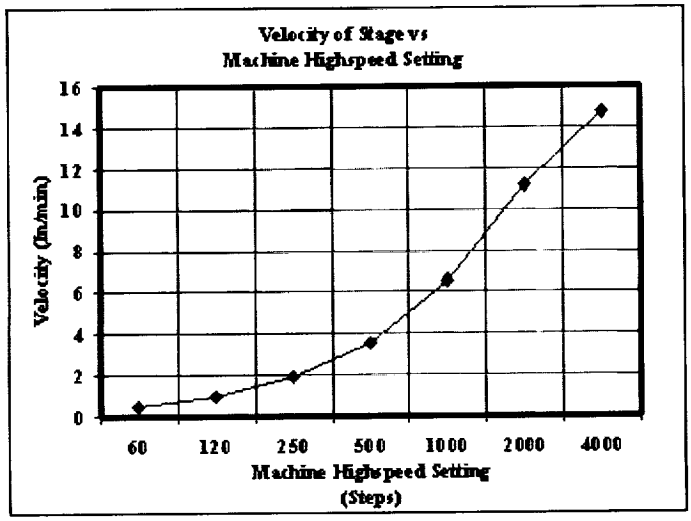

Figure 9c: Stage Velocity at Various Machine Highspeed Settings

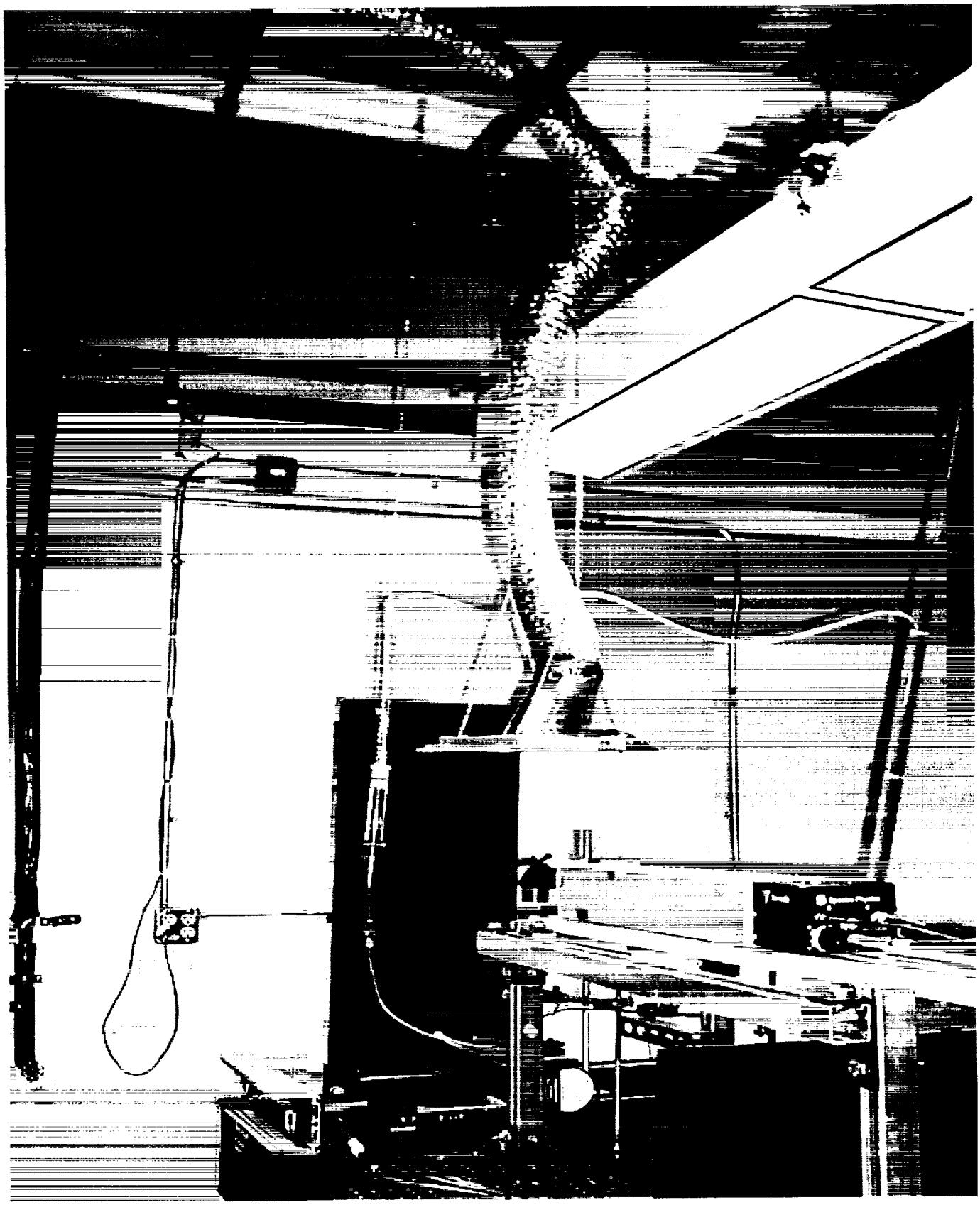

Figure 10: Ventilation System

Figure 11: Powder Delivery System

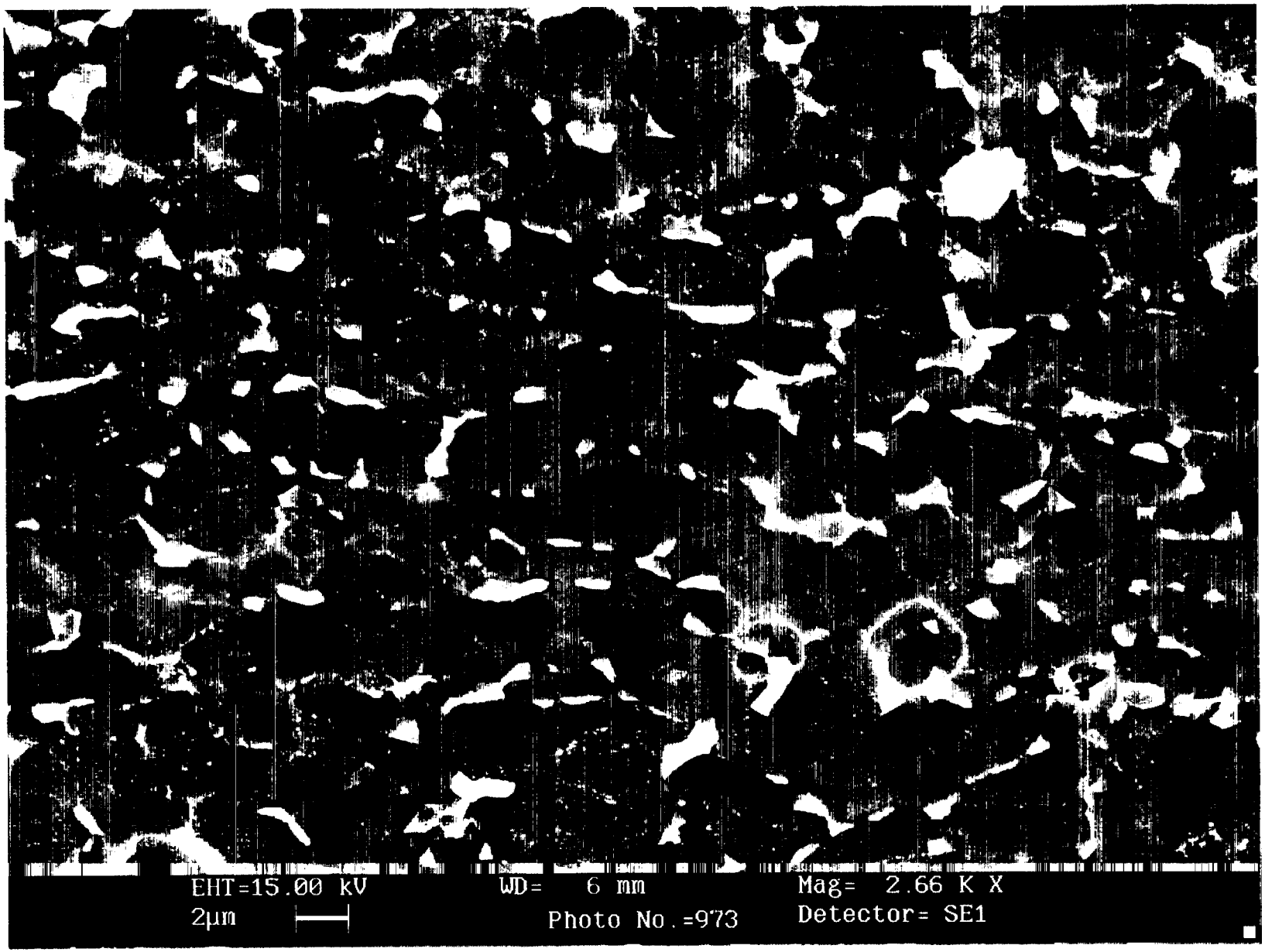

Figure 12a: As-Received Ti-6Al-4V (2660x)

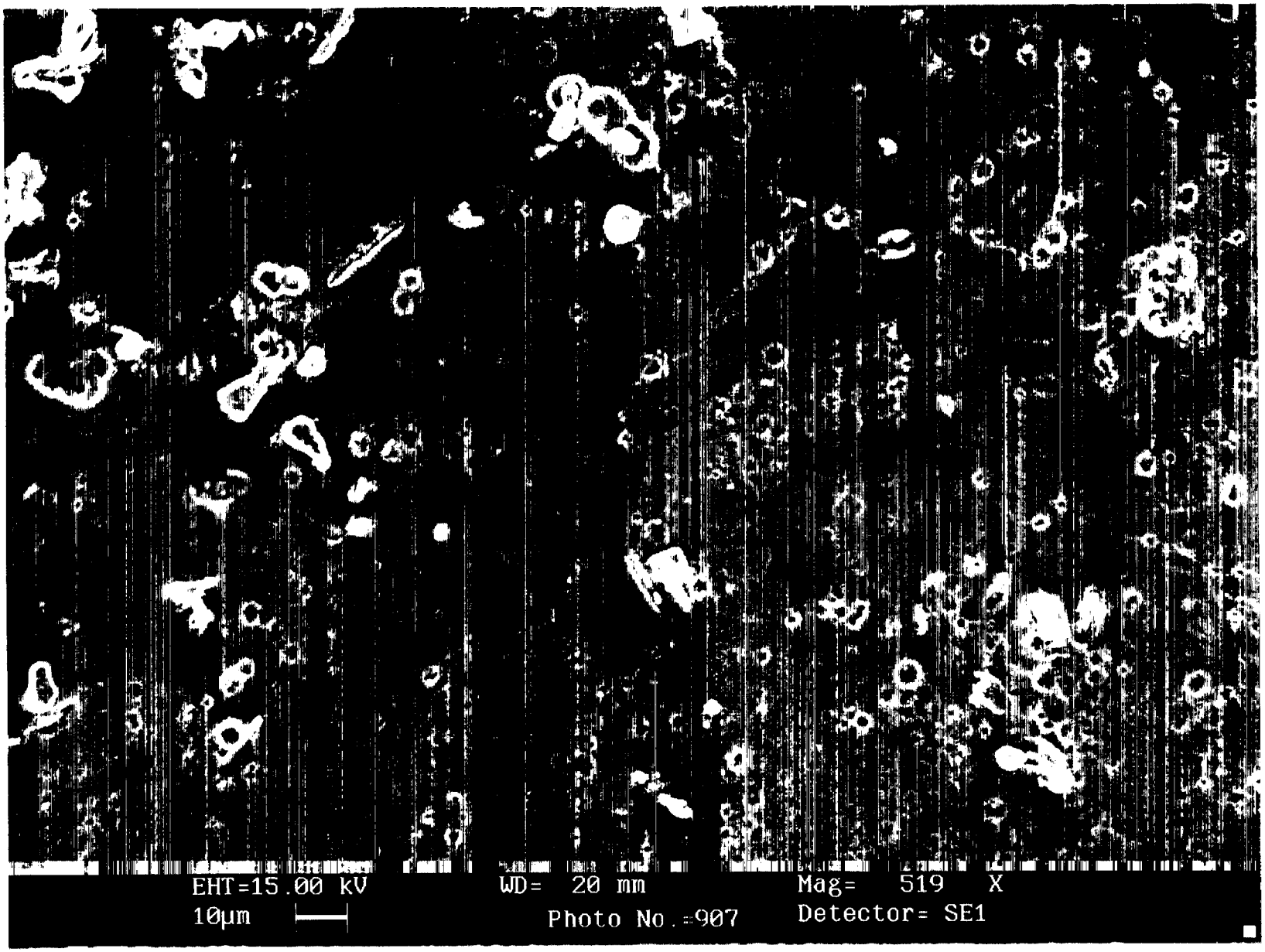

Figure 12b: As-Received Al-2219 (519x)

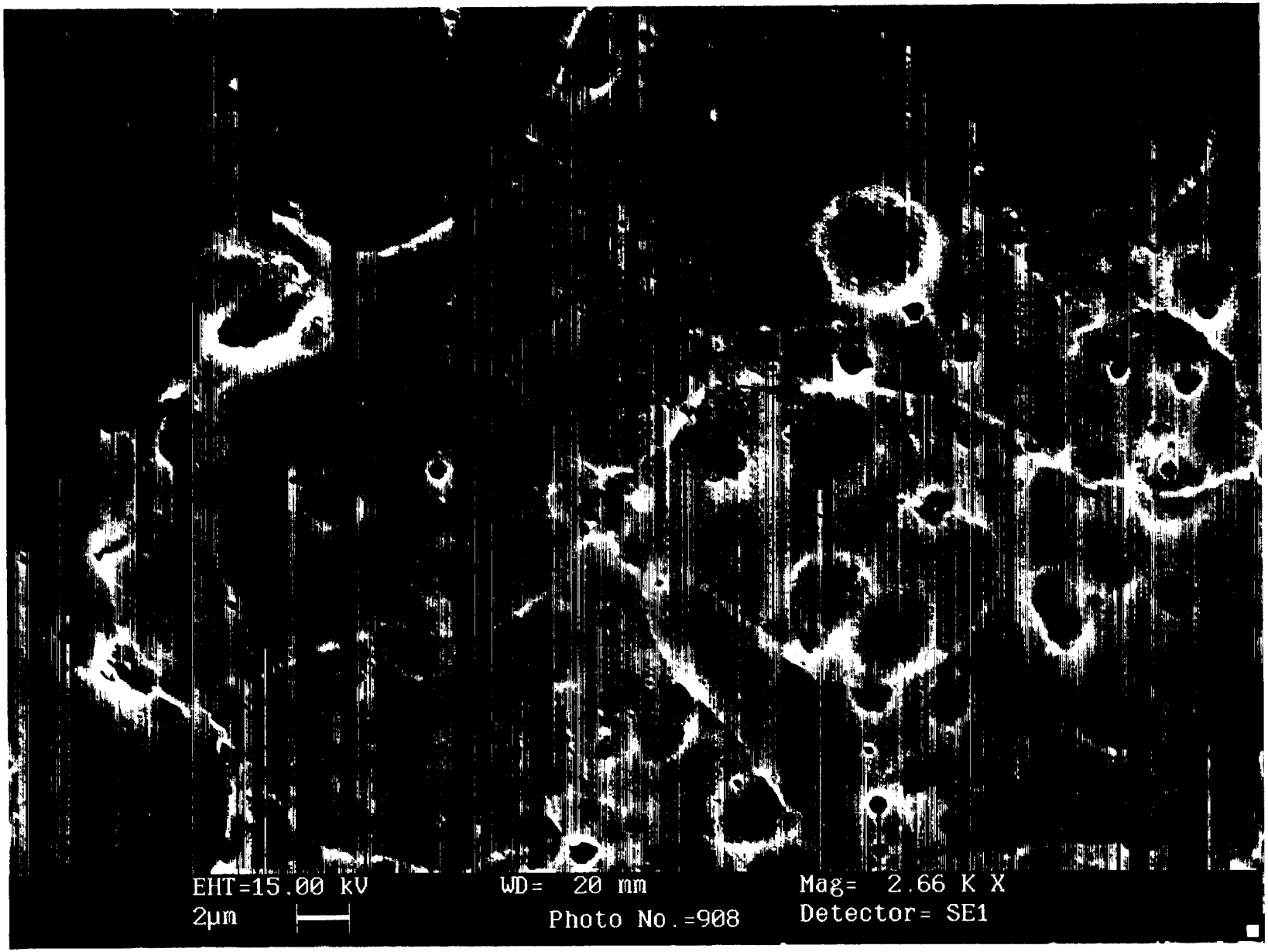

Figure 12c: As-Received Al-2219 (2660x)

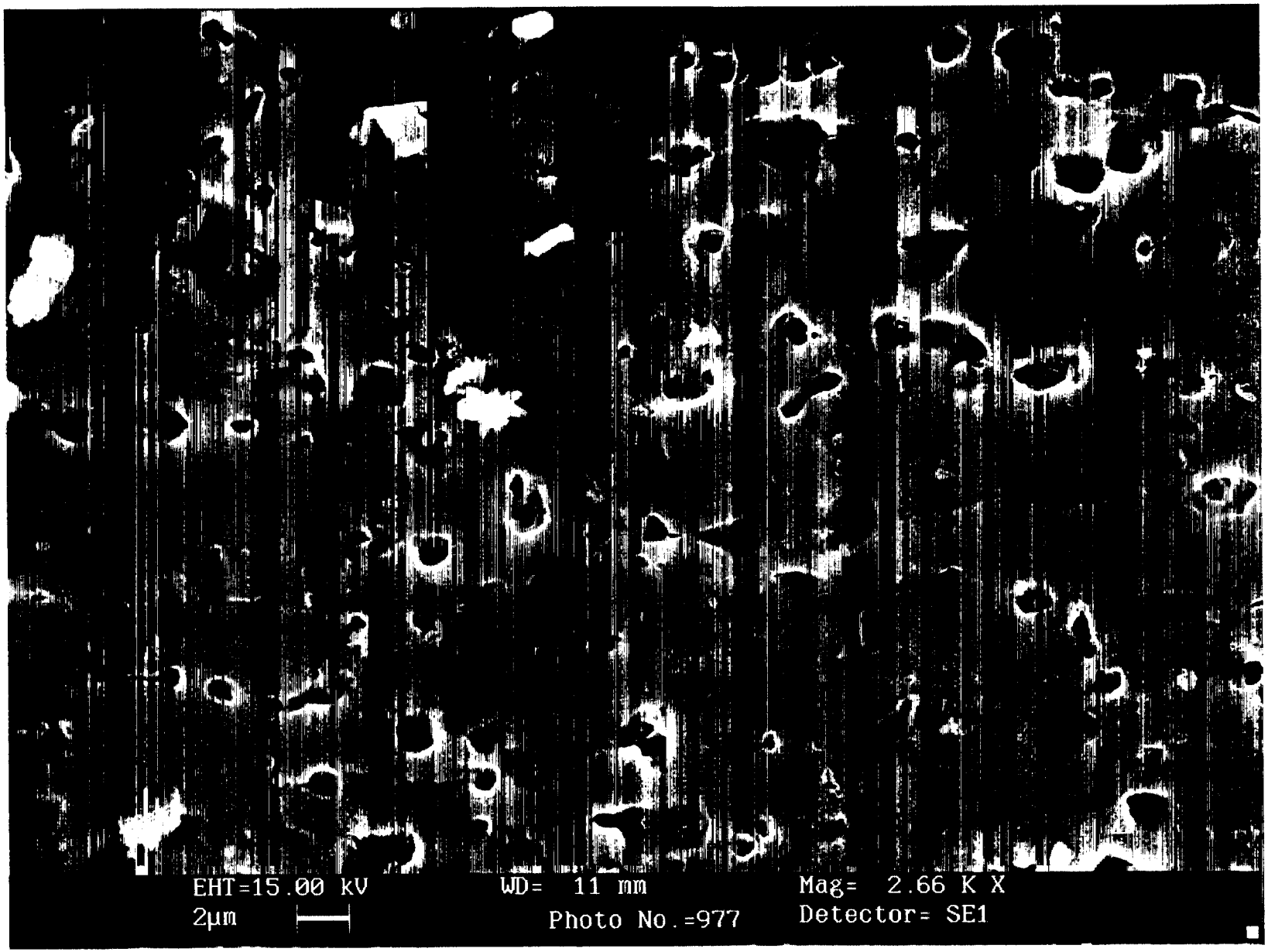

Figure 12d: As-Received Al-2090 (2660x)

Figure 12e: As-Received Al-2090 (5220x)

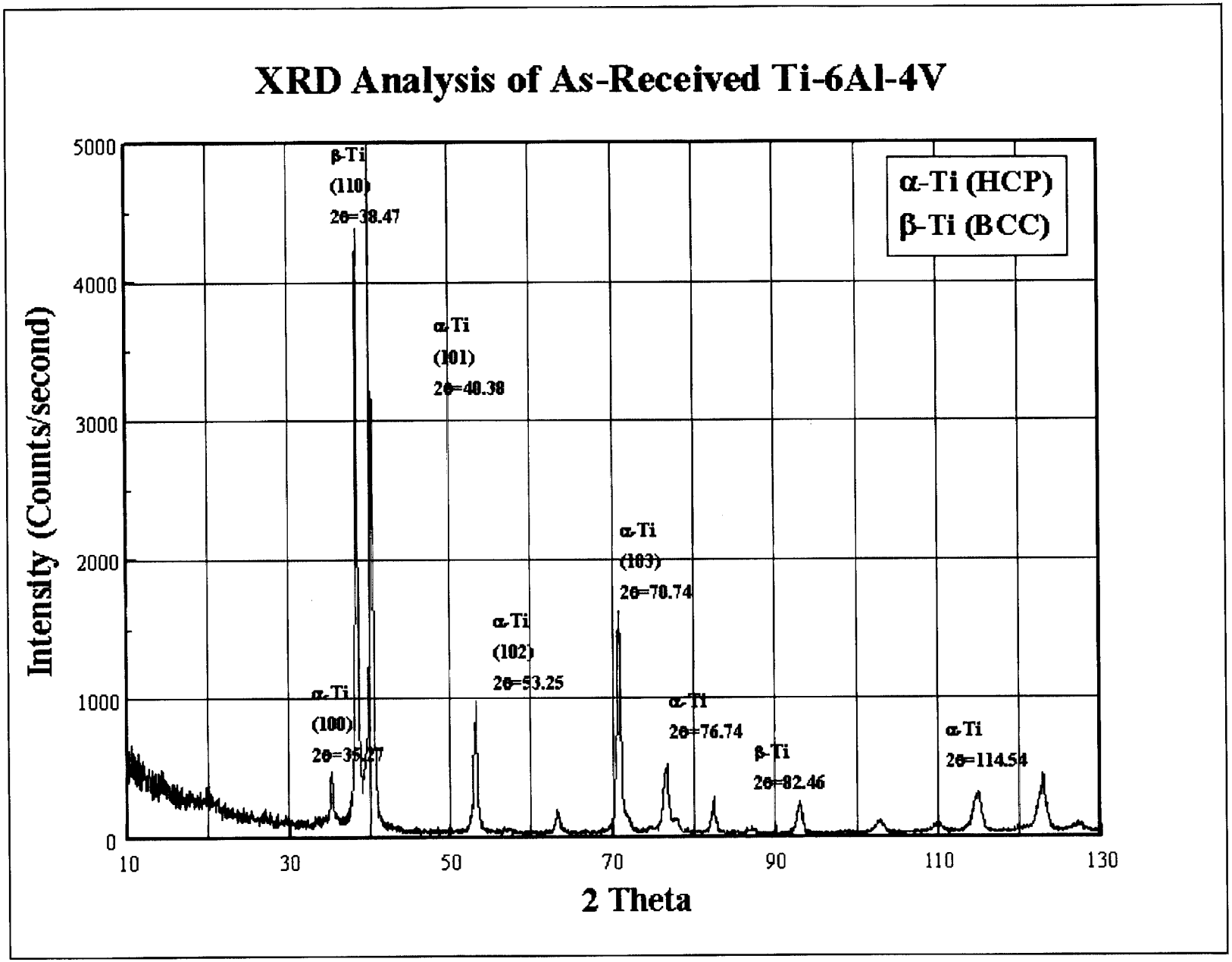

Figure 13a: XRD Scan of As Received Ti-6Al-4V

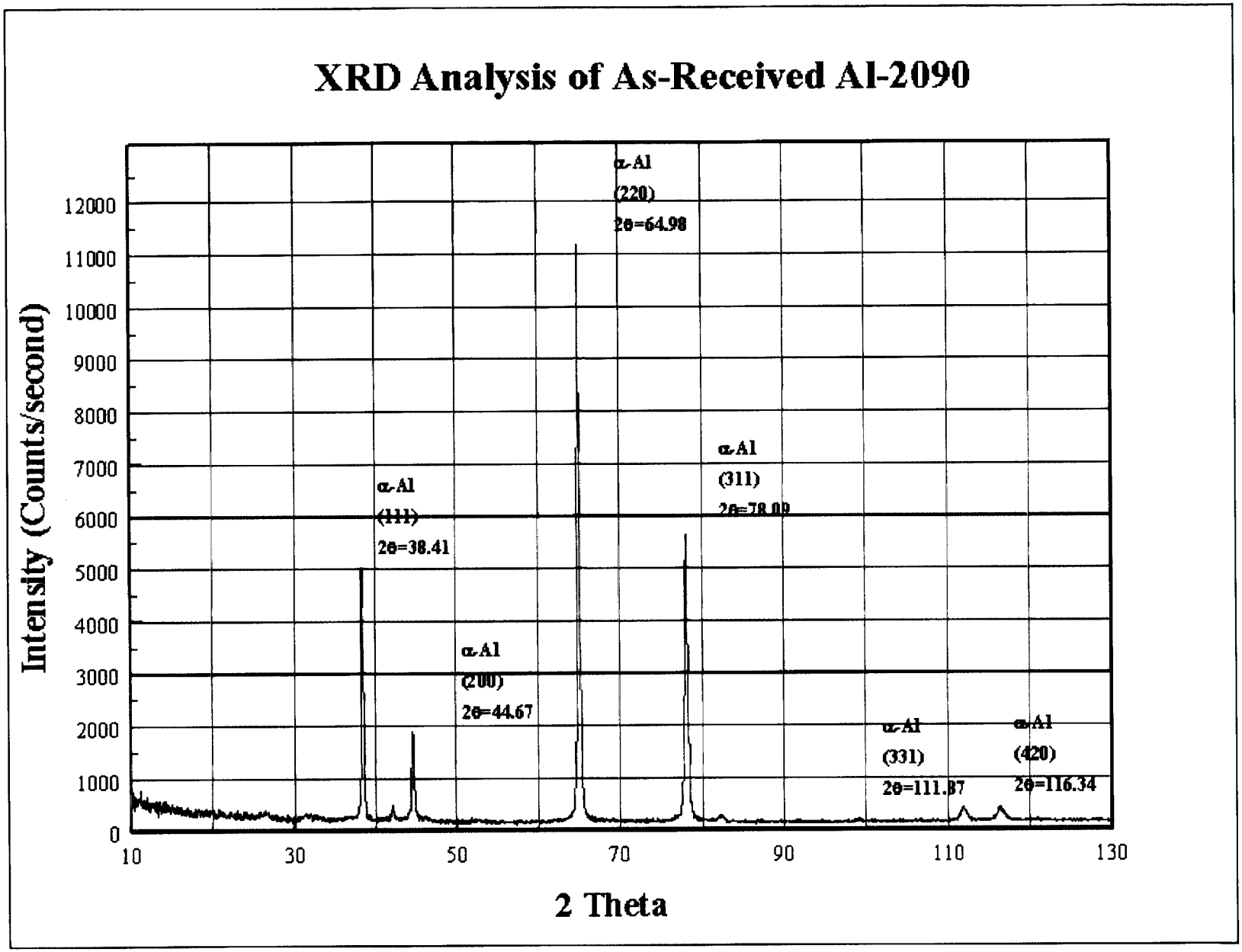

Figure 13b: XRD Scan of As Received Al-2090

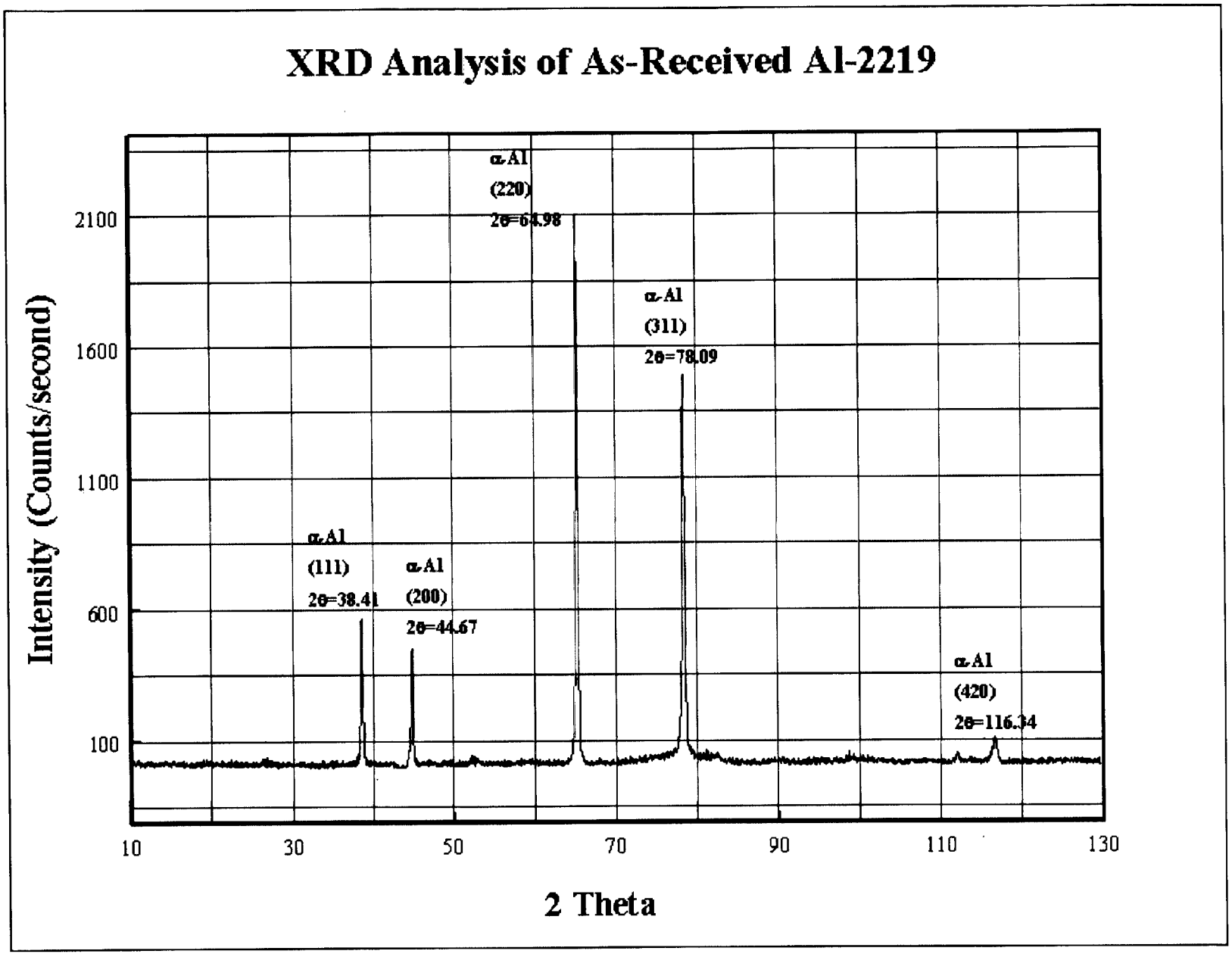

Figure 13c: XRD Scan of As Received Al-2219

Figure 14a: Laser Processed Ti-6Al-4V
(10-3-2000 TC1-4)

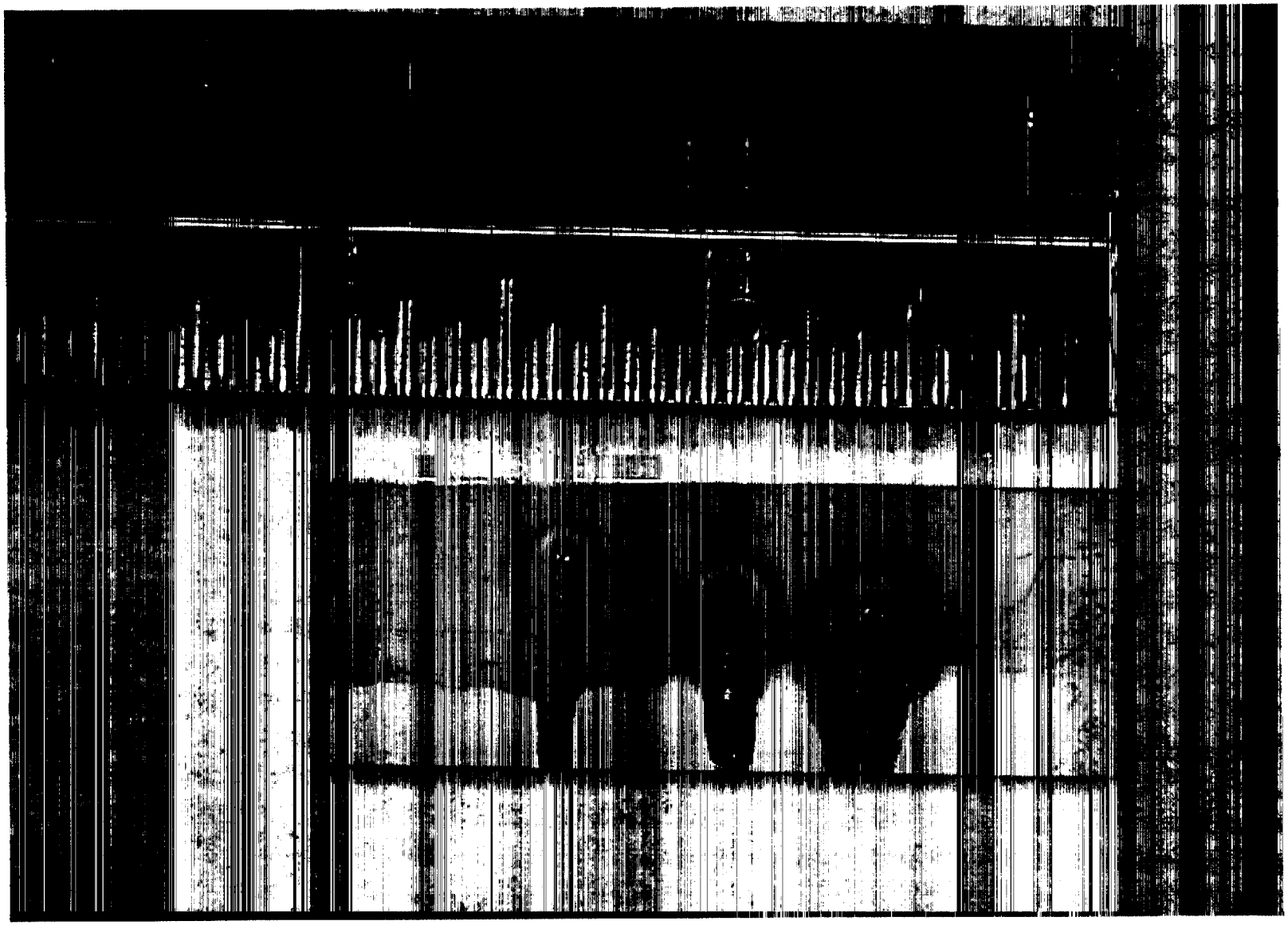

Figure 14b: Laser Processed Ti-6Al-4V
(After Partial Chemical Etching)
(10-9-2000 TC2)

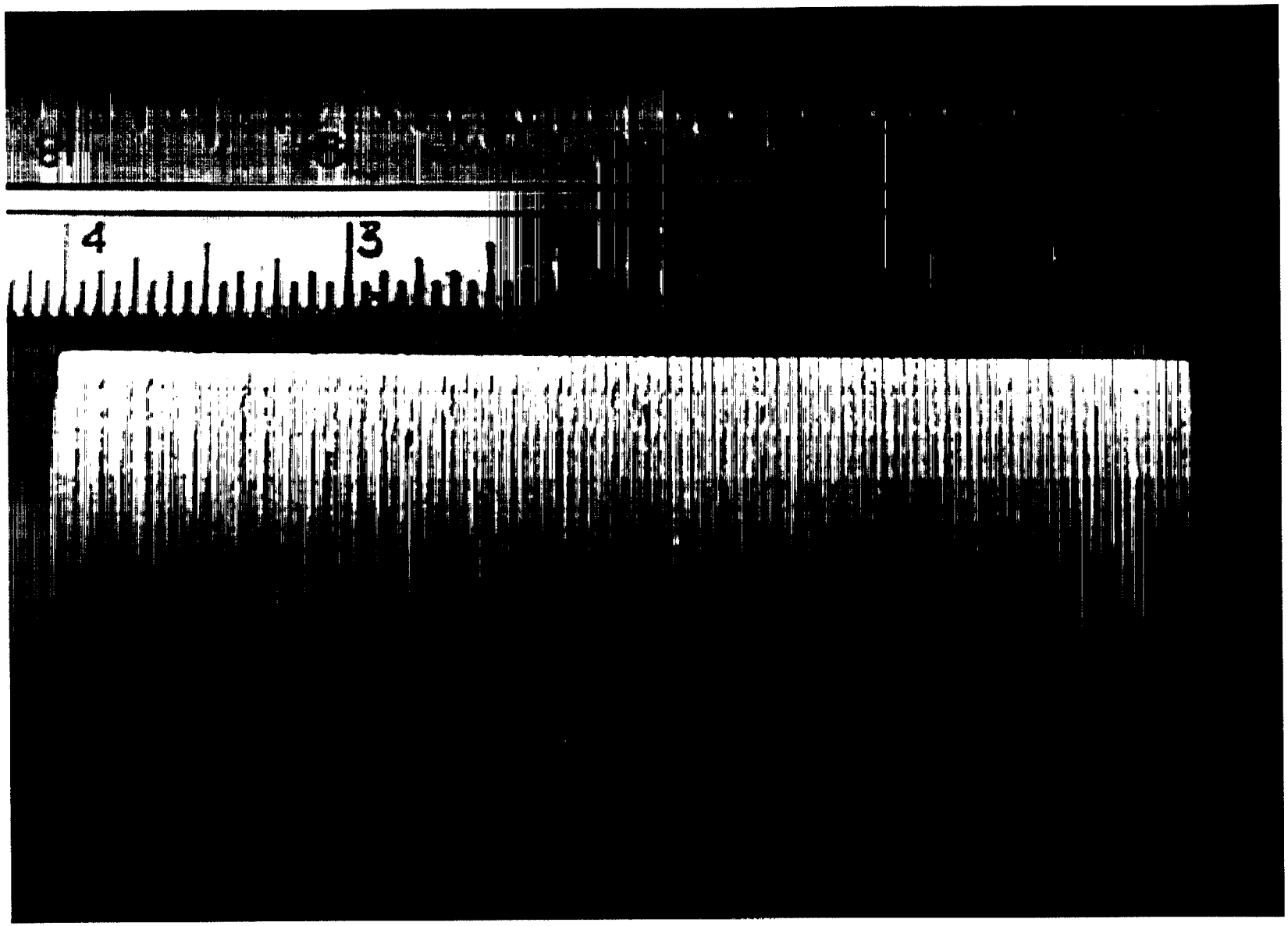

Figure 14c: Laser Processed Al-2219
(10-9-2000 TC3)

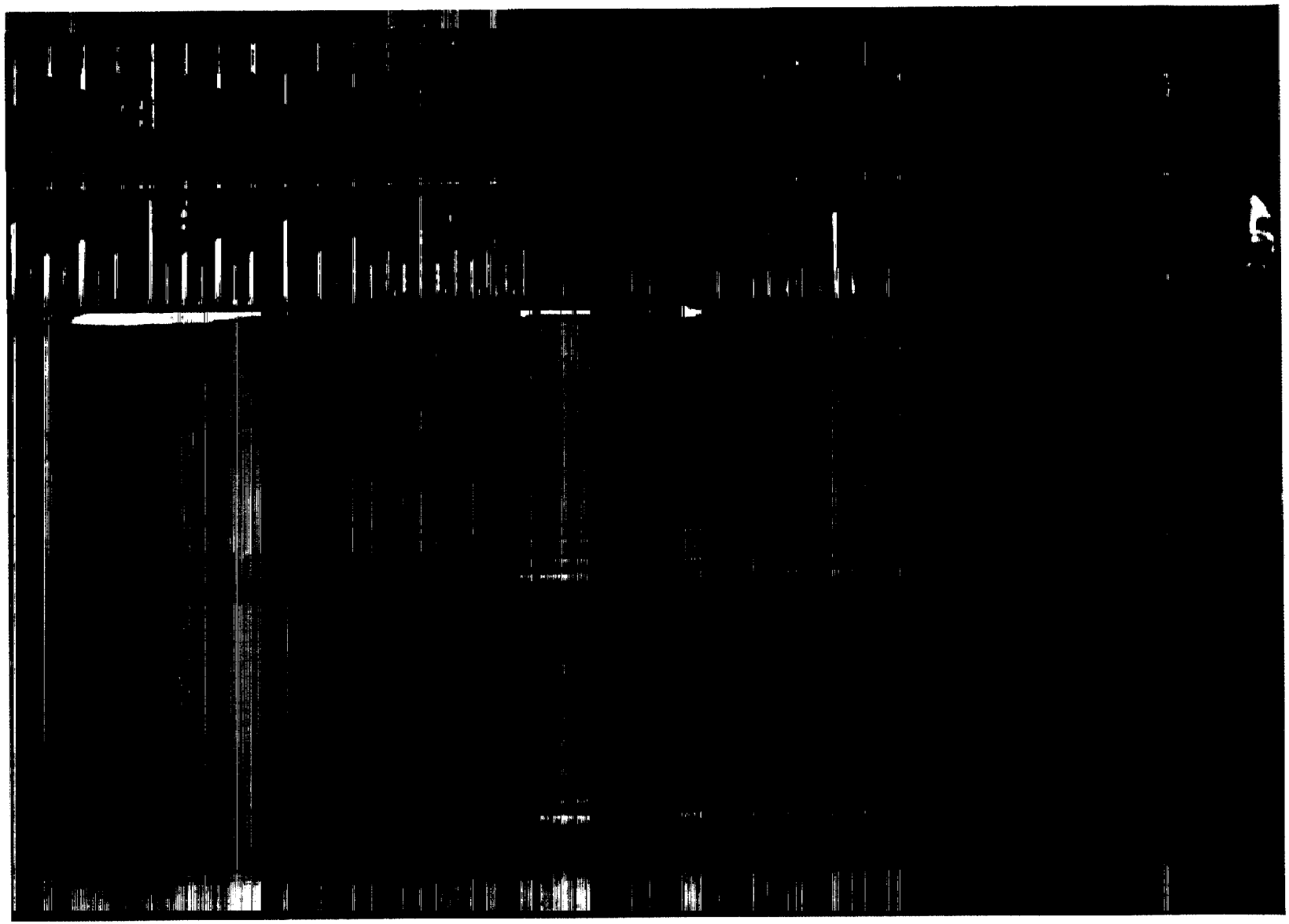

Figure 14d: Laser Processed Ti-6Al-4V
(10-13-2000 TC1)

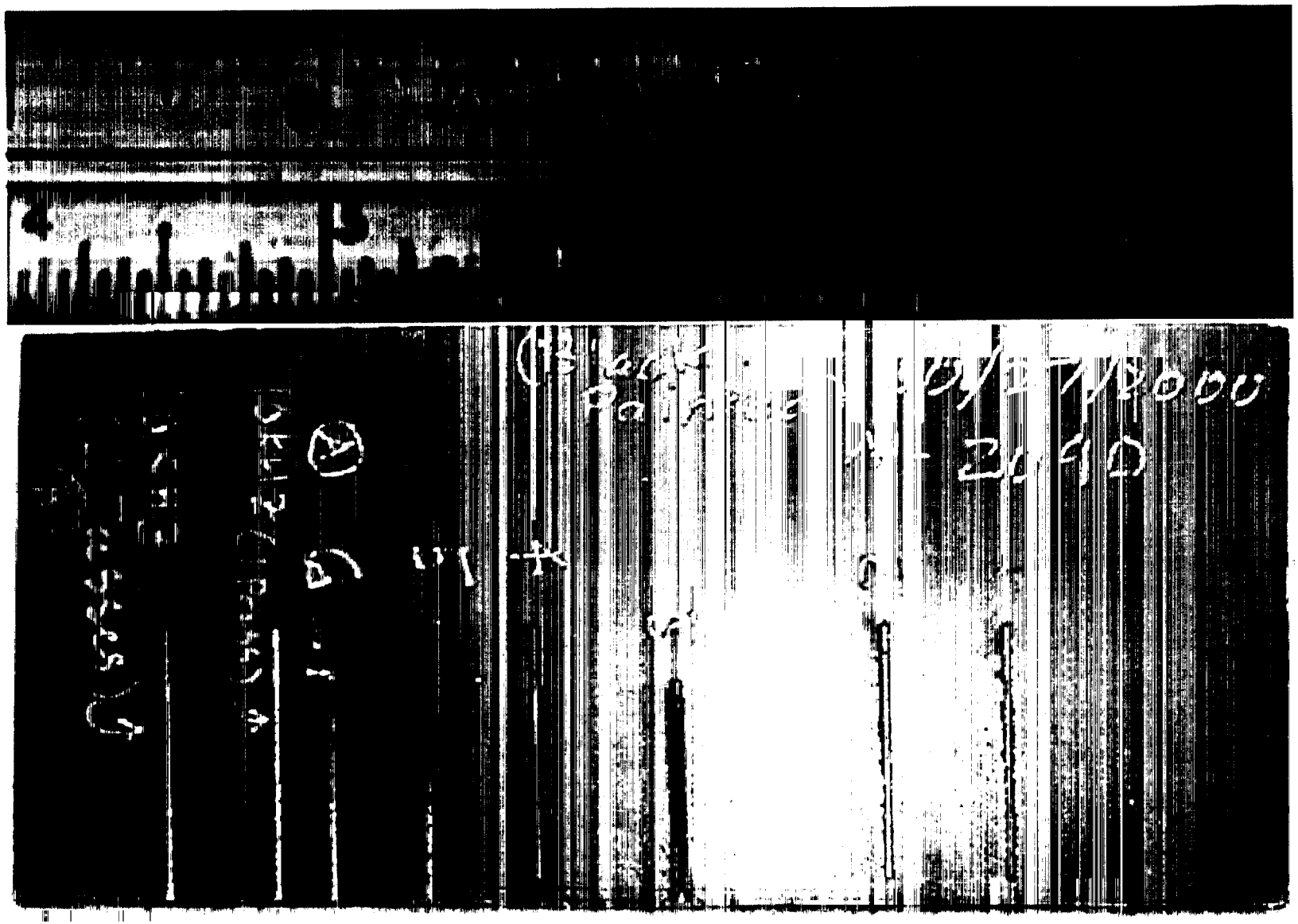

Figure 14e: Black Painted Al-2090
(10-27-2000 TC1)

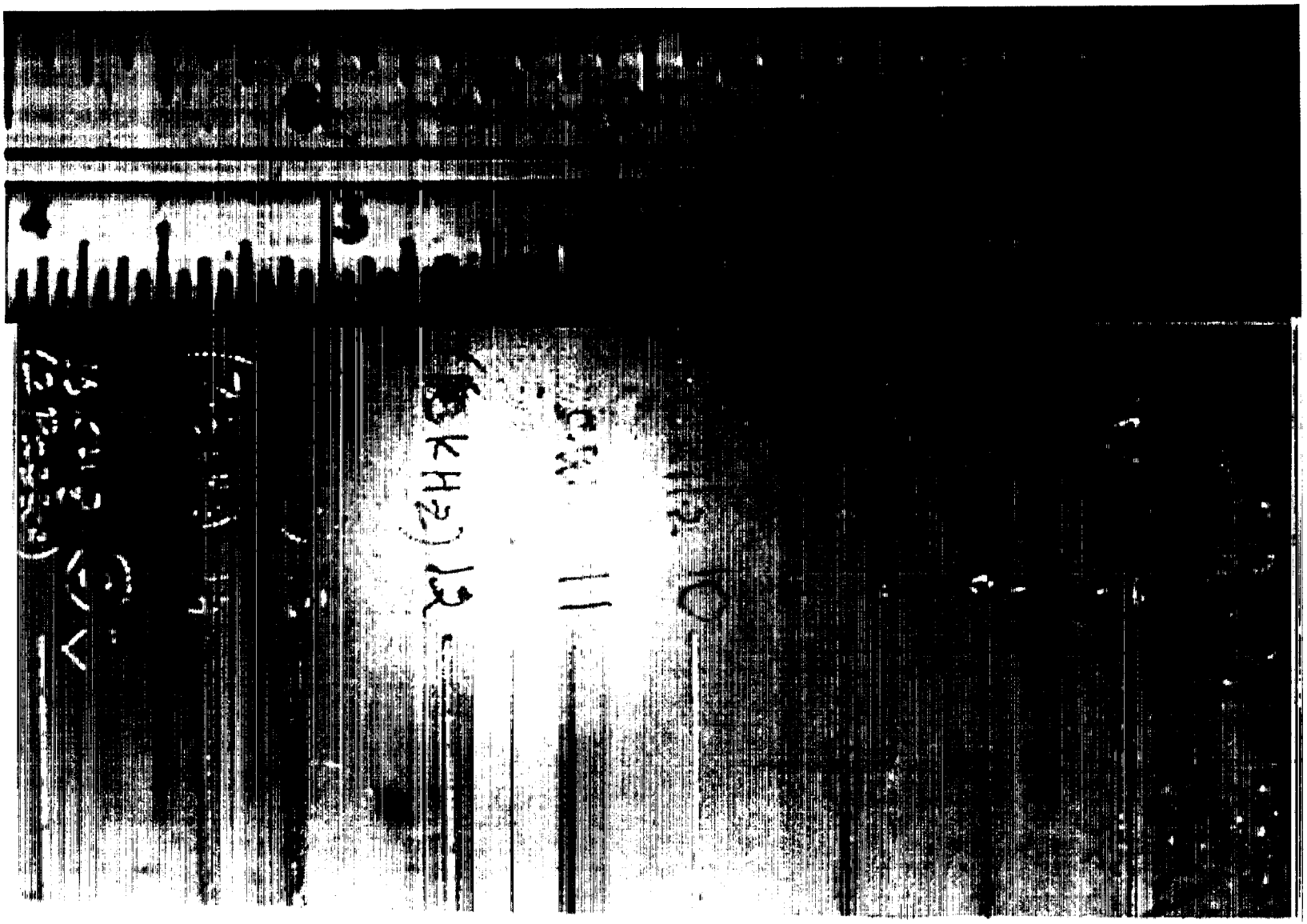

Figure 14f: Laser Processed Al-2090
(10-27-2000 TC2)

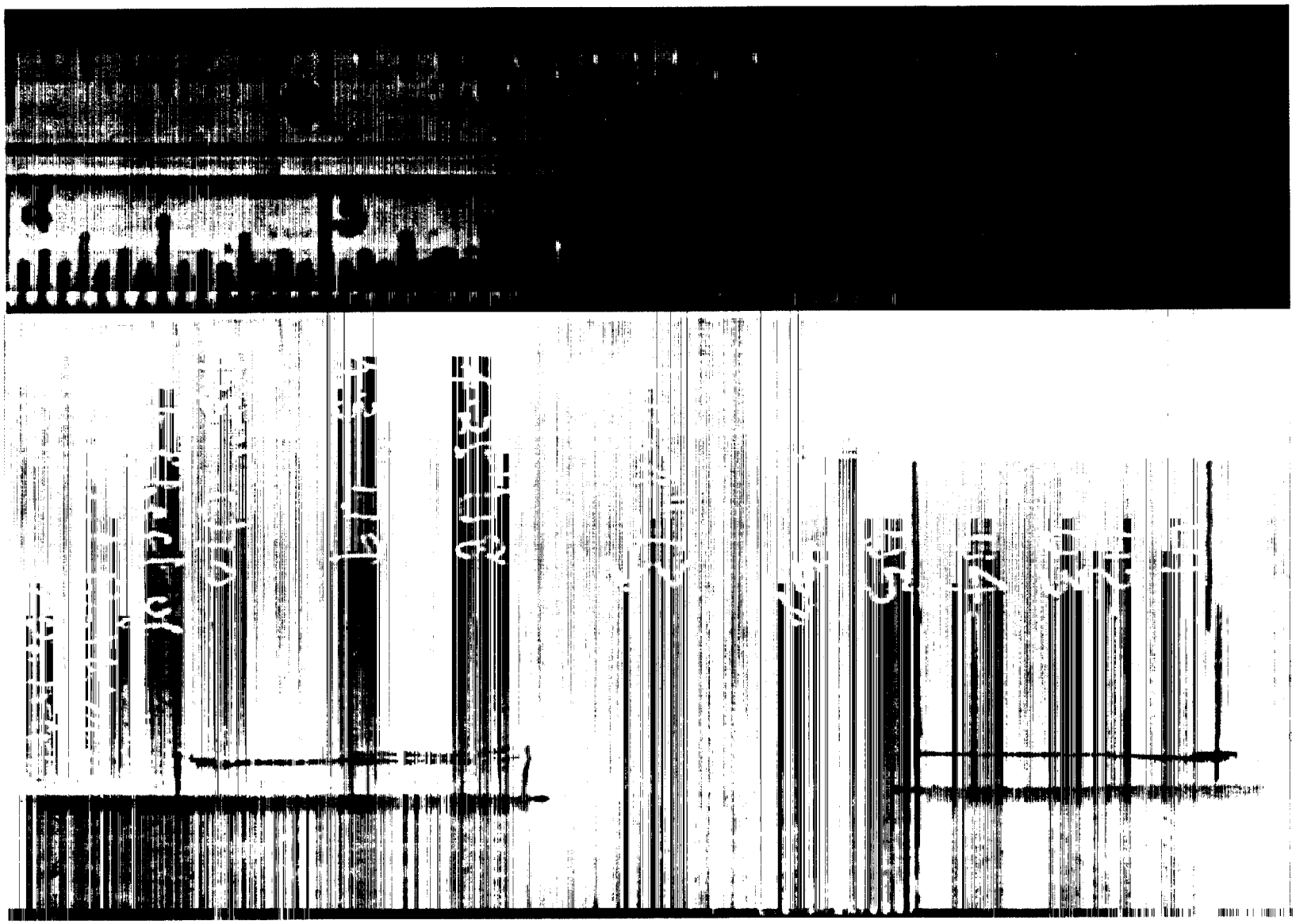

Figure 14g: Laser Processed Al-2219
(10-30-2000 TC3)

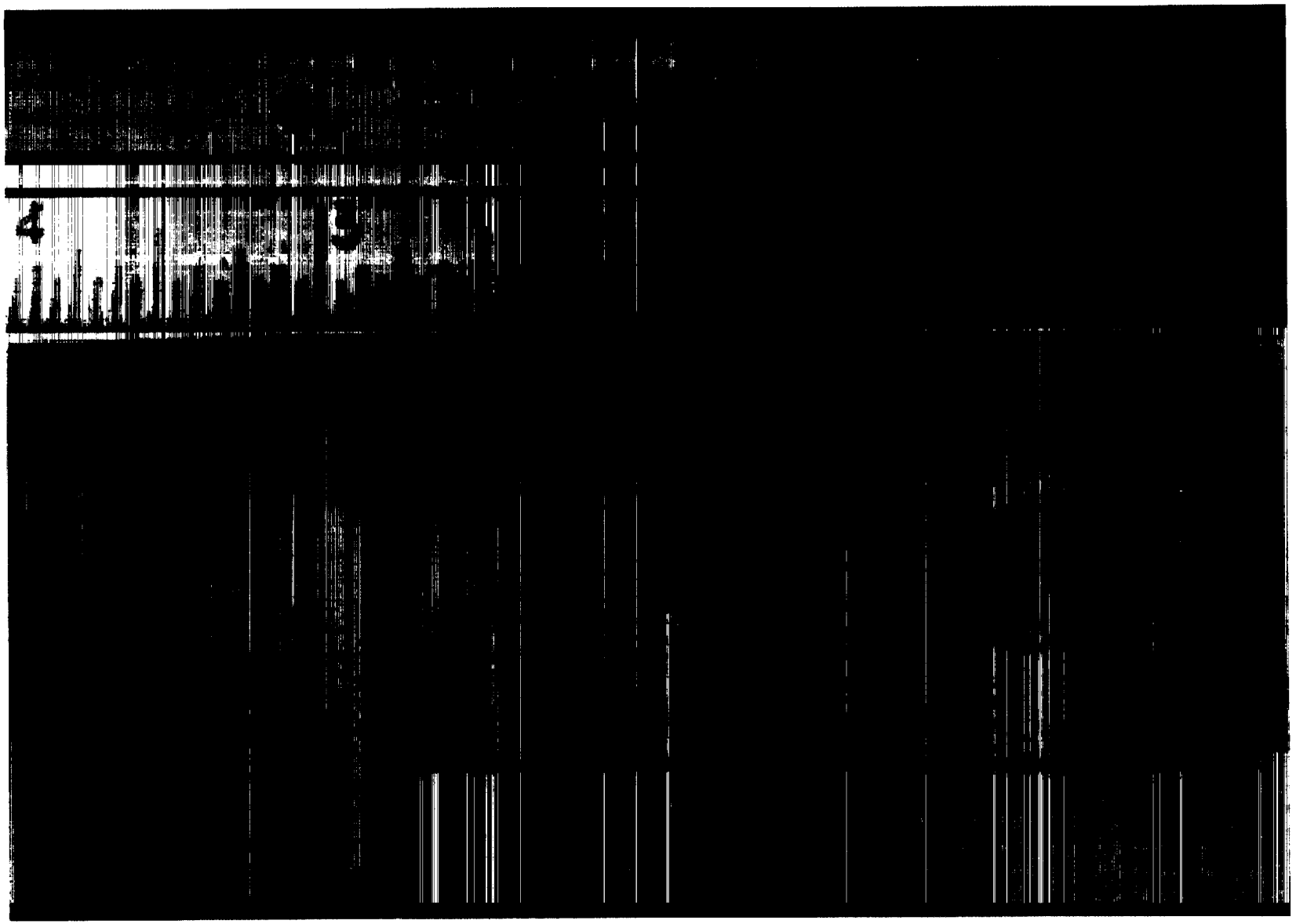

Figure 14h: Black Painted Ti-6Al-4V Substrate & Al-2219 PPP (10-30-2000 TC4)

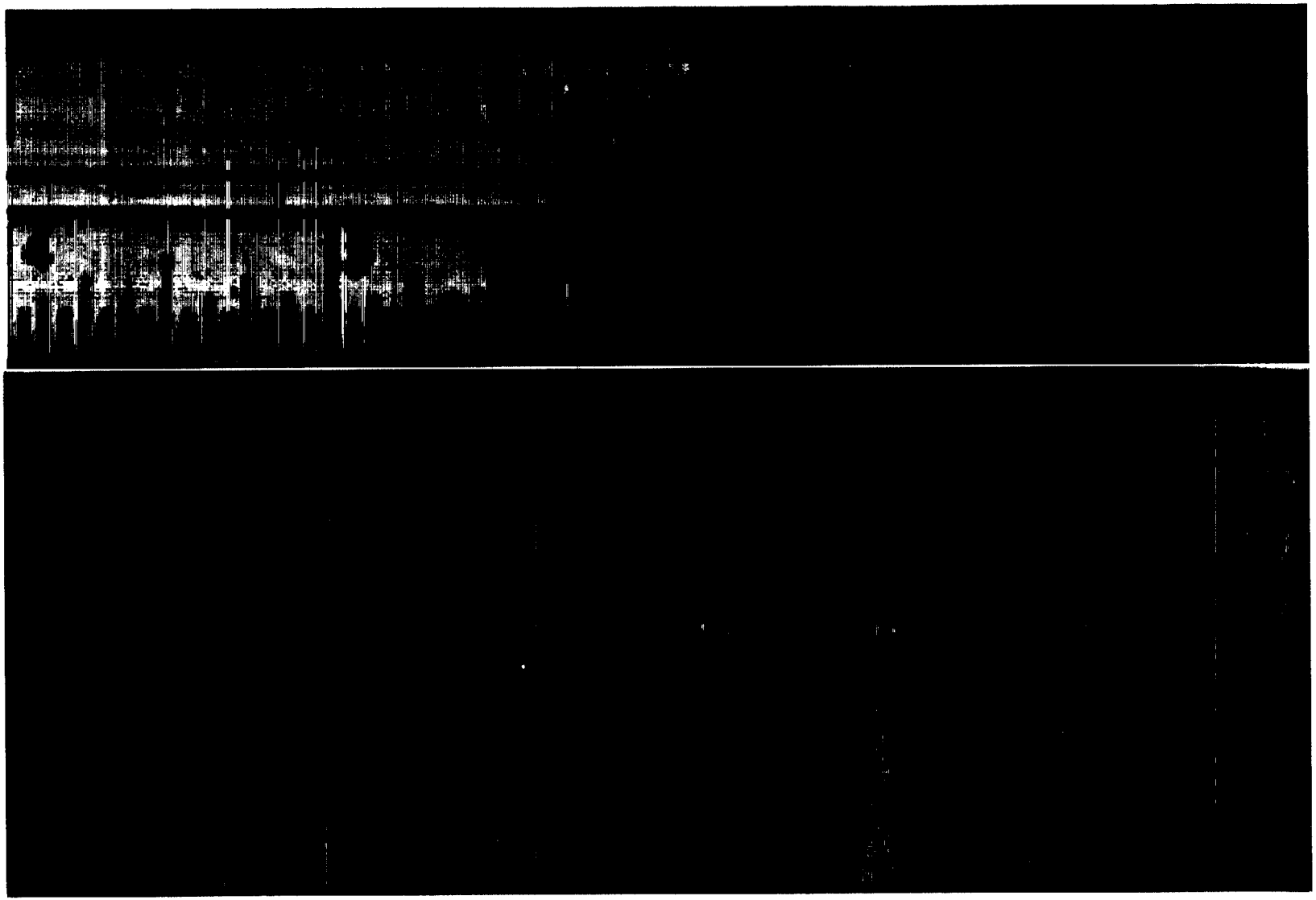

Figure 14i: Black Painted Al-2090 Substrate & Ti-6Al-4V PPP (11-1-2000 TC1)

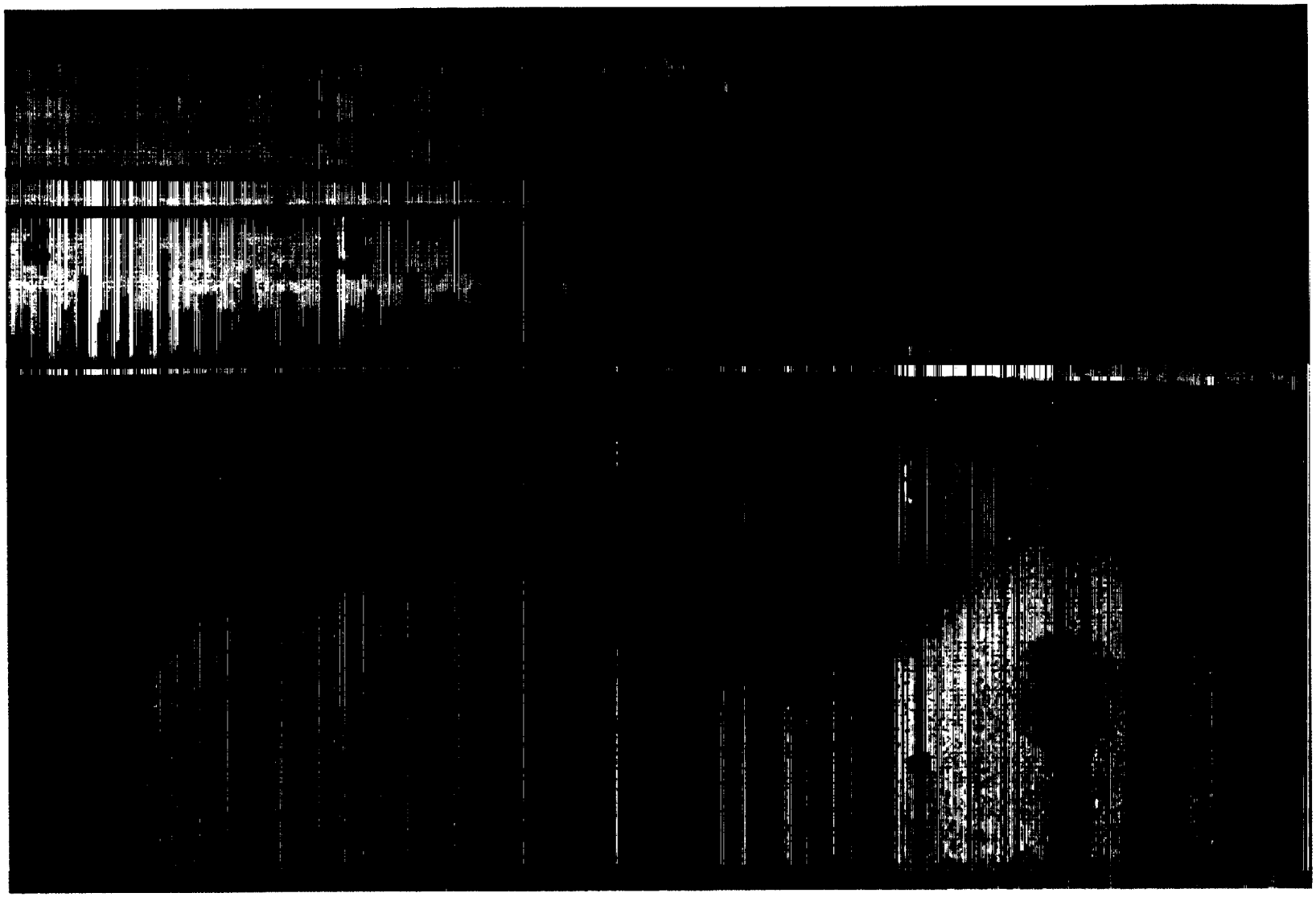

Figure 14j: Black Painted Ti-6Al-4V Substrate & Al-2219 PPP (11-1-2000 TC2)

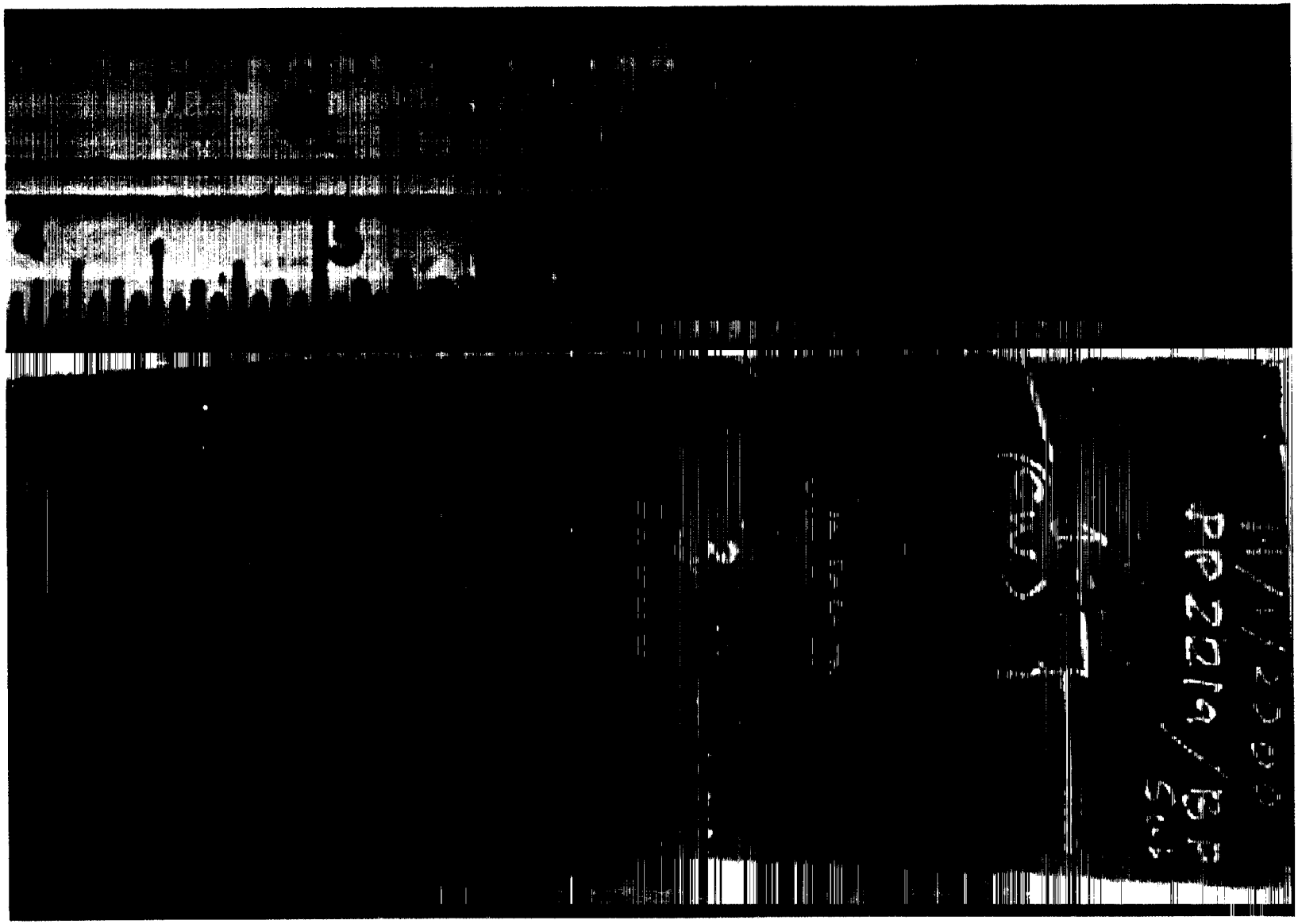

Figure 14k: Black Painted Al-2219 Substrate & Ti-6Al-4V PPP (11-1-2000 TC3)

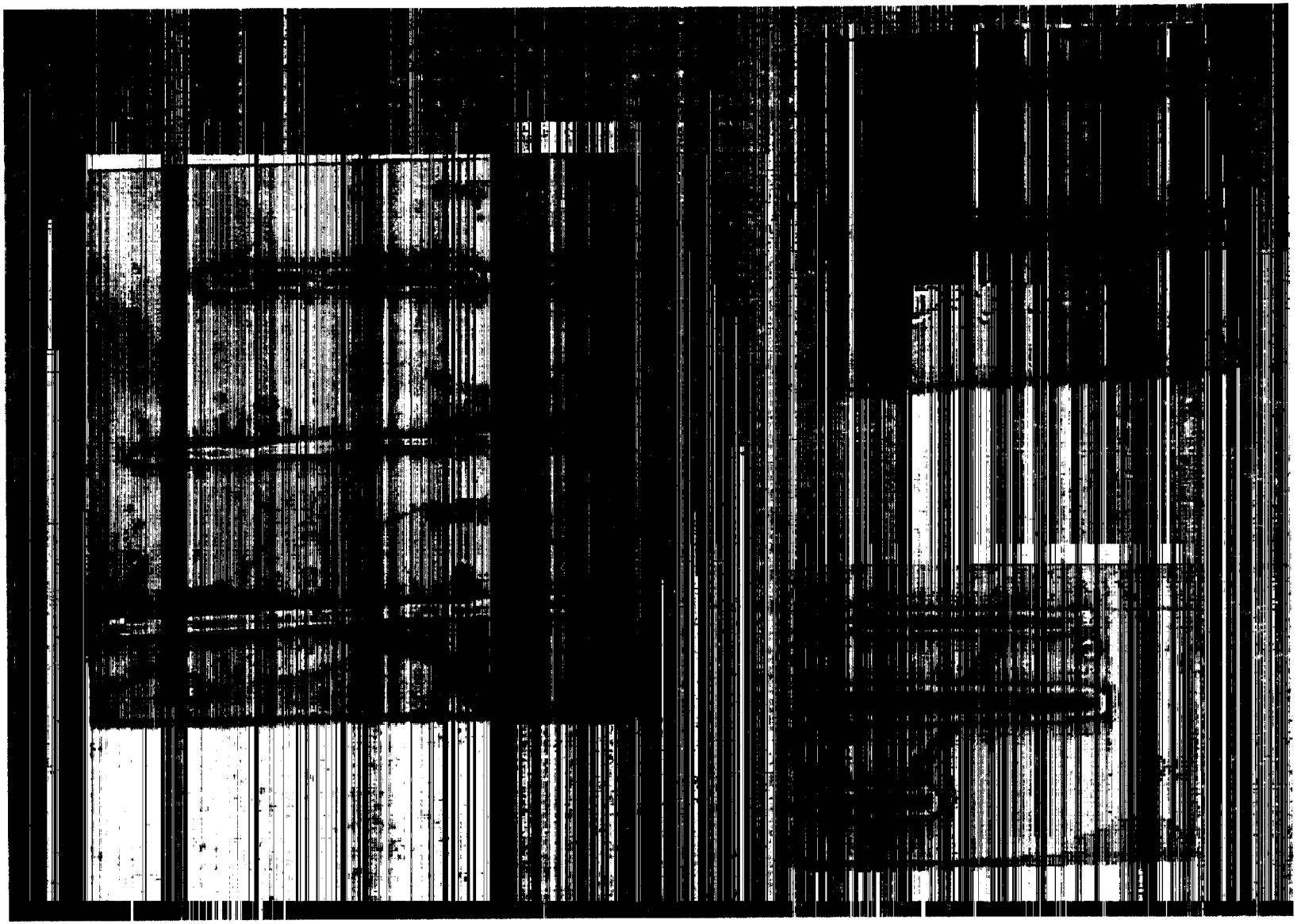

Figure 14l: Laser Nitrided Ti-6Al-4V
(11-1-2000 TC4)

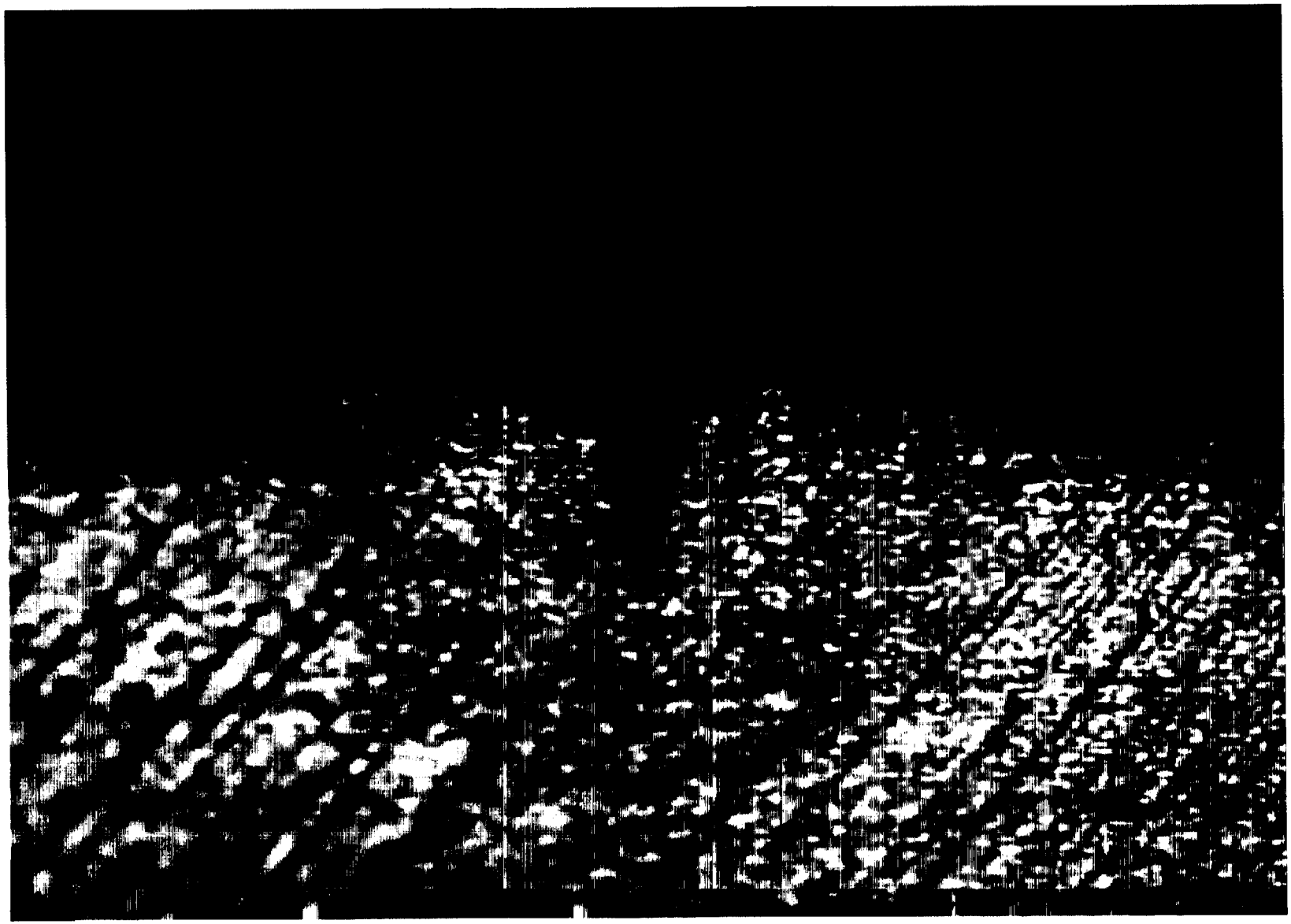

Figure 15a: Laser Cutting on Untreated Ti-6Al-4V
(PRF = 1 kHz)
(10-03-2000 TC4 R1 20x)

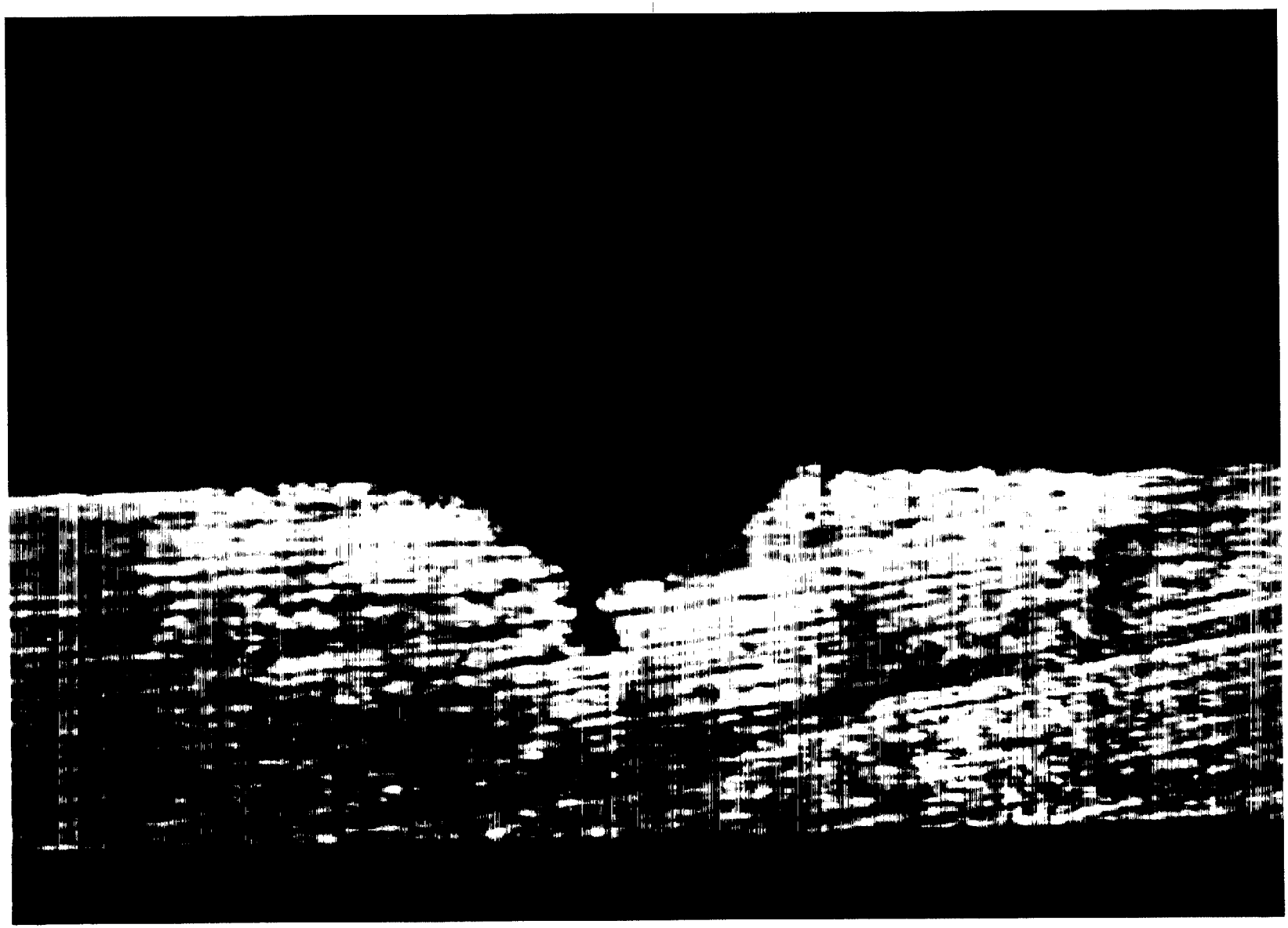

Figure 15b: Black Painted Ti-6Al-4V Substrate & Al-2219 PPP
Pulsed Mode; PRF : 20 kHz; Speed:12.7 mm/min
(11-1-2000 TC2 R3 20x)

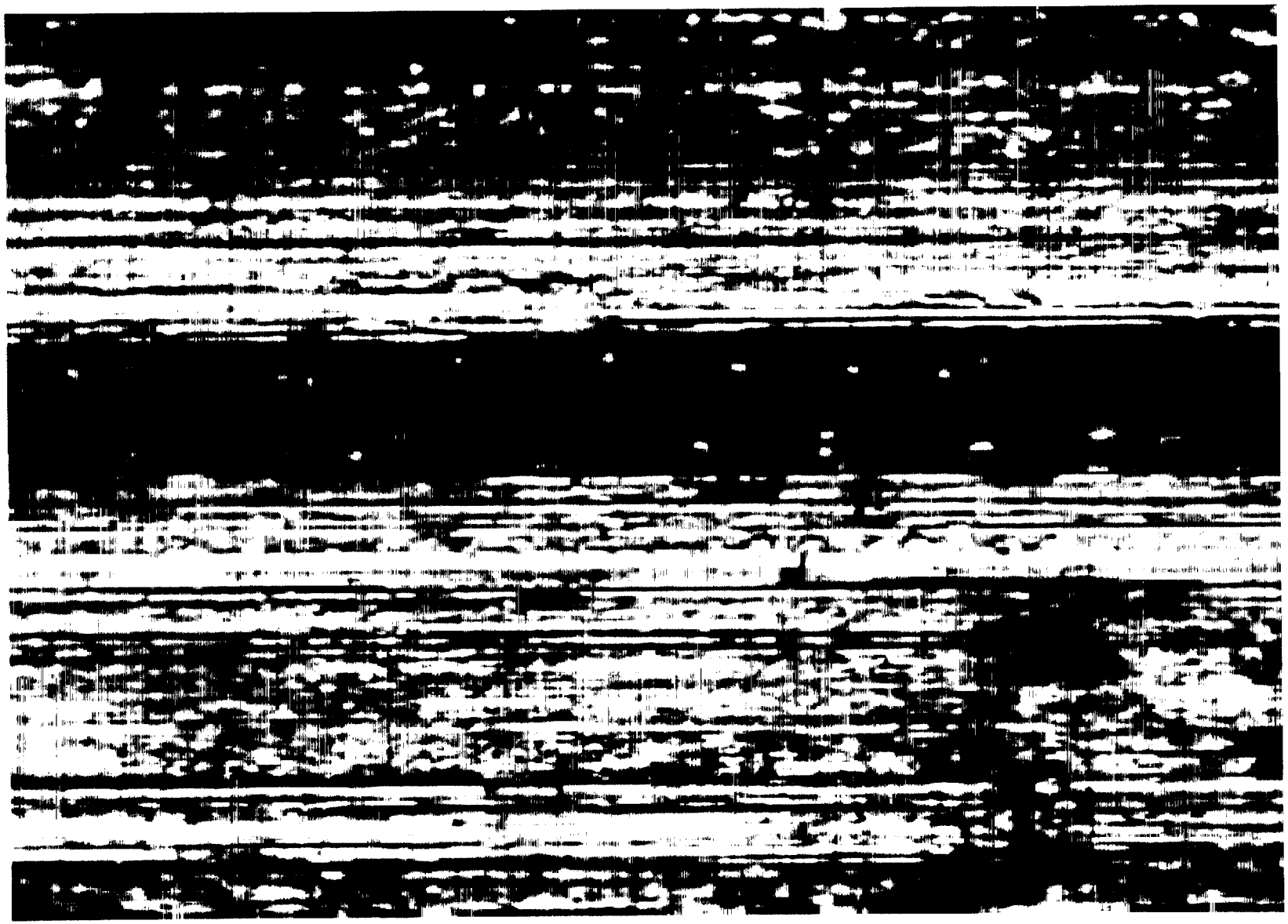

Figure 15c: Black Painted Al-2219
(10-30-2000 TC2 R2 05x Top)

Figure 15d: Black Painted Al-2219
(10-30-2000 TC2 R2 20x Top)

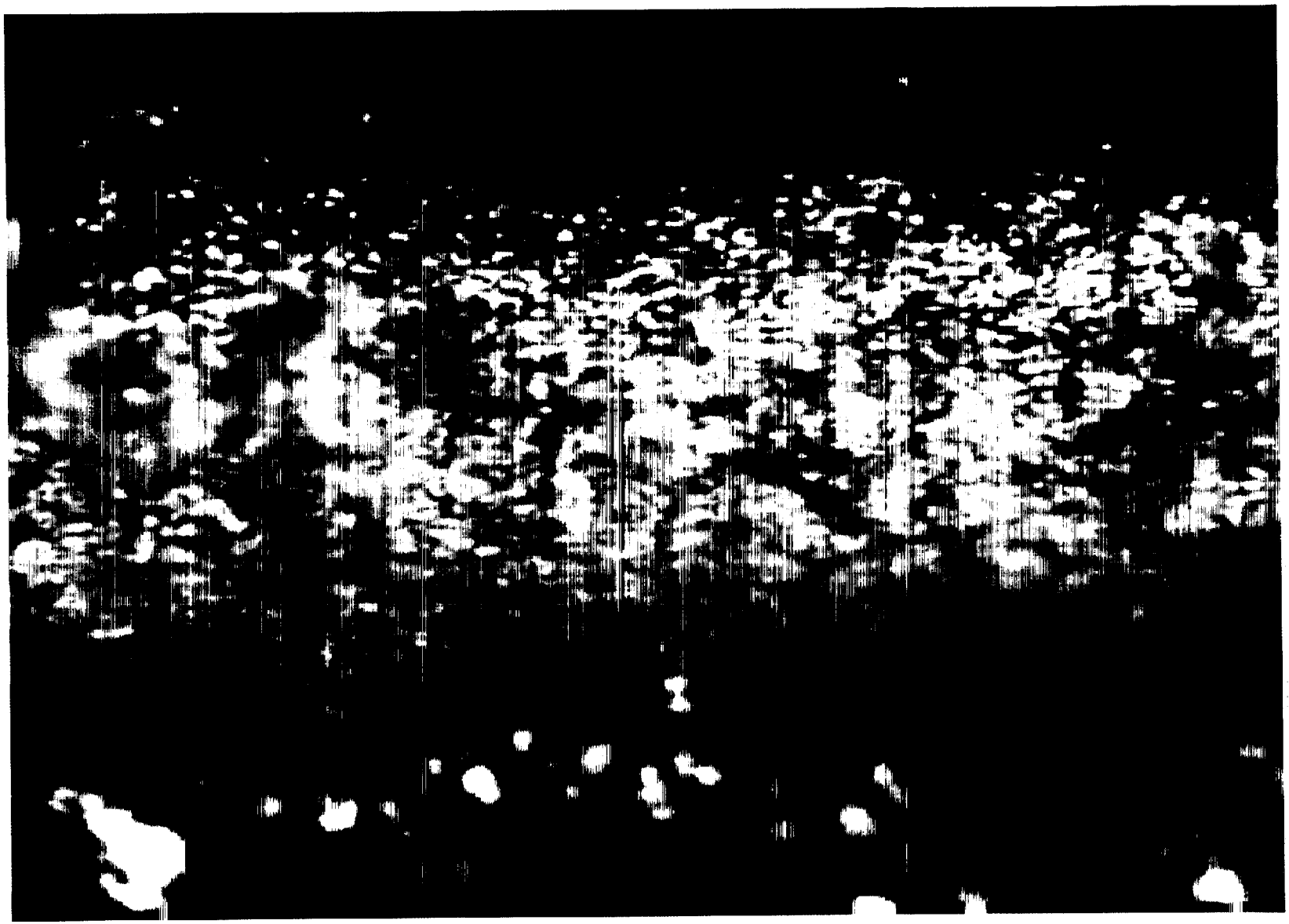

Figure 15e: Black Painted Al-2219
(10-30-2000 TC2 R3 20x Top)

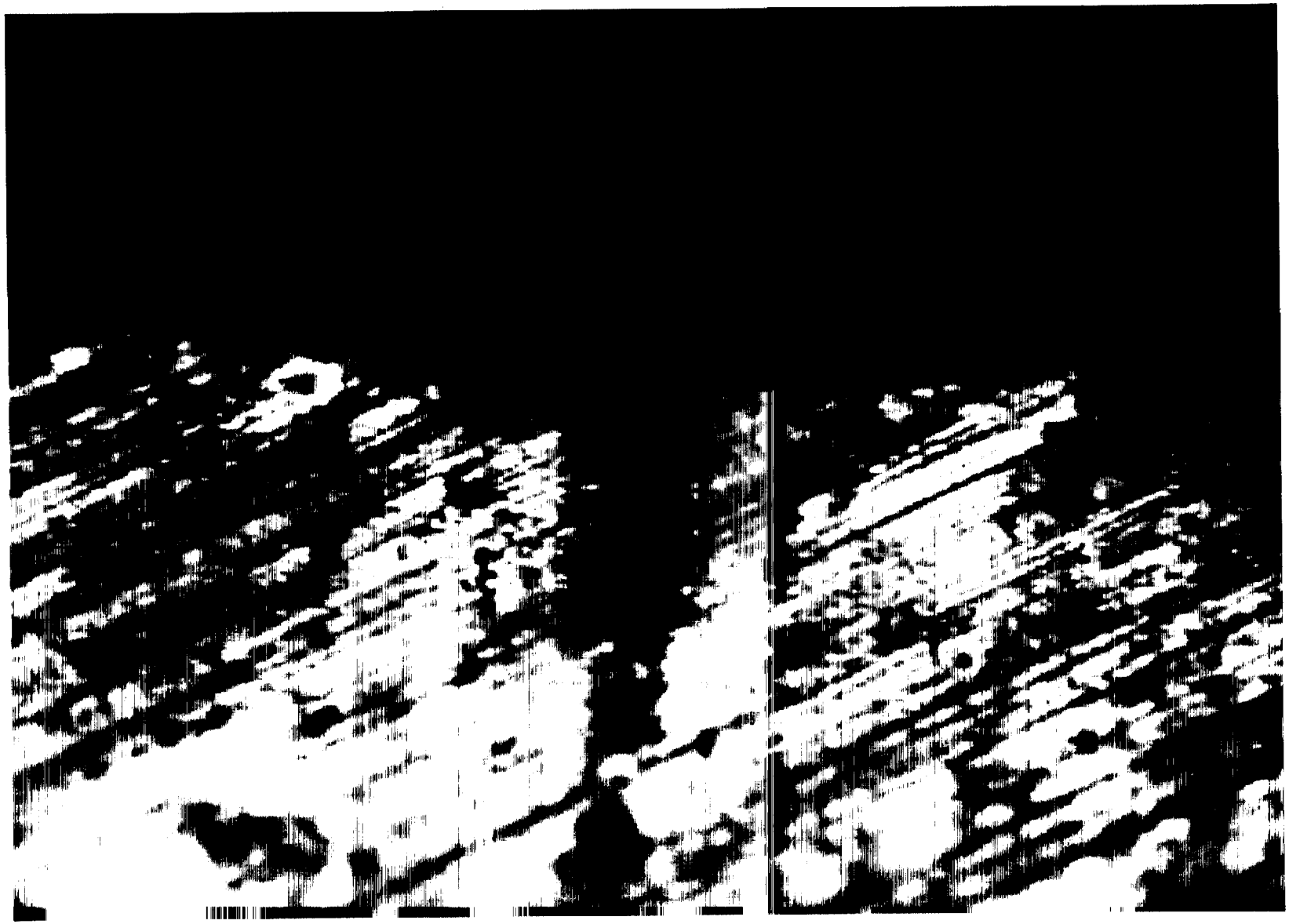

Figure 15f: Untreated Al-2219
(10-30-2000 TC3 R2 20x)

Figure 15g: Untreated Al-2219
(10-30-2000 TC3 R3 20x Top)

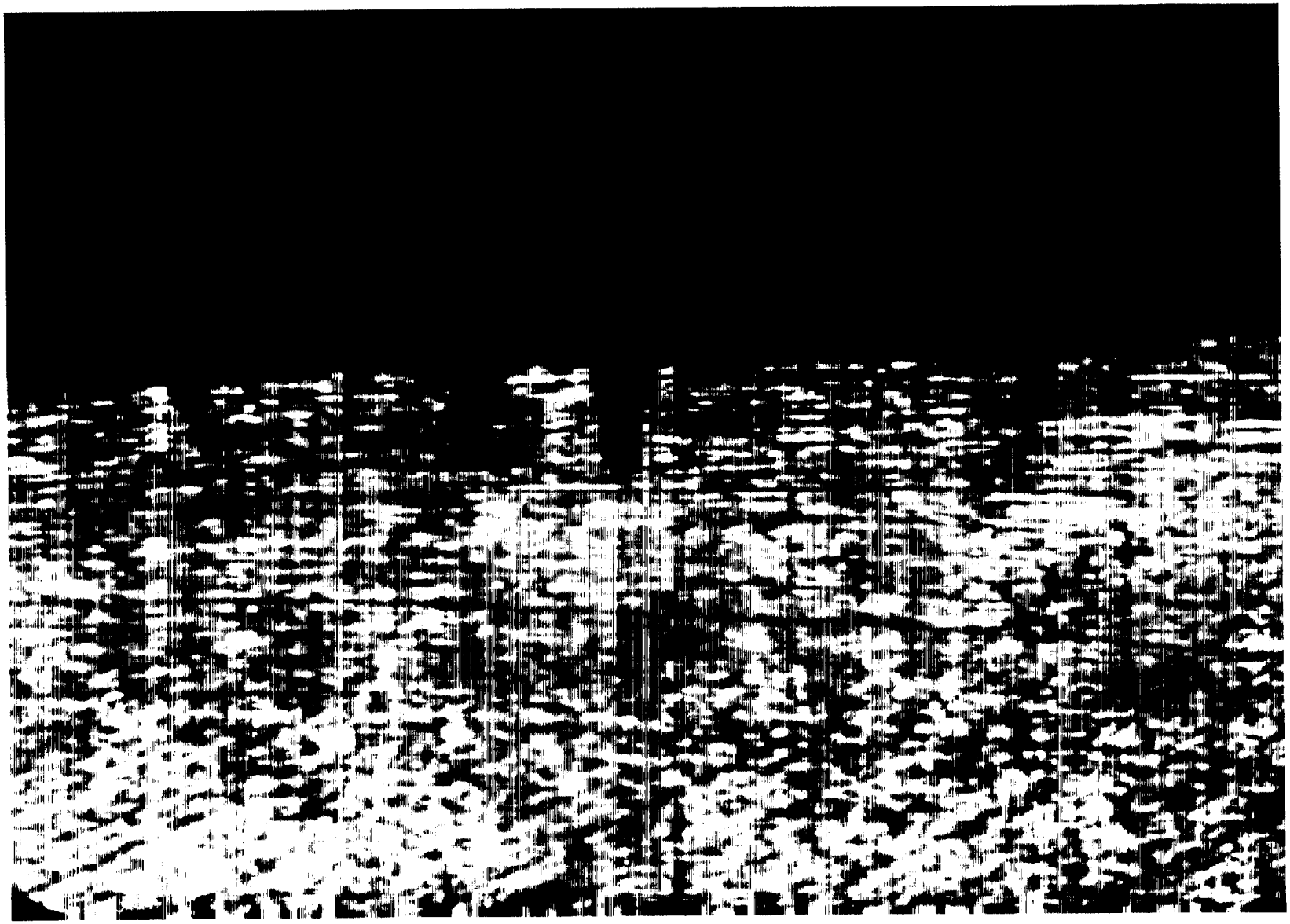

Figure 15h: Untreated Al-2219
(10-30-2000 TC3 R4 5x)

Figure 15i: Black Painted Al-2090
(Top Surface; Pulsed Mode-PRF: 20 kHz; Speed: 12.7 mm/min)
(10-27-2000 TC1 R4 10x Top)

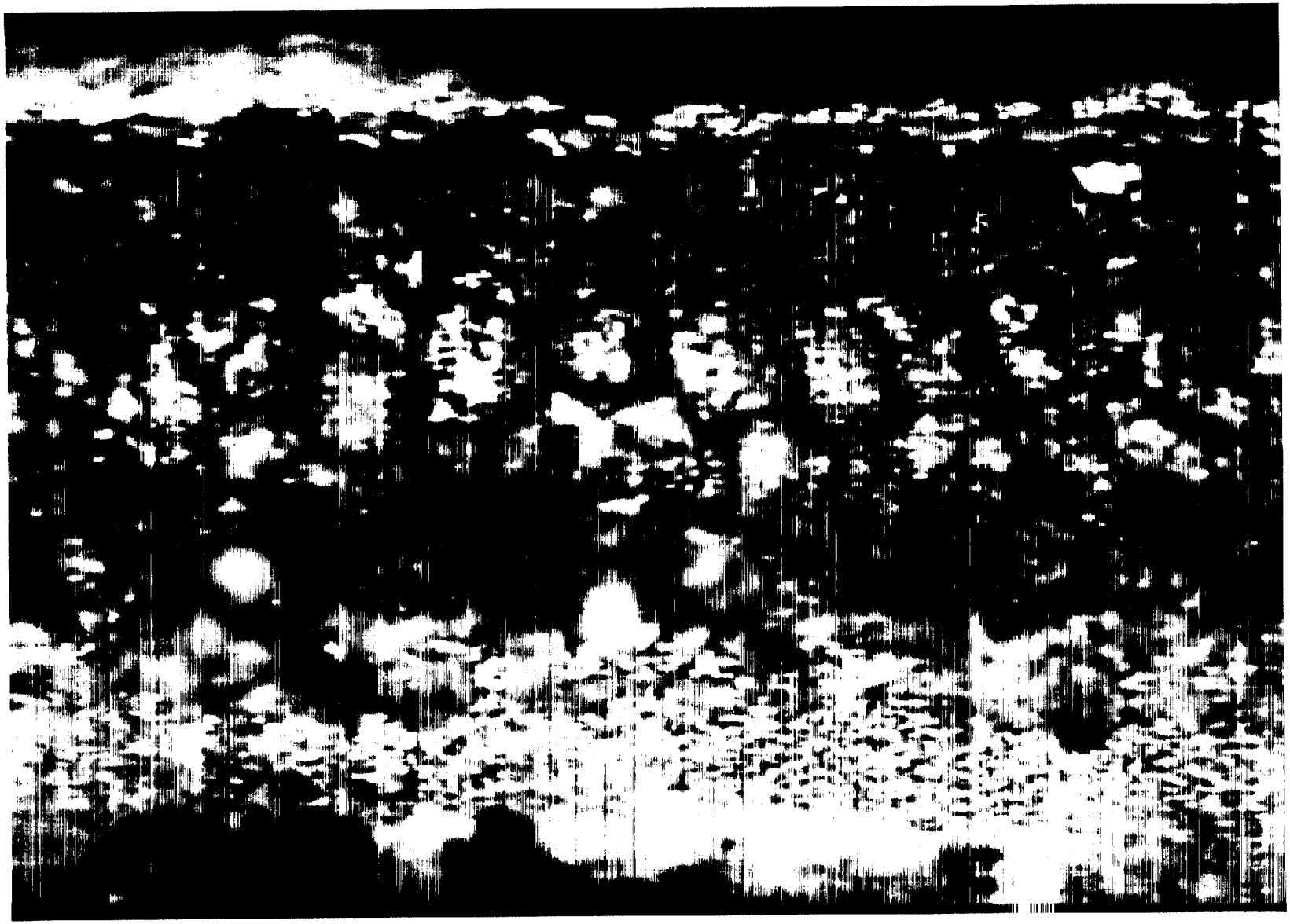

Figure 15j: Black Painted Al-2090
(10-27-2000 TC1 R4 20x Top)

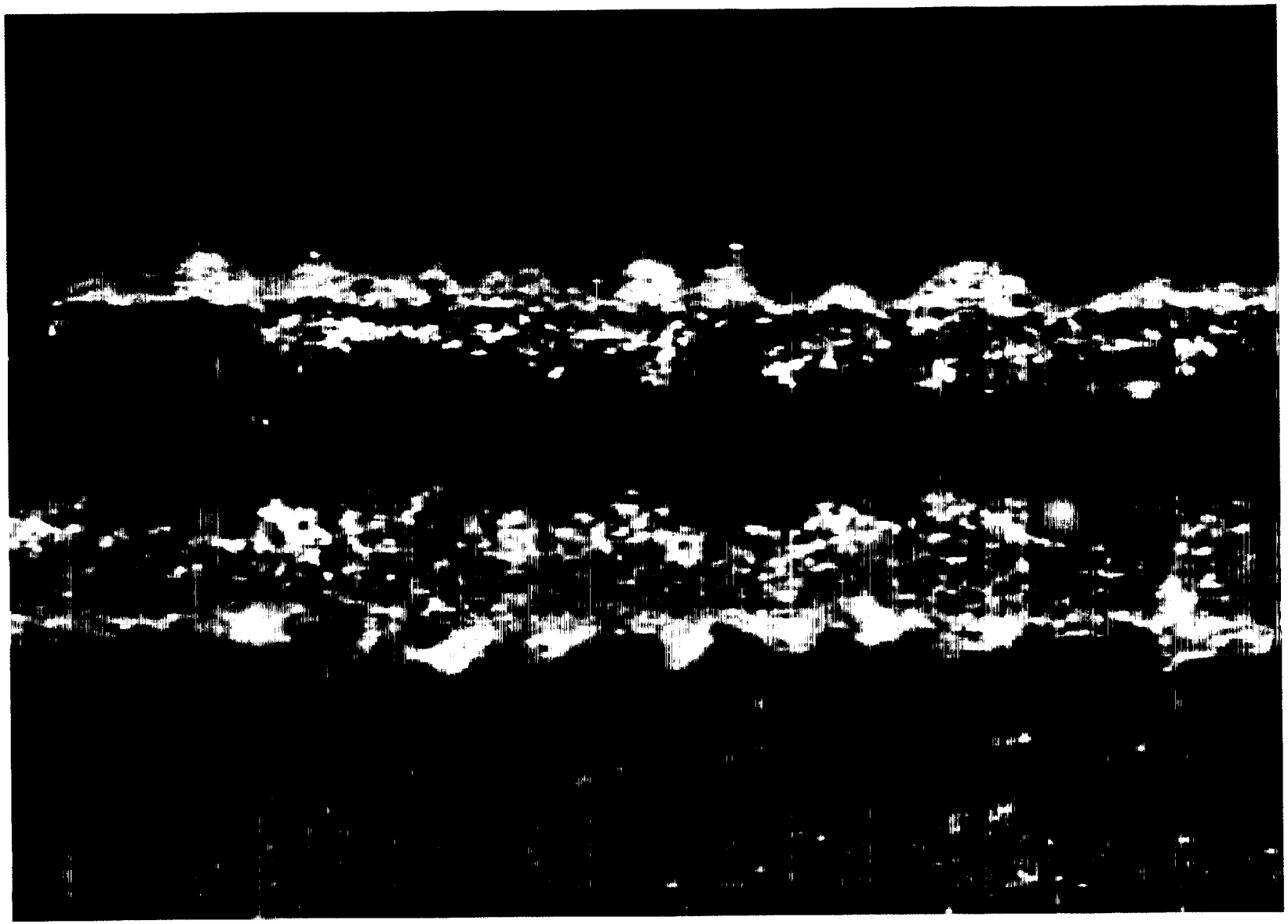

Figure 15k:Black Painted Al-2090 ()
(Top Surface; Pulsed Mode-PRF: 1 kHz; Speed: 12.7 mm/min)
(10-27-2000 TC1 R5 10x Top)

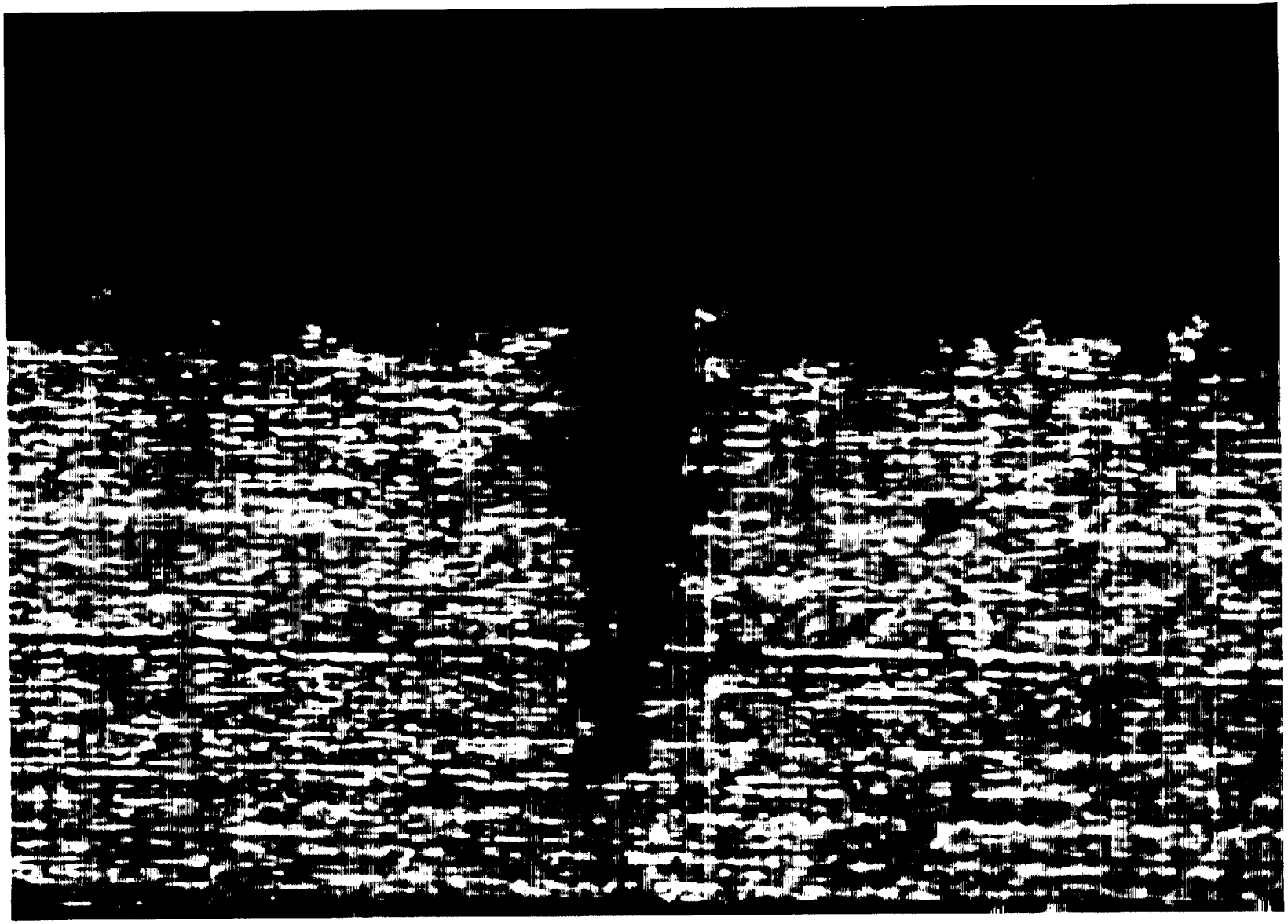

Figure 15l: Black Painted Al-2090 (Transverse Section)
(10-27-2000 TC1 R5 10x)

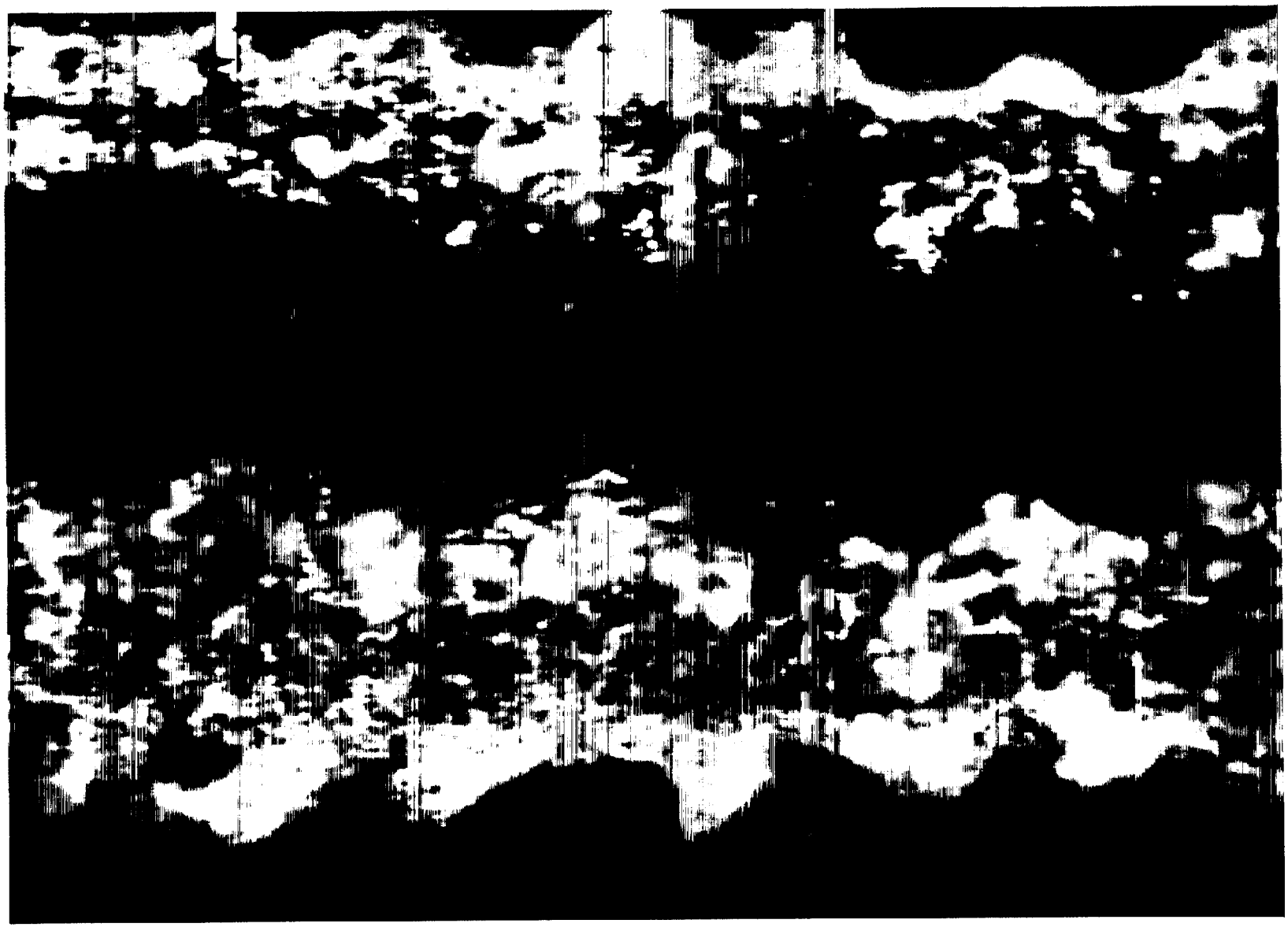

Figure 15m: Black Painted Al-2090
(10-27-2000 TC1 R5 20x Top)

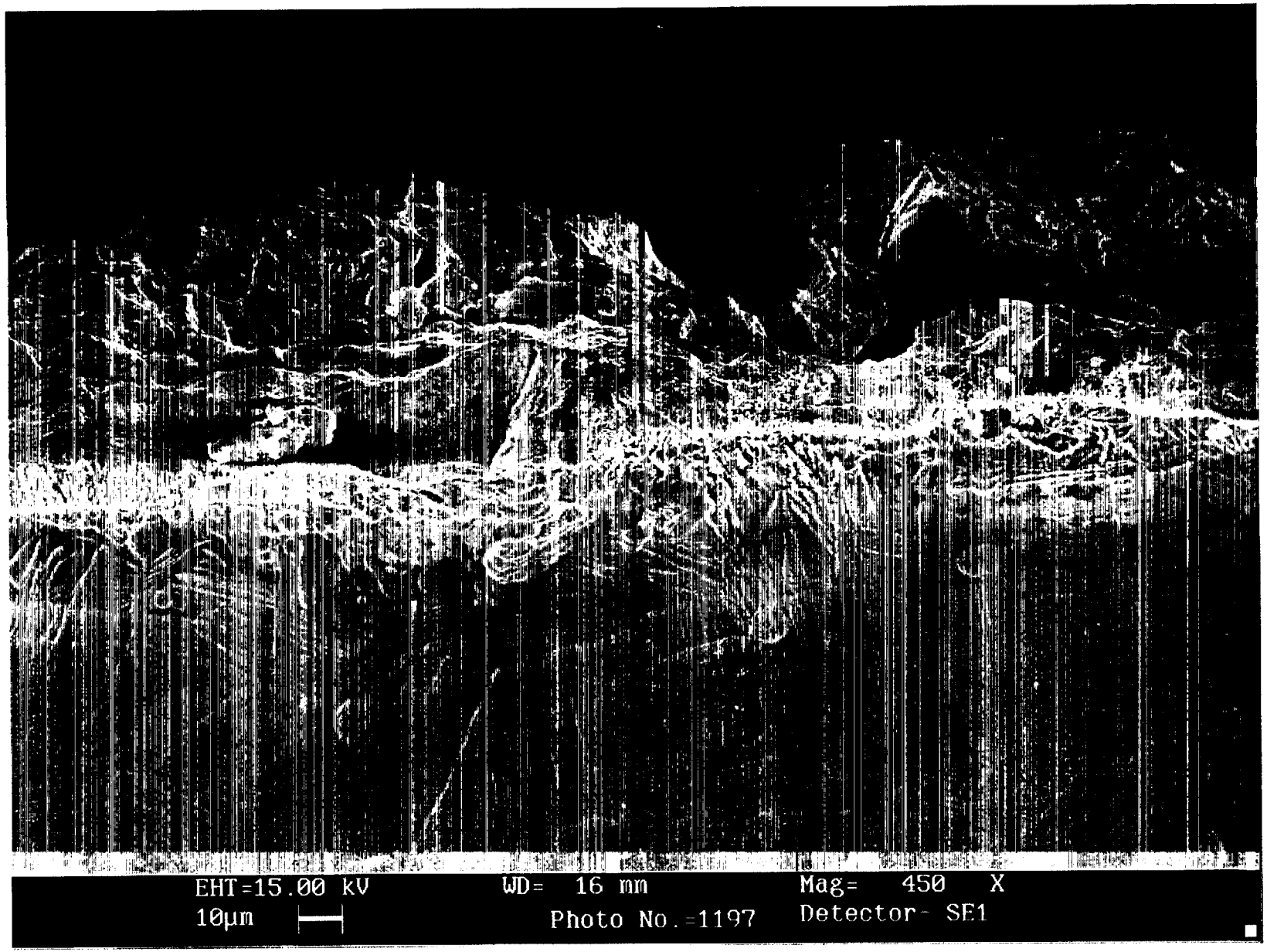

Figure 16a: Untreated Ti-6Al-4V Substrate and Ti-6Al-4V PPP
(cw mode; Power: 46.3 W; Speed: 25.4 mm/min)
(10-10-2000 TC1 R3 0450x)

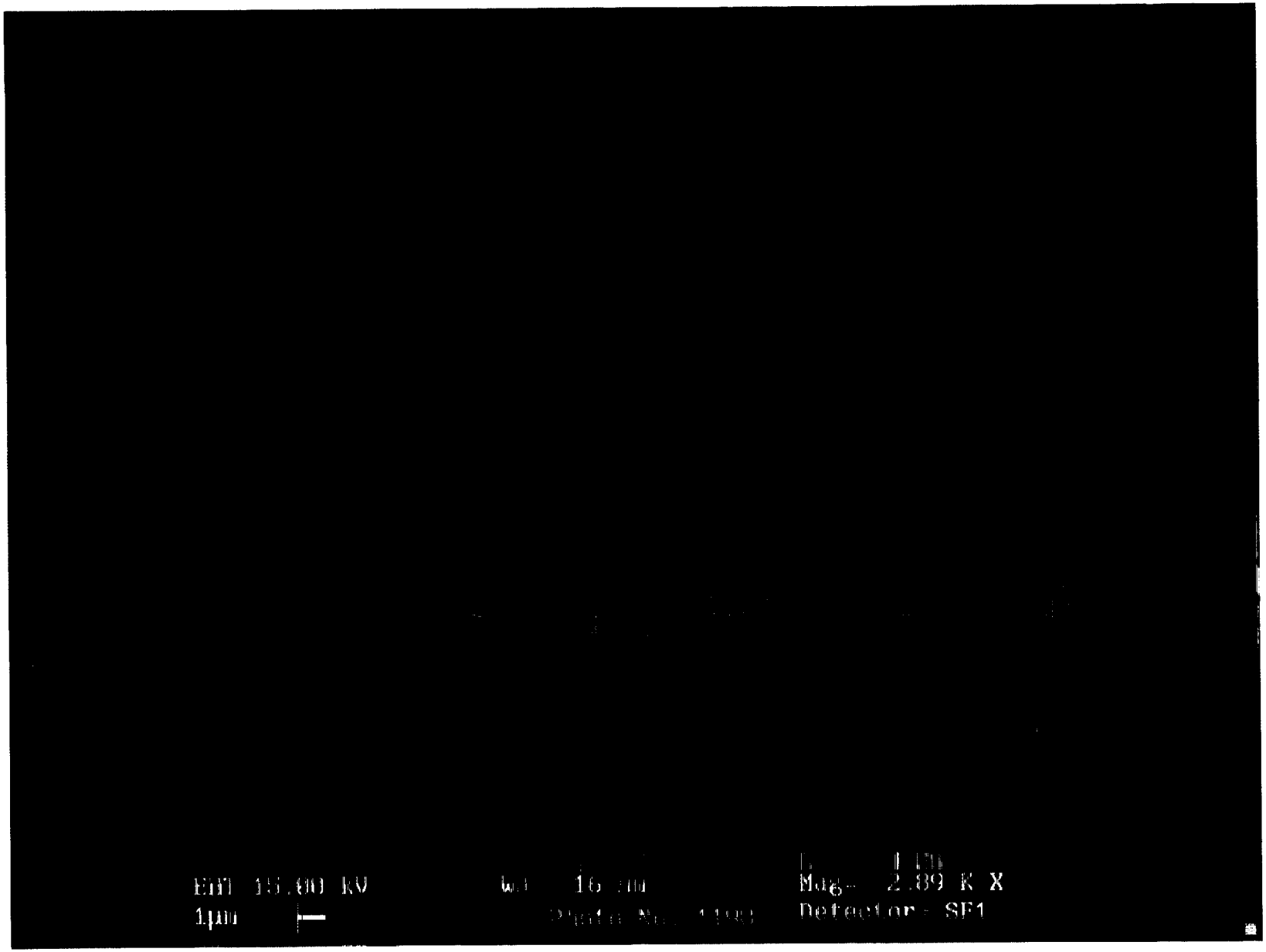

Figure 16b: Untreated Ti-6Al-4V Substrate and Ti-6Al-4V PPP (Interface)
(10-10-2000 TC1 R3 2890x)

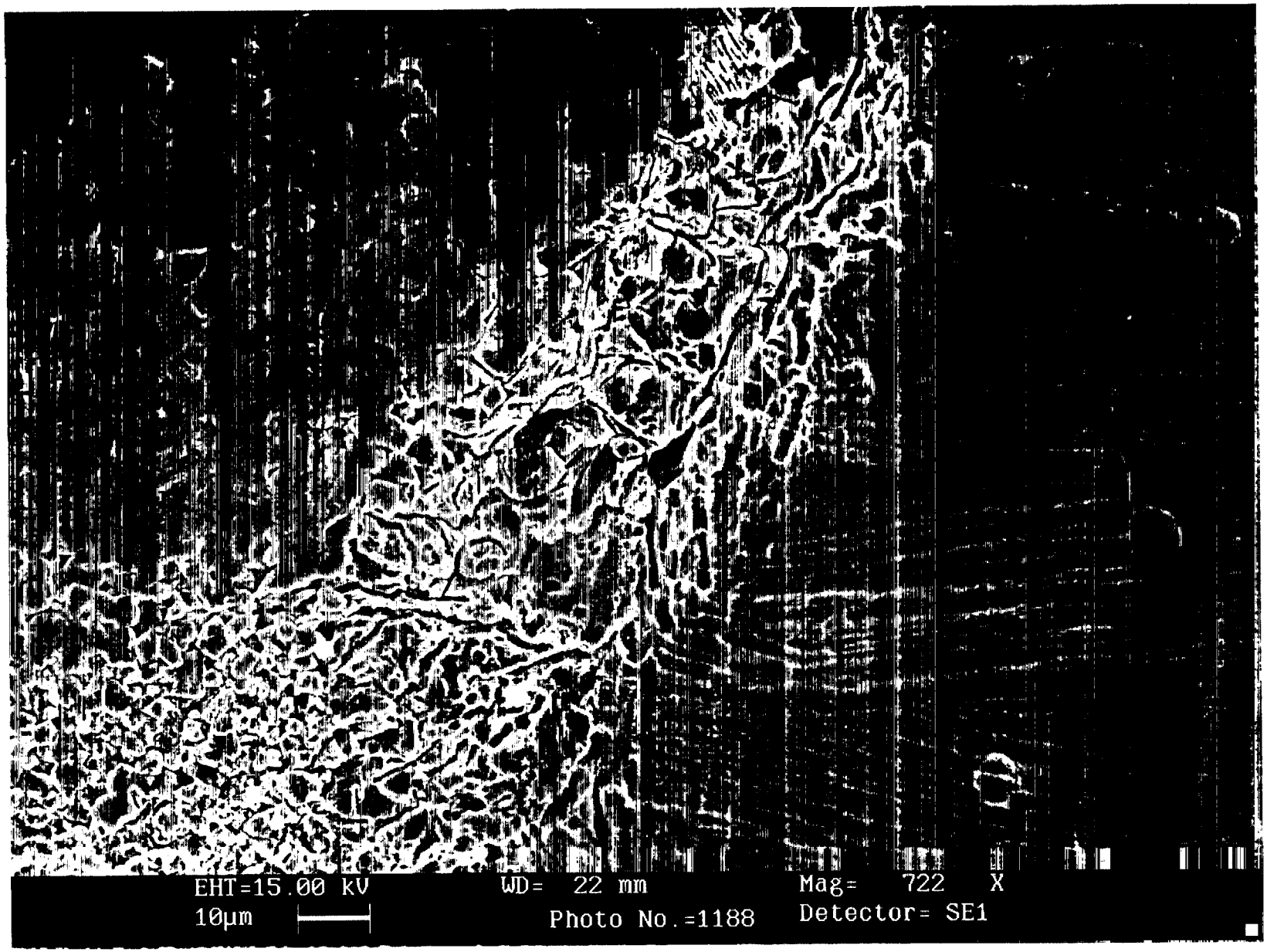

Figure 16c: Black Painted Ti-6Al-4V Substrate & Al-2219 PPP
(10-30-2000 TC4 R5 0637x (Top Center of Coating))

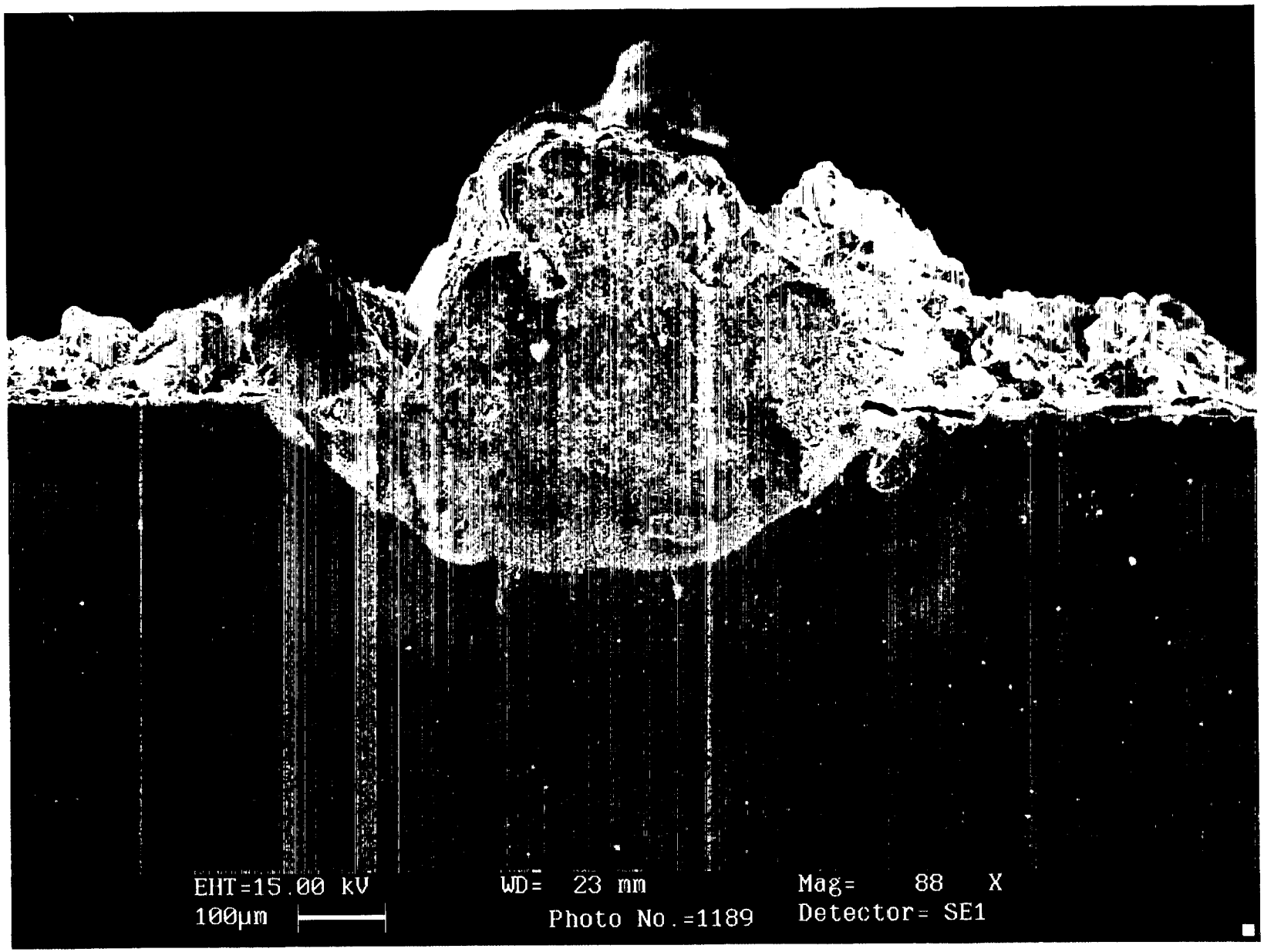

Figure 16d: Black Painted Ti-6Al-4V Substrate & Al-2219 PPP
(10-30-2000 TC4 R5 88x)

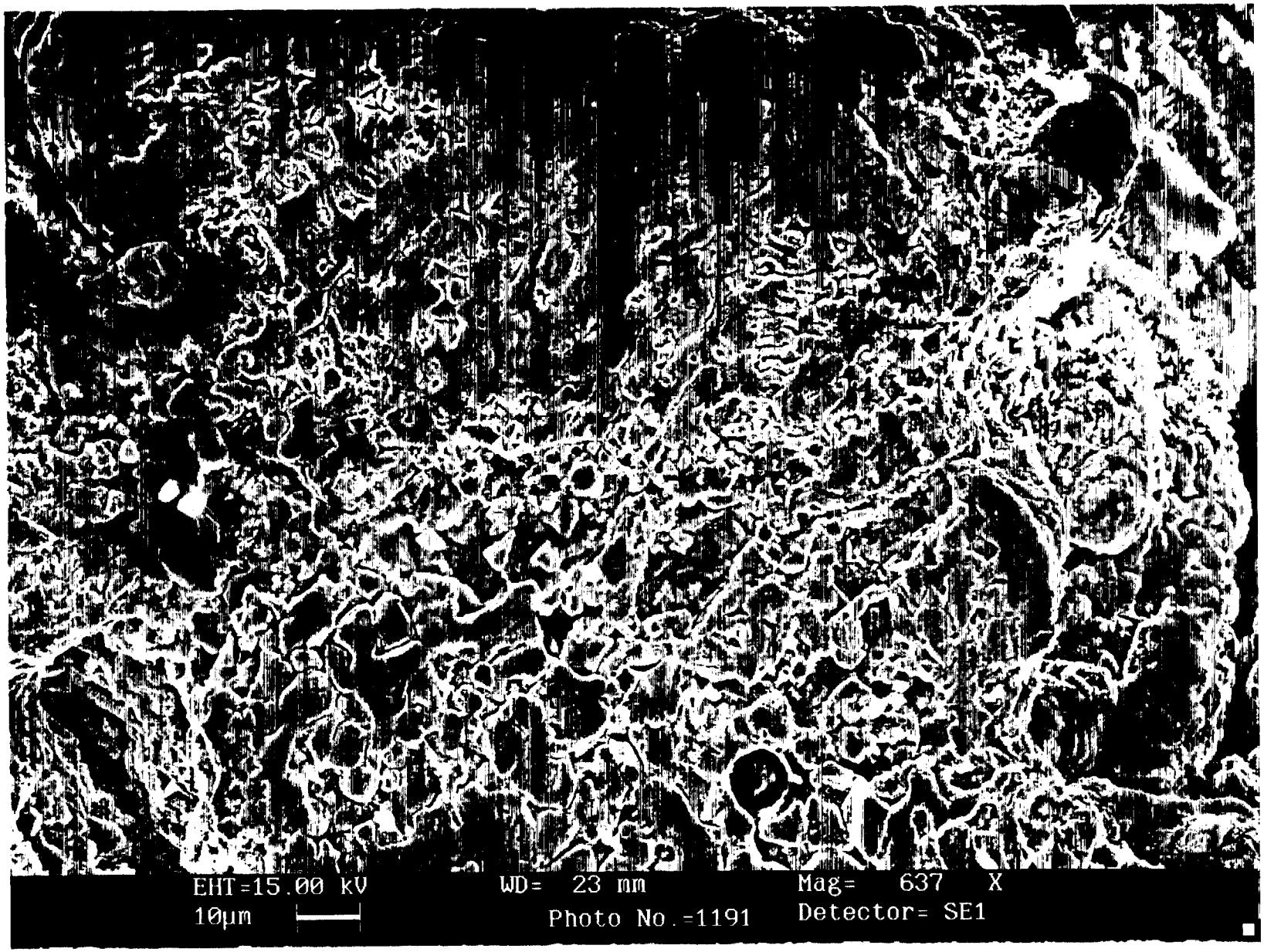

Figure 16e: Black Painted Ti-6Al-4V Substrate & Al-2219 PPP
(10-30-2000 TC4 R5 0637x (Top Center of Coating))

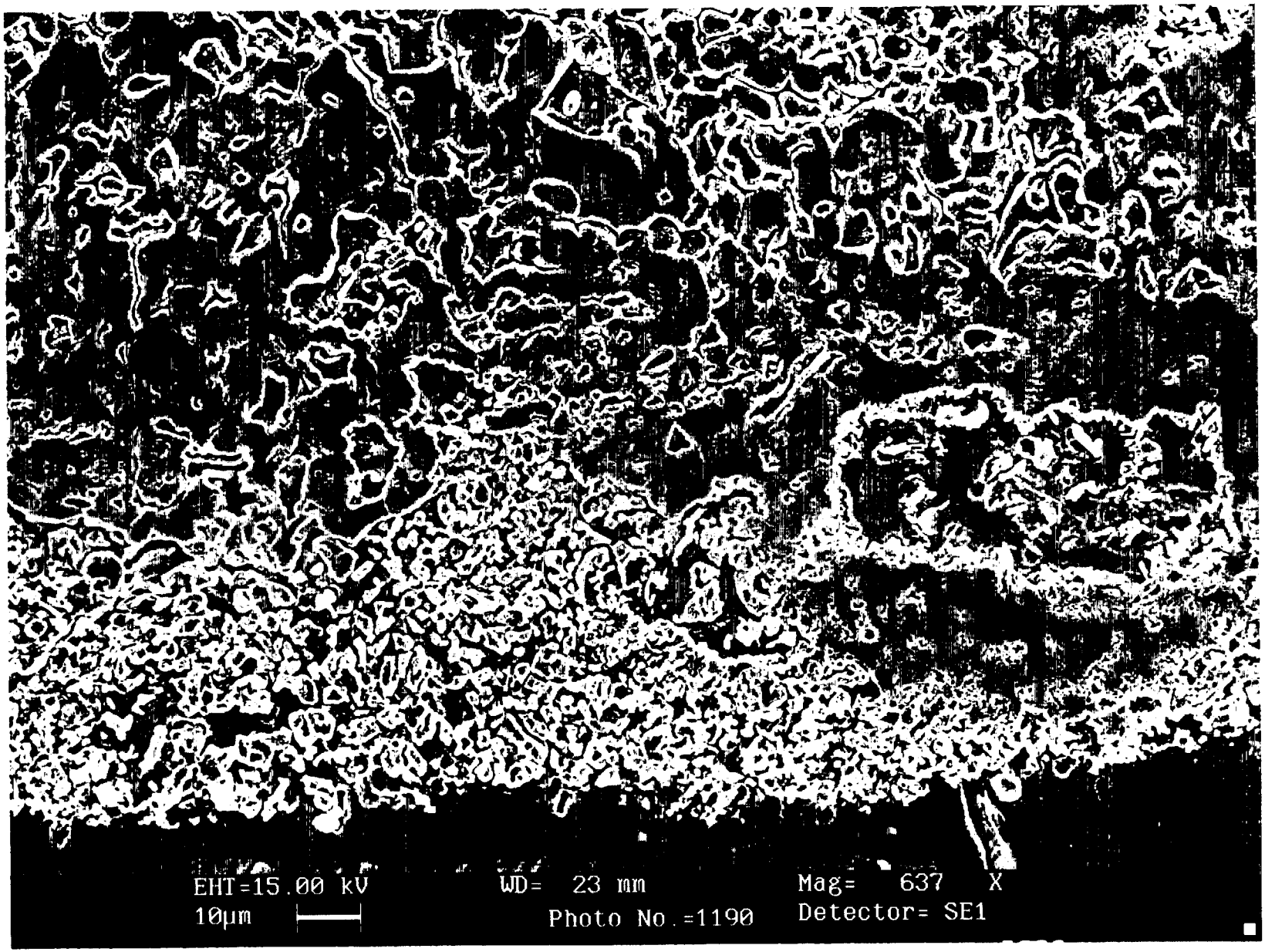

Figure 16f: Black Painted Ti-6Al-4V Substrate & Al-2219 PPP
(10-30-2000 TC4 R5 0637x SC Interface)

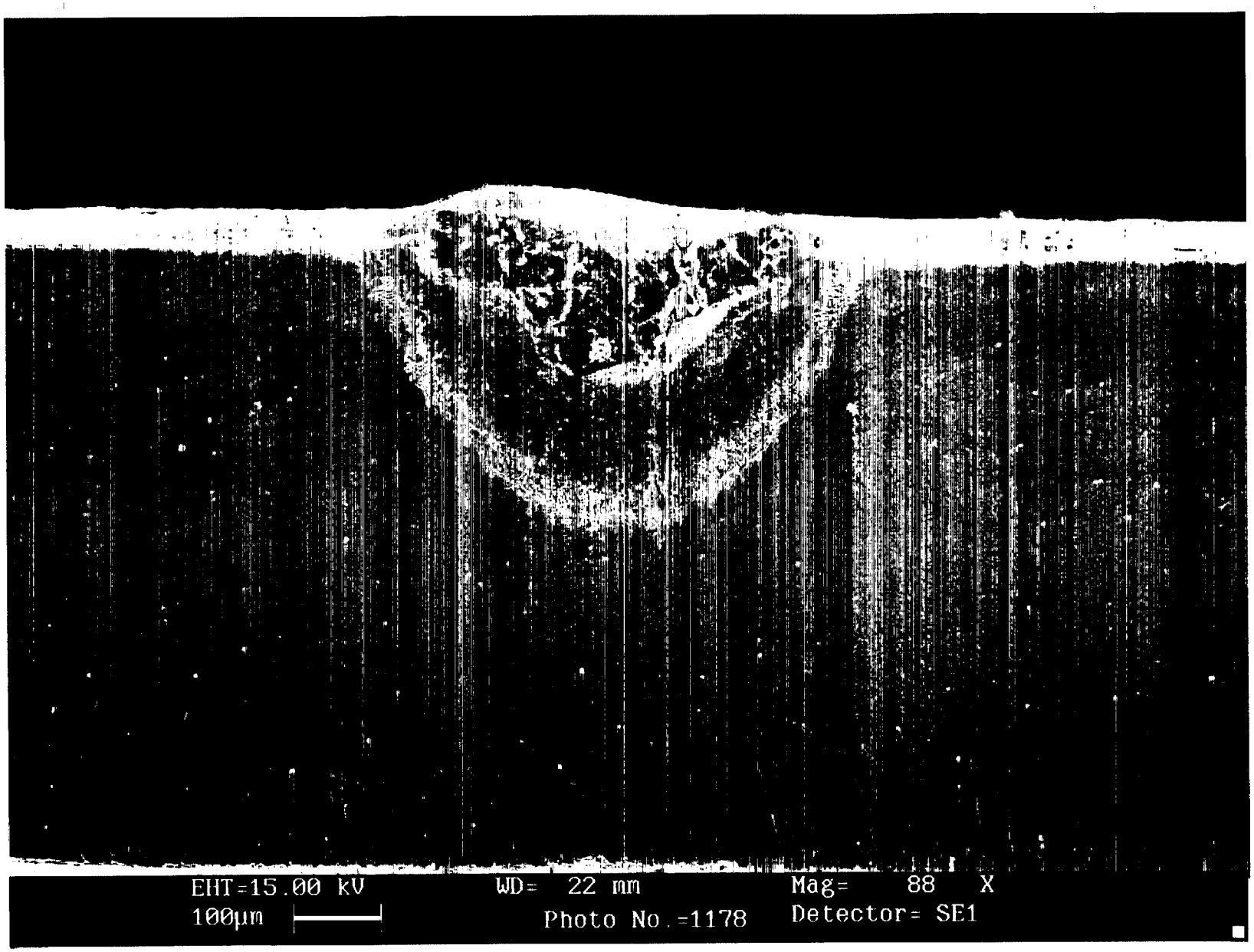

Figure 16g: Laser Nitridation of Untreated Ti-6Al-4V (11-1-2000 TC4 R1 88x)

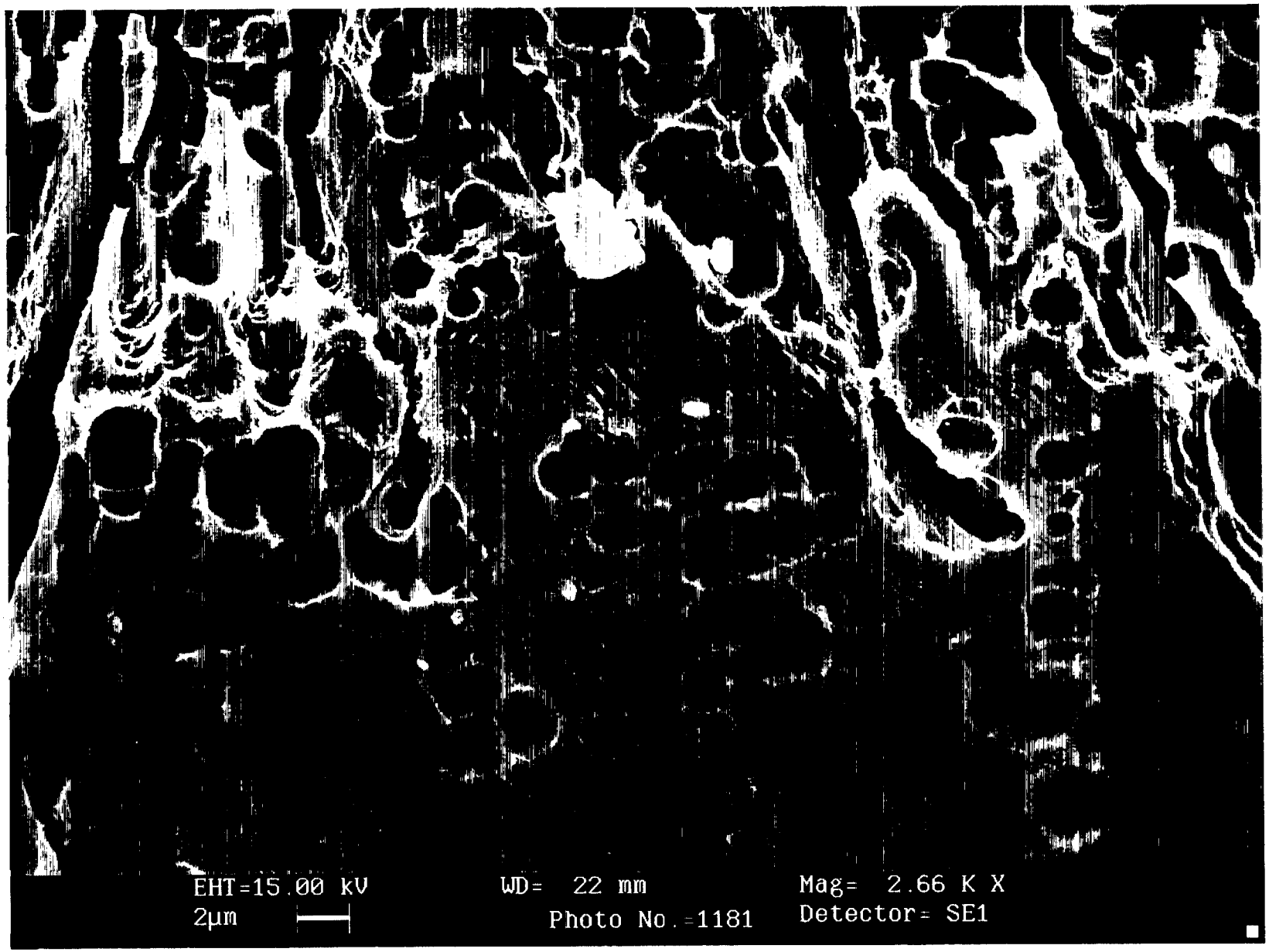

Figure 16h: Laser Nitridation of Untreated Ti-6Al-4V(Interface)
(11-1-2000 TC4 R1 2660x)

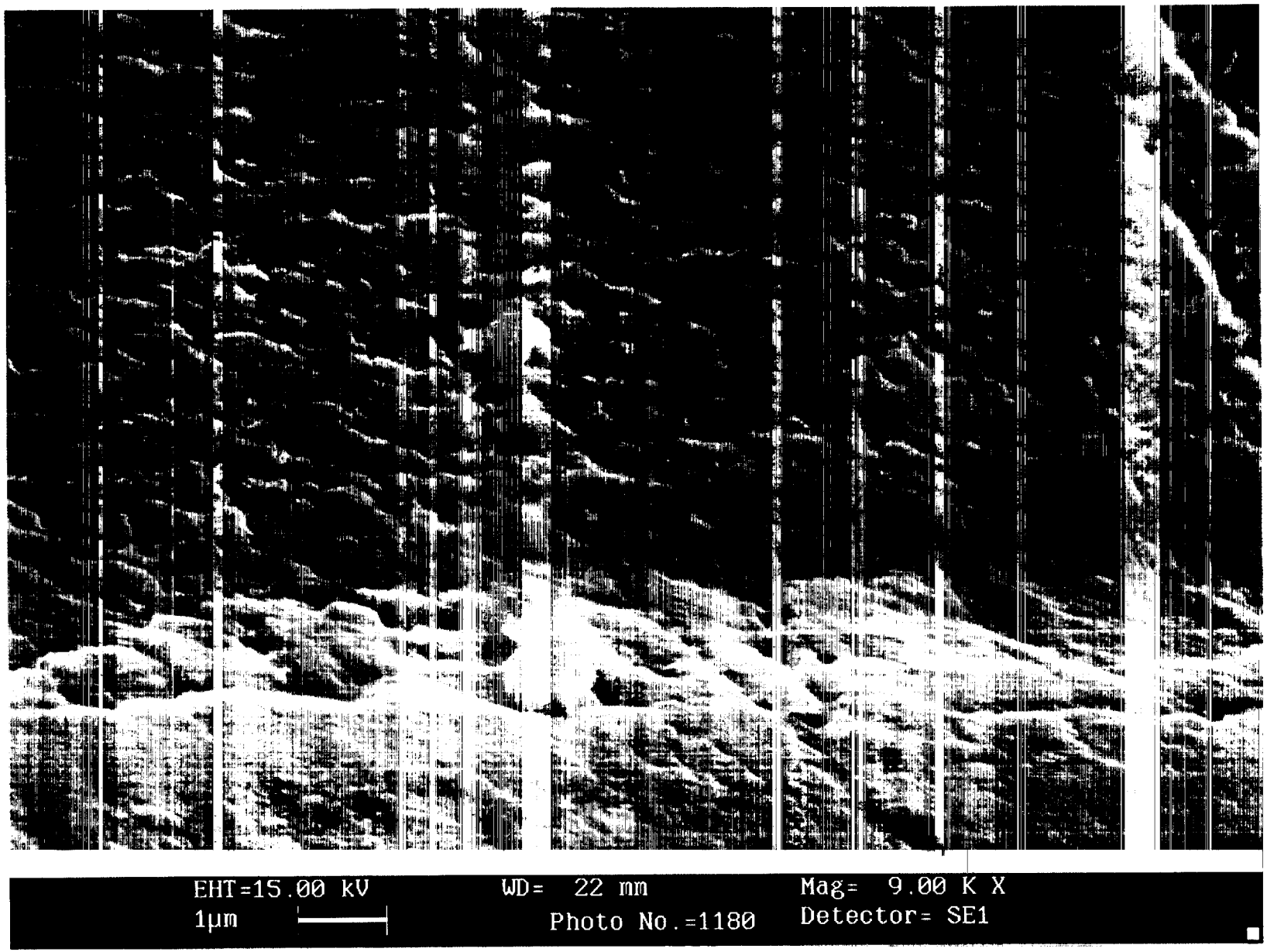

Figure 16i: Laser Nitridation of Untreated Ti-6Al-4V(Top Surface)
(11-1-2000 TC4 R1 9000x)

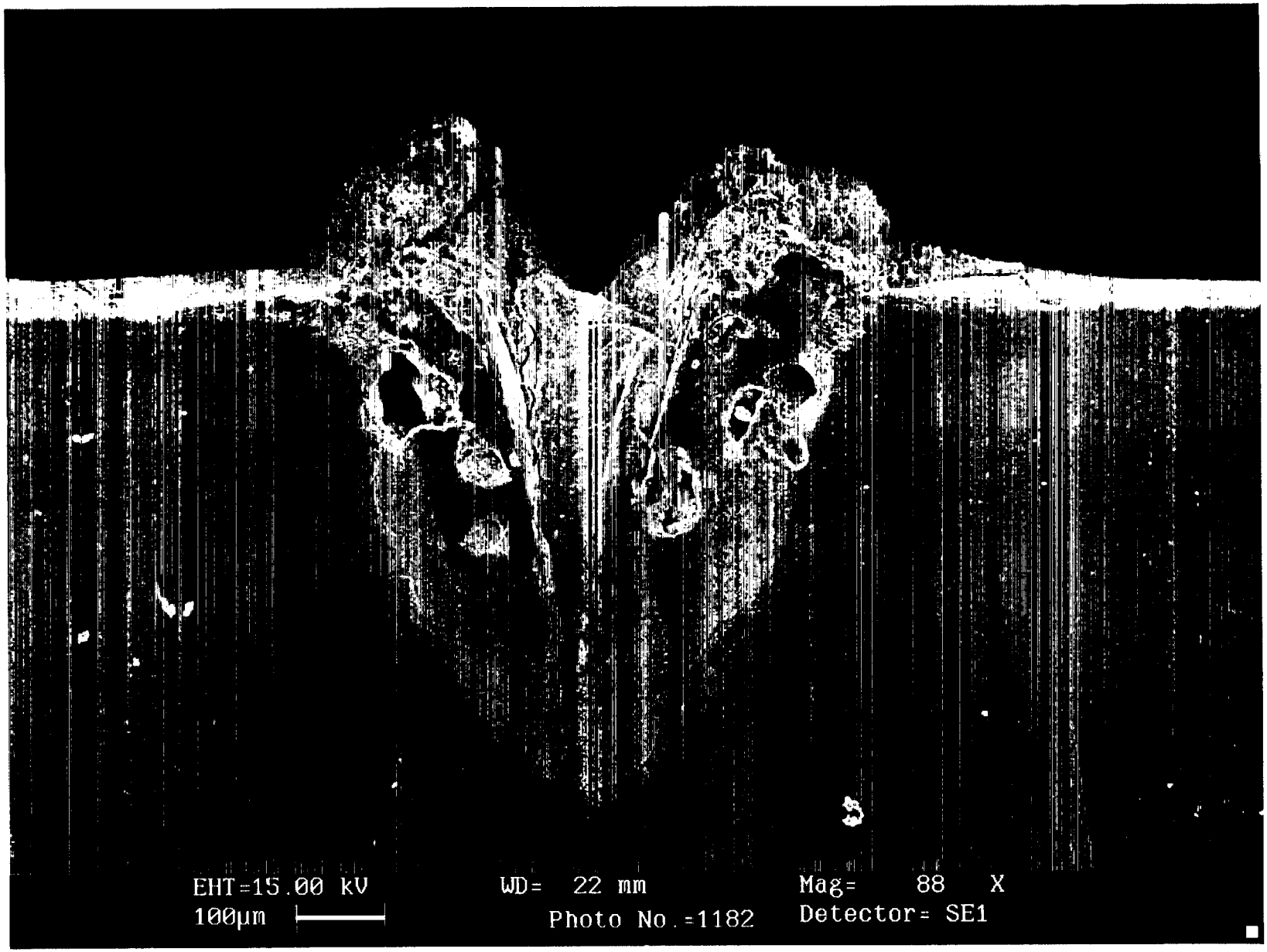

Figure 16j: Laser Nitridation of Untreated Ti-6Al-4V(PRF = 10 kHz)
(11-1-2000 TC4 R7 88x)

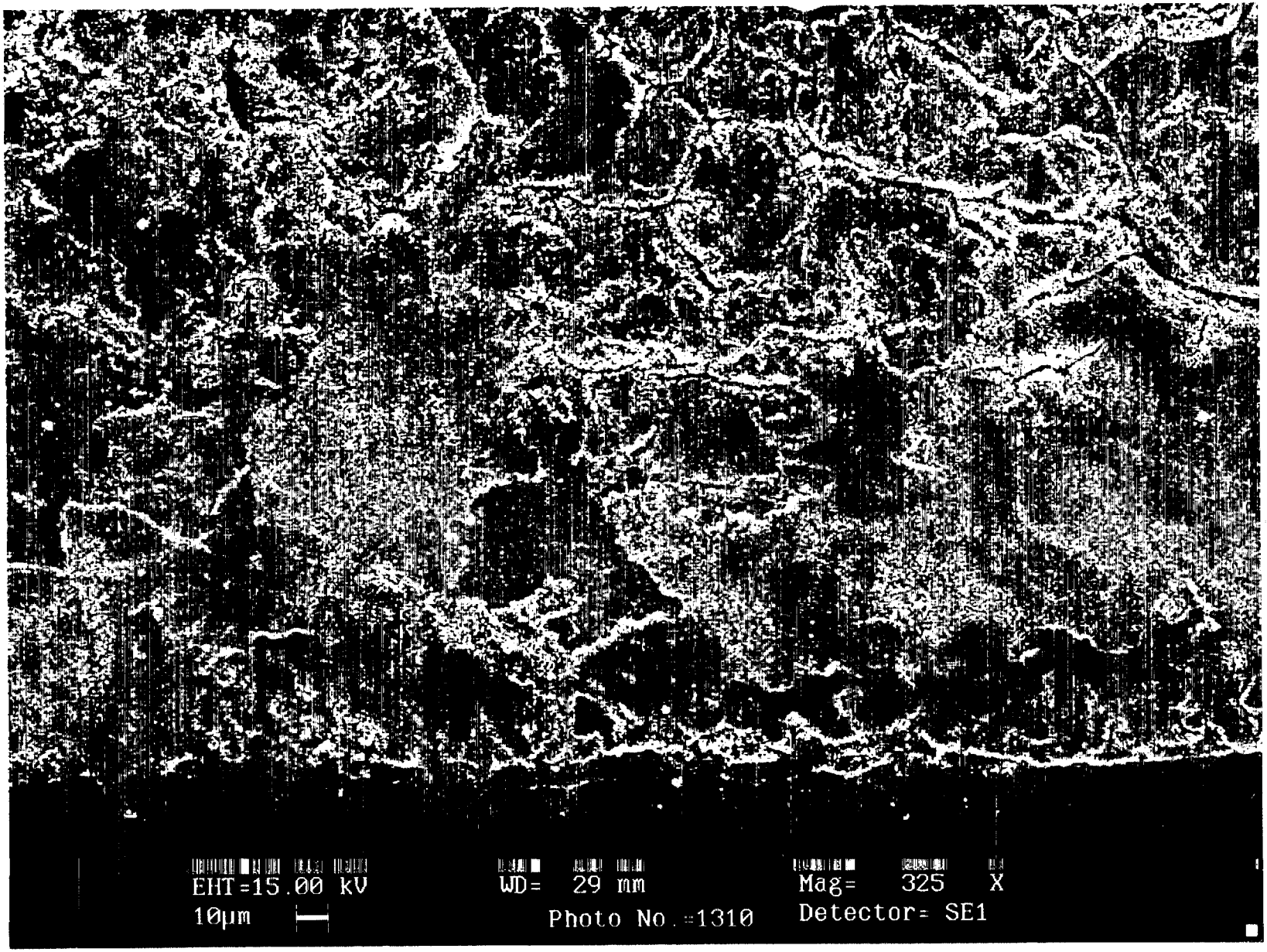

Figure 16k: Untreated Al-2219
(10-30-2000 TC2 R3 325x)

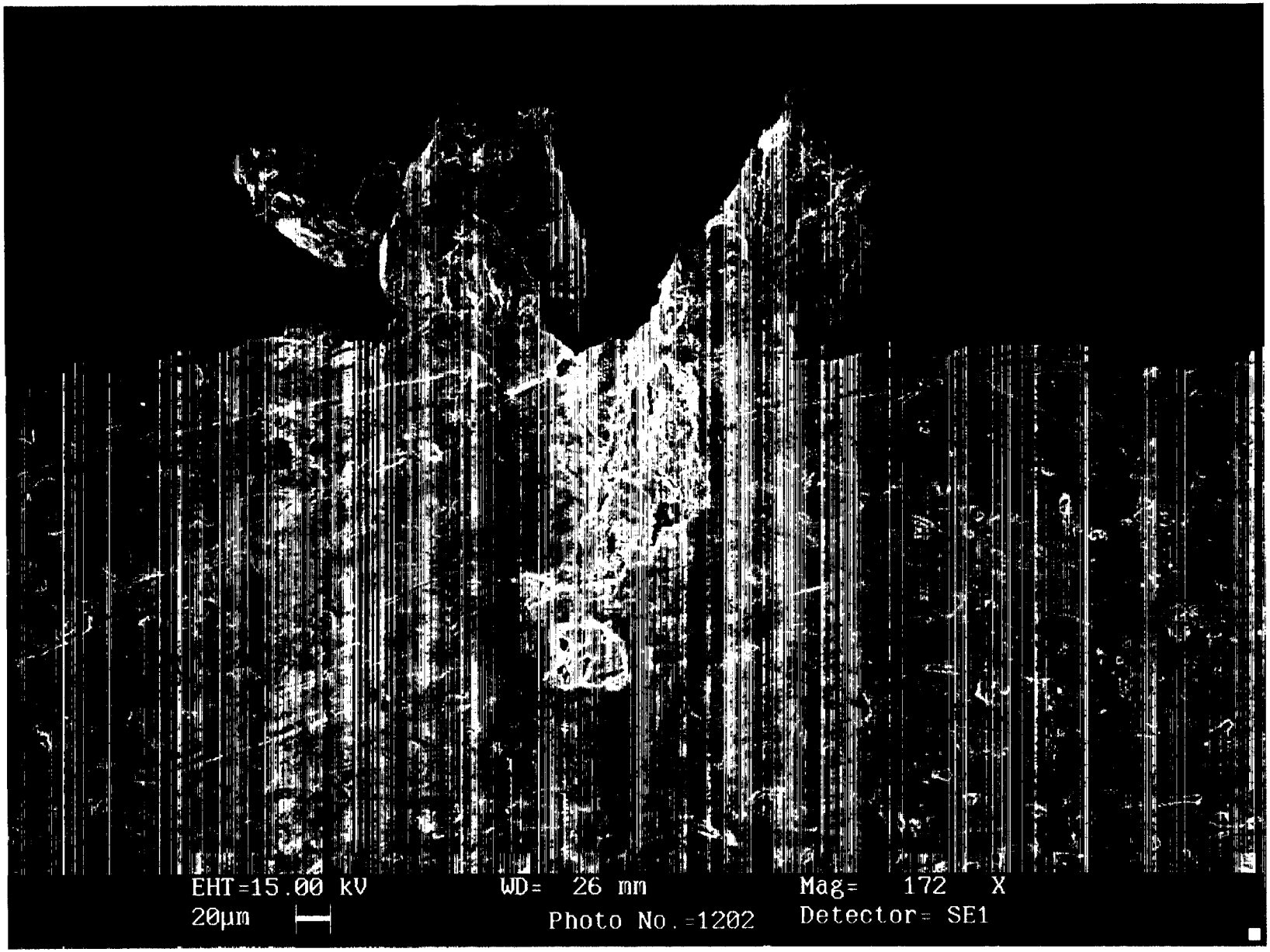

Figure 16l: Untreated Al-2219
(10-30-2000 TC3 R6 172x)

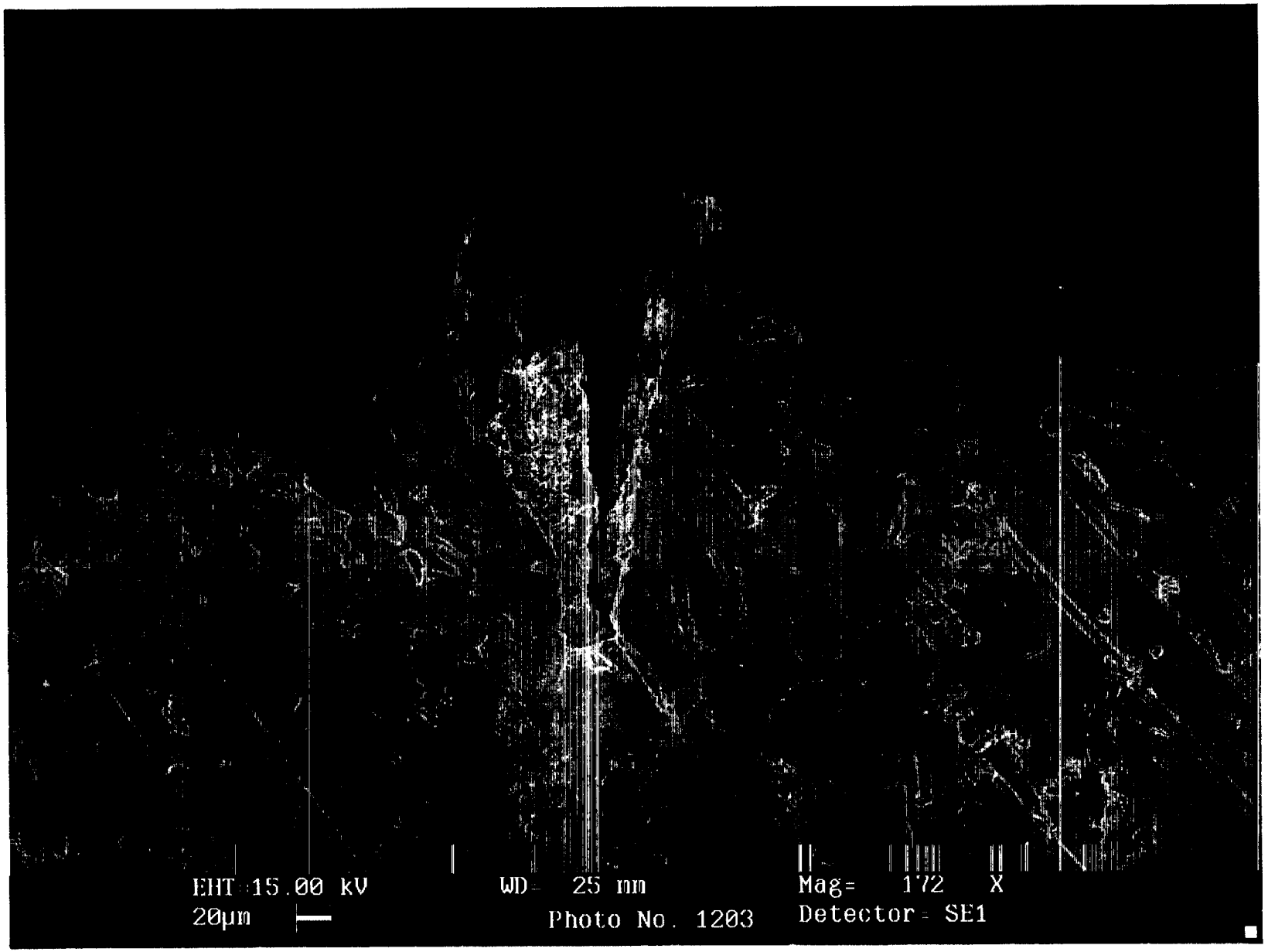

Figure 16m: Untreated Al-2219
(10-30-2000 TC3 R10 172x)

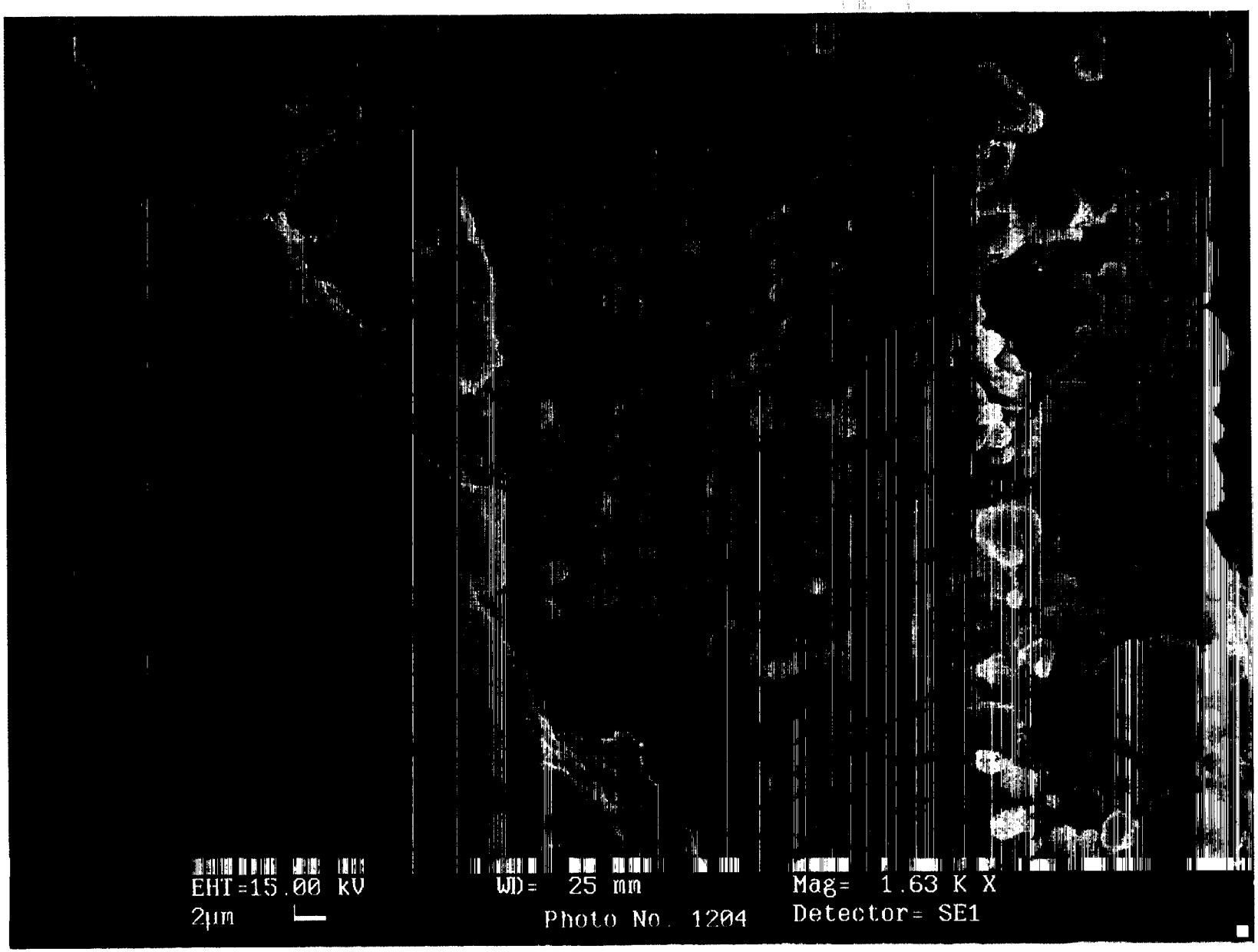

Figure 16n: Untreated Al-2219
(10-30-2000 TC3 R10 1630x)

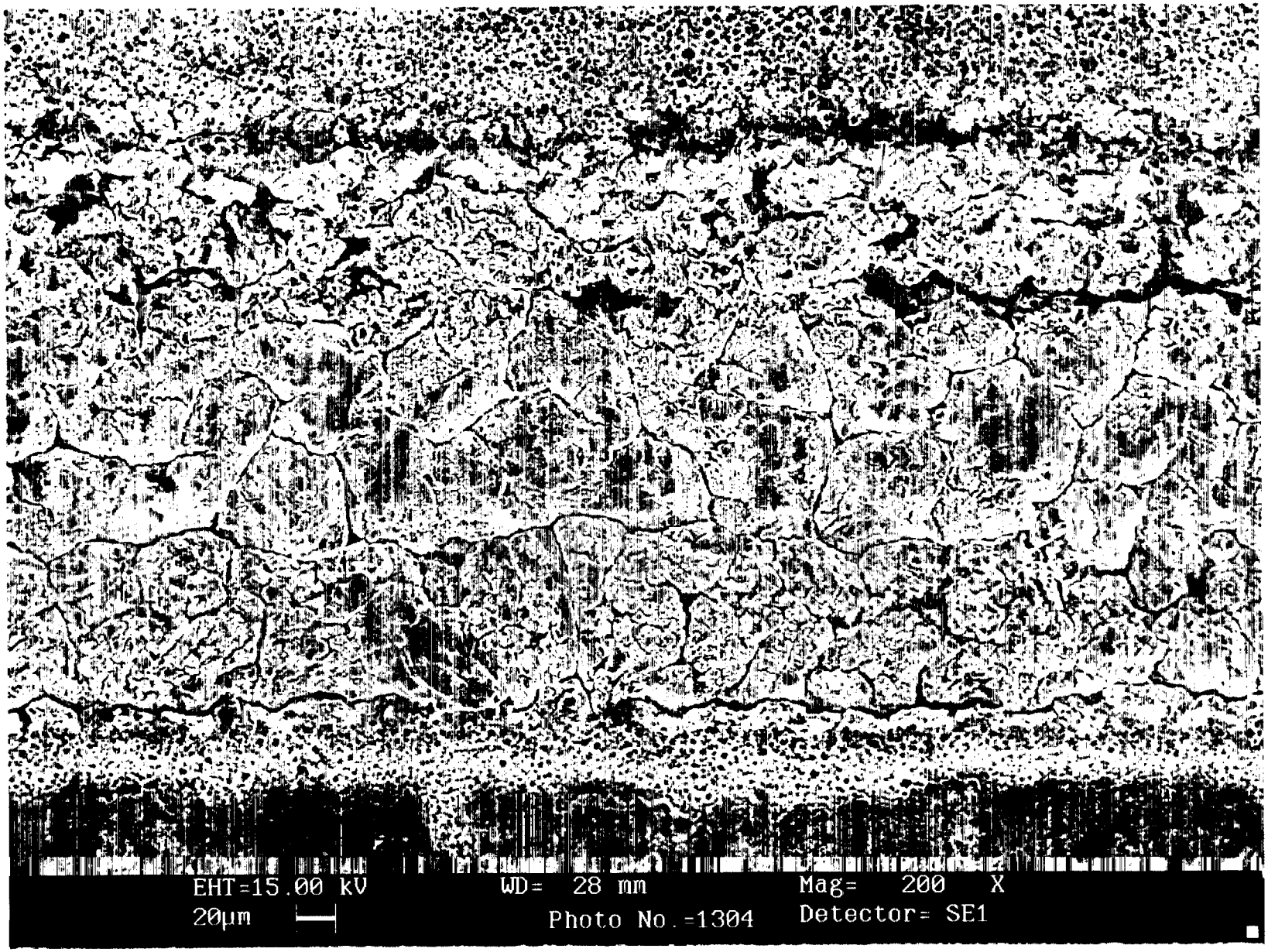

Figure 16o: Black Painted Al-2090 (Top Surface)
(Pulsed Mode; PRF: 20 kHz; Speed: 12.7 mm/min)
(10-27-2000 TC1 R4 200x)

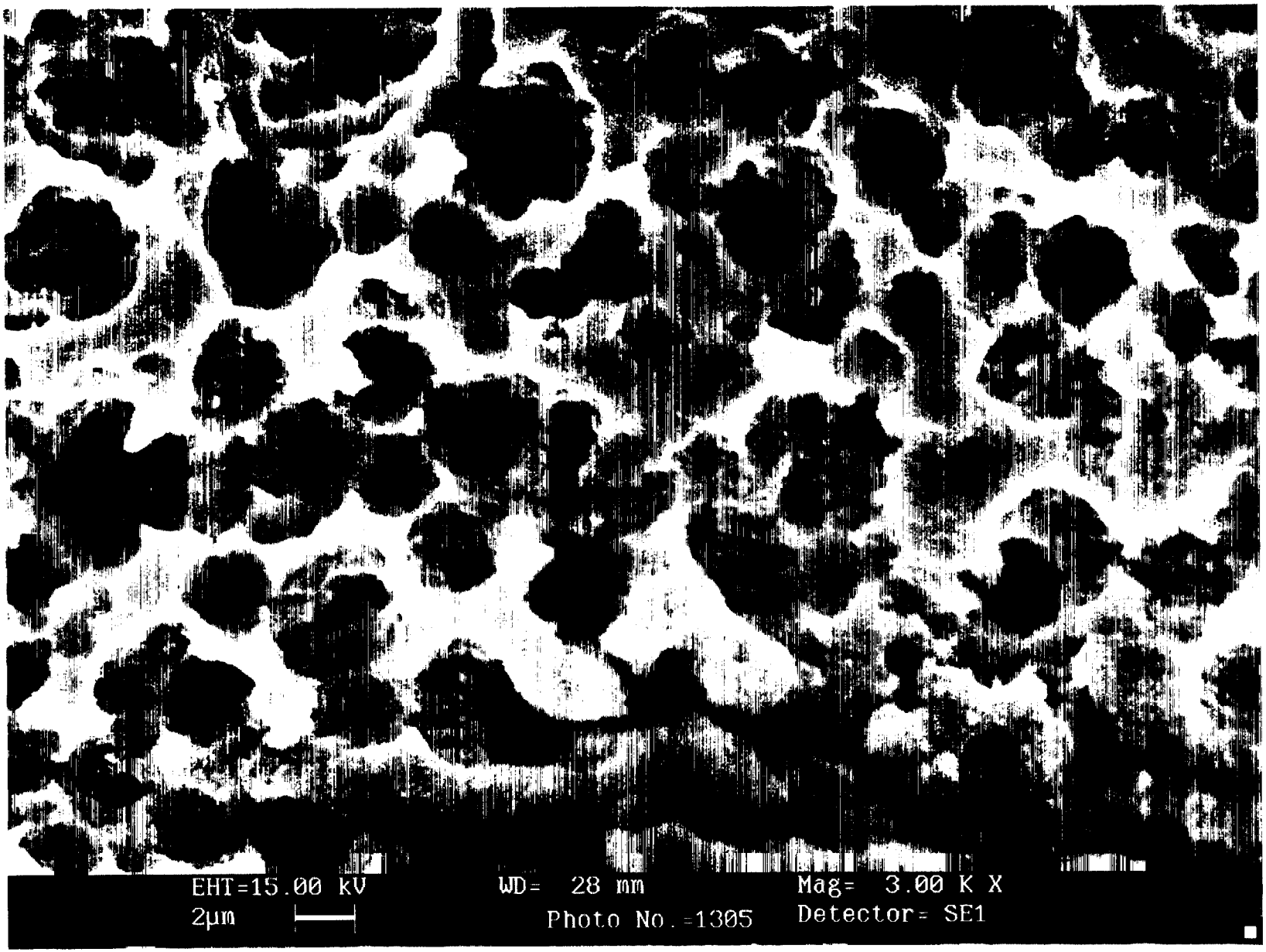

Figure 16p: Black Painted Al-2090
(10-27-2000 TC1 R4 3000x)

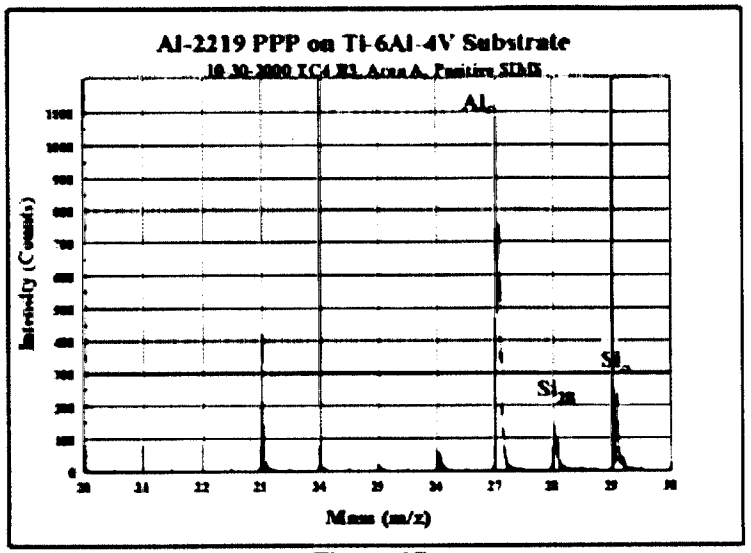

Figure 17a

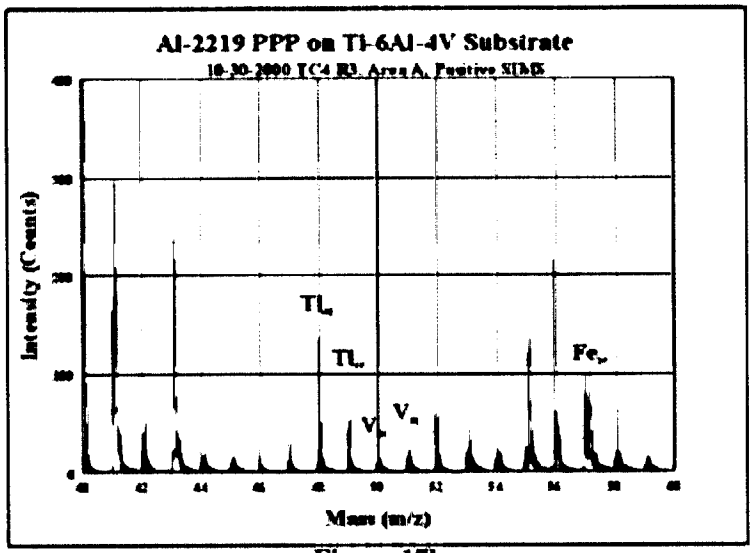

Figure 17b

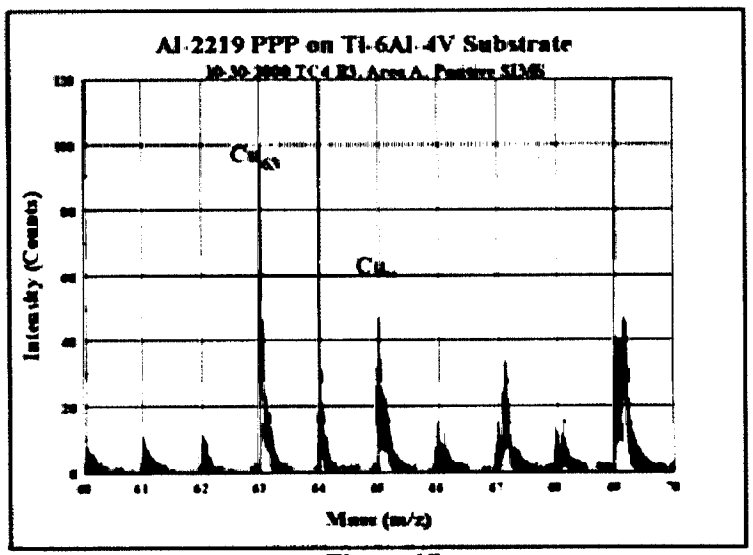

Figure 17c

Figures 17a-c: SIMS Analysis of Al-2219 PPP on Ti-6Al-4V Substrate

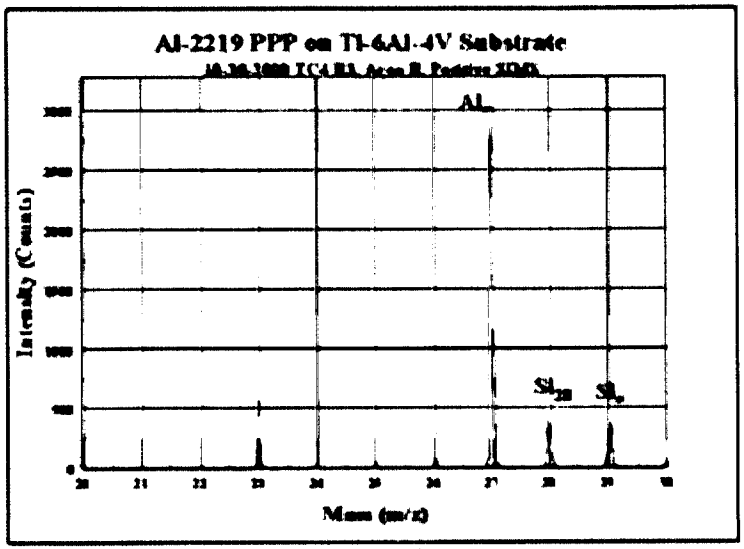

Figure 17d

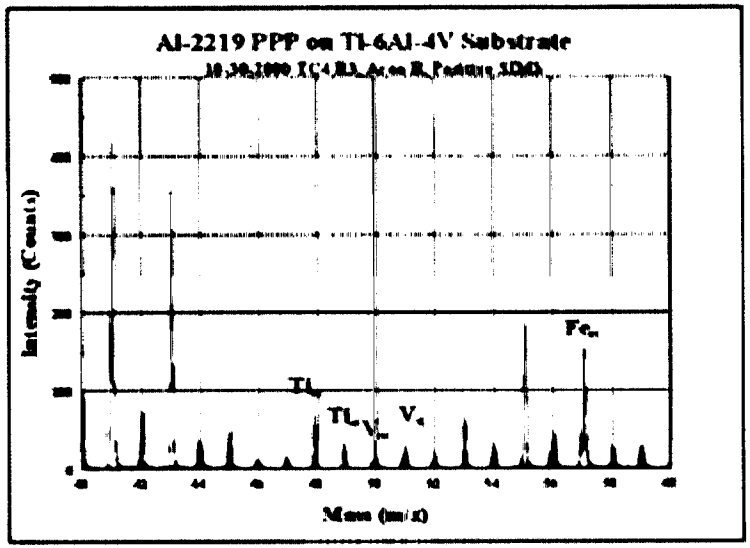

Figure 17e

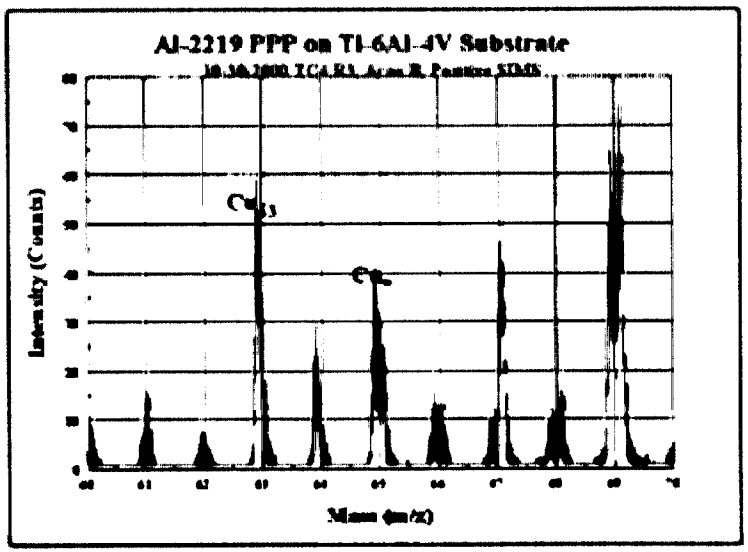

Figure 17f

Figures 17d-f: SIMS Analysis of Al-2219 PPP on Ti-6Al-4V Substrate

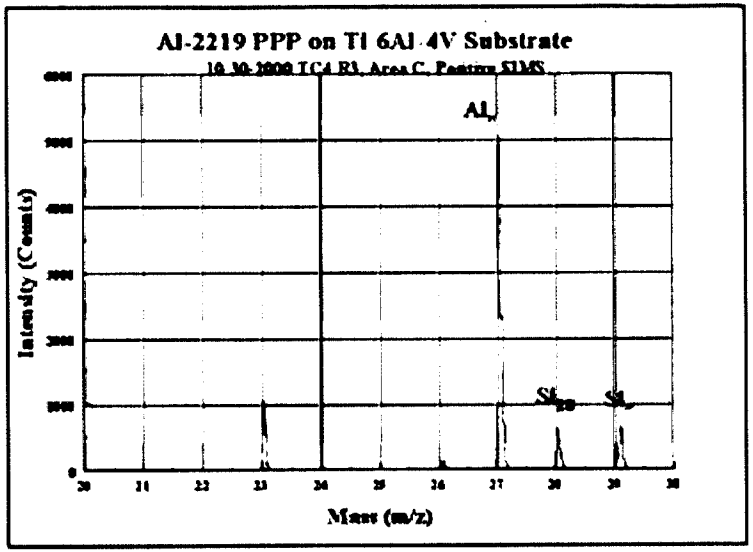

Figure 17g

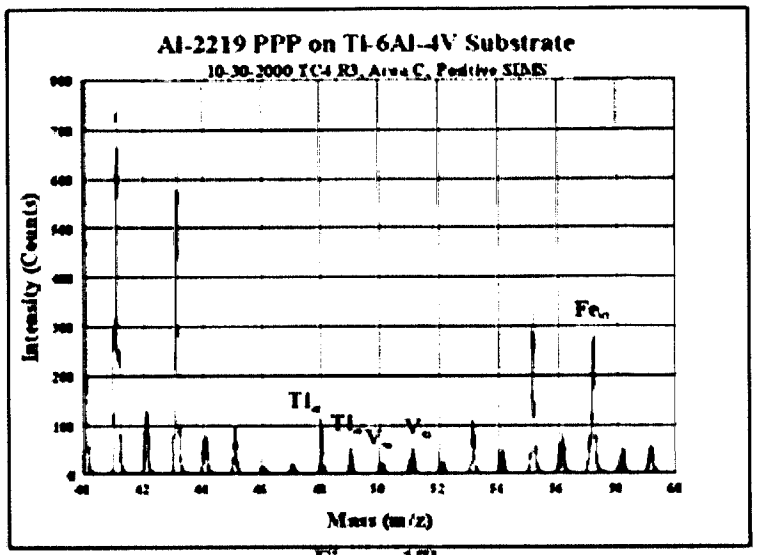

Figure 17h

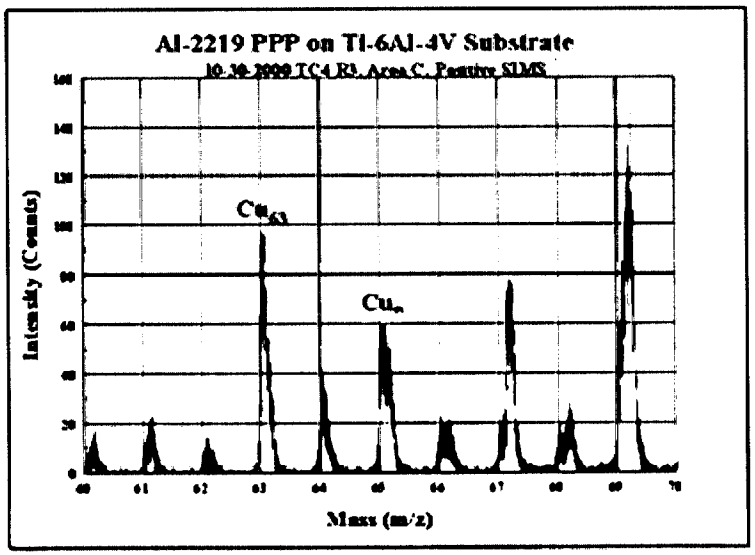

Figure 17i

Figures 17g-i: SIMS Analysis of Al-2219 PPP on Ti-6Al-4V Substrate

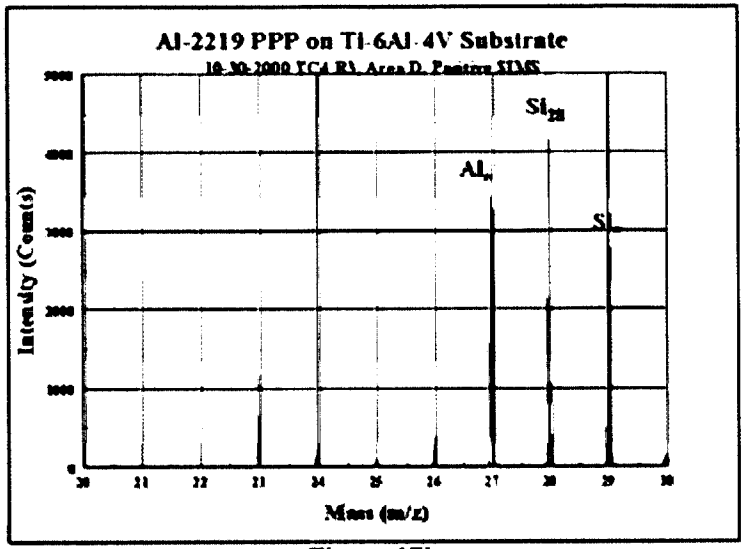

Figure 17j

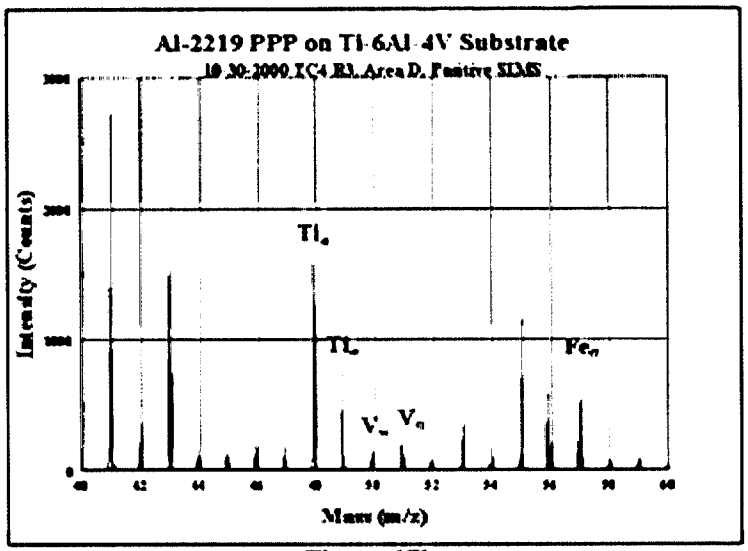

Figure 17k

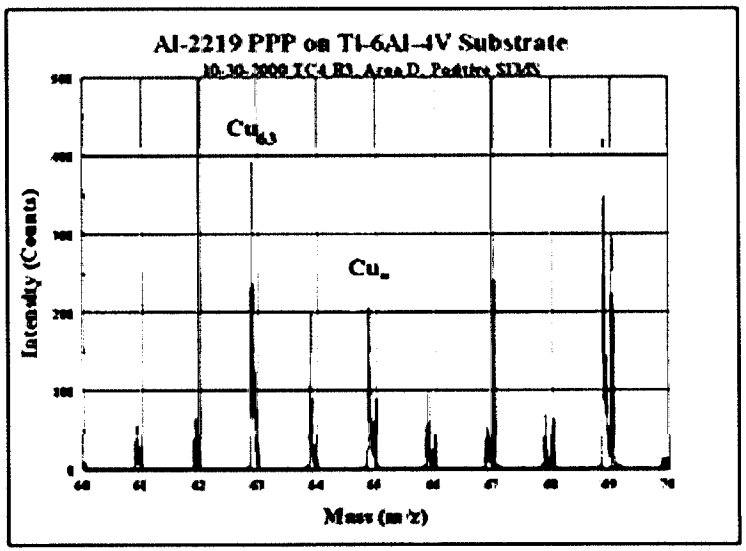

Figure 17l

Figures 17j-l: SIMS Analysis of Al-2219 PPP on Ti-6Al-4V Substrate

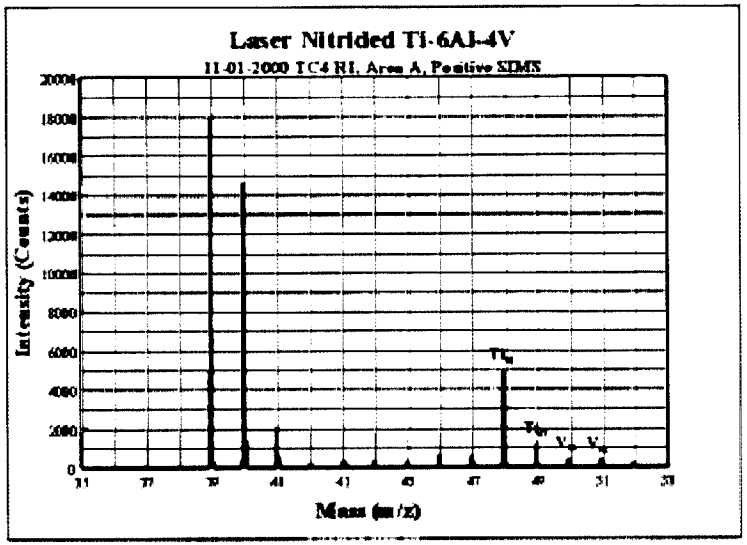

Figure 17m

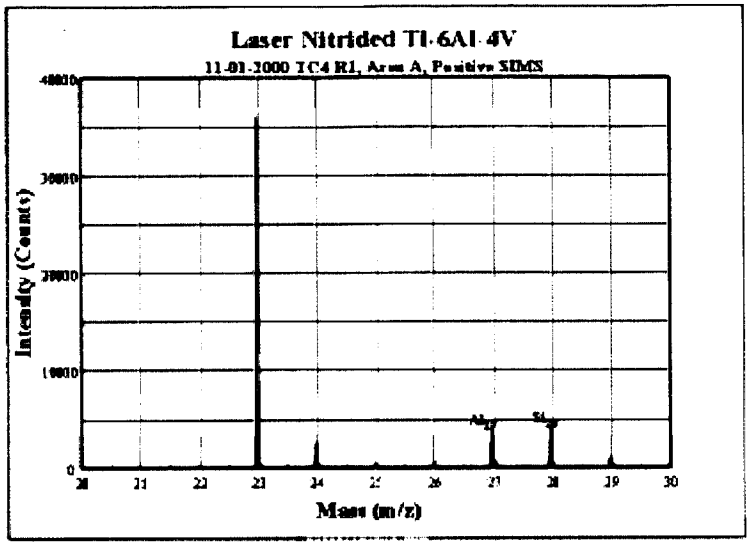

Figure 17n

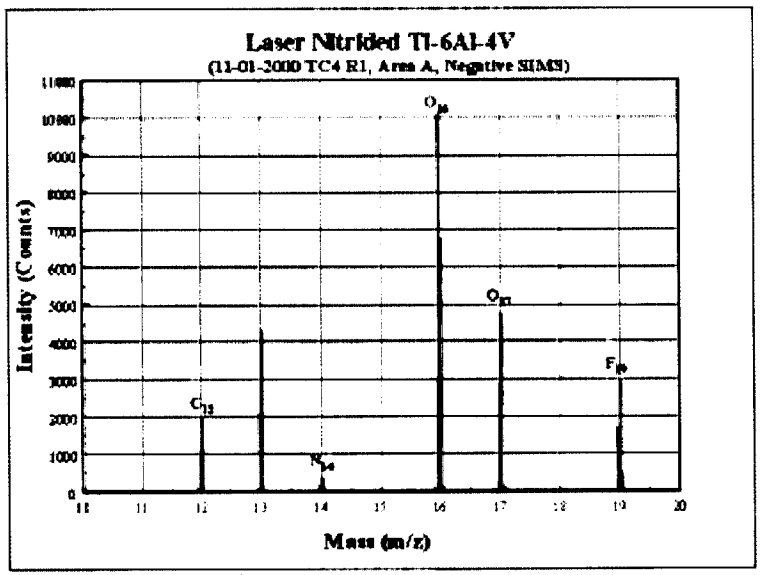

Figure 17o

Figures 17m-o: SIMS Analysis of Al-2219 PPP on Ti-6Al-4V Substrate

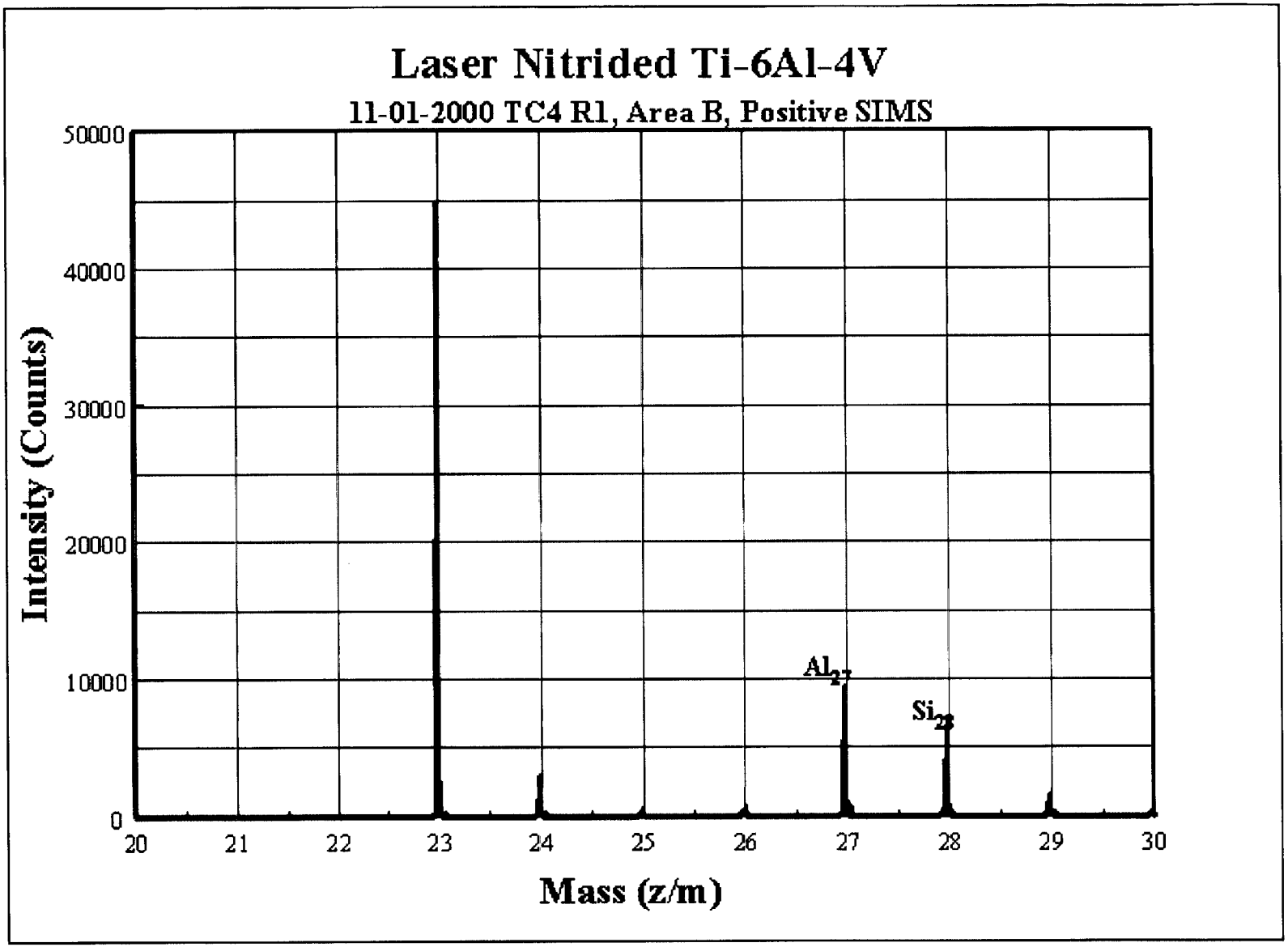

Figure 17p: Laser Nitrided Ti-6Al-4V

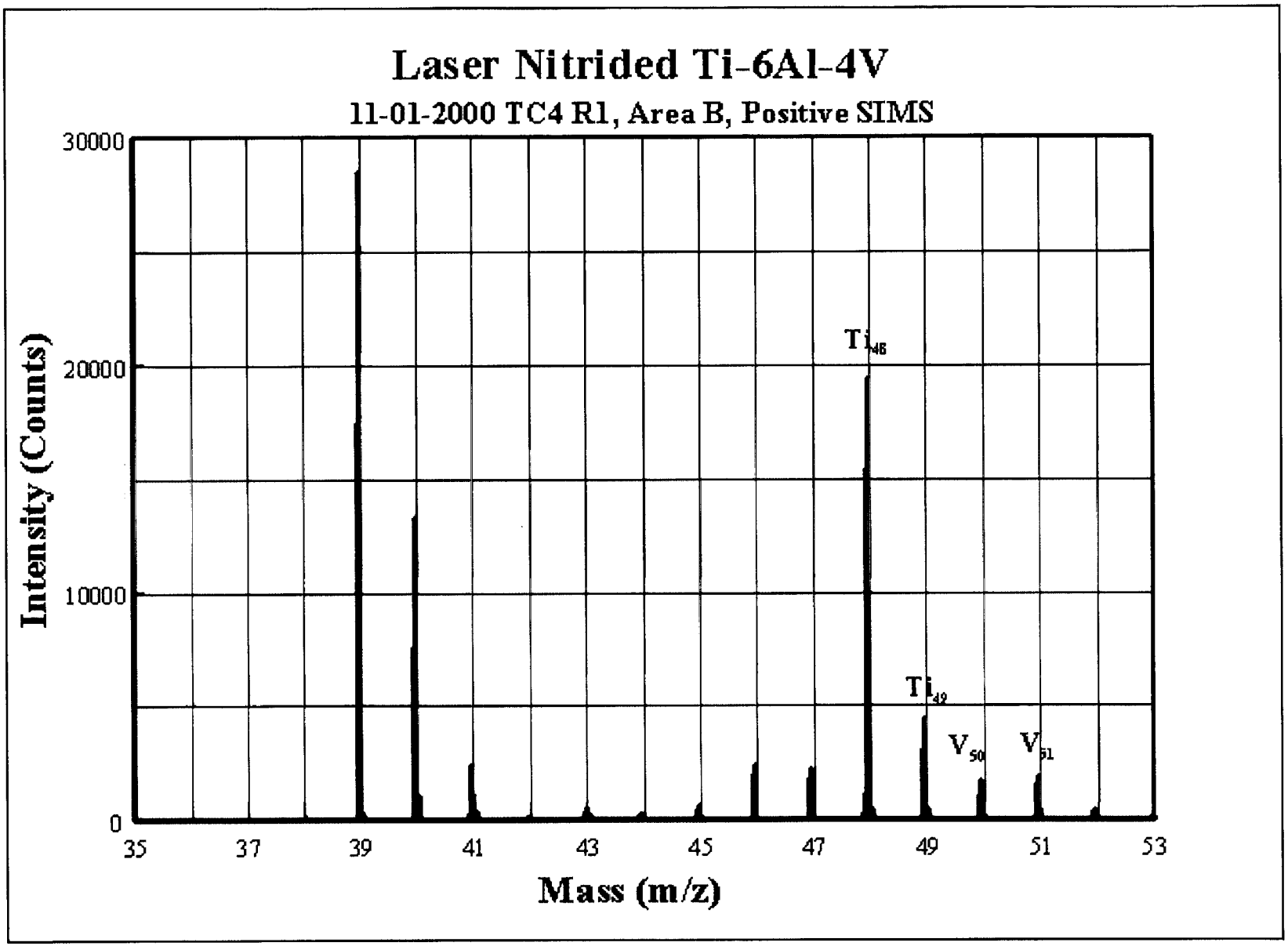

Figure 17q: Laser Nitrided Ti-6Al-4V

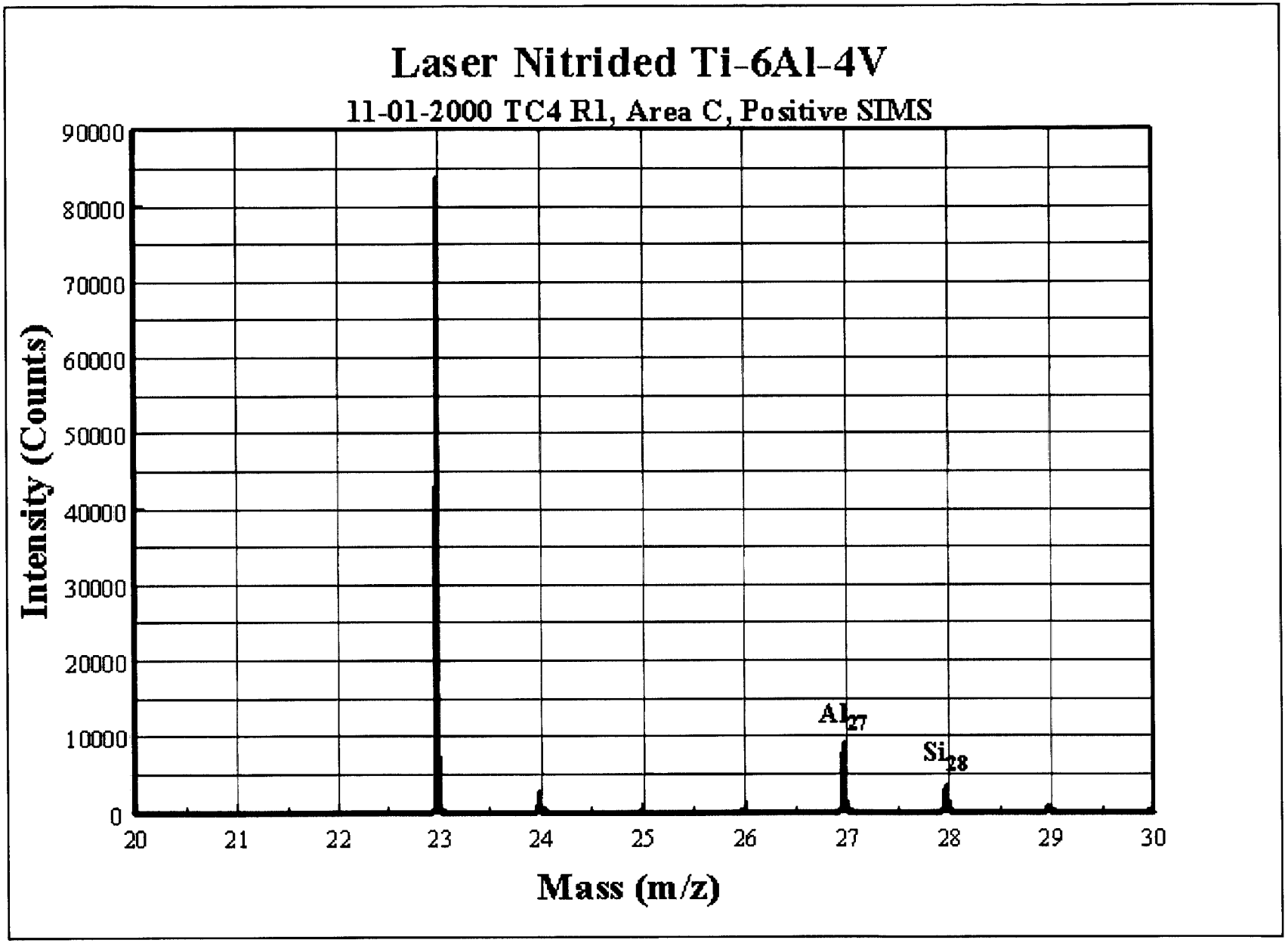

Figure 17r: Laser Nitrided Ti-6Al-4V

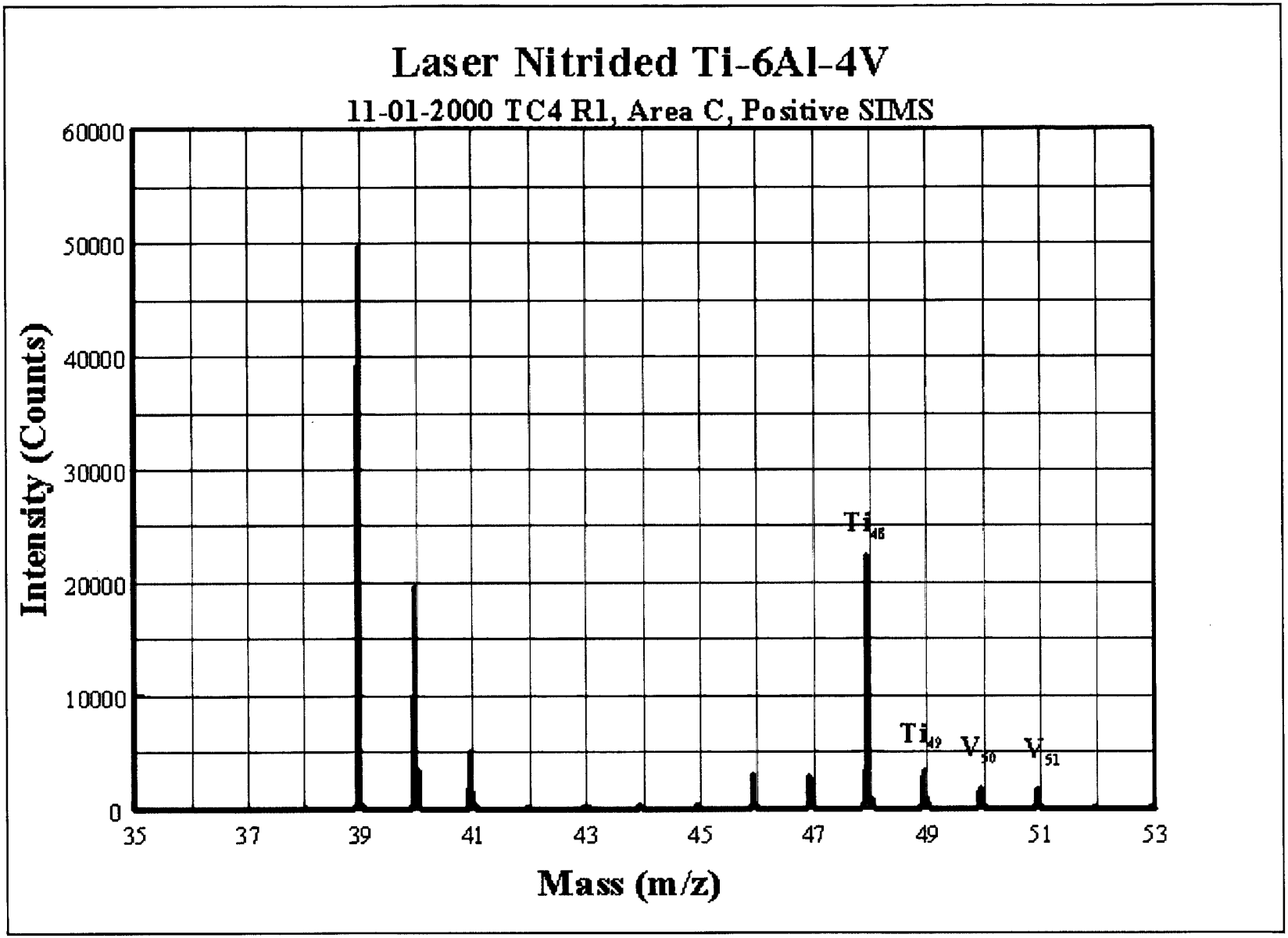

Figure 17s: Laser Nitrided Ti-6Al-4V

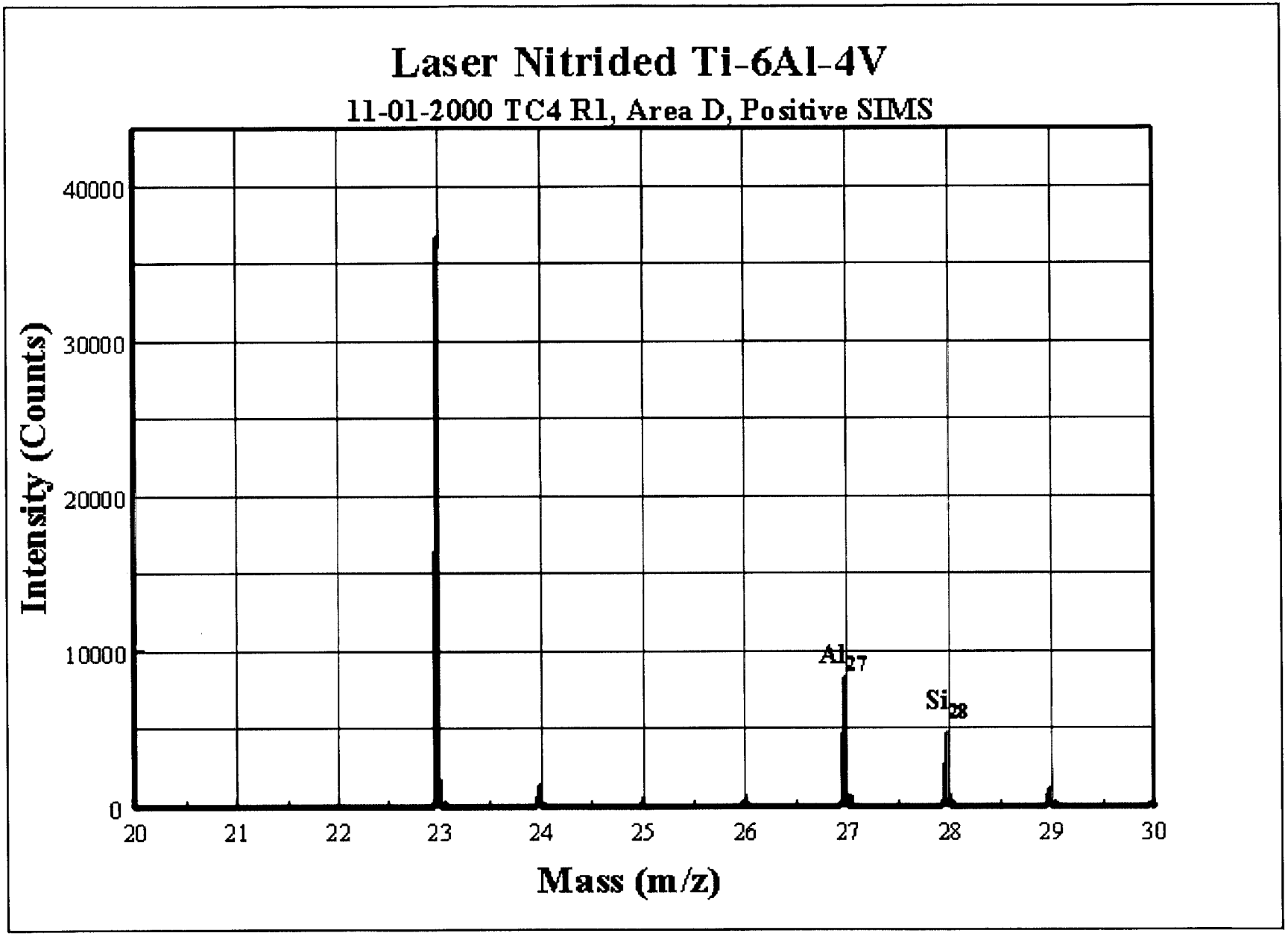

Figure 17t: Laser Nitrided Ti-6Al-4V

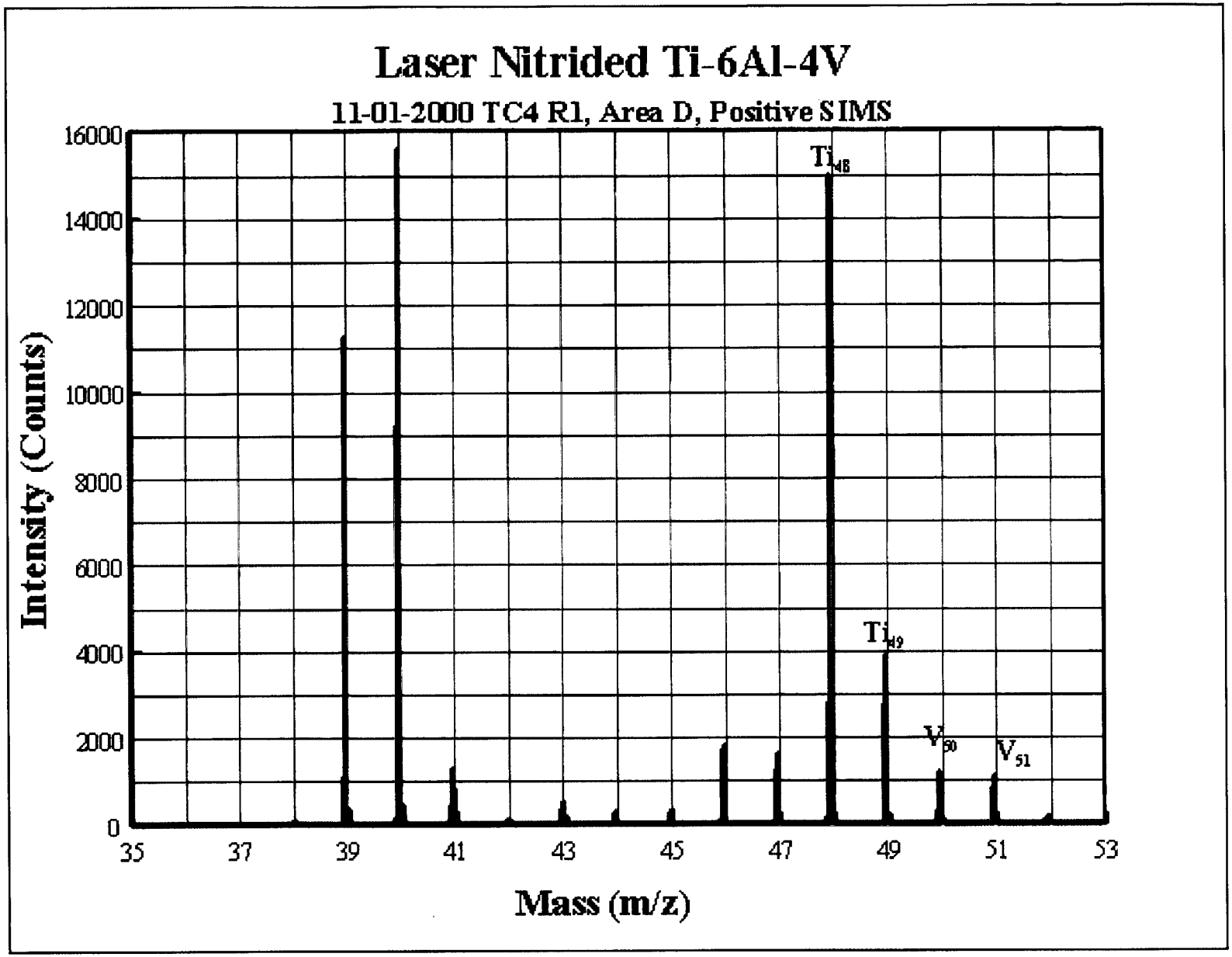

Figure 17u: Laser Nitrided Ti-6Al-4V

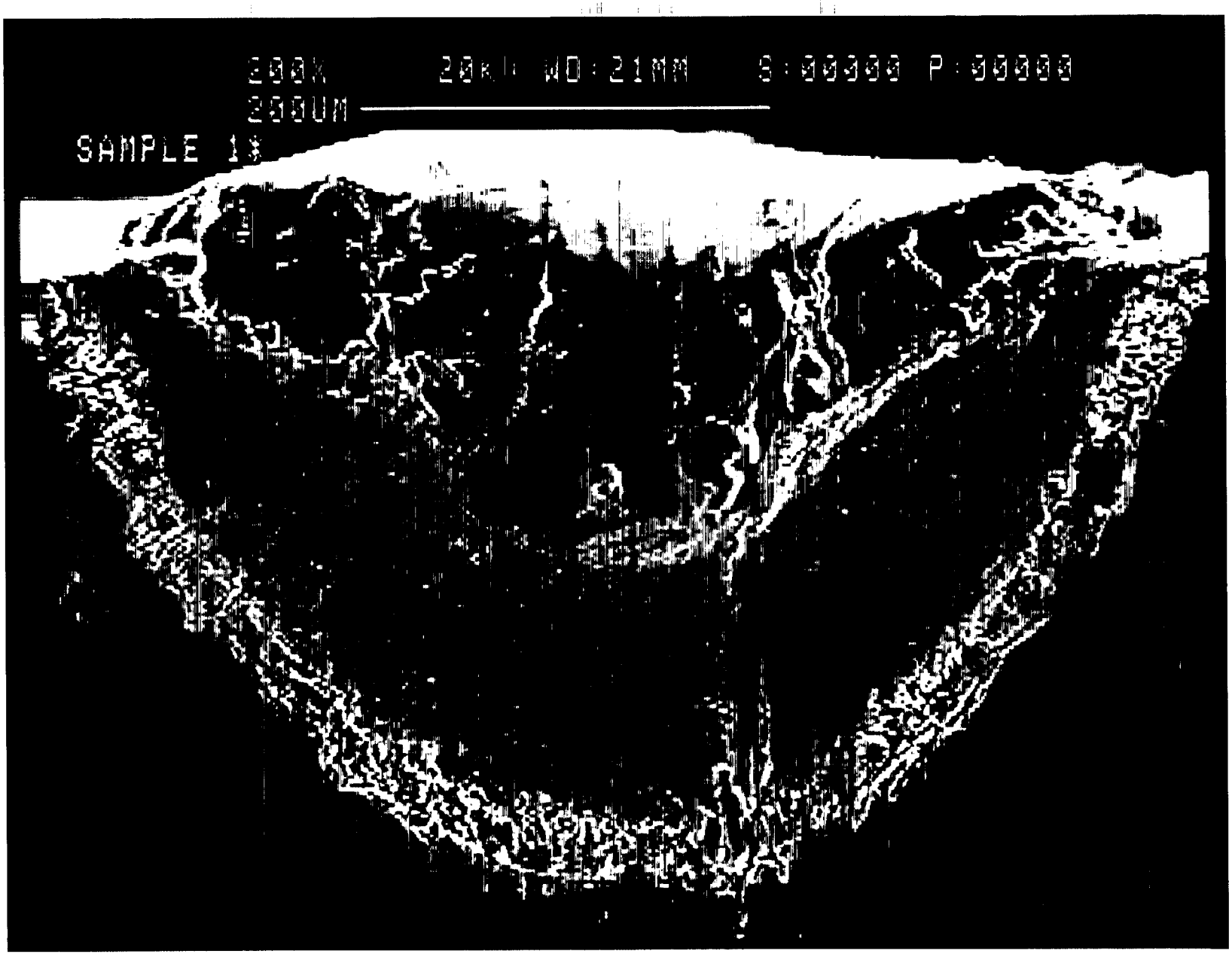

Figure 18a: SEM Cross-Section of Laser Nitrided Ti-6Al-4V
(Sample 11-01-2000 TC4 R1)

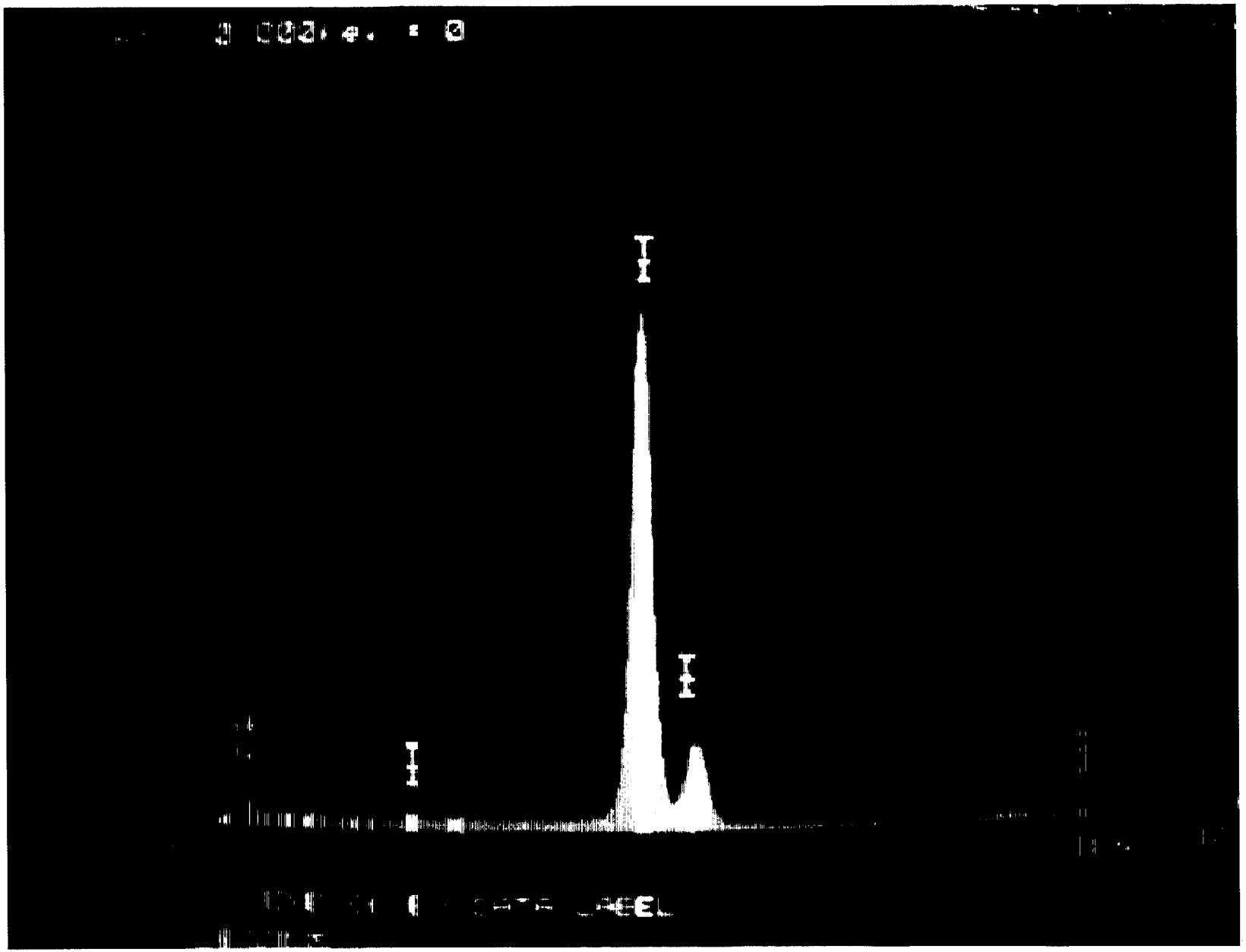

Figure 18b: EDS Analysis of Entire Cross-Section of Laser Nitrided Ti-6Al-4V (Sample 11-01-2000 TC4 R1)

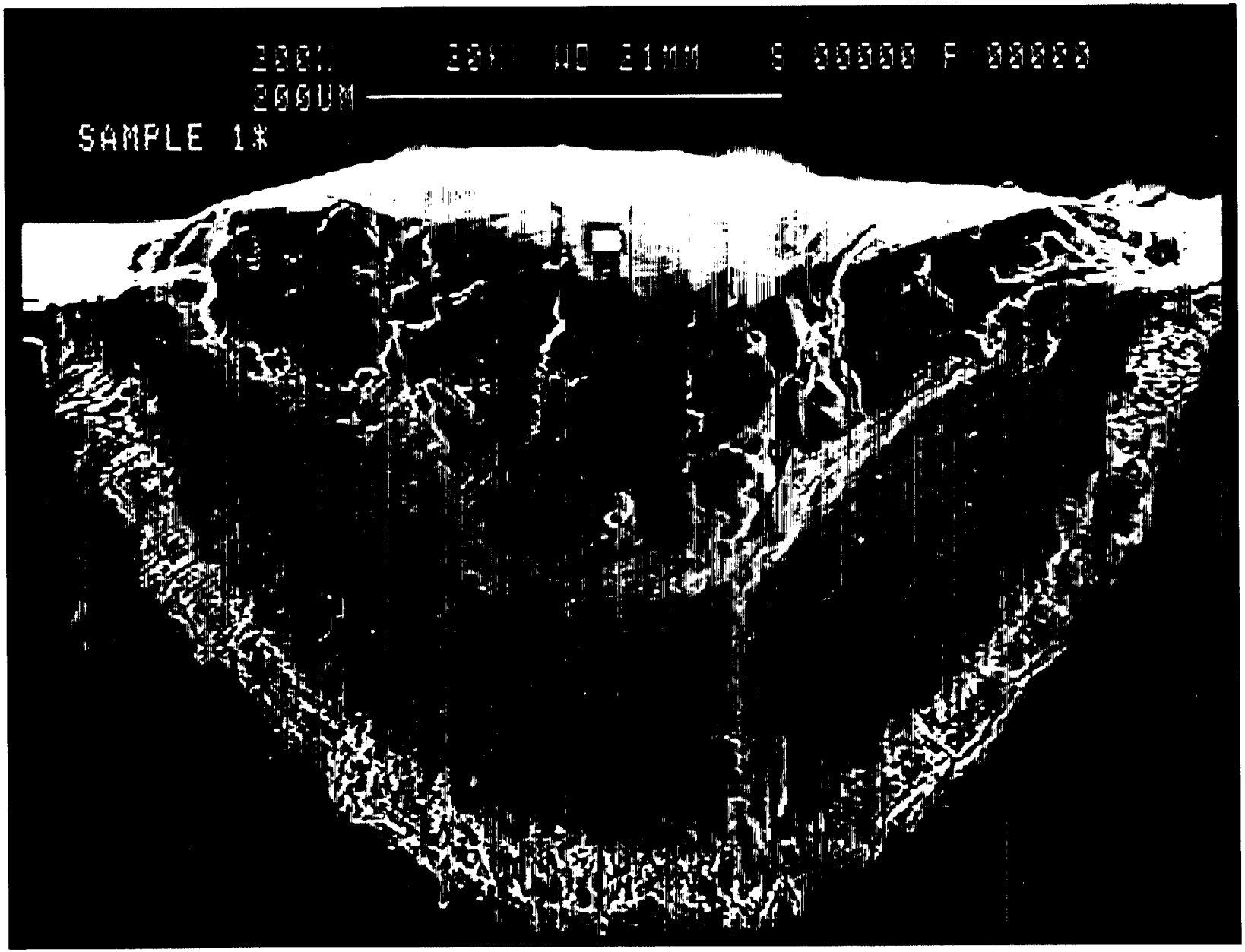

Figure 18c: SEM Cross-Section of Laser Nitrided Ti-6Al-4V Showing Location of Selected Analysis Point Sample 11-01-2000 TC4 R1)

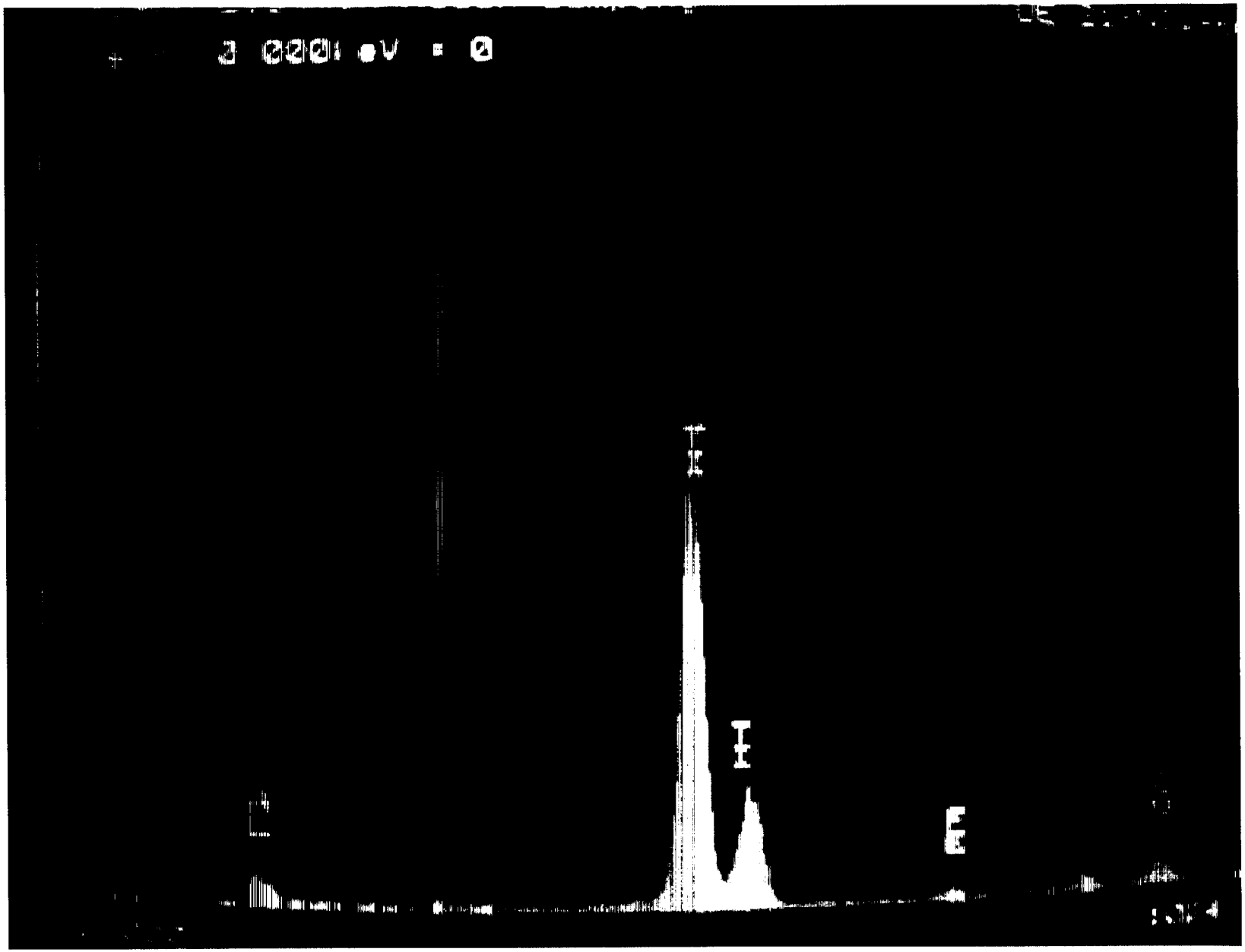

Figure 18d: EDS Analysis of Selected Area of Laser Nitrided Ti-6Al-4V (Sample 11-01-2000 TC4 R1)

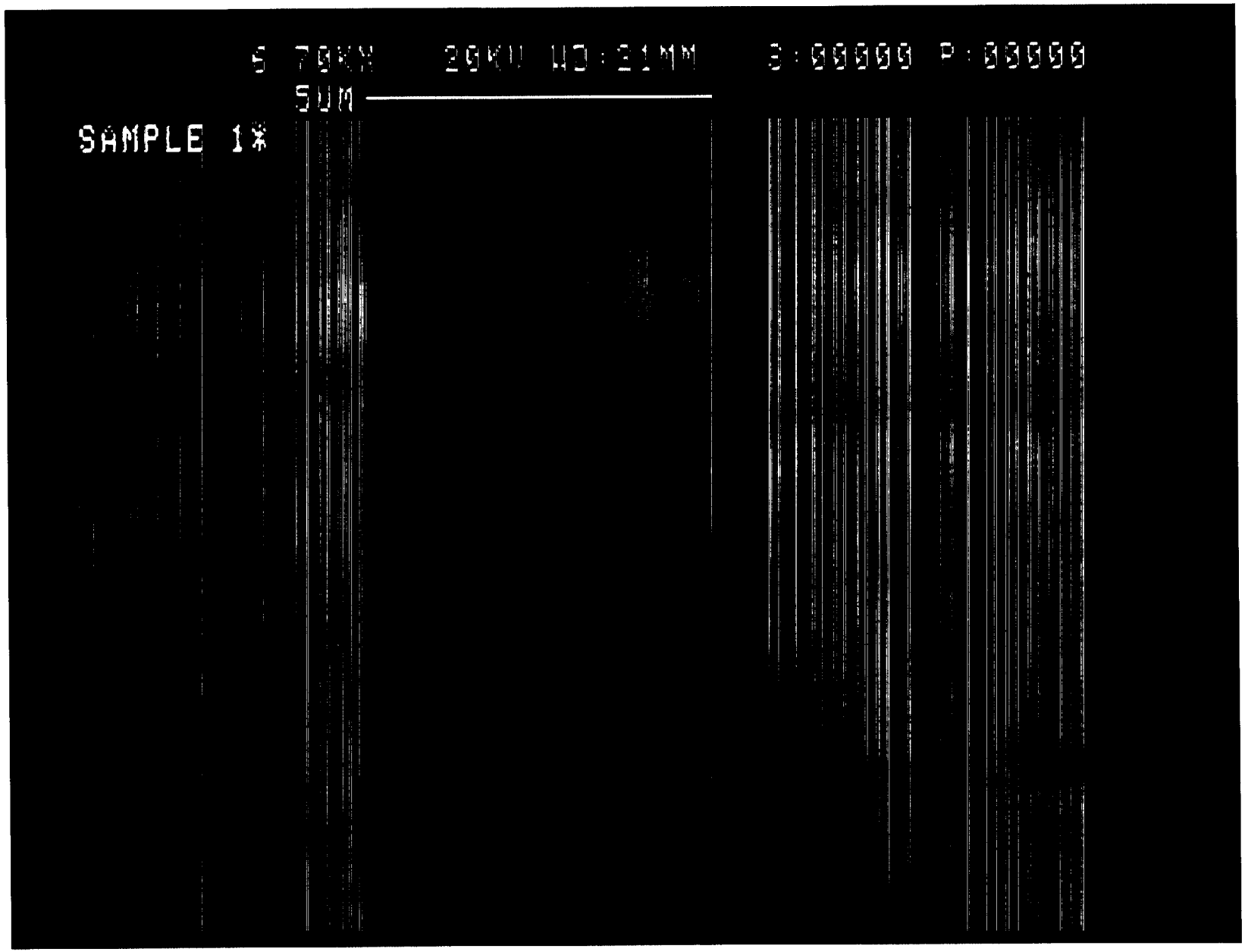

Figure 18e: High Magnification SEM Micrograph of Selected Analysis Point of Laser Nitrided Ti-6Al-4V (Sample 11-01-2000 TC4 R1)

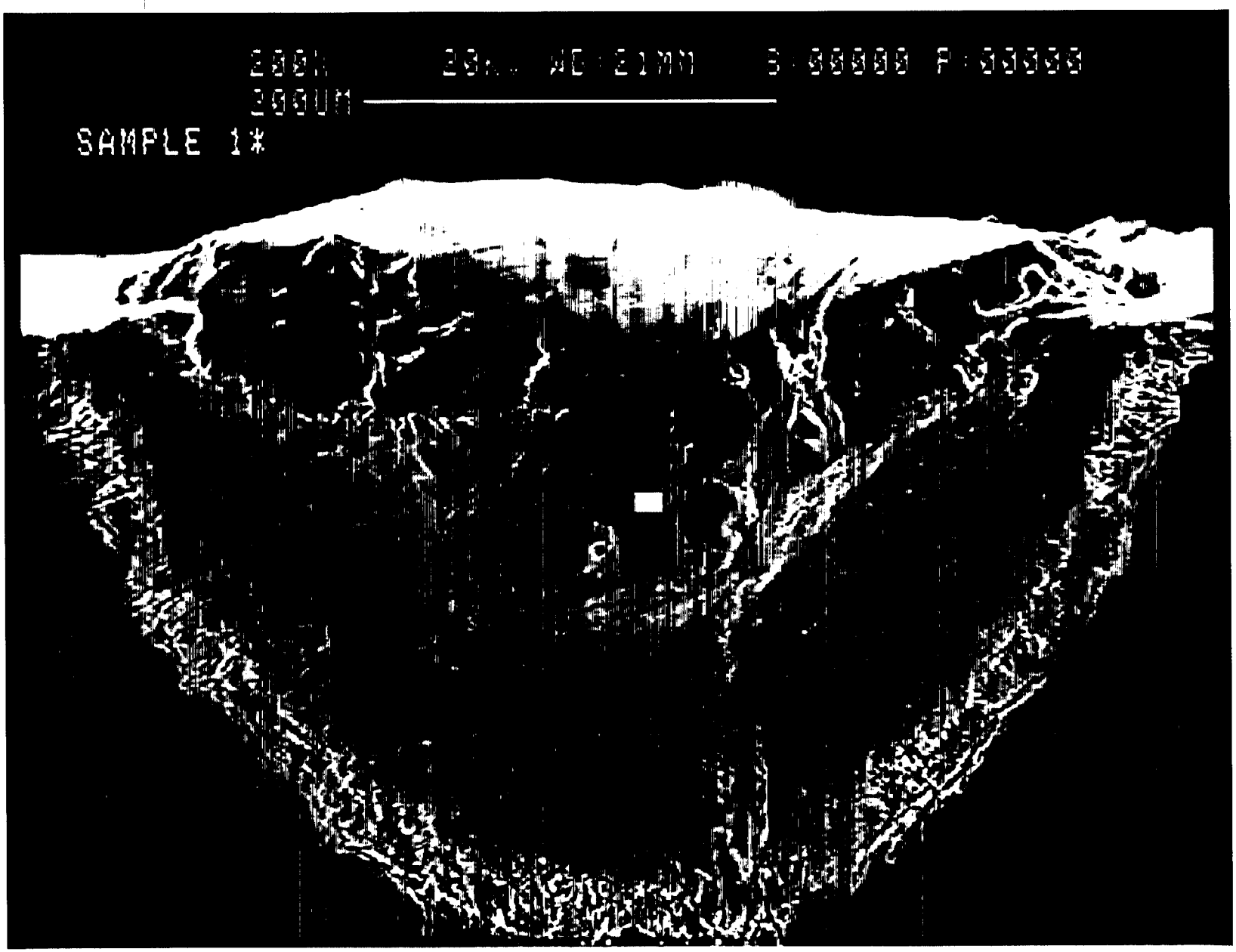

Figure 18f: SEM Cross-Section of Laser Nitrided Ti-6Al-4V Showing Location of Selected Analysis Point (Sample 11-01-2000 TC4 R1)

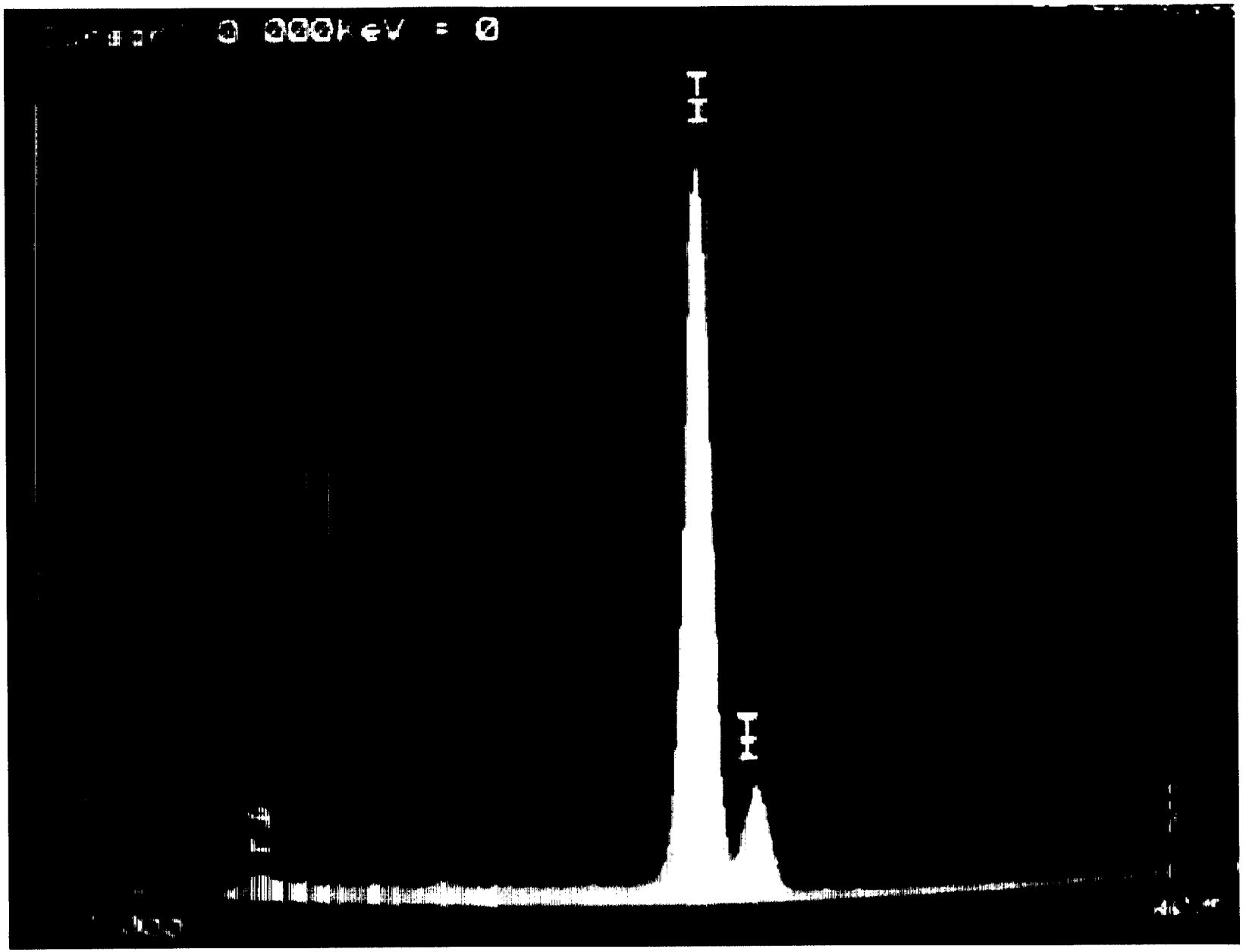

Figure 18g: EDS Analysis of Selected Area of Laser Nitrided Ti-6Al-4V (Sample 11-01-2000 TC4 R1)

Figure 18h: High Magnification SEM Micrograph of Selected Analysis Point of Laser Nitrided Ti-6Al-4V (Sample 11-01-2000 TC4 R1)

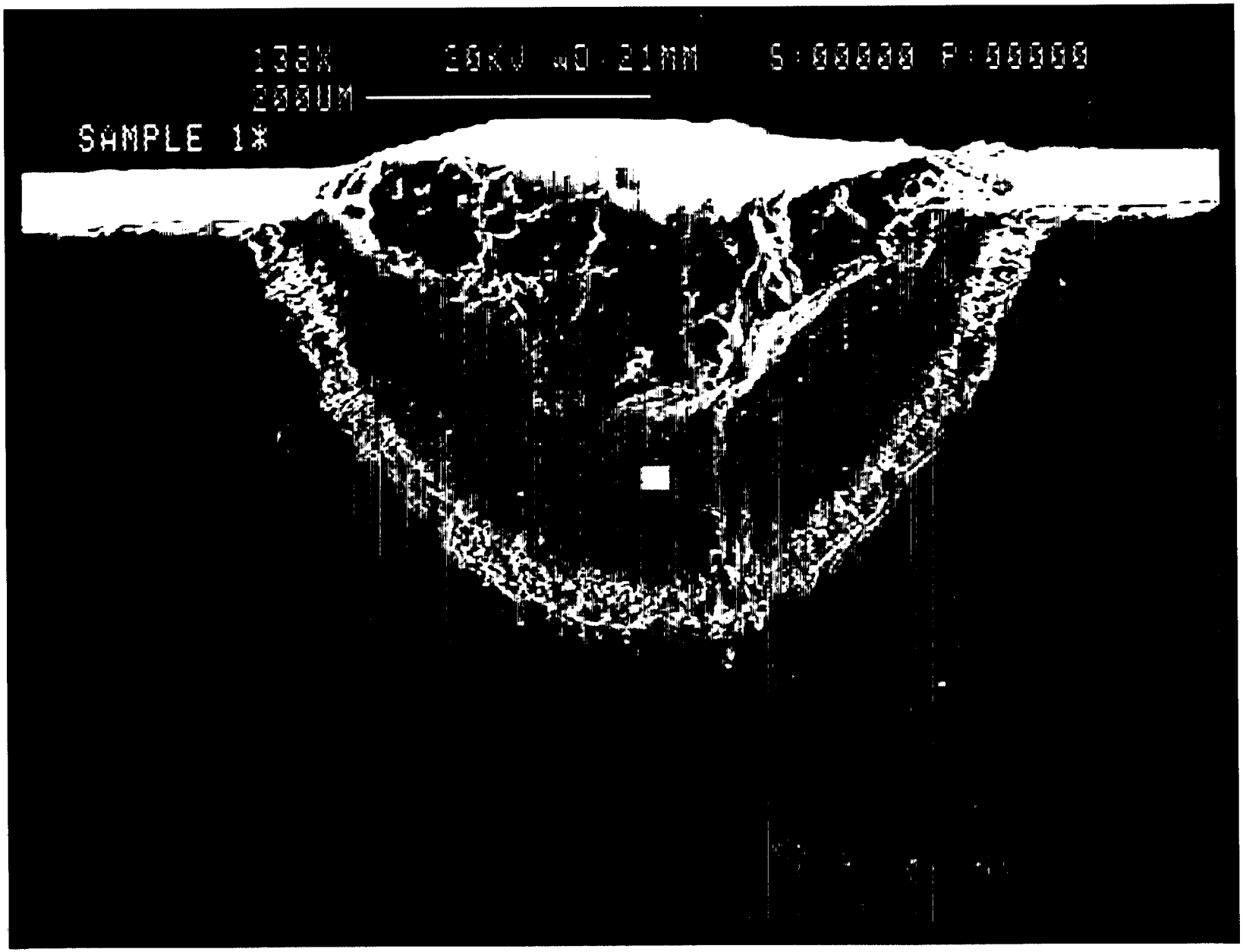

Figure 18i: SEM Cross-Section of Laser Nitrided Ti-6Al-4V Showing Location of Selected Analysis Point (Sample 11-01-2000 TC4 R1)

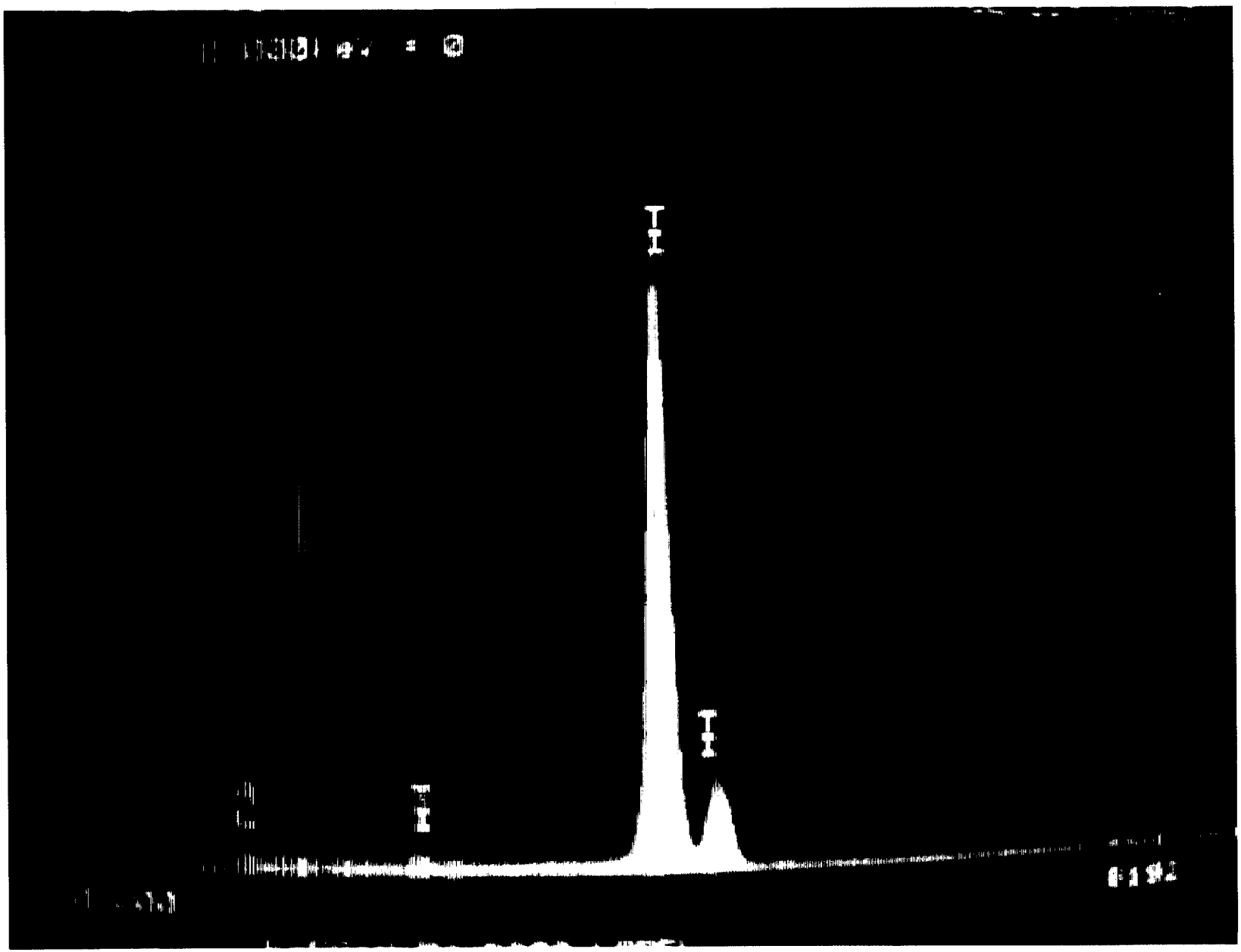

Figure 18j: EDS Analysis of Selected Area of Laser Nitrided Ti-6Al-4V (Sample 11-01-2000 TC4 R1)

Figure 18k: High Magnification SEM Micrograph of Selected Analysis Point of Laser Nitrided Ti-6Al-4V (Sample 11-01-2000 TC4 R1)

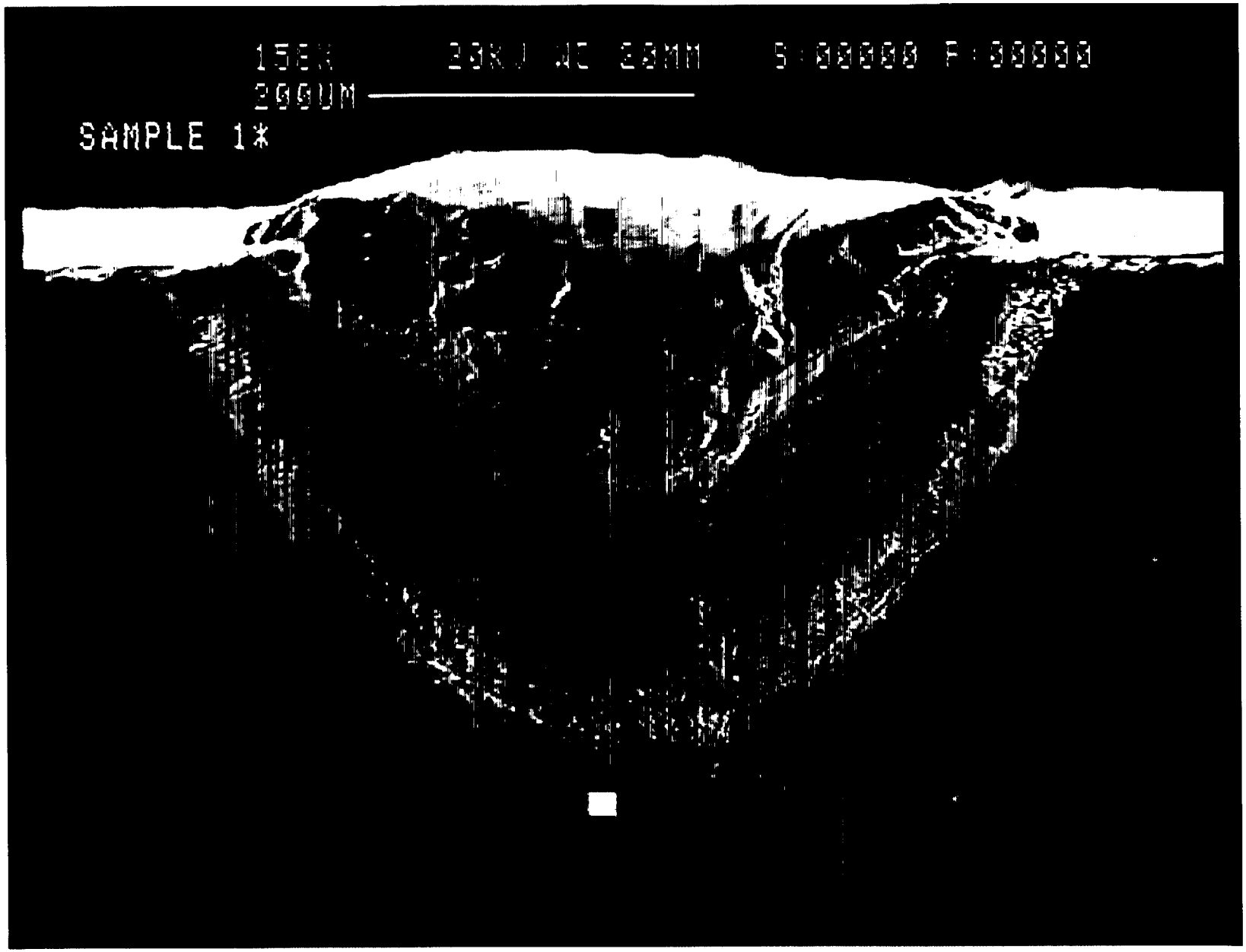

Figure 18l: SEM Cross-Section of Laser Nitrided Ti-6Al-4V Showing Location of Selected Analysis Point (Sample 11-01-2000 TC4 R1)

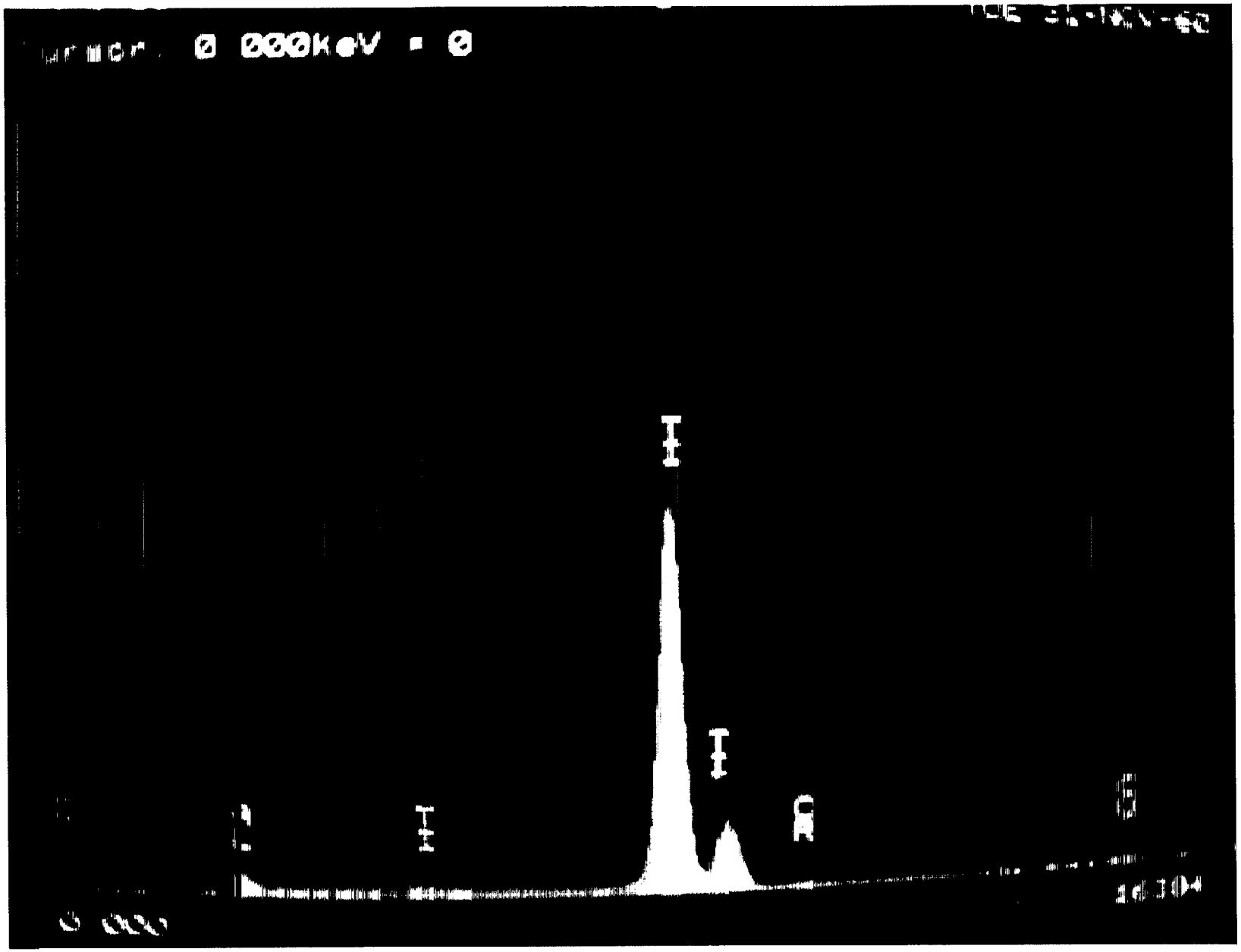

Figure 18m: EDS Analysis of Selected Area of Laser Nitrided Ti-6Al-4V (Sample 11-01-2000 TC4 R1)

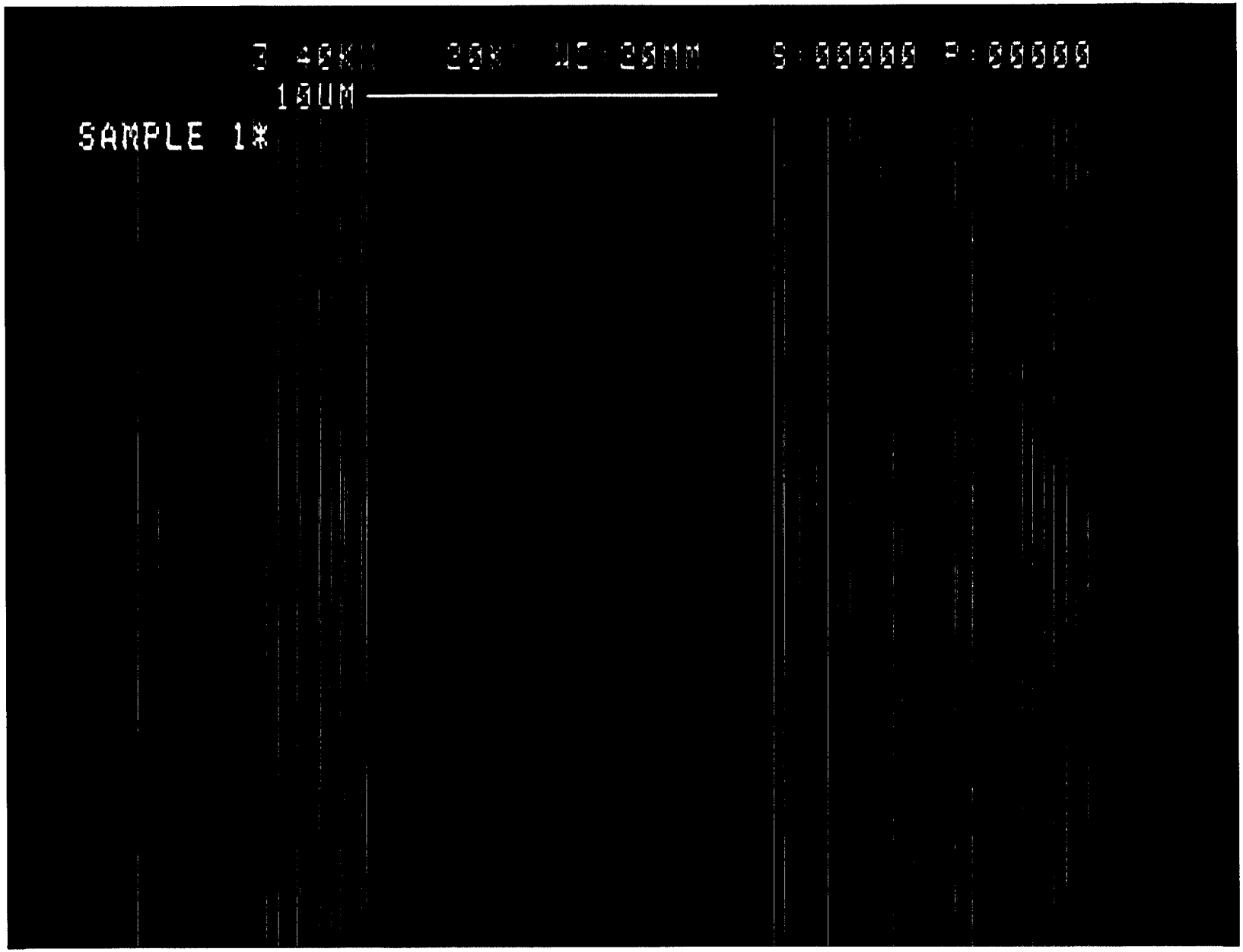

Figure 18n: High Magnification SEM Micrograph of Selected Analysis Point of Laser Nitrided Ti-6Al-4V (Sample 11-01-2000 TC4 R1)

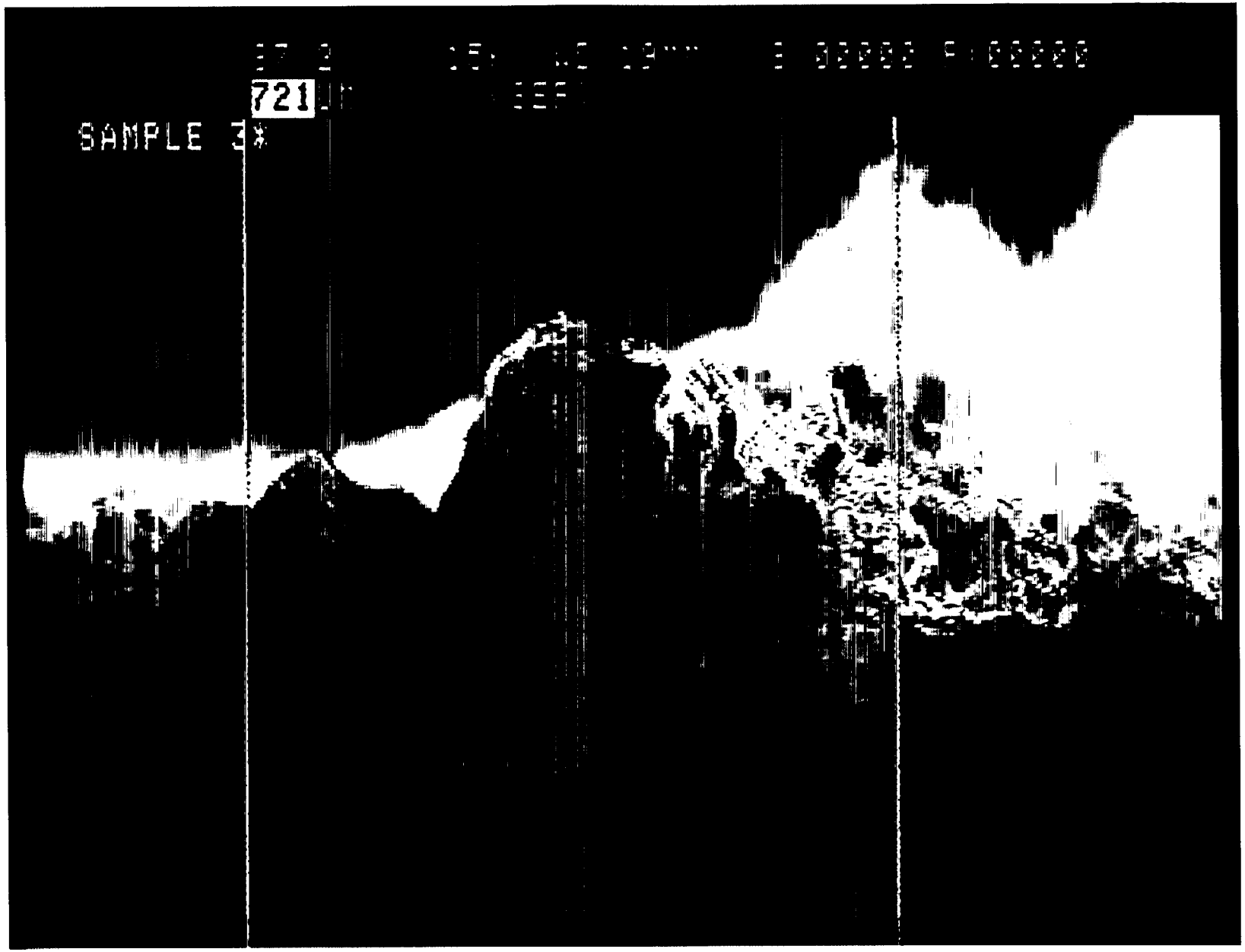

Figure 18o: SEM Cross-Section of Al-2219 PPP on Ti-6Al-4V Substrate (Sample 10-30-2000 TC4 R3)

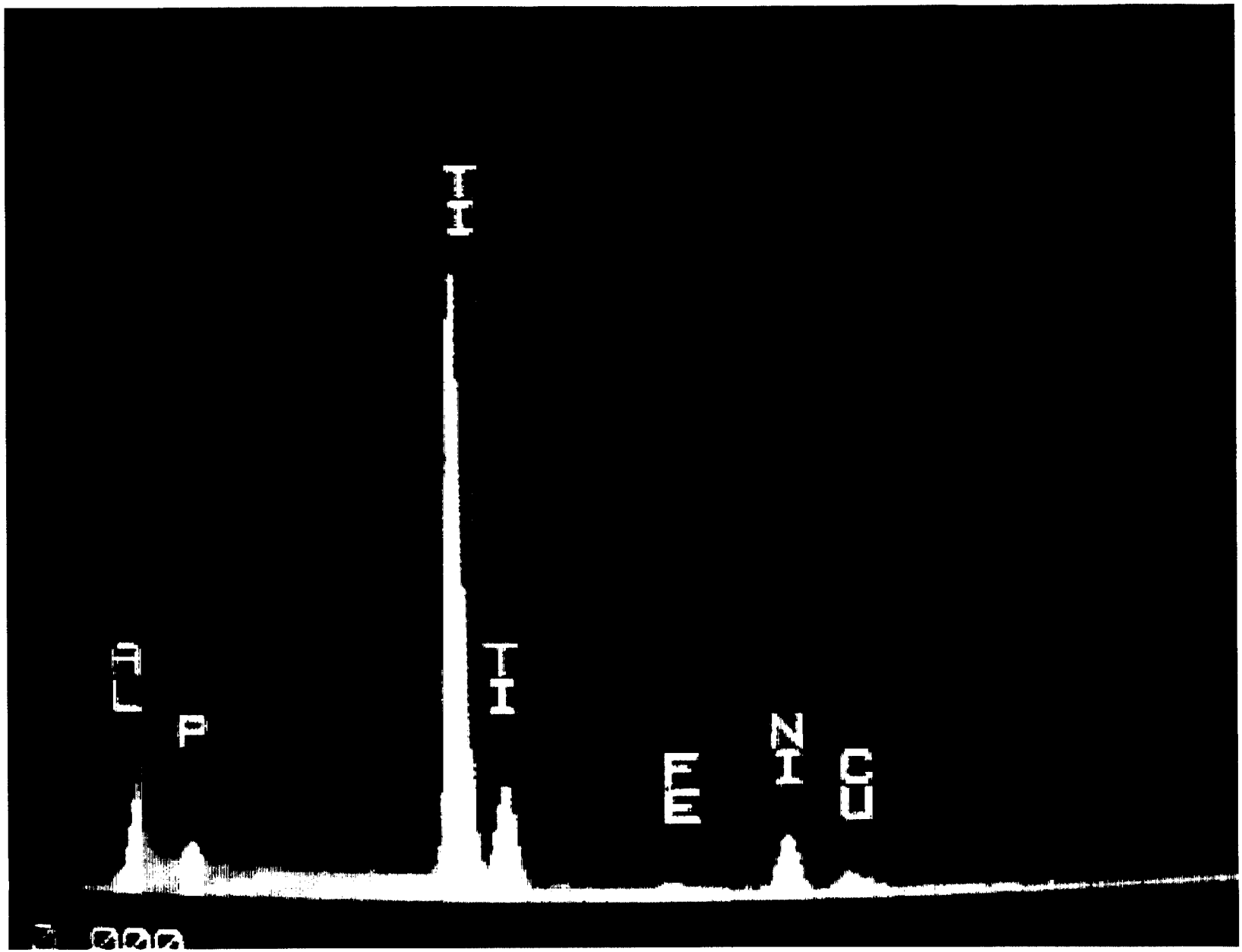

Figure 18p: EDS Analysis of Entire Cross-Section of Al-2219 PPP on Ti-6Al-4V Substrate (Sample 10-30-2000 TC4 R3)

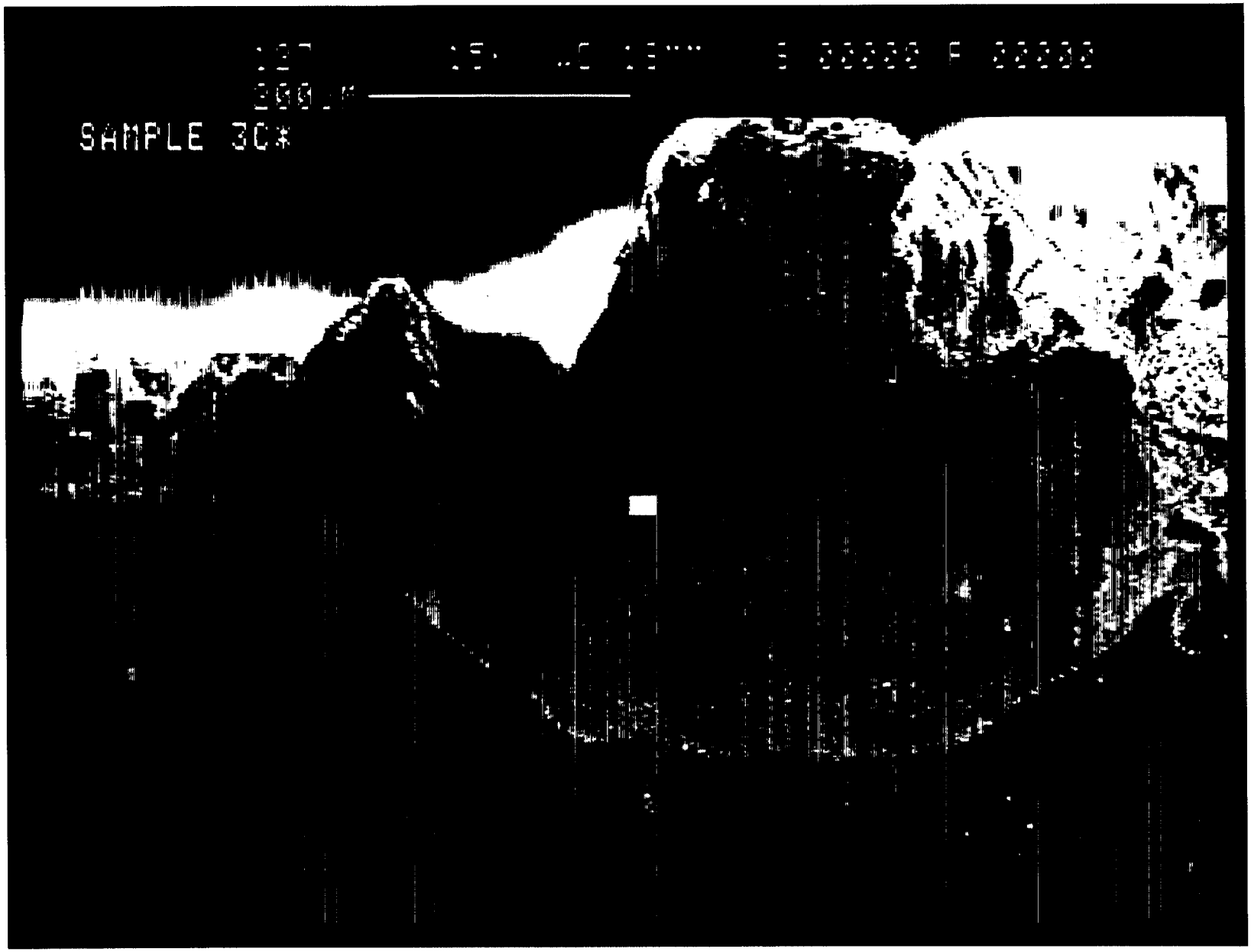

Figure 18q: SEM Cross-Section of Al-2219 PPP on Ti-6Al-4V Substrate Showing Location of Selected Analysis Point (Sample 10-30-2000 TC4 R3)

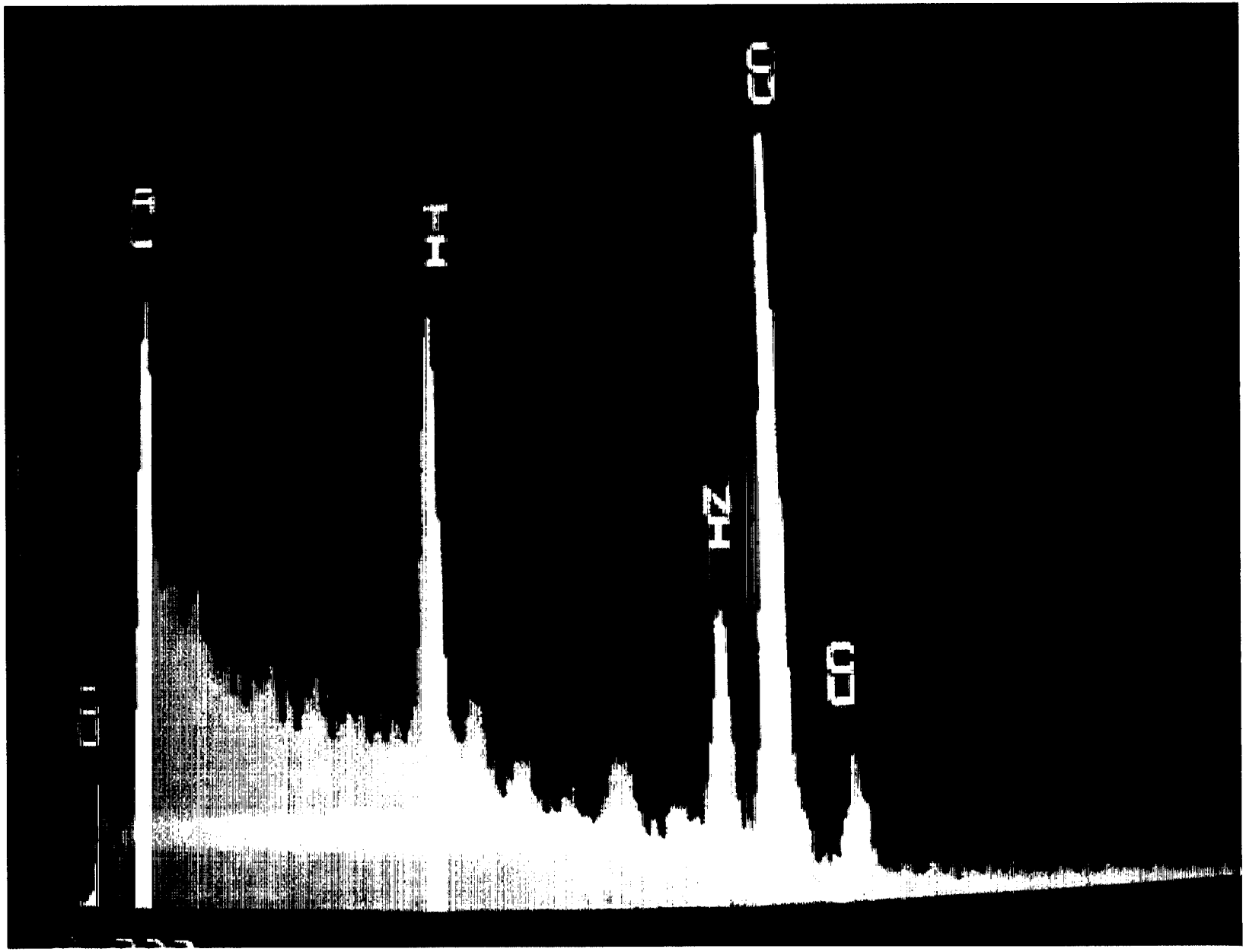

Figure 18r: EDS Analysis of Selected Area of Al-2219 PPP on Ti-6Al-4V Substrate (Sample 10-30-2000 TC4 R3)

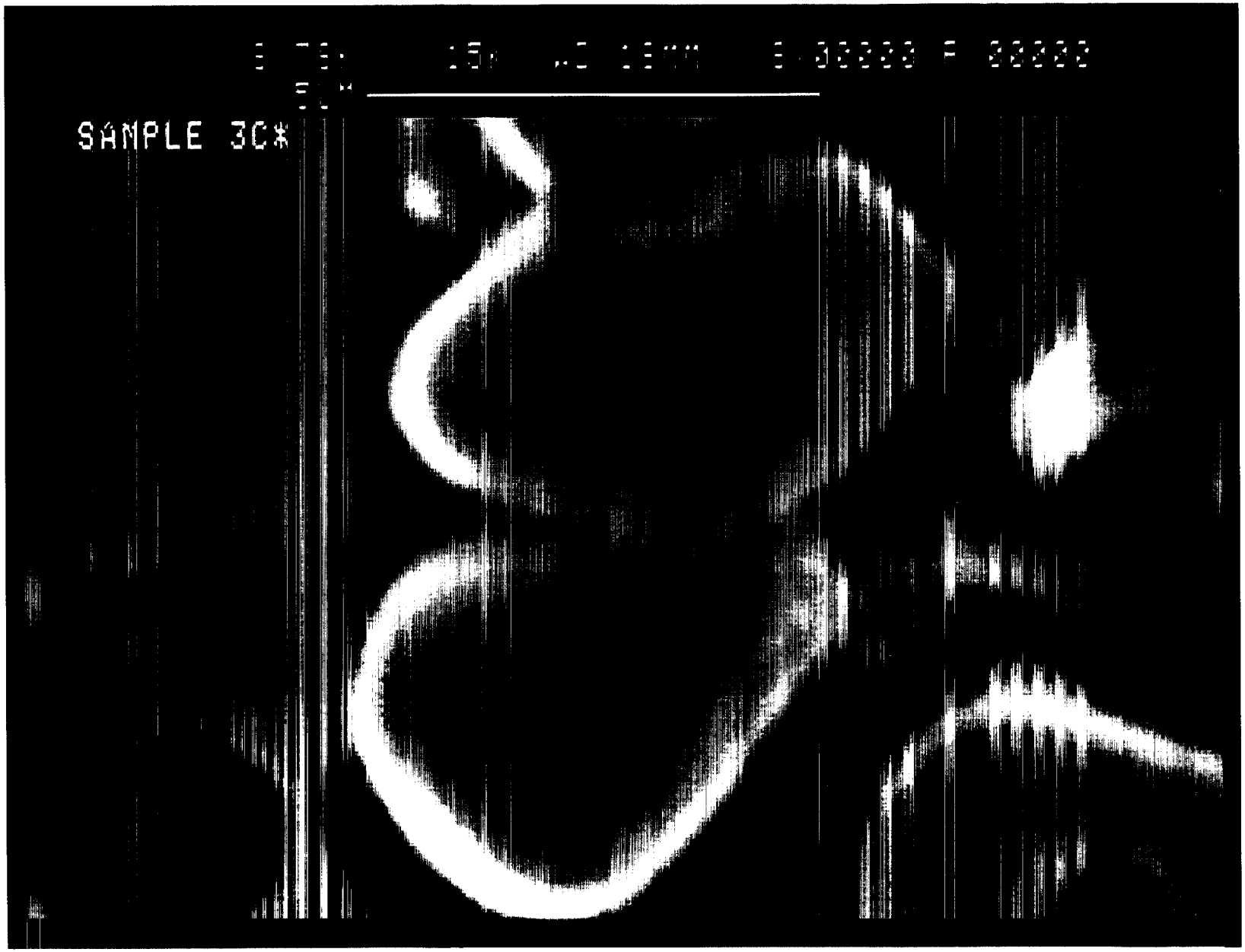

Figure 18s: High Magnification SEM Micrograph of Selected Analysis Point of Al-2219 PPP on Ti-6Al-4V Substrate (Sample 10-30-2000 TC4 R3)

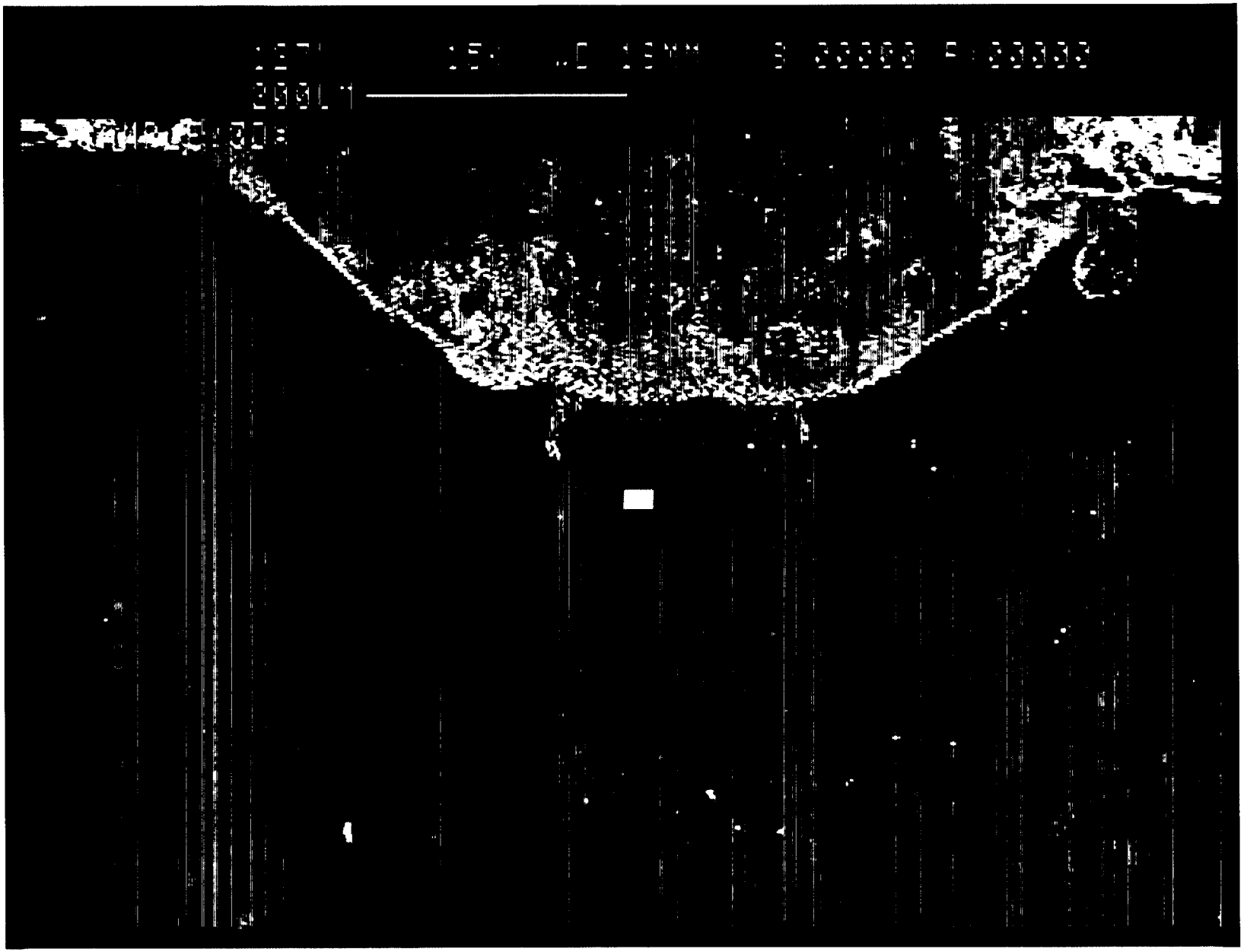

Figure 18t: SEM Cross-Section of Al-2219 PPP on Ti-6Al-4V Substrate Showing Location of Selected Analysis Point (Sample 10-30-2000 TC4 R3)

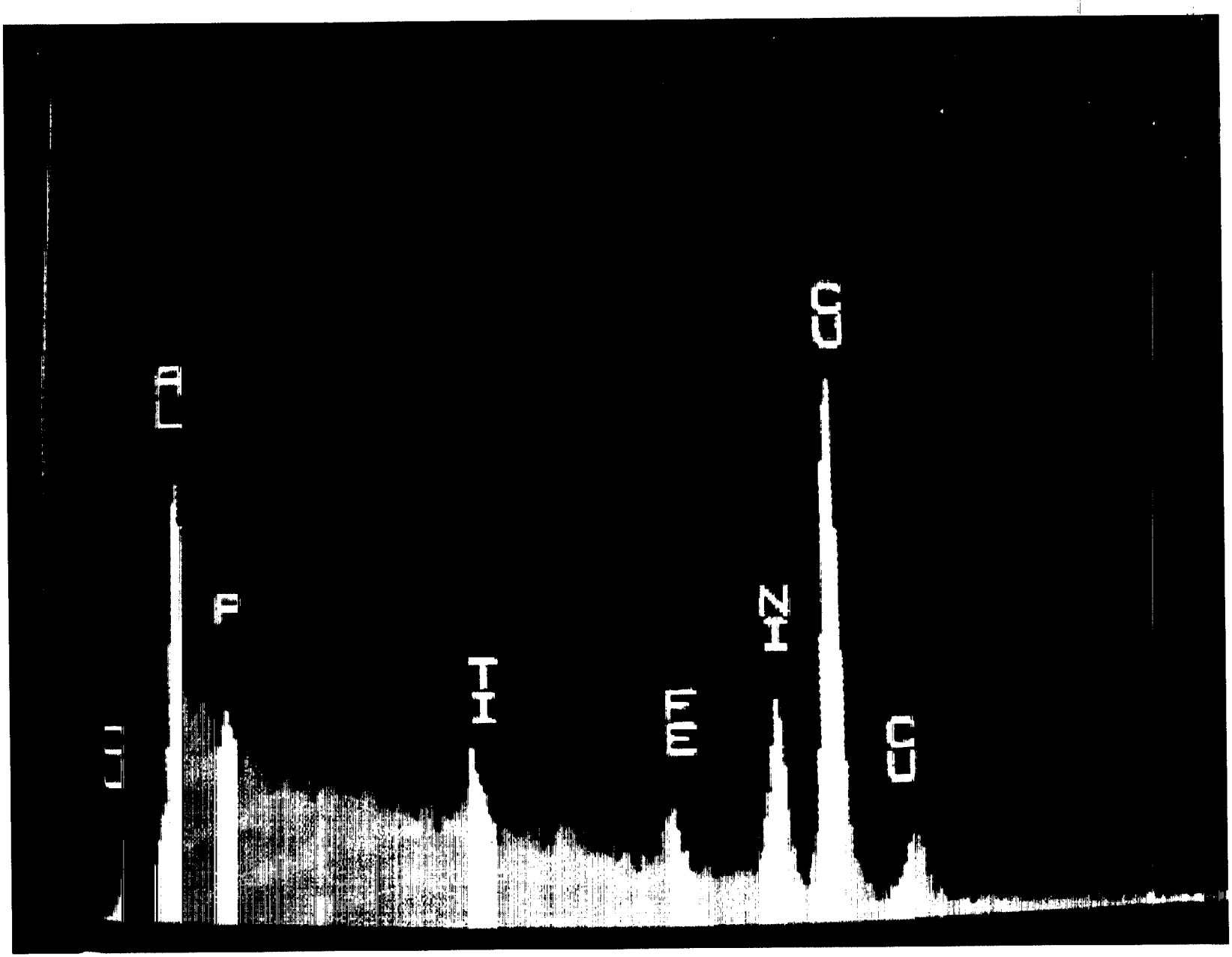

Figure 18u: EDS Analysis of Selected Area of Al-2219 PPP on Ti-6Al-4V Substrate (Sample 10-30-2000 TC4 R3)

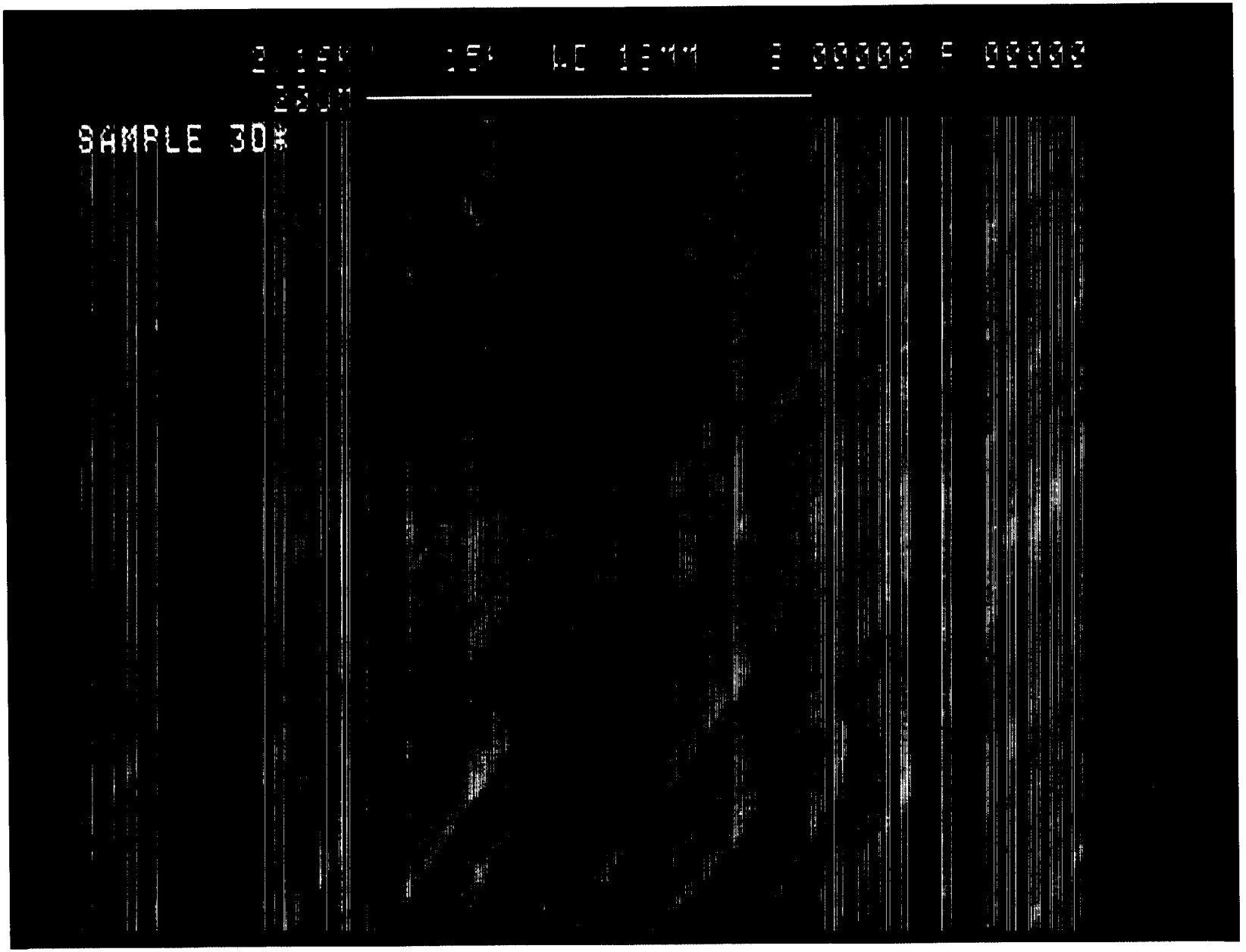

Figure 18v: High Magnification SEM Micrograph of Selected Analysis Point of Al-2219 PPP on Ti-6Al-4V Substrate (Sample 10-30-2000 TC4 R3)

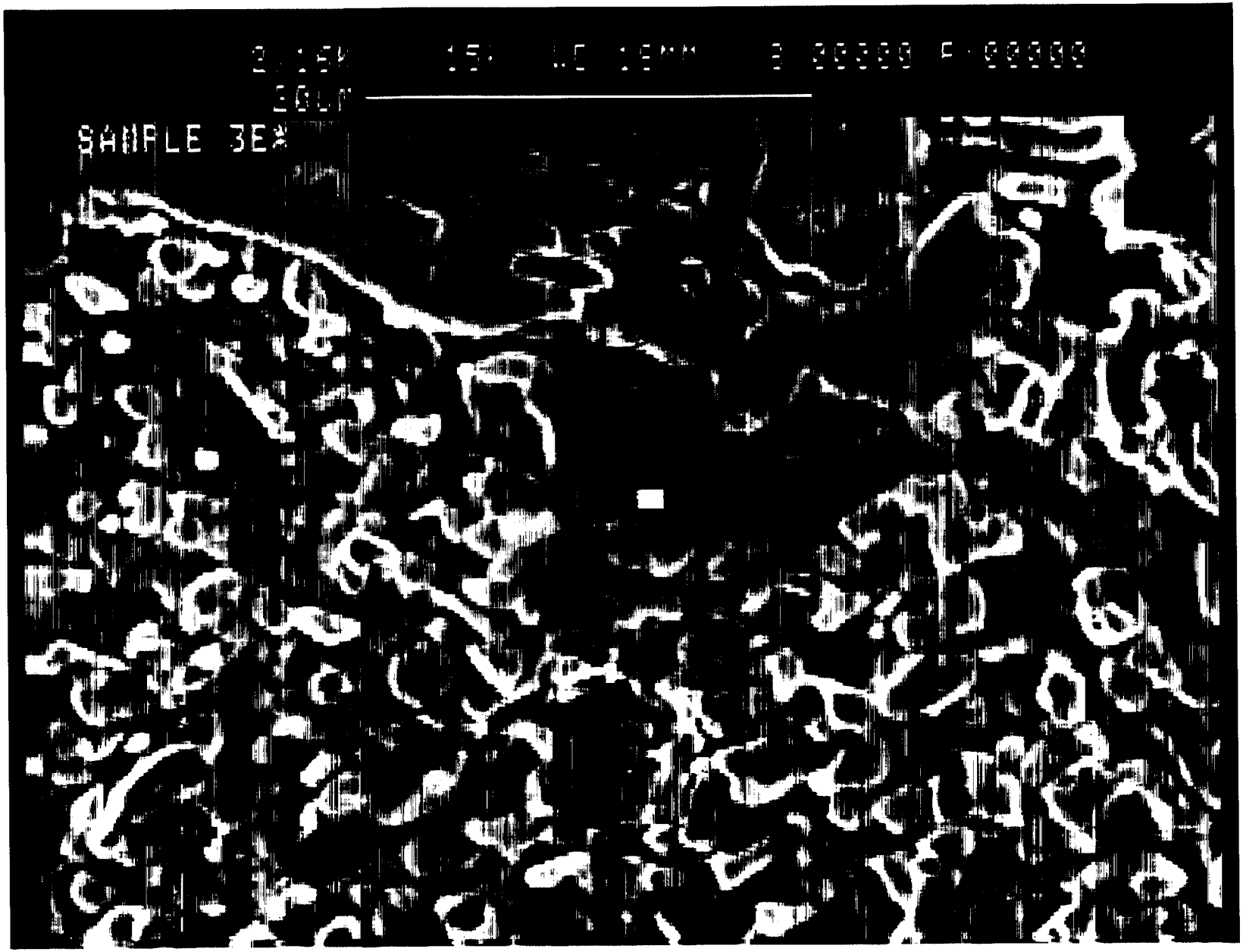

Figure 18w: SEM Cross-Section of Al-2219 PPP on Ti-6Al-4V Substrate Showing Location of Selected Analysis Point (Sample 10-30-2000 TC4 R3)

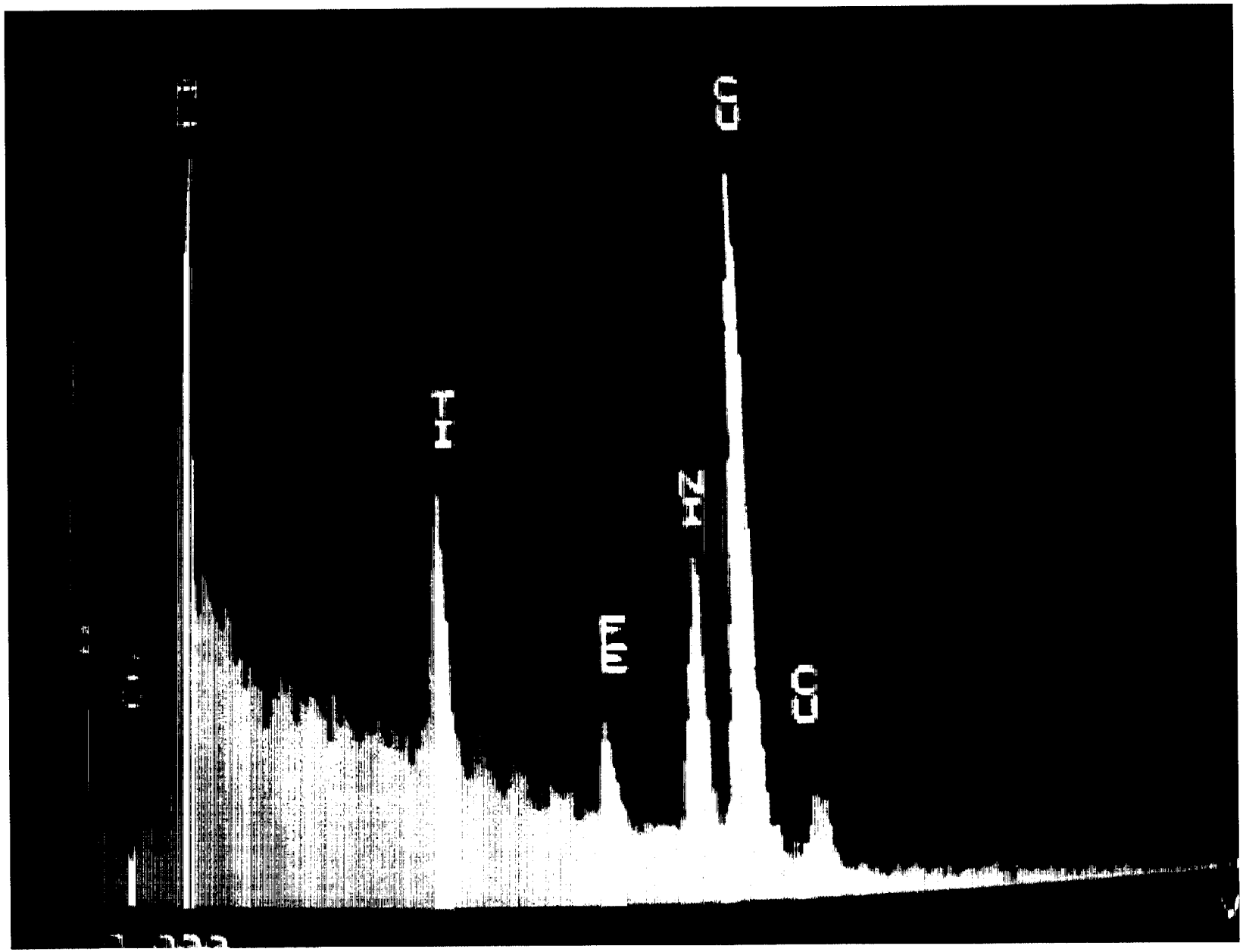

Figure 18x: EDS Analysis of Selected Area of Al-2219 PPP on Ti-6Al-4V Substrate (Sample 10-30-2000 TC4 R3)

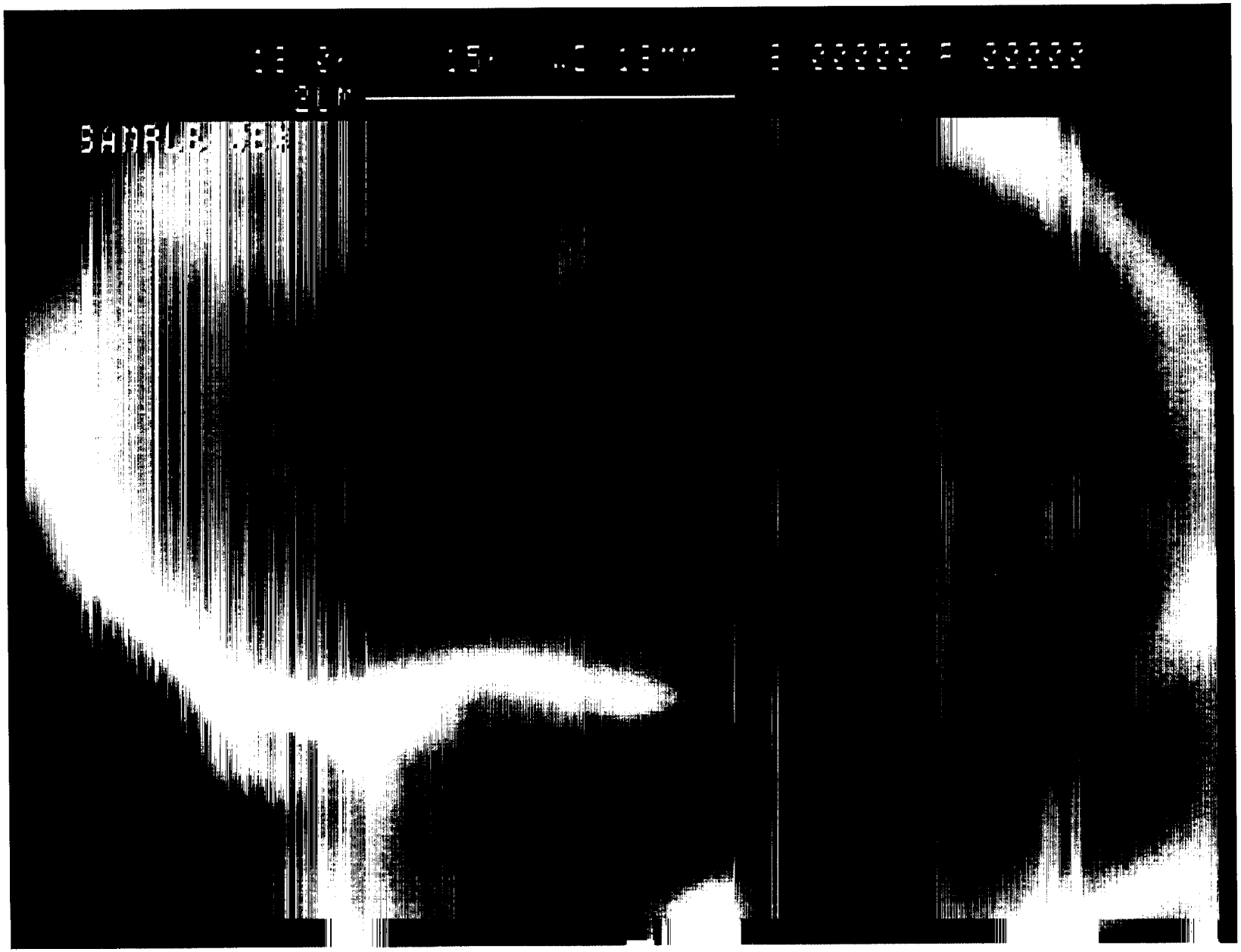

Figure 18y: High Magnification SEM Micrograph of Selected Analysis Point of Al-2219 PPP on Ti-6Al-4V Substrate (Sample 10-30-2000 TC4 R3)

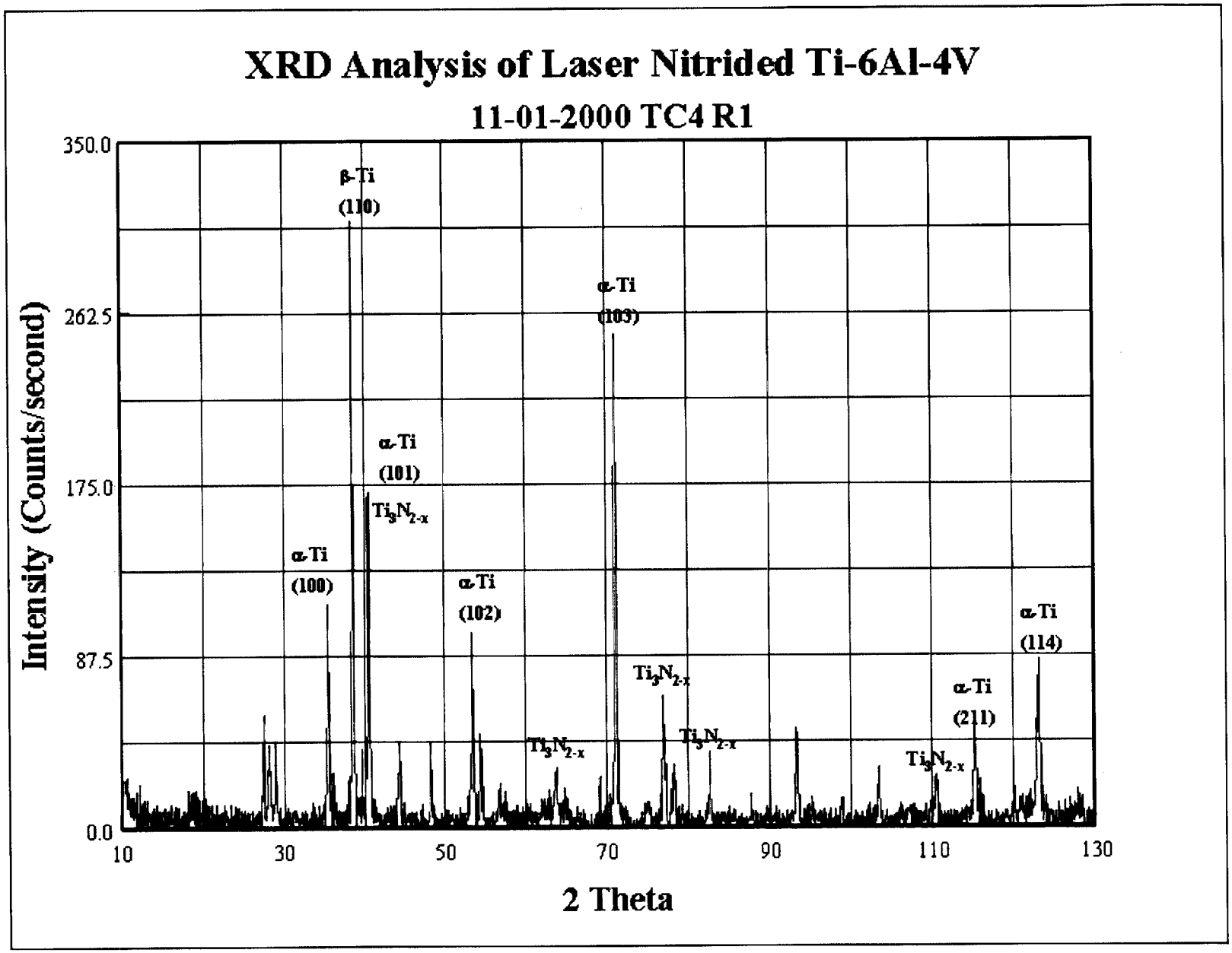

Figure 19a: XRD Analysis of Laser Nitrided Ti-6Al-4V (11-01-2000 TC4 R1)

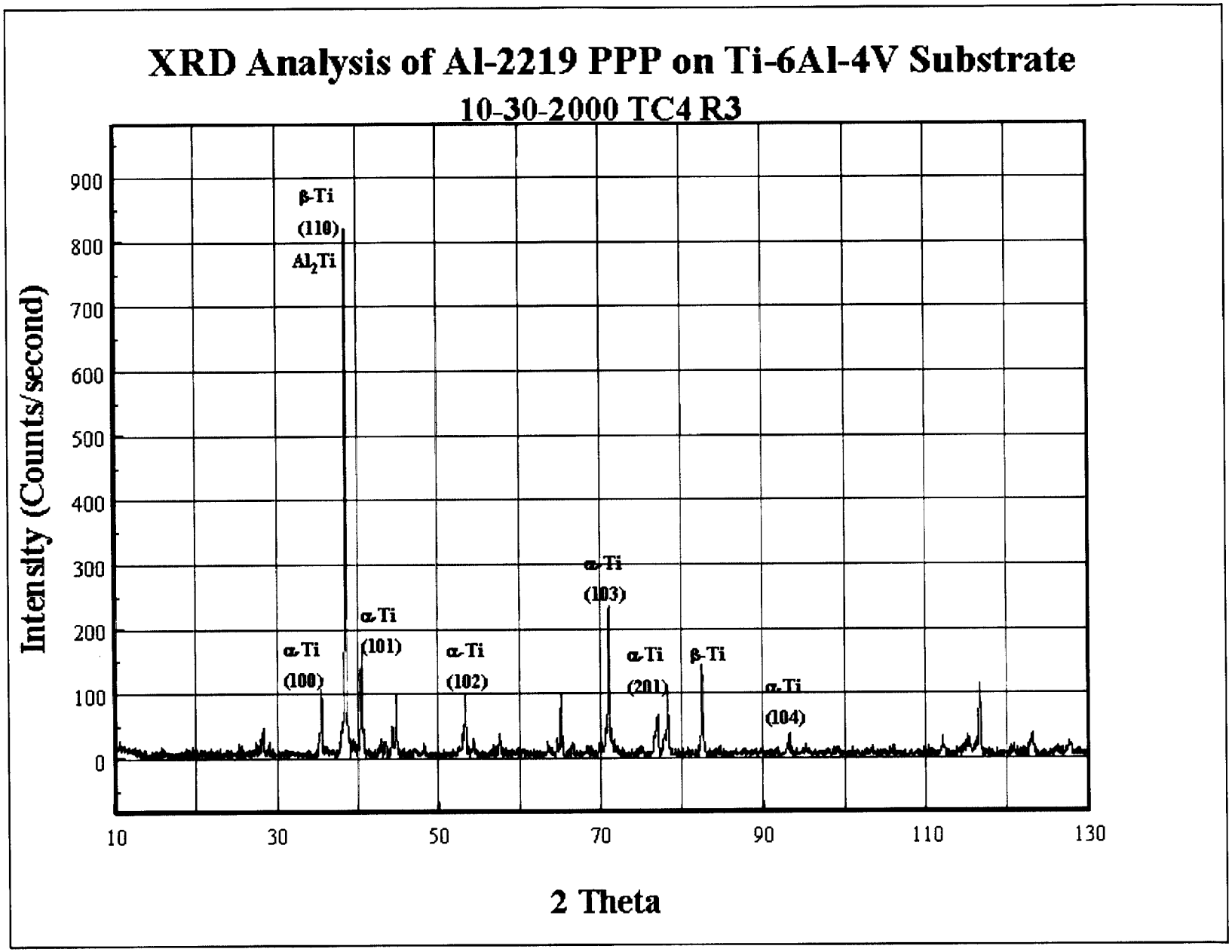

Figure 19b: XRD Analysis of Al-2219 PPP on Ti-6Al-4V Substrate (10-3002000 TC4 R3)

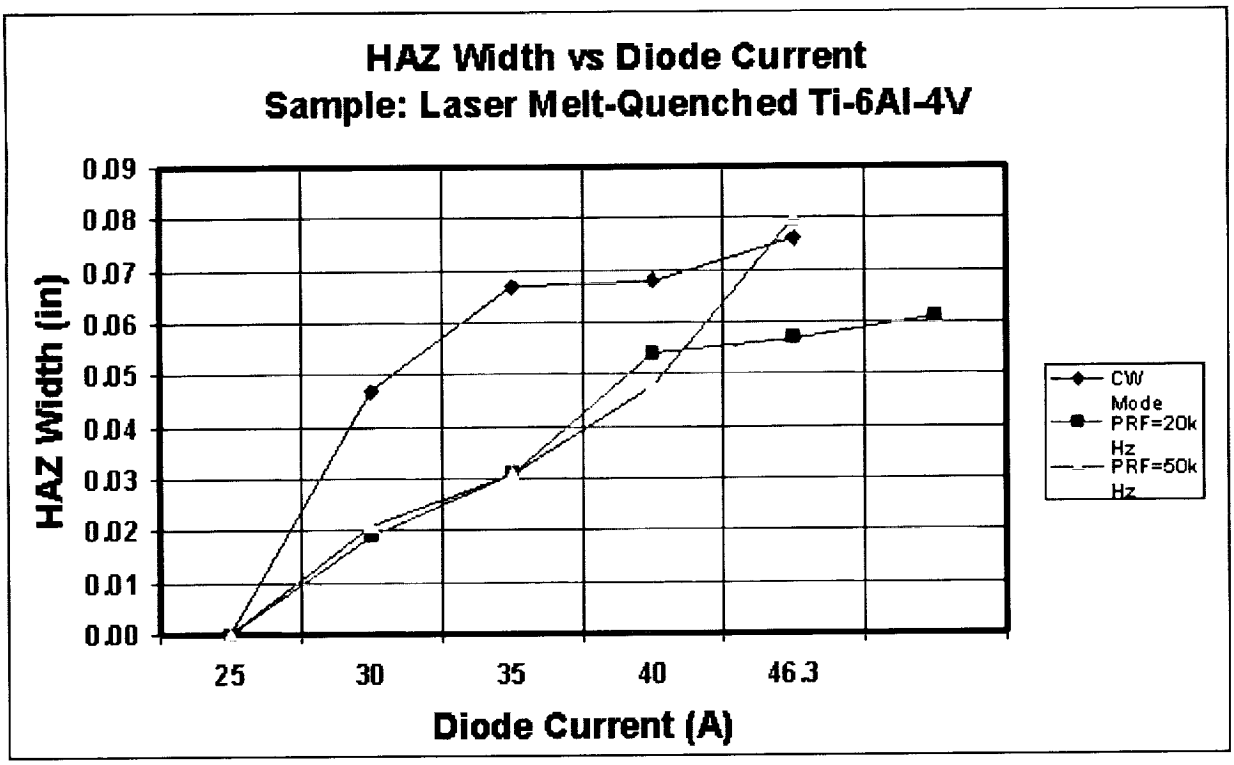

Figure 20a: HAZ Width vs. Diode Current

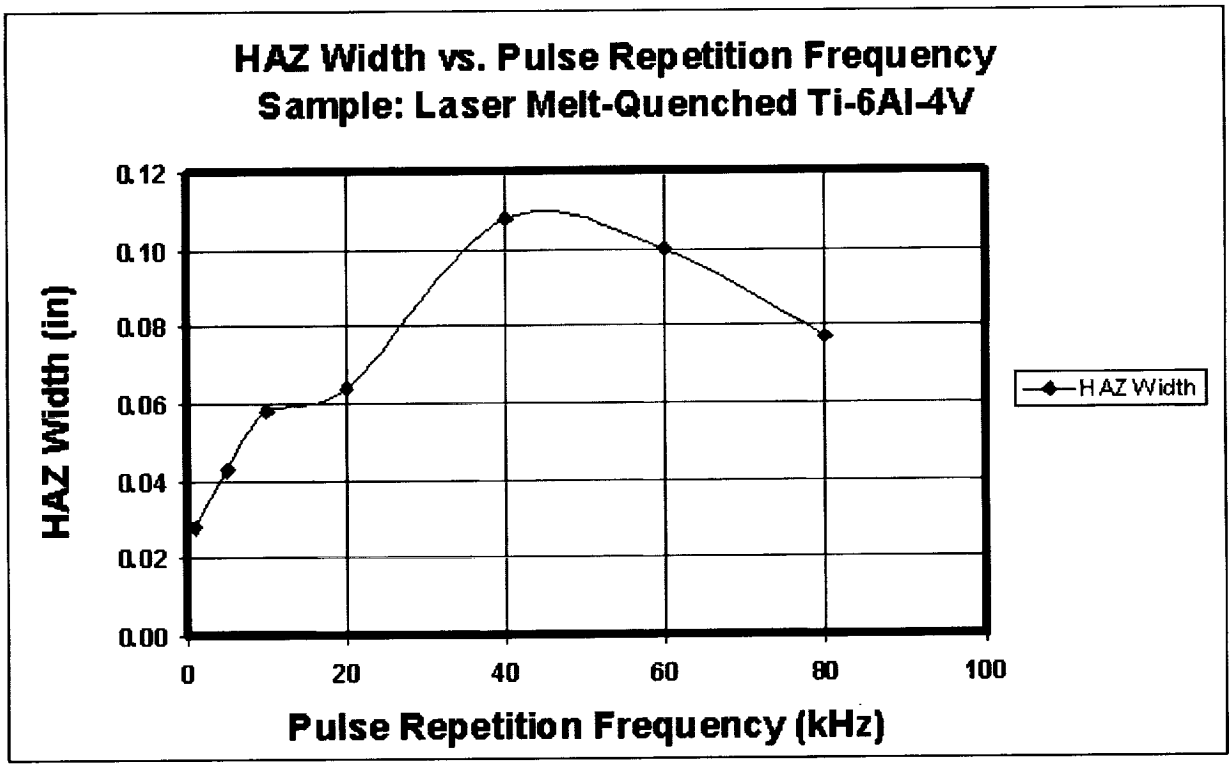

Figure 20b: HAZ Width vs. Pulse Repetition Frequency

APPENDIX A:
CONTINUOUS WAVE CO_2 LASER BEAM WELDING DATA FOR AL-ALLOYS

MATERIAL: Al-ALLOYS
LASER BEAM TYPE: CONTINUOUS WAVE

Material Specification	Laser Type & Beam Mode	Average Power (kW)	Beam Diameter (mm)	Process Speed (mm/s)	Power Density (kW/cm^2)	Specific Energy (kJ/cm^2)	Interaction Time (s)	Shielding Gas & Flow Rate (m^3/hr)	Weld Characteristics	Ref.
A5052P-H32 t=1mm to 6mm	CO2	1.800		16.33				Ar		Masumato, et al, 1992
	CO2	1.800		108.33				Ar		Masumato, et al, 1992
A7075P-T6	CO2							Ar		Masumato, et al, 1992
5083 t=1mm to 3mm	CO2	5.000		100.00					BW & LW	Yoshikawa, M., et al, 1995
5251 t=1mm to 3mm	CO2	5.000		100.00					BW & LW	Yoshikawa, M., et al, 1995
6061 t=1mm to 3mm	CO2	5.000		100.00					BW & LW	Yoshikawa, M., et al, 1995
	CO2	5.000		100.00					BW & LW	Yoshikawa, M., et al, 1995
6082 t=1mm to 3mm	CO2	5.000		100.00					BW & LW	Yoshikawa, M., et al, 1995
	CO2	5.000		100.00					BW & LW	Yoshikawa, M., et al, 1995
Al 5251, t=2mm	CO2	5.000		100.00					BW	Riches, S.T., 1993
Al 6061, t=2mm	CO2	5.000		100.00					BW	Riches, S.T., 1993
A2219-T3 t=4mm & 10mm	CO2	3.000	0.291	16.67	4499.88	61.78	0.017481	Ar, 2.41	BOP	Kutsuna, M., et al, 1993
	CO2	3.000	0.291	33.33	4499.88	30.89	0.0087405	Ar, 2.41	BOP	Kutsuna, M., et al, 1993
	CO2	3.000	0.291	50.00	4499.88	20.59	0.005827	Ar, 2.41	BOP	Kutsuna, M., et al, 1993
	CO2	4.000	0.291	16.67	5999.85	82.38	0.017481	Ar, 2.41	BOP	Kutsuna, M., et al, 1993
	CO2	4.000	0.291	33.33	5999.85	41.19	0.0087405	Ar, 2.41	BOP	Kutsuna, M., et al, 1993
	CO2	4.000	0.291	50.00	5999.85	27.46	0.005827	Ar, 2.41	BOP	Kutsuna, M., et al, 1993
	CO2	6.000	0.291	16.67	8999.77	123.56	0.017481	Ar, 2.41	BOP	Kutsuna, M., et al, 1993
	CO2	6.000	0.291	33.33	8999.77	61.78	0.0087405	Ar, 2.41	BOP	Kutsuna, M., et al, 1993
	CO2	6.000	0.291	50.00	8999.77	41.19	0.005827	Ar, 2.41	BOP	Kutsuna, M., et al, 1993
	CO2	8.000	0.291	16.67	11999.69	164.75	0.017481	Ar, 2.41	BOP	Kutsuna, M., et al, 1993
	CO2	8.000	0.291	33.33	11999.69	82.38	0.0087405	Ar, 2.41	BOP	Kutsuna, M., et al, 1993
	CO2	8.000	0.291	50.00	11999.69	54.92	0.005827	Ar, 2.41	BOP	Kutsuna, M., et al, 1993
A5052	CO2		0.291	16.67			0.017481	Ar, 2.41	BOP	Kutsuna, M., et al, 1993
A5083	CO2	1.900	0.291	3.33	2849.93	195.84	0.087405	He, 1.19	BOP	Kutsuna, M., et al, 1993
	CO2	1.900	0.291	5.00	2849.93	130.43	0.05827	He, 1.19	BOP	Kutsuna, M., et al, 1993
	CO2	1.900	0.291	8.33	2849.93	78.26	0.034962	He, 1.19	BOP	Kutsuna, M., et al, 1993
A5083P-O t=80x40x6 (mm) & t=80x40x4 (mm)	CO2	1.900	0.291	5.00	2849.93	130.43	0.05827	He, 1.51	BOP	Kutsuna, M., et al, 1993
	CO2	1.900	0.291	5.00	2849.93	130.43	0.05827	He, 0.9 & N2, 0.612	BOP	Kutsuna, M., et al, 1993
A6063 t=4mm	CO2		0.291						BOP	Kutsuna, M., et al, 1993
	CO2 @ TEM01	1.000		50.00				Ar, 2.99	BOP & IBW	Kutsuna, M., et al, 1993
	CO2 @ TEM01	2.000		50.00				Ar, 2.99	BOP & IBW	Kutsuna, M., et al, 1993
	CO2 @ TEM01	2.500		50.00				Ar, 2.99	BOP & IBW	Kutsuna, M., et al, 1993
	CO2 @ TEM01	3.100		50.00				Ar, 2.99	BOP & IBW	Kutsuna, M., et al, 1993
	CO2 @ TEM01	3.500		50.00				Ar, 2.99	BOP & IBW	Kutsuna, M., et al, 1993
	CO2 @ TEM01	4.200		50.00				Ar, 2.99	BOP & IBW	Kutsuna, M., et al, 1993
	CO2 @ TEM01	4.500		50.00				Ar, 2.99	BOP & IBW	Kutsuna, M., et al, 1993
	CO2 @ TEM01			100.00					BOP & IBW	Kutsuna, M., et al, 1993

BOP (Bead-on-plate), BW (Butt Weld), FP (Full Penetration), IBW (I-Butt Weld), LW (Lap Weld)

APPENDIX A: (CONT'D):
CONTINUOUS WAVE CO_2 LASER BEAM WELDING DATA FOR AL-ALLOYS

MATERIAL: Al-ALLOYS
LASER BEAM TYPE: CONTINUOUS WAVE

Material Specification	Laser Type & Beam Mode	Average Power (kW)	Beam Diameter (mm)	Process Speed (mm/s)	Power Density (kW/cm^2)	Specific Energy (kJ/cm^2)	Interaction Time (s)	Shielding Gas & Flow Rate (m^3/hr)	Weld Characteristics	Ref.
Al-Li-Cu-Mg-Zr 8090 t=4.3mm	CO2	1.500		10.00					BOP & LW	Kamalu, J.N., et al, 1991
	CO2	1.800		21.40					BOP & LW	Kamalu, J.N., et al, 1991
	CO2	1.800		25.60					BOP & LW	Kamalu, J.N., et al, 1991
	CO2	1.100		7.00					BOP & LW	Kamalu, J.N., et al, 1991
	CO2	2.000		7.00					BOP & LW	Kamalu, J.N., et al, 1991
	CO2			10.00					BOP & LW	Kamalu, J.N., et al, 1991
	CO2			25.00					BOP & LW	Kamalu, J.N., et al, 1991
Al-Li Alloy (2090) t=1.6mm	CO2	1.300		42.33					BOP & BW	Mollan, P.A., et al, 1988
	CO2	1.300		254.00					BOP & BW	Mollan, P.A., et al, 1988
Al 5083	CO2 @ TEM01	7.000	0.800	13.00	1392.61	67.31	0.061538462	Ar	BW	Blake, A., et al, 1985
	CO2 @ TEM01	8.000	0.800	17.00	1591.55	58.82	0.047058824	Ar	BW	Blake, A., et al, 1985
Al5083 t=6.35mm	CO2	3.000	0.800	5.08	596.83	73.82	0.157480315		FP	Blake, A., 1982
	CO2	5.000	0.800	5.08	994.72	123.03	0.157480315		FP	Blake, A., 1982
	CO2	7.400	0.800	5.08	1472.18	182.09	0.157480315		FP	Blake, A., 1982
	CO2	5.000	0.800	8.47	994.72	73.79	0.094451004		BOP	Blake, A., 1982
	CO2	4.000	0.800	6.35	795.77	78.74	0.125984252	He	BOP	Blake, A., 1982
	CO2	5.000	0.800	6.35	994.72	98.43	0.125984252	He	BOP	Blake, A., 1982
	CO2	6.000	0.800	6.35	1193.66	118.11	0.125984252	He	BOP	Blake, A., 1982
	CO2	8.000	0.800	6.35	1591.55	157.48	0.125984252	He	BOP	Blake, A., 1982
	CO2	4.000	0.800	10.58	795.77	47.26	0.075614367	He	BOP	Blake, A., 1982
	CO2	5.000	0.800	10.58	994.72	59.07	0.075614367	He	BOP	Blake, A., 1982
	CO2	6.000	0.800	10.58	1193.66	70.89	0.075614367	He	FP	Blake, A., 1982
	CO2	8.000	0.800	10.58	1591.55	94.52	0.075614367	He	FP	Blake, A., 1982
	CO2	6.000	0.800	19.05	1193.66	39.37	0.041994751	He	BOP	Blake, A., 1982
	CO2	8.000	0.800	19.05	1591.55	52.49	0.041994751	He	BOP	Blake, A., 1982
	CO2	6.000	0.800	12.70	1193.66	59.06	0.062992126	He	FP	Blake, A., 1982
	CO2	8.000	0.800	12.70	1591.55	78.74	0.062992126	He	FP	Blake, A., 1982
	CO2	6.000	0.800	31.75	1193.66	23.62	0.02519685	He	BOP	Blake, A., 1982
	CO2	8.000	0.800	31.75	1591.55	31.50	0.02519685		BOP	Blake, A., 1982
Al-6061-O t=12.7mm	CO2 @ TEM01	5.000	0.800	6.35	994.72	98.43	0.125984252	He	BOP	Blake, A., 1982
	CO2 @ TEM01	7.000	0.800	6.35	1392.61	137.80	0.125984252	He	BOP	Blake, A., 1982
	CO2 @ TEM01	5.000	0.800	8.47	994.72	73.79	0.094451004	He	BOP	Blake, A., 1982
	CO2 @ TEM01	7.000	0.800	8.47	1392.61	103.31	0.094451004	He	BOP	Blake, A., 1982
	CO2 @ TEM01	1.000	0.800		200.00				BOP	Blake, A., 1982
	CO2 @ TEM01	2.000	0.800		400.00				BOP	Blake, A., 1982
	CO2 @ TEM01	3.000	0.800		600.00				BOP	Blake, A., 1982
	CO2 @ TEM01	4.000	0.800		800.00				BOP	Blake, A., 1982
	CO2 @ TEM01	5.000	0.800		1000.00				BOP	Blake, A., 1982
	CO2 @ TEM01	6.000	0.800		1200.00				BOP	Blake, A., 1982

BOP (Bead-on-plate), BW (Butt Weld), FP (Full Penetration), IBW (I-Butt Weld), LW (Lap Weld)

APPENDIX B:
PULSED LASER BEAM WELDING DATA FOR AL-ALLOYS

MATERIAL: Al-ALLOYS
LASER BEAM TYPE: PULSED

Material Specification & Geometry	Laser Type & Beam Mode	Average Power (kW)	Beam Diameter (mm)	Process Speed (mm/s)	Power Density (kW/cm^2)	Specific Energy (kJ/cm^2)	Pulse Duration (s)	Frequency (Hz)	Duty Cycle (%)	Interaction Time (s)	Shielding Gas & Flow Rate (m^3/hr)	Weld Characteristics	Ref.
A5052P-H32 t=1mm to 6mm	CO2	1.400		6.67				200			Ar		Masumato, et al, 1992
	CO2	1.400		10.00				200			Ar		Masumato, et al, 1992
	CO2	1.400		16.67				200			Ar		Masumato, et al, 1992
	CO2	1.400		33.33				200			Ar		Masumato, et al, 1992
	CO2	1.400		50.00				200			Ar		Masumato, et al, 1992
6061, t=3mm	YAG	2.000		5.00				110			Ar, 1.5	BW & LW	Yoshikawa, M., et al, 1995
	YAG	2.000		5.00				110			He	BW & LW	Yoshikawa, M., et al, 1995
	YAG	2.000		5.00				110			N2	BW & LW	Yoshikawa, M., et al, 1995
	YAG	2.000		6.67				110			He	BW & LW	Yoshikawa, M., et al, 1995
	YAG	2.000		6.67				110			N2	BW & LW	Yoshikawa, M., et al, 1995
	YAG	2.000		25.00				110			Ar, 1.5	BW & LW	Yoshikawa, M., et al, 1995
5083, t=2mm	YAG	2.000		25.00				110			He	BW & LW	Yoshikawa, M., et al, 1995
	YAG	2.000		25.00				110			N2	BW & LW	Yoshikawa, M., et al, 1995
	YAG	2.000		16.67				110			Ar, 1.5	BW & LW	Yoshikawa, M., et al, 1995
	YAG	2.000		16.67				110			He	BW & LW	Yoshikawa, M., et al, 1995
	YAG	2.000		16.67				110			N2	BW & LW	Yoshikawa, M., et al, 1995
6061, t=2mm	YAG	2.000		25.00				110			Ar, 1.5	BW & LW	Yoshikawa, M., et al, 1995
	YAG	2.000		25.00				110			He	BW & LW	Yoshikawa, M., et al, 1995
	YAG	2.000		25.00				110			N2	BW & LW	Yoshikawa, M., et al, 1995
5083, t=3mm	YAG	2.000		8.33				110			He	BW & LW	Yoshikawa, M., et al, 1995
6061, t=3mm	YAG	2.000		4.17				110			He, Ne	BW & LW	Yoshikawa, M., et al, 1995
6061	Nd:YAG	0.020	0.400				0.007	1			Ar		Coyle, R.J., et al, 1987
413	Nd:YAG	0.020	0.400				0.007	1			Ar		Coyle, R.J., et al, 1987
4047 7.1mm dia. x 0.3mm	Nd:YAG	0.020	0.400				0.007	1			Ar		Coyle, R.J., et al, 1987
5000 series t=1.25mm	Nd:YAG	3.000		38.33								BW	Riches, S.T., 1993
8000 series t=1.25mm	Nd:YAG	3.000		33.33								BW	Riches, S.T., 1993
AlMgSi 1 F28 t=5mm	CO2 @ TEM00	1.400	0.100		17825.35			20000			O2,N2,He or Ar 1.8 to 2.41		Michaelis, A., et al, 1994

BW (Butt Weld), LW (Lap Weld)

APPENDIX C:
CONTINUOUS WAVE CO2 LASER BEAM WELDING DATA FOR TITANIUM ALLOYS

Material Specification	Laser Type & Beam Mode	Average Power (kW)	Beam Diameter (mm)	Process Speed (mm/s)	Power Density (kW/cm^2)	Specific Energy (kJ/cm^2)	Interaction Time (s)	Shielding Gas & Flow Rate (m^3/hr)	Weld Characteristics	Ref.
Ti-6Al-4V,	CO2	1.000	0.250	23.00	2037.18	17.39	0.010869565	He, Ar	BW	Mazumder, J., et al, 1982
AMS 4911-Ta10 BSS	CO2	1.000	0.250	34.00	2037.18	11.76	0.007352941	He, Ar	BW	Mazumder, J., et al, 1982
t=1mm	CO2	1.000	0.250	15.00	2037.18	26.67	0.016666667	He, Ar	BW	Mazumder, J., et al, 1982
t=1mm	CO2	1.000	0.250	11.00	2037.18	36.36	0.022727273	He, Ar	BW	Mazumder, J., et al, 1982
t=0.89mm	CO2	1.480	0.250	60.00	3015.03	9.87	0.004166667	He, Ar	BW	Mazumder, J., et al, 1982
t=0.89mm	CO2	1.480	0.250	50.00	3015.03	11.84	0.005	He, Ar	BW	Mazumder, J., et al, 1982
t=0.89mm	CO2	1.480	0.250	23.00	3015.03	25.74	0.010869565	He, Ar	BW	Mazumder, J., et al, 1982
t=0.81mm	CO2	1.500	0.250	60.00	3055.77	10.00	0.004166667	He, Ar	BW	Mazumder, J., et al, 1982
t=0.81mm	CO2	1.500	0.250	50.00	3055.77	12.00	0.005	He, Ar	BW	Mazumder, J., et al, 1982
t=0.81mm	CO2	1.500	0.250	23.00	3055.77	26.09	0.010869565	He, Ar	BW	Mazumder, J., et al, 1982
t=2.03mm	CO2	1.500	0.250	7.00	3055.77	85.71	0.035714286	He, Ar	BW	Mazumder, J., et al, 1982
t=2.03mm	CO2	1.500	0.250	9.00	3055.77	66.67	0.027777778	He, Ar	BW	Mazumder, J., et al, 1982
t=2.03mm	CO2	1.500	0.250	13.00	3055.77	46.15	0.019230769	He, Ar	BW	Mazumder, J., et al, 1982
t=1mm	CO2	1.110	0.250	6.00	2261.27	74.00	0.041666667	He, Ar	BW	Mazumder, J., et al, 1982
t=1mm	CO2	1.500	0.250	23.00	3055.77	26.09	0.010869565	He, Ar	BW	Mazumder, J., et al, 1982
t=1mm	CO2	1.540	0.250	50.00	3137.26	12.32	0.005	He, Ar	BW	Mazumder, J., et al, 1982
t=1mm	CO2	1.540	0.250	60.00	3137.26	10.27	0.004166667	He, Ar	BW	Mazumder, J., et al, 1982

BW (Butt Weld)

APPENDIX D:
LASER SHOCK PROCESSING DATA OF ALUMINUM ALLOYS

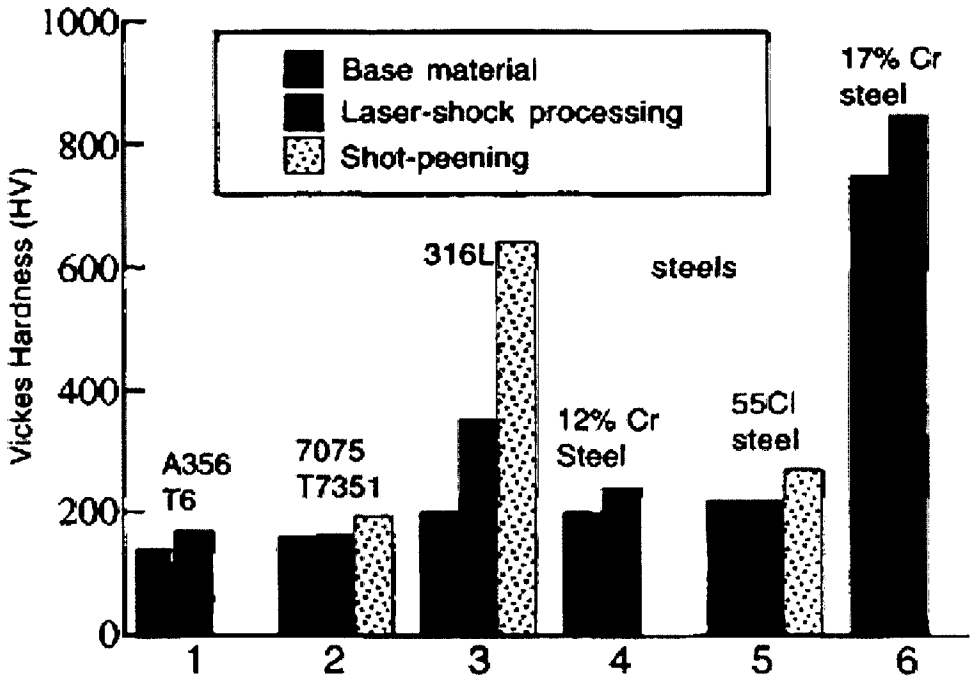

Maximum surface hardening induced in a typical LSP configuration (20-30 ns, 5-10 GW/ cm^2, water confined regime, ambient atmosphere) - Comparison with shot-peening.[27,28,30]

APPENDIX D (CONT'D) :
LASER SHOCK PROCESSING DATA OF ALUMINUM ALLOYS

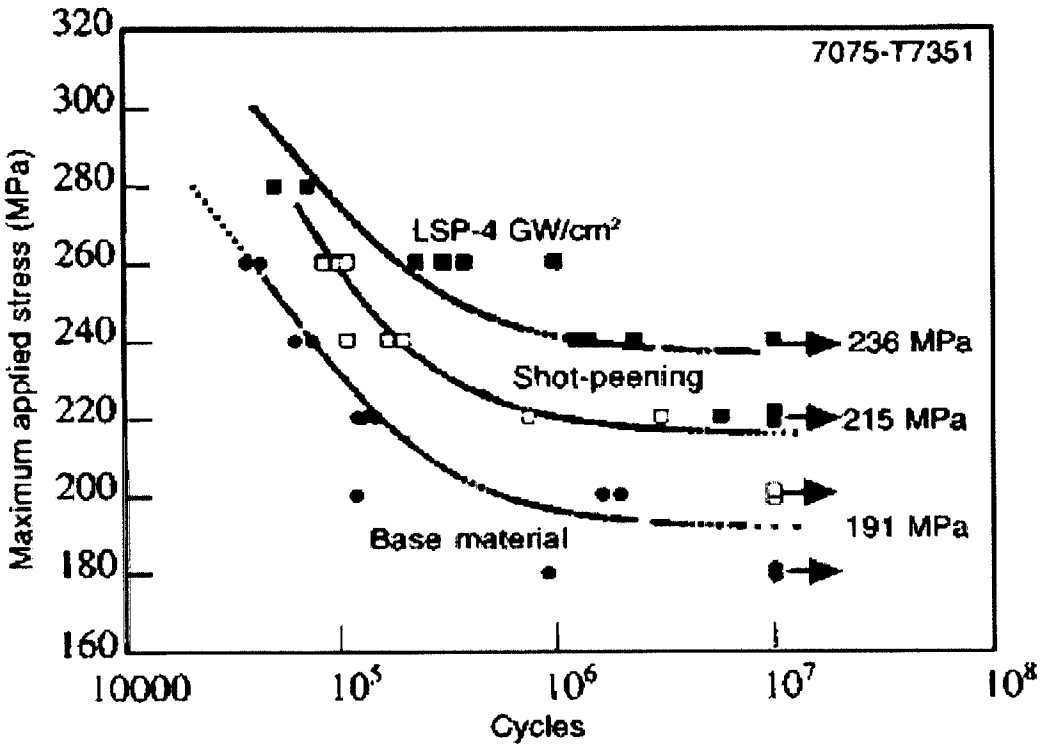

S-N curves on a 7075-T7351 aluminium alloy. Influence of shot-peening and laser-shock processing surface treatments (notched samples, bending-fatigue at 30 Hz - R = 0.1).[28]

APPENDIX D (CONT'D) :
LASER SHOCK PROCESSING DATA OF ALUMINUM ALLOYS

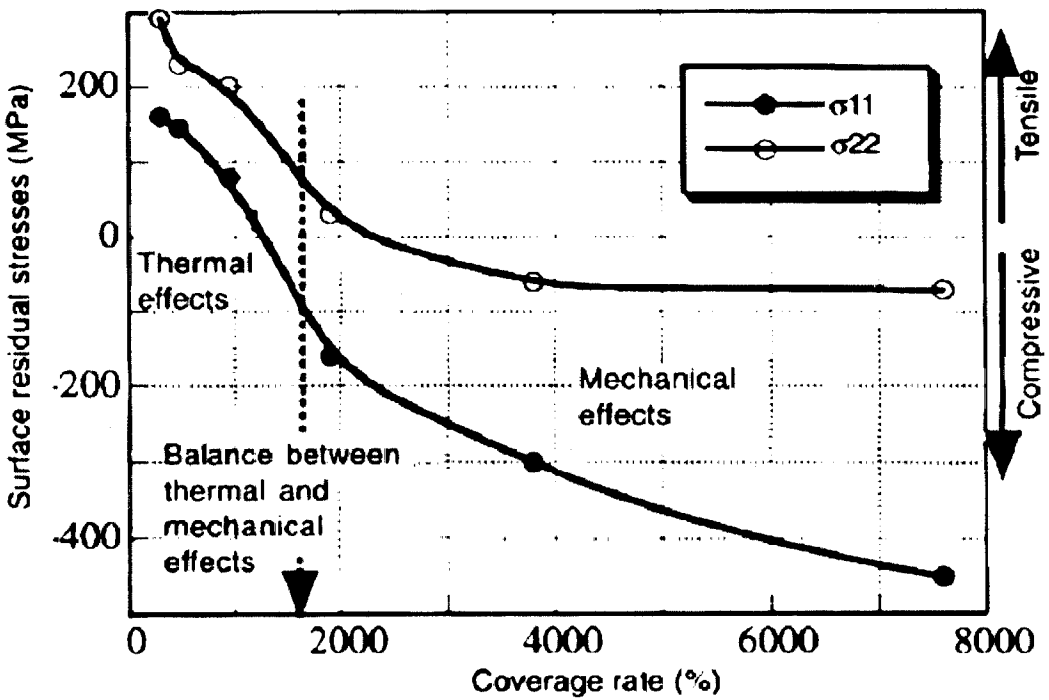

LSP without protective coating : surface stress dependence on coverage factor (AISI304 steel -5 ns pulses- 0.75 mm spots).

APPENDIX E:
TORNADO ND:YAG LASER SPECIFICATIONS

General Characteristics

Model	TN50-106Q
Wavelength	1064 nm
Average Power	>35 W @ 10 kHz
Pulse Width (nominal)	120 ns @ 10 kHz
Pulse Eenergy, 5 kHz	>5 mJ
Pulse Energy, 10 kHz	>3.5 mJ
Pulse Duration, 1 kHz	>80ns
Pulse Duration, 5 kHz	90 ns, nominal
Pulse Duration, 10 kHz	110 ns, nominal
Repetition Rate Range	Single shot to 80 kHz
Spatial Mode	Flat-Top (Multi Mode Beam) $M^2 < 14$ at 10 kHz
Polarization	Unpolarized Beam

Beam Specifications

M^2	< 15
Polarization	Random
Beam Diameter (at waist) Beam Diameter @ 10 kHz	1.9 mm (nominal) 2.0 mm @ OC
Beam Ellipticity @ 10 kHz	< 10% difference in any orthogonal axes
Beam Divergence	4.5 mrad ($M^2 = 14$)
Boresight:	0.1 mm position of output
Stability	3
Beam Pointing	<20 ~rad per oC
Pulse-to-pulse Stability	Energy (5-10 kHz) <2% rms Peak Power (5-10 kHz): 3.5% rms
Long-term Stability :	3% non-cumulative, over 8 hours Environmental Characteristics
Warm-up Time	<10 minutes (cold start to 90% of full power)
Temperature Range	18°-35° C

Altitude	0-3,000 meters
Humidity	8-95%, non-condensing Non-Operating Conditions
Temperature	0-50°C

Physical Characteristics

Electrical Requirements	220-240 Vac, 50/60 Hz
Power Consumption	3 kW (typical)
Cooling Internal Fan	200 CFM
Weight	
Laser Head	5.9 kg (13 Ibs)
S240 Power Supply	13.8 kg (30.5 Ibs)
Chiller	39 kg (86 Ibs)

Chiller Requirements

Electrical Requirements	200- 240 Vac, 10 A, 50 or 60 Hz
Temperature	20°C
Flow Rate	(0.5 Gal/min)
Pressure	344 kPa (50 psi)
Cooling Capacity	> 1 kW
Coolant	Deionized Water

Diode Module Specifications

Lifetime	5250 hours
Field Replaceable	(8760 hrs is 1 year)

APPENDIX E (CONT'D):
TORNADO ND:YAG LASER SPECIFICATIONS

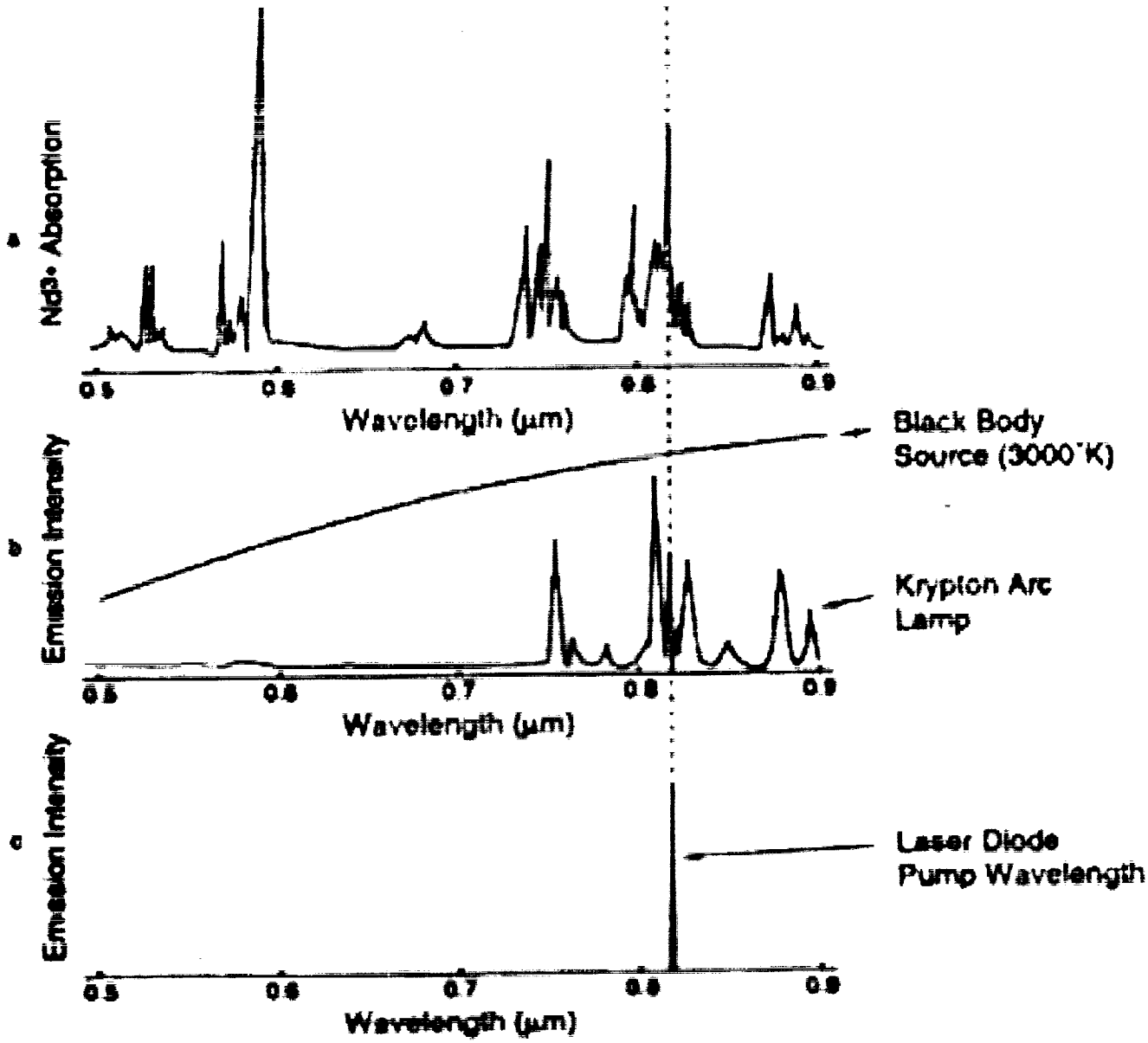

APPENDIX E (CONT'D):
TORNADO ND:YAG LASER SPECIFICATIONS

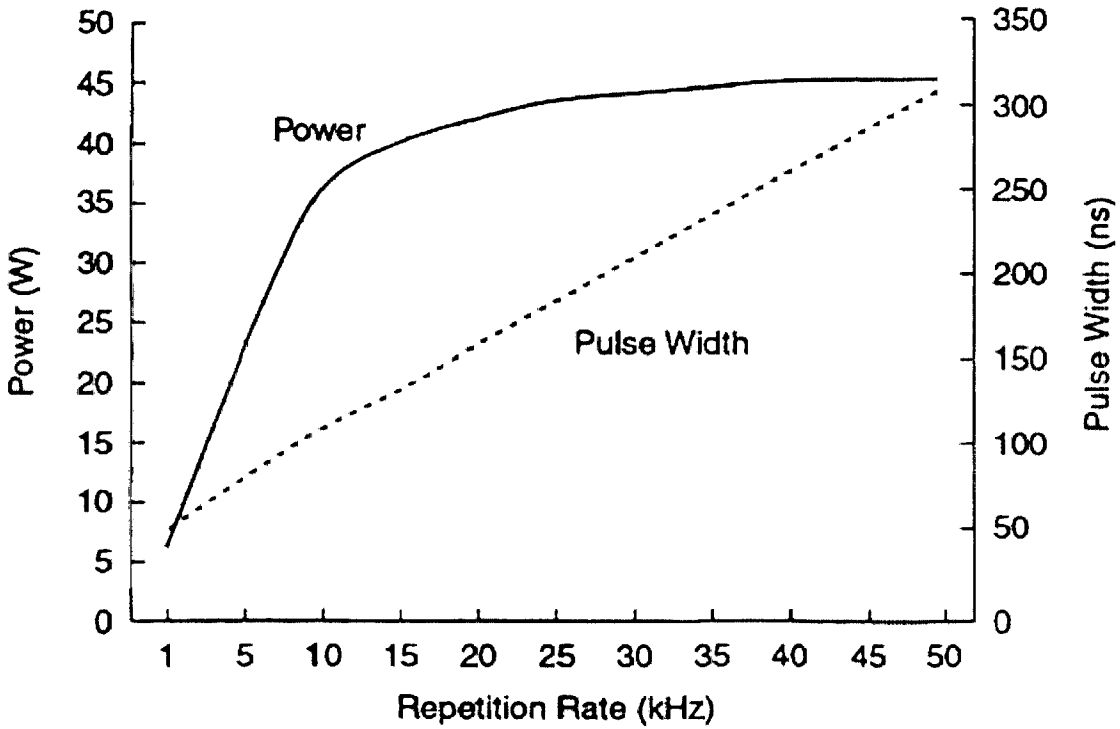

APPENDIX F:
GLOSSARY OF TERMS FOR LASER CHARACTERISTICS

AVERAGE POWER (Watts) = Pulse Energy (Joules) x Pulse Repetition Rate (Hz)

$$Pa = ER$$

AVERAGE POWER (Watts) = Peak Power Pulse (Watts) x Pulsewidth (Sec.) x Pulse Repetition Rate (Hz

$$Pa = P_pTR$$

BRIGHTNESS $$= \frac{\text{Power (Watts)}}{[\text{Beam Diameter (MM)} \times \text{Beam Divergence (mr)}]^2}$$

$$B = \frac{P}{(\Theta D)^2}$$

PULSE ENERGY (Joules) = Peak Power Pulse (Watts) x Pulsewidth (Sec.)

$$E = P_pT$$

LIGHT TRANSMISSION $$= \frac{\text{Intensity of light after passing through filter}}{\text{Intensity of light}} = T\lambda$$

OPTICAL DENSITY = −1 Log (Light transmission)

$$T\lambda = 10^{-OD}$$

SPOT SIZE = Diffraction Limited spot + Spherical Aberration

$$d_s = 1.27\ \frac{\lambda f M^2}{D}$$

APPENDIX F (CONT'D):
GLOSSARY OF TERMS FOR LASER CHARACTERISTICS

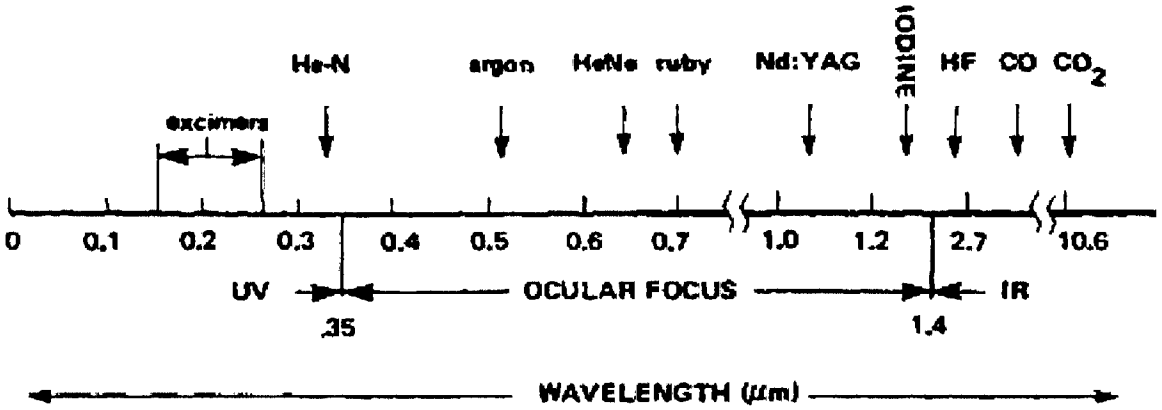

Wavelength spectrum of typical lasers

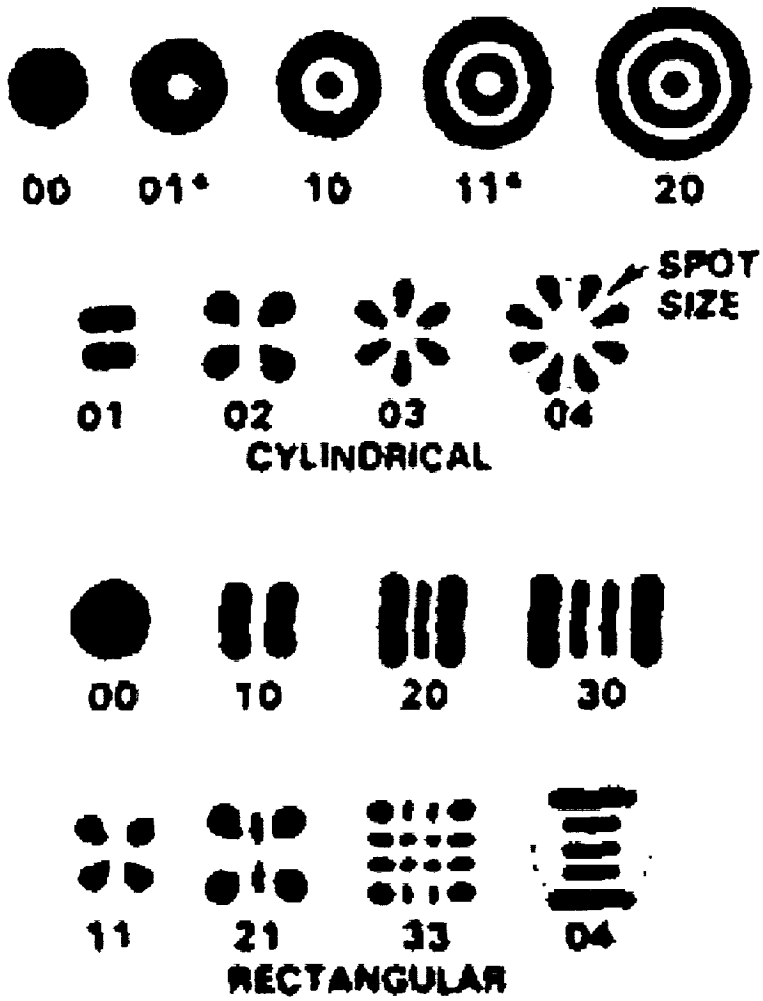

Transverse Electromagnetic Modes
TEM_{mn}

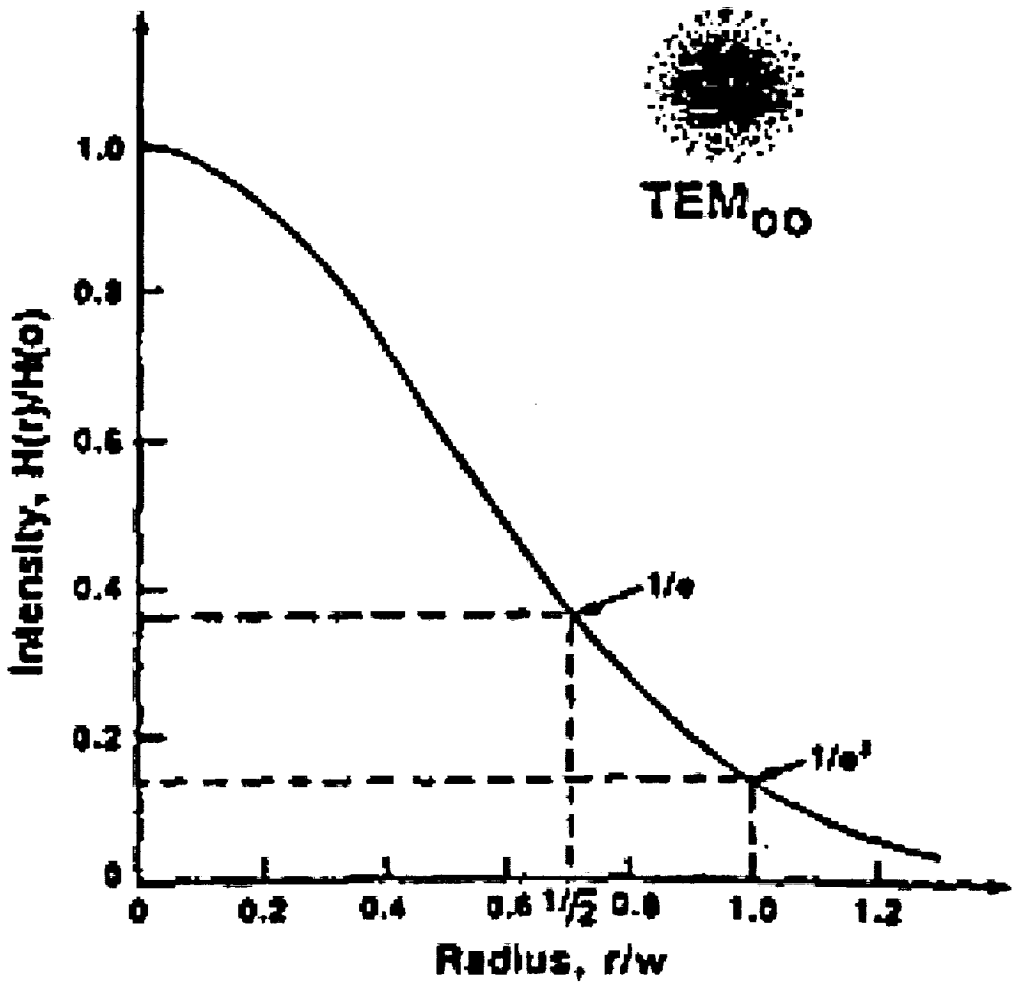

Gaussian Distribution of TEM_{00}

APPENDIX G:
TYPICAL MELT ENERGY CALCULATIONS FOR TITANIUM AND ALUMINUM ALLOYS

Alloy Component Percentage by Weight							
Material	Ti	Al	V	Cu	Li	Mn	TOTALS
Ti-6Al-4V	0.900	0.060	0.040	0	0	0	1.000
Al 2090	0	0.950	0	0.027	0.023	0	1.000
Al 2219	0	0.930	0	0.067	0	0.003	1.000

Empirical and Calculated Alloy Thermal Property Values						
Material	Density (kg/m^3)	Melting Point (°C)	Heat Capacity (J/kg-°C)	Thermal Conductivity (W/m-K)	Heat of Fusion (J/kg)	Melt Energy (J/mm^3)
Ti-6Al-4V	4430	1660	526.30	6.7	427653.20[a]	5.7182[b]
Al 2090	2590	650	1203.00	88	376235.60[a]	2.9374[b]
Al 2219	2840	643	864.00	120	374351.60[a]	2.5919[b]

Values in blue obtained from www.matweb.com

Values in green obtained from Alcoa Green Letter, #226, 1988

Values in red calculated from obtained values

a: Weighed average calculated using primary alloying elements

b: Calculated by: $E_M = 1_{mm}{}^3 \times \rho \times \left[(C_P \times \Delta T) + \Delta H_f\right]$

Where:
- **T = (Melting Point – 20°C)**
- **C_P= Specific Heat**
- **ΔH_f=Enthalpy of Formation**
- **ρ=Density**

APPENDIX H:
COMPARISON CHART OF VARIOUS LASERS

Manufacturer & Model	Wavelength (μm)	Pumping Medium	Beam Mode	Output Power (W)	Approx. Cost (US$)	Electrical Requirements
Spectra Physics Tornado- TN50-106Q (new) TN100-106Q (new)	1064 1064	diode diode	pulsed/ cw	50 100	32, 700 57, 500	208V, 3PH, 20A
GSI Lumonics JK500 (used)	1064	lamp	cw	500	70, 000	460V, 3PH, 100A
USLaser 406-1 (new) 406-2 (new)	1064 1064	lamp lamp	cw cw	500 1000	47, 000 95, 000	208V, 3PH 208V, 3PH
Lee Laser 8250M/500 (new) LDP-200MQG (new)	1064 532	lamp diode	cw pulsed/cw	500 100	38, 000 108, 000	220V, 1PH, 20A
Trump HL703D (new)	1064	lamp	cw	700	106, 000	440V, 3PH, 100A 208V, 3PH, 192A
Raytheon SS550 (used)	1064	lamp	pulsed	400	39, 000	480V, 3PH
Nuvonyx* ISL-1000L (new)	810	direct diode laser	cw	1000	125, 000	
Roffin-Sinar RSY-500 RSY-1000	1064 1064	lamp lamp	cw cw	500 1000	110000 175000	208V, 3PH (excluding chiller)

* Typical Wall Plug Efficiency: CO_2: 12%, Lamp Pumped Nd:YAG: 1-2%, Diode Pumped ND:YAG: 8-12%, Direct Diode Laser: 40%